BIS-MPA DENDRIMERS AS A PLATFORM FOR MOLECULAR IMAGING APPLICATIONS

BIS-MPA DENDRIMERS AS A PLATFORM FOR MOLECULAR IMAGING APPLICATIONS

By LUKAS P SADOWSKI, B.Sc.

A Thesis Submitted to the School of Graduate Studies in Partial Fulfillment of the Requirements for the Degree of PHD of CHEMISTRY

Title: Bis-MPA Dendrimers as a Platform for Molecular Imaging Applications

Author: Lukas P. Sadowski

Hon. Dbl. Major B.Sc. (Chemistry and Biology)

York University, Toronto, Canada.

Supervisor: Dr. Alex Adronov

Number of Pages: xv, 189

Abstract

The objective of this research was to develop and validate new macromolecular imaging agents to detect and characterize malignant tumours. Using well-defined, highly branched macromolecules called dendrimers as the structural scaffold, efficient functionalization of the periphery was demonstrated using "click" chemistry in order to prepare multivalent imaging probes. Furthermore, a transmetalation was demonstrated to displace chelated copper with technetium, enabling "click" reactions to be performed in the presence of the dipicolylamine (DPA), a ligand known to chelate many metals.

The dendritic scaffold was functionalized with either hydrophobic or hydrophilic targeting vectors. The hydrophobic ligand, an acyloxymethyl ketone targeting the overexpression of cathepsin B exhibited poor *in vitro* affinity when coupled to either G1 or G2 dendrimers, despite the use of various linkers. A glu-urea-lys dipeptide, representing a hydrophilic prostate specific membrane antigen targeting vector, demonstrated excellent affinity *in vitro*. The lead compound, a G2 dendrimer bearing four PSMA targeting vectors attached via an alkyl spacer was further investigated *in vitro* and *in vivo*. Unfortunately, poor tumor uptake was observed and the compound was hypothesized to hydrolyze readily (<15min), based on the *in vitro* plasma stability data. To rectify the aforementioned problem, non neo-pentyl esters were replaced with either carbamate or ether linkages. *In vitro* plasma stability analysis of the analogous compounds demonstrated increased stability. In particular, the ether analogue was found to be most stable, with minimal degradation observed after 4 hours.

Acknowledgements

I would like to acknowledge my supervisor, Alex Adronov, for giving me the opportunity to carry out research in his lab. I would also like to thank my committee members, John Valliant and Michael Brook for their useful discussions and suggestions throughout the project, as well as Kirk Green for all of the training and help received throughout my time at McMaster University. Additionally, I would like to extend a huge thank you to many of the group members, both past and present. In particular, I would like to thank Spencer Knight - Live Long and Prosper, Mr. Knight. To Greg Bahun, who was particularly helpful in getting me started in the lab and who is continually a source of fruitful discussions. To Sabrina Hodgson, thank you for being you and for being an amazing friend – there is never a dull moment with you around! The trypod would also be incomplete without Victoria Mackey – thanks little buddy!

This body of work was also made possible due to the continual love and support that I have received from my family. To my parents, who have endured endless discussions over dinner while I try to explain my research, I thank you. You gave me the means to pursue my dreams. I would also like to thank my brother, Radek, for challenging me to better myself in all walks of life and to Micah for bringing me joy beyond words!

Most importantly, I would like to acknowledge my undergraduate supervisor, the late Professor Michael M. Pollard. You are one of the most charismatic, brightest and creative people that I have ever met in my entire life. You continue to inspire me to be better – thank you.

Table of Contents

Table of Figures

Table of Schemes

1.1. Introduction to Polymers and Polymer Architecture

Polymer chemistry, involving the synthesis and properties of polymers, encompasses a wide-range of diverse subdisciplines. The field of polymer chemistry, also referred to as macromolecular chemistry, ranges from natural polymers such as deoxyribonucleic acids (DNA) and proteins, which are vital to all living things, to synthetic polymers such as poly(ethylene) and poly(styrene) which are common plastics manufactured on hundred million-ton scales worldwide and are invaluable for modern-day living.[1] The countless innovations in polymer chemistry over the past several decades are undoubtedly due to the continuous dedication to research in this field by scientists across the world. There are numerous examples of polymers with exceptional properties, including, but not limited to, classic examples such as Teflon[2] and Kevlar,[3] which are based on fluorinated polymers and polymers with a rigid network of H-bonds, respectively. Furthermore, it is possible to prepare biocompatible, degradable polymers that are specifically designed for biomedical applications such as *in vivo* stents,[4] drug delivery,[5–7] or even tissue engineering.[8–10] The wide-range of material possibilities, potential applications, and tunable properties are just a few of the reasons polymer chemistry has become so successful and world-renowned to date.

Polymer architecture is one of the fundamental concepts within polymer chemistry. Similar to proteins, the architecture of synthetic polymers can have a pronounced effect on the resulting properties and therefore, controlling the architecture is of great interest. This type of control can be achieved through tuning the properties of the monomeric unit, and controlling the degree of branching within the polymer backbone.

Branched polymers are known to have considerably different properties compared to their linear analogues, such as crystallinity, hydrodynamic radius and solubility.[11] The ability to fine-tune these parameters allows for the preparation of modular materials with a diverse array of potential applications. Dendrimers are one class of branched polymers that have unique properties and characteristics (Figure 1.1). These properties make dendrimers highly suitable for many biomedical applications, and will be the focus of this thesis.

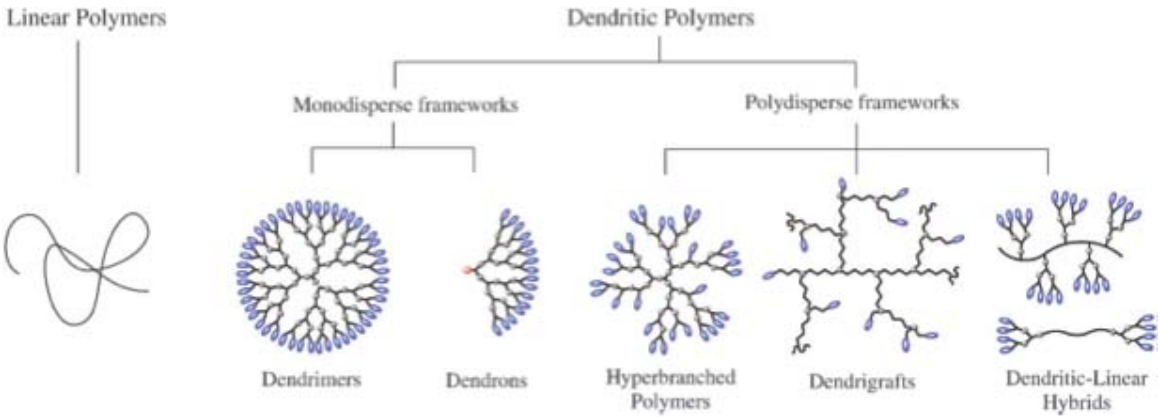

Figure 1.1. Schematic diagram of linear and dendritic polymer architectures. Reproduced from Ref 12 with permission of The Royal Society of Chemistry.

1.2. Introduction to Dendrimers

Dendrimers are a class of polymers that are highly branched and structurally perfect. Unlike hyperbranched polymers, which have random branching points, the structural perfection of dendrimers, and therefore their monodispersity, is a direct result of the step-wise growth that is employed when synthesizing this class of compounds.

Each dendrimer is comprised of a multifunctional core, from which branching units emanate. Each layer of branching constitutes one generation, while each "wedge" of the dendrimer is referred to as a dendron, as outlined in Figure 1.2.

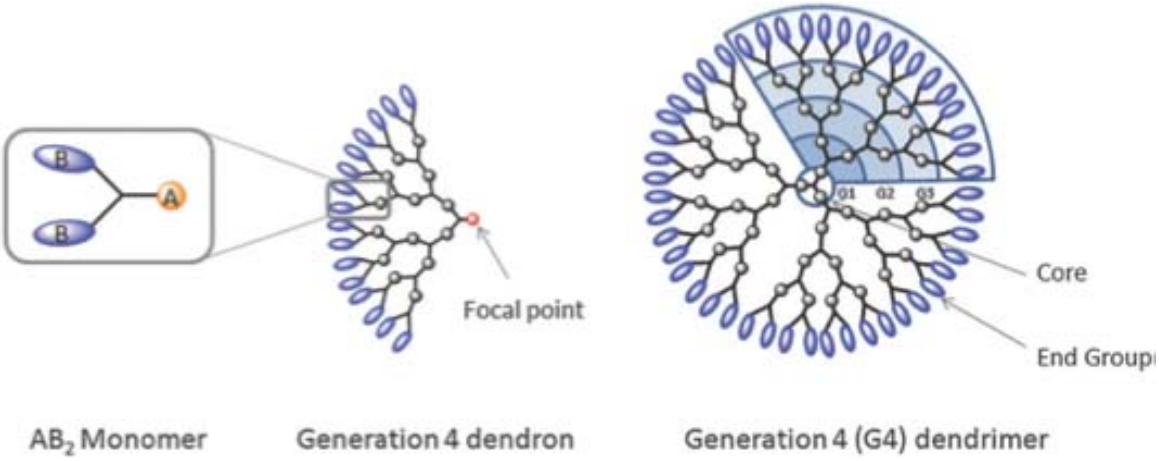

Figure 1.2. Cartoon scheme representing the main structural components of a dendrimer. Reproduced from Ref 12 with permission of The Royal Society of Chemistry.

The outermost layer of the dendrimer is referred to as the periphery and typically comprises approximately half of the dendrimer's mass. The periphery dictates the macroscopic properties of the dendrimer, such as solubility. The high number of peripheral groups often contributes to site isolation of the core, creating a unique microenvironment. This core microenvironment has the ability to encapsulate guest molecules of different sizes, leading to host-guest interactions, in a phenomenon referred to as the "dendritic box", which has been shown to release the guest molecules in a controlled manner and has potential for numerous biomedical applications.[13,14]

1.3. History of Dendrimers

The synthesis of branched architectures in a controlled manner by using AB_2 monomers was first hypothesized by P.J. Flory in 1952.[15] An AB_2 monomer refers to a molecule that contains one type of a certain functionality (A) and two of another functionality (B). By controlling the reactivity of A and B, it is possible to create a hyperbranched polymer, provided that crosslinking can be suppressed. In 1978, Vogtle became the first chemist to report the synthesis of branched molecular architectures, which he referred to as "cascade polymers", based on an iterative stepwise process of Michael additions of an amine onto acrylonitrile, followed by reduction of the nitrile functionality using a combination of Co(III) and $NaBH_4$.[16] Unfortunately, the reduction was plagued by low yields and side reactions, thereby limiting the synthesis to low molecular weight branched polymers (Figure 1.3a). Nevertheless, this seminal report on cascade polymers was the foundation of what later led to the synthesis and commercialization of polypropylene imine (PPI) dendrimers, which have been used extensively in research (Figure 1.3b). Using the same sequence of reactions, Meijer was able to circumvent the problematic reduction of the nitrile moieties using Raney cobalt and hydrogen,[17] while Mülhaupt reported the successful reduction using Raney nickel in lieu of Raney cobalt.[18]

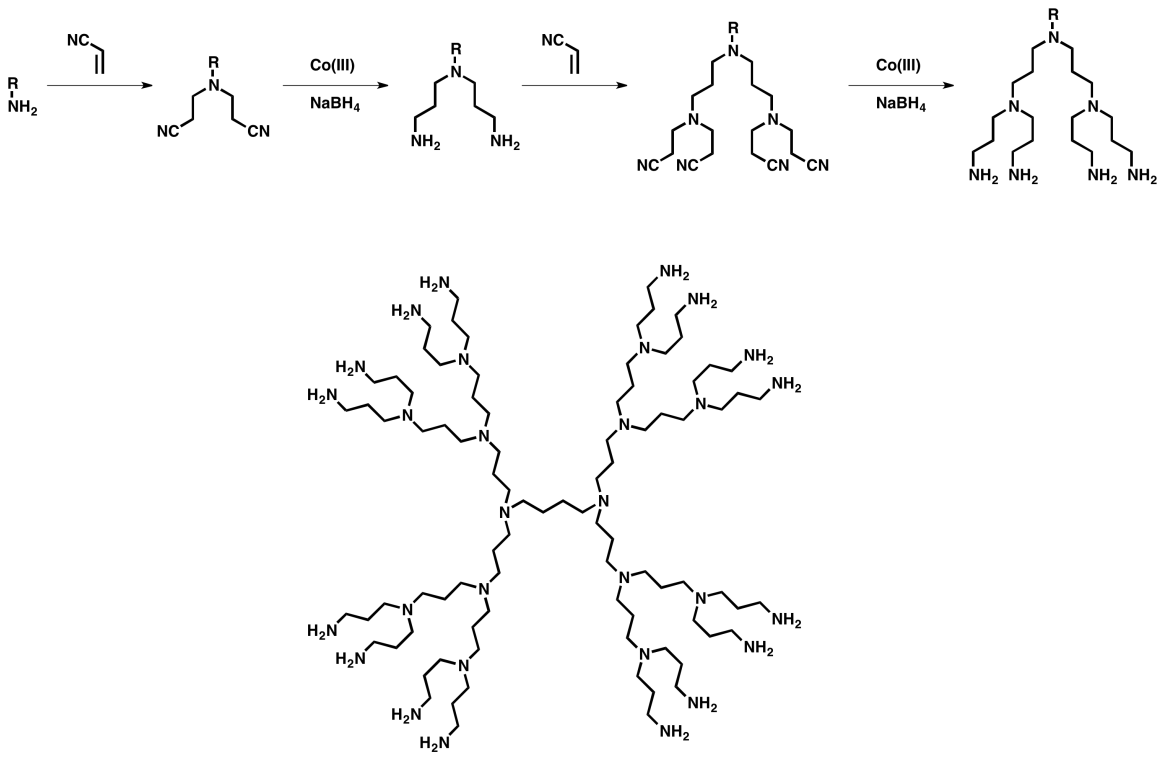

Figure 1.3. Vogtle's original synthetic approach to prepare cascade polymers (top) and structure of a third generation PPI dendrimer prepared independently by Meijer and Mulhaupt (bottom).[16-18]

The term "dendrimer" was first coined by Tomalia in 1985, when he described the synthetic protocols for preparing dendrimers up to the 7th generation using ethylene diamine as the core.[19] The elegant step-wise synthesis relied on two high yielding reactions: a Michael addition of an amine to an acrylate monomer, followed by amidation between a methyl ester and an amine (Figure 1.4). Therefore, the dendrimer is synthesized in half-generation steps, with the amine periphery corresponding to whole number generations (x.0) and the methyl ester periphery corresponding to half

generations (x.5). Remarkably, by using a large excess of diamine during the amidation step, crosslinking and intramolecular side reactions are negligible. Due to the alternating amine and amide functional groups found within the dendrimer, they are referred to as polyamidoamine (PAMAM) dendrimers. PAMAM dendrimers are produced commercially, leading to their broad availability, and are the most prevalent dendrimer within this class of materials.

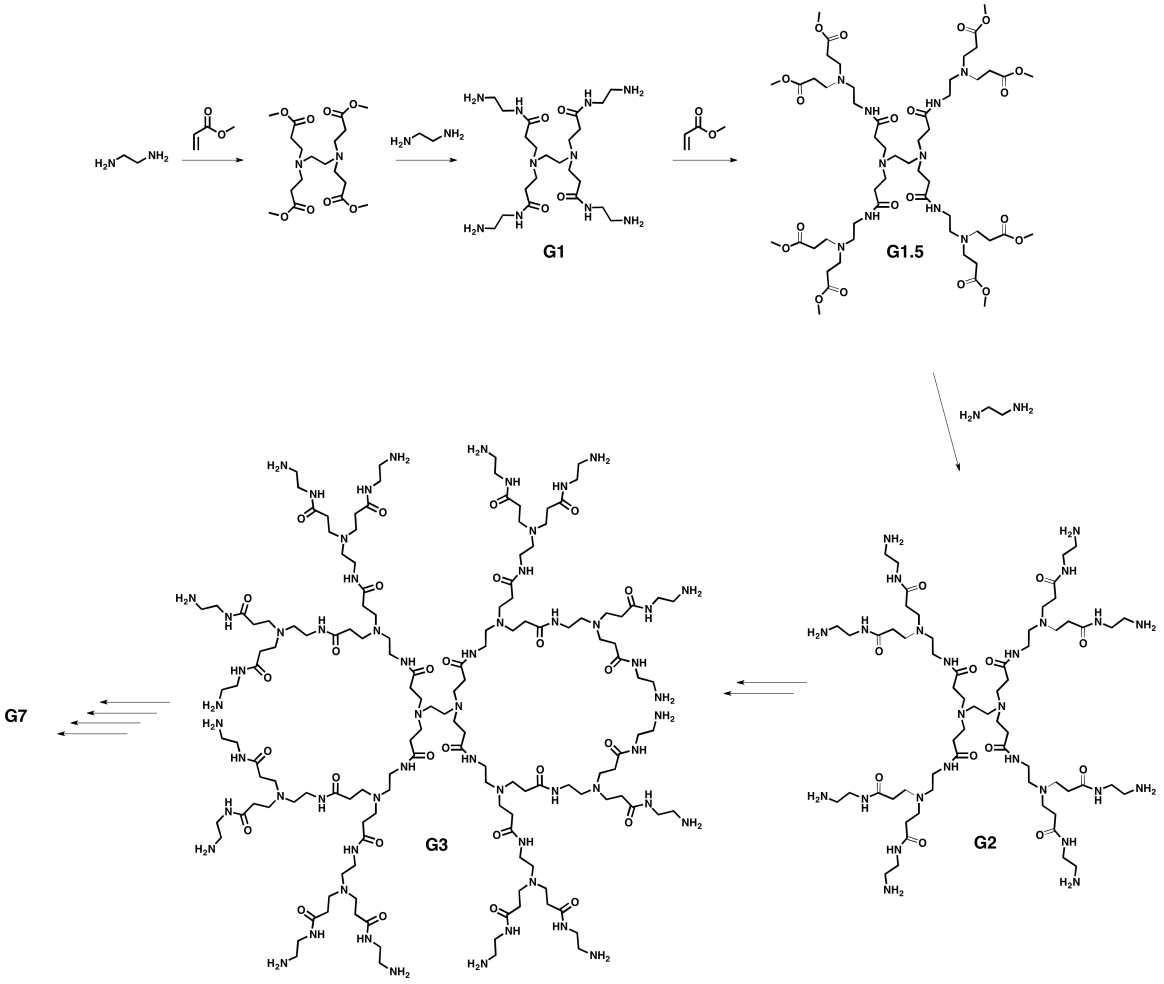

Figure 1.4. PAMAM dendrimer synthesis described by Tomalia.[19]

The synthetic strategy employed by Vogtle and Tomalia to prepare dendrimers is referred to as the divergent approach. This approach, however, relies on high yielding reactions in order to obtain complete functionalization at the periphery. To circumvent this problem, Fréchet and Hawker developed a convergent dendrimer synthesis.[20] In this approach, synthesis of the dendrimer starts with the peripheral groups and builds inwards, with coupling to the core occurring in the final step. This strategy has been credited with drastically expanding the interest in dendrimers owing to the structural control and the ability to precisely prepare and purify high generation, defect-free dendrimers that this method provides.

1.4. Dendrimer Synthesis

As described above, there are two general strategies for preparing dendrimers: divergent growth and convergent growth. While each method has advantages and disadvantages, both synthetic strategies are still used extensively to prepare different dendritic architectures.

1.4.1. Divergent Dendrimer Synthesis

The divergent synthesis of dendrimers was first employed by Vogtle[16] and is the same method that was later be used by Tomalia[19] and Newkome.[21] In this approach, the dendrimer synthesis starts at the core, with the addition of each layer of branching occurring in a stepwise manner. The reaction of the monomer with the core yields the first

generation (G1) dendrimer. Each dendrimer generation typically requires two steps: a branching step and an activation step (Figure 1.5). The branching step adds the monomeric unit and thus doubles the number of functional groups at the dendrimer periphery. The "activation" step is used to make the periphery reactive, so that another layer of branching can be added. This activation step typically involves functional group conversion (such as reducing the nitriles to amines in PPI dendrimers), addition of a non-branching reactive unit (such as ethylene diamine in PAMAM dendrimers) or removal of a protecting group.

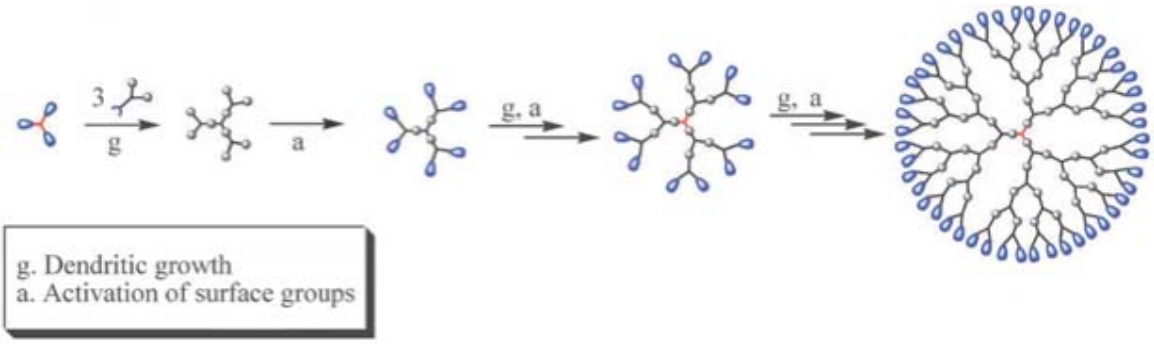

Figure 1.5. Cartoon representation of a divergent synthetic strategy. Reproduced from Ref 22 with permission of The Royal Society of Chemistry.

The divergent synthetic strategy relies on highly efficient reactions that are able to quantitatively functionalize the periphery of the dendrimer during both activation and growth steps. This is because purification of dendrimers with defects at the periphery is not viable, particularly at higher generations. Nevertheless, there are advantages that are realized by employing a divergent synthetic protocol. Purification is typically simple,

involving removal of the monomer from the product dendrimer, thus making the process amenable to commercialization.

1.4.2. Convergent Dendrimer Synthesis

A major milestone that re-invented the dendrimer field came from Fréchet and Hawker in 1990.[20] Recognizing that the synthesis of high generation, perfectly monodisperse dendrimers was limited through divergent means, an alternative synthetic strategy was proposed: start at the periphery and couple to the core in the final step. This method was aptly termed the convergent synthesis.

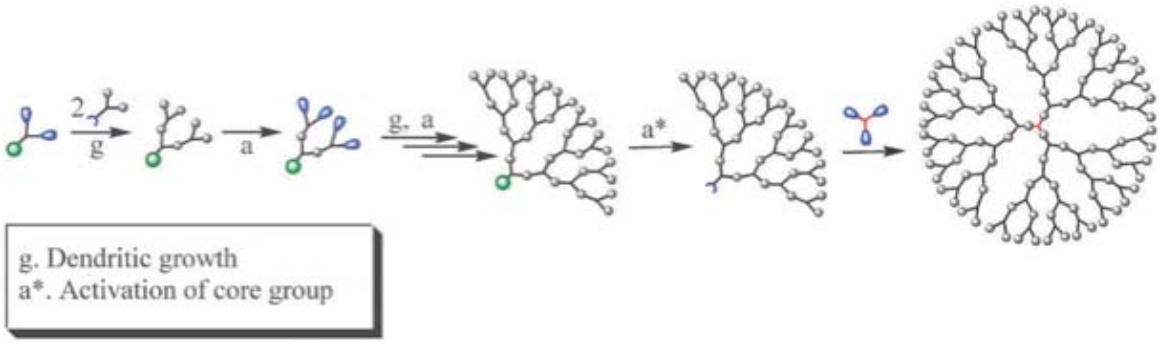

Figure 1.6. Cartoon scheme of convergent dendrimer synthesis. Reproduced from Ref 22 with permission of The Royal Society of Chemistry.

Unlike the divergent synthesis, this method did not rely on quantitative conversions at every step because the product is easily separable from partially functionalized side products. Another advantage that is conferred by this method is the

exquisite control over surface functionality.[22] Unfortunately, these advantages are realized at the expense of a more involved purification process that is required at each step, typically involving column chromatography. The purification requirement not only increases the time needed for dendrimer synthesis, but also the cost. However, the convergent strategy is still the most reliable method for obtaining high purity dendrimers and is recognized for re-igniting the interest in this class of macromolecules.

1.4.3. Accelerated Dendrimer Synthesis

The desire to prepare dendrimers in a reduced number of steps has led to many innovative strategies. For example, hypermonomer approaches (AB_x, where $x > 2$) have been used to increase the degree of branching with each generation growth.[23,24] Another approach to expedite the synthesis of high generation dendrimers is referred to double stage convergent growth.[25] This method relies on the parallel synthesis of low generation dendrons and low generation dendrimer (sometimes referred to as a hypercore). The final step consists of coupling dendrons to the hypercore, yielding a high generation dendrimer. Alternatively, a double stage exponential growth relies on functionalizing a portion of the same dendrimer material at the core and the other portion at the periphery (Figure 1.7).

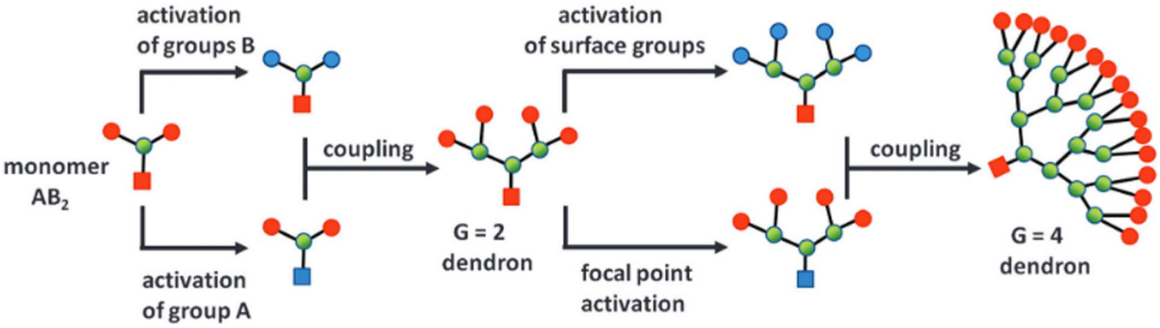

Figure 1.7. Cartoon schematic of a double stage exponential growth dendrimer synthesis. Reproduced from Ref 27 with permission of The Royal Society of Chemistry (RSC) on behalf of the European Society for Photobiology, the European Photochemistry Association and the RSC.

The accelerated synthesis of dendrimers takes advantage of two monomers with orthogonal reactivity, typically referred to as AB_2 and CD_2, in order to grow each dendrimer generation in a single synthetic step (Figure 1.8). This confers a major advantage in preparing high generation dendrimers, as the iterative two-step process of coupling followed by activation to prepare each generation of a dendrimer can be reduced to a single step.

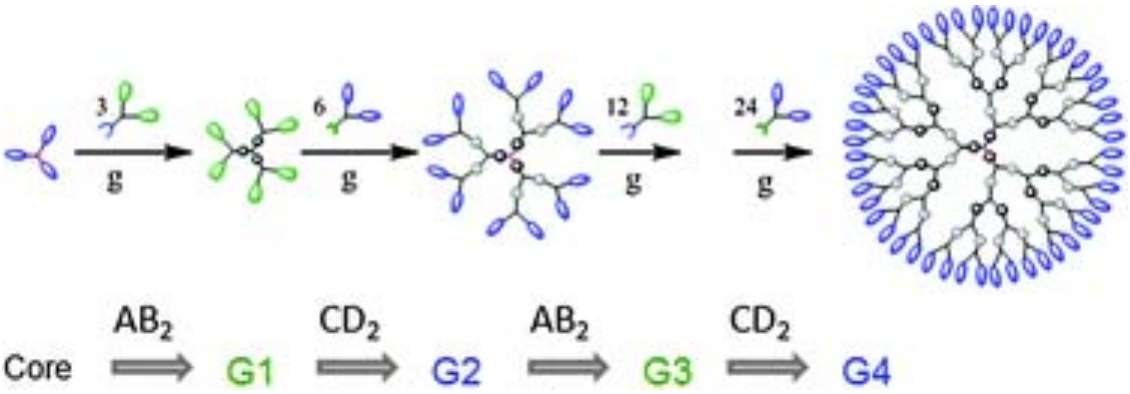

Figure 1.8. Cartoon scheme of an accelerated dendrimer synthesis using AB_2 and CD_2 monomers. Reproduced from Ref 12 with permission of The Royal Society of Chemistry.

This concept was first reported by Fréchet and Spindler, however, the limitations of their synthetic approach precluded the synthesis of high generation dendrimers.[26] The first successful accelerated dendrimer synthesis to prepare high generation dendrimers was first reported by Zimmerman, which was based on the iterative Mitsunobu esterification and Sonogashira couplings.[27] Since the pioneering work of Fréchet and Zimmerman, there have been many successful reports on the accelerated synthesis of dendrimers.[28,29] For example, an elegant "activated" monomer design enabled the preparation of a poly(benzyl ester) dendrimer in a facile manner.[30] The concept has been applied to many different dendritic scaffolds, including phosphorus based dendrimers, as reported by Majoral and co-workers.[31] With the advent of "click" chemistry,[32] Malkoch reported the accelerated synthesis of dendrimers based on the Cu(I) catalyzed alkyne azide cycloaddition (CuAAC) and etherification reactions.[33] The ability to prepare high generation dendrimers in an accelerated and timely manner was further demonstrated by

utilizing two orthogonal click reactions: CuAAC and thiol-ene click (TEC).[34] The facile and elegant monomer design, coupled with minimal purification culminated in the synthesis of a sixth generation dendrimer in a single day, starting from the two monomers.

1.5. Dendrimers for Materials Applications

Despite the many properties that are unique to dendrimers, their long synthetic protocols have limited their use in materials applications. Nevertheless, there are numerous fundamental studies and academic endeavors that have made use of dendrimers for catalysis,[35] light harvesting,[36] surfactants,[37] sensors[38] and supramolecular architectures.[39] The aforementioned examples highlight the versatility of potential applications that dendrimers possess in a broad range of sub-disciplines. Figure 1.9 illustrates the advantage of a dendritic scaffold for a) light harvesting by acting like an antenna and b) signal amplification via a self-immolative backbone. For bulk materials, hyperbranched polymers are often used in lieu of dendrimers. For example, the commercially available Boltorn™, which are polydisperse hyperbranched polymer analogues of bis-MPA dendrimers are used to enhance the mechanical properties in epoxy and polyurethane resins.[40,41]

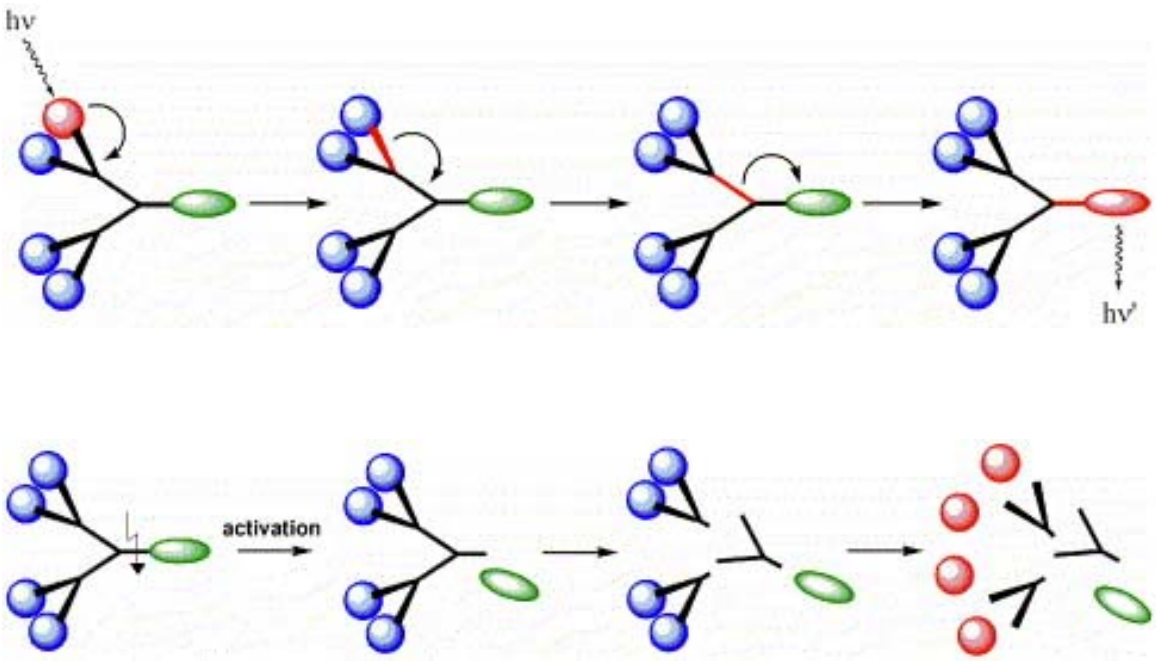

Figure 1.9. Schematic representation of a light harvesting dendrimer antenna (top) and self-immolative dendrimers used for signal amplification or drug delivery (bottom). Reprinted from Journal of Luminescence, 111, Flomenbom, O., Amir, R.J., Shabat, D., Klafter, J. Some New Aspects of Dendrimer Applications, 315-325, Copyright 2005, with permission from Elsevier.

1.6. Dendrimers for Biomedical Applications

The vast majority of research within the dendrimer community is geared toward biomedical applications. This is largely due to the fact that dendrimers are relatively more time consuming and thus expensive to prepare compared to hyperbranched polymers. This high cost is offset by the exquisite synthetic control and reproducibility that is afforded by the dendritic scaffold, two features that are particularly important when

preparing materials for biomedical applications. Nevertheless, commercial availability of PAMAM, PPI, 2,2-Bis(hydroxymethyl)propionic acid (Bis-MPA) and phosphorus containing dendrimers has allowed for their continued exploration in a variety of fields. With respect to biomedical applications, the periphery of positively charged dendrimers such as PAMAM and PPI leads to cytotoxicity problems due to cell membrane disruption. In particular, the ability for cells to transport biomolecules through the cell membrane is lost due to the interaction between the cationic dendrimer periphery and the anionic groups present on the cell surface.[42,43] To avoid the issue of cytotoxicity, peripheral modification is necessary to mask the cationic character of these dendrimers. For example, PAMAM dendrimers that have been peripherally-functionalized with PEG do not display the same cytotoxicity as unfunctionalized PAMAM dendrimers.[44] Given the variety of dendritic scaffolds that have been reported, there are just a few that have been extensively investigated for biomedical applications owing to their commercial availability, ease of synthesis, and/or ease of functionalization and biocompatibility (Figure 1.10).

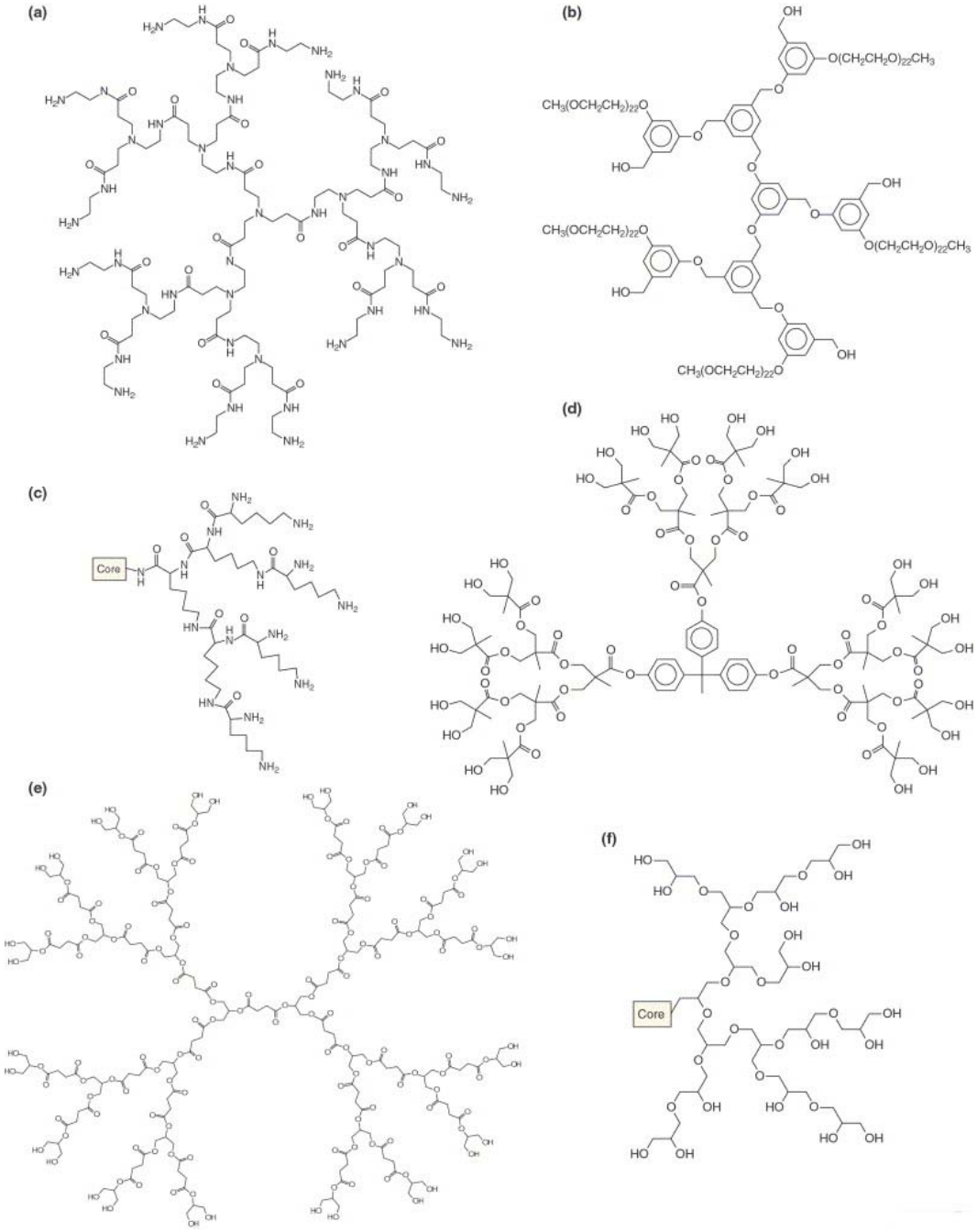

Figure 1.10. Dendrimer architectures that have been at the forefront of biomedical applications: a) PAMAM b) poly(aryl) ether c) poly(lysine) d) bis-MPA e) Poly(glycerol-

co-maleic acid) and f) poly(glycerol) ether. Reprinted from Drug Discovery Today, 10, Gillies, E., Fréchet, J.M.J. Dendrimers and Dendritic Polymers in Drug Delivery, 35-43, Copyright 2005, with permission from Elsevier.

1.6.1. Dendrimers for Drug Delivery

The purpose of drug delivery vehicles is to deliver the payload to the target while minimizing the toxic effects that chemotherapeutics are known to have on healthy tissues and organs. To accomplish this feat, drug delivery platforms need to posses a number of important features, which include facile drug loading, increased solubility and favorable pharmacokinetics, which corresponds to increased circulation times and the ability to target the site of disease.[5,45] A successful drug delivery system would be one that is able to deliver the drug to the site of disease and release it in a steady and continuous manner, without causing harmful effects to the rest of the body.

Dendrimers as drug delivery vehicles represent a highly active and constantly evolving area of research. Ever since the introduction of the "dendritic box",[13,14] dendrimers been investigated for drug delivery through host-guest interactions, supramolecular interactions and covalent functionalization. Due to their size and architecture, dendrimers typically exhibit longer circulation times *in vivo*, compared to linear polymers of the same MW, an intrinsic property that is highly desirable in drug delivery applications. Unlike linear polymers, which can chain extend and be filtered readily via the renal pores, dendrimers of the same molecular weight retain a 3-dimensional globular shape, allowing them to bypass the renal filtration system of the

kidneys, as long as they are above the hydrodynamic volume of renal filtration pores (Figure 1.11). Therefore, by controlling the degree of branching and hydrodynamic volume of the dendrimer, it is possible to tune the dendrimer circulation time *in vivo*. For example, a G1 dendrimer peripherally-functionalized with two 20 kDa PEG chains and a G3 dendrimer with eight 5 kDa PEG chains both have similar molecular weights, yet the plasma circulation half life for the G3 dendrimer was found to be 31 hours versus 1.4 hours for the G1 dendrimer.[46]

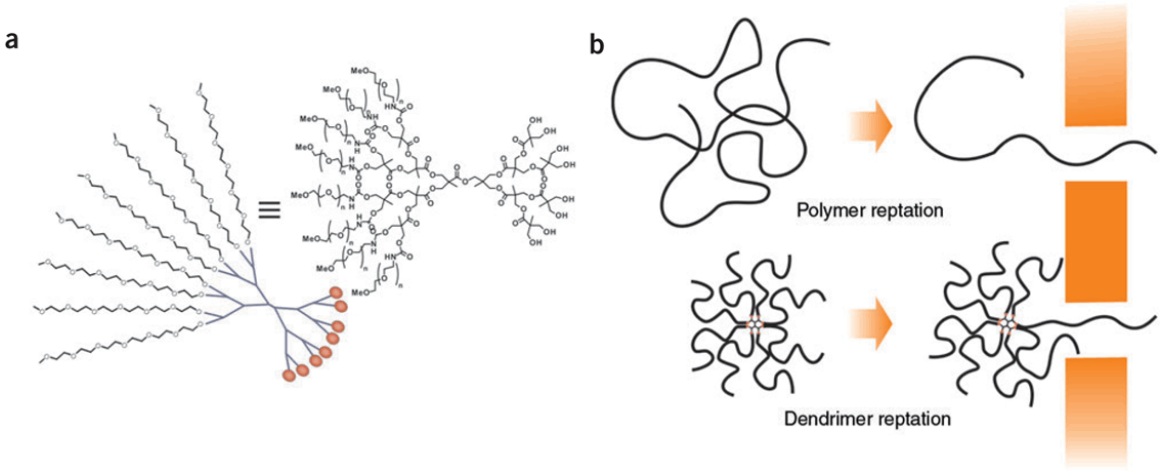

Figure 1.11. Cartoon schematic illustrating the comparative ease of kidney filtration of a linear polymer versus a dendrimer. Adapted with permission from Macmillan Publishers Ltd: Nature Biotechnology (2005, *23* (12), 1517–1526), copyright 2005.

By increasing circulation times *in vivo,* through higher generation dendrimers, it is possible to achieve passive tumour targeting due to the enhanced permeation and retention effect (EPR).[47] This phenomenon is due to rapidly formed vasculature in the

vicinity of a tumour that is highly permeable, coupled with the lack of lymphatic drainage in the area. Macromolecules can accumulate due to the leaky vasculature, yet are unable to be cleared readily. Upon reaching the tumour, drug delivery vehicles must be able to release the drug, preferably in a steady and controlled manner. This can be achieved through hydrolysable linkages or through passive diffusion. Fréchet and coworkers demonstrated the feasibility of this approach by attaching doxorubicin (DOX) to the aforementioned PEGylated dendrimers using acid labile hydrazone linkages.[48] Complete tumour regression in mice bearing C-26 colon carcinomas was observed after a single treatment of the DOX containing dendrimer. Furthermore, DOX uptake by the tumour was nine-fold higher and over ten-fold less toxic compared to freely administered DOX.

Dendrimers have also been investigated for their potential ability to act as microbicides. Vivagel®, an anionic dendrimer based on the PAMAM scaffold has been actively investigated for the prevention of human immunodeficiency virus (HIV) and sexually transmitted diseases (STDs).[49] Vivagel is also being investigated as a treatment for recurring bacterial vaginosis and is currently in phase 3 clinical trials. In addition to Vivagel®, Ocuseal® is the other commercial product that uses dendrimers for *in vivo* use.[50] The product is a PEG based hydrogel with dendritic components that is used primarily as a wound dressing after cataract surgery.

Lastly, the precise and facile incorporation of carboranes into the bis-MPA dendritic scaffold has been demonstrated by Adronov and co-workers.[51] By incorporating carboranes within the dendritic scaffold, the resulting polyhydroxylated dendrimers were found to exhibit excellent water solubility. The high boron content within the dendrimer

paves the way toward the use of this class of compounds for boron neutron capture therapy (BNCT) via irradiation of the ^{10}B atoms with thermal neutrons.

1.6.2. Dendrimers for Imaging

While a considerable effort has been made to implement dendrimers in drug delivery applications, the use of dendrimers as molecular imaging agents has led to many innovative and remarkable discoveries. Imaging agents based on dendritic scaffolds take advantage of the multivalent periphery for the attachment of imaging moieties and/or targeting vectors. Furthermore, the presence of orthogonal chemistry at the periphery and core facilitates the attachment of multiple imaging modalities, allowing for the facile preparation of targeted dual modality imaging agents.

1.6.2.1. Principles of Magnetic Resonance Imaging

Magnetic resonance (MR) imaging is a technique that takes advantage of spin active nuclei (most commonly protons) to visualize tissues. MR imaging is capable of achieving remarkable resolution and contrast, which only increases with higher magnetic field strength, enabling visualization of smaller features. These properties make MR imaging a highly useful diagnostic tool for imaging the brain, cardiovasculature and musculoskeletal tissue, as well as in the field of oncology. Additionally, contrast agents, which are typically based on gadolinium (Gd) or paramagnetic iron oxide can further aid in obtaining higher quality images.

1.6.2.1.1. Dendrimers as MRI Contrast Agents

The use of dendrimers to enhance contrast in magnetic resonance imaging (MRI) is a strategy that has been investigated in depth.[52] This strategy typically takes advantage of the multivalent periphery of dendrimers by attaching multiple Gd-DOTA complexes to decrease the relaxation time of water in the vicinity, thereby improving contrast. By using large macromolecules, the rate of diffusion of these compounds is reduced, resulting in greater relaxation time differences and improved image quality. The first account of using dendrimers for *in vivo* MRI applications involved PAMAM dendrimers that were chelated to gadolinium atoms via diethylenetriaminepentaacetic acid (DTPA).[53] The same strategy has been used with PPI dendrimers, enabling visualization of sub-millimeter tumours.[54]

1.6.2.2. Nuclear Imaging

The use of radioisotopes for imaging applications, broadly referred to as nuclear imaging, is a mainstay for modern diagnostic medicine, with 40 million procedures being carried out in hospitals each year.[55,56] This imaging modality can be further differentiated into positron emission tomography (PET) and single photon emission computed tomography (SPECT) depending on the radionuclide that is employed. This is because different radionuclides can decay using different mechanisms.

SPECT imaging detects photons that are directly emitted from the radionuclide as it decays. Some of the more commonly used SPECT radionuclides include: ^{99m}Tc, ^{123}I, ^{111}In and ^{67}Ga, which typically have longer half-lives compared to PET radionuclides.

The most utilized SPECT radionuclide in diagnostic medicine is ^{99m}Tc, accounting for 85% of nuclear scans.[55,56] ^{99m}Tc has a half-life of 6.02 hours and an emission energy of 140 keV, making it ideal for imaging applications. It is made readily available through the decay of ^{99}Mo in ^{99}Mo/^{99m}Tc generators, which enables the transport of these generators due to the longer half-life of ^{99}Mo (2.75 days).[57] Approximately 40% of the world's ^{99}Mo is produced at Canada's Chalk River reactor.[56] Additionally, production of ^{99m}Tc has been demonstrated using a cyclotron, which reduces the previously encountered supply dependence.[58–60] Further adding to the utility of ^{99m}Tc, is the accessibility of different oxidation states that this radionuclide can posses, ranging from +7 to +1. One of the most successful imaging agents based on ^{99m}Tc is sestamibi, a myocardial perfusion agent that is used to image blood flow in the heart and has shown to be advantageous compared to ^{201}Th.[61] Sestamibi has uptake in certain types of tumour tissue, underscoring the importance of this radioimaging agent in nuclear diagnostic imaging.[62]

PET isotope decay involves formation of a positron, which almost instantaneously comes into contact with an electron, resulting in positron annihilation. This, in turn, produces two gamma photons that are emitted at an angle of 180° to each other with an energy of 511 keV. Gamma detectors located in a circular array around the patient detect the simultaneous collisions of emitted photon pairs and use an algorithm to calculate their origin, thus resulting in image reconstruction. Radionuclides that are useful for PET imaging include ^{18}F, ^{11}C, ^{64}Cu and ^{89}Zr, and are typically produced by a cyclotron. By far the most widely used PET isotope is ^{18}F, owing to the wide spread use of [^{18}F]fluorideoxyglucose (^{18}FDG). FDG is a non-natural fluorinated analogue of glucose,

which is taken up in areas of high metabolism, such as tumour tissue, and is widely used in diagnostic oncology.

PET and SPECT imaging does not give any anatomical information and must be combined with another imaging modality, typically x-ray computed tomography (CT), to provide a reference for the location of the imaging agent within the body. More recently, nuclear imaging, and in particular, PET imaging is being combined with MRI, termed PET/MRI, in order to combine the sensitivity of PET imaging with the resolution of MR imaging.

1.6.2.2.1. Radiolabeled Dendrimers for Molecular Imaging Applications

The development of novel radiopharmaceuticals based on dendritic scaffolds is a rapidly growing field of research. Unlike CT images, which look at anatomical features, molecular imaging is used to look at biological processes. By visualizing biological processes that are associated with a particular type of disease, it may be possible to achieve earlier detection, while reducing the rate of false-positives or negatives. Molecular imaging of tumours is particularly appealing due to the possibility of differentiating tumours that are metastatic from those that are benign in nature based on the targeted biological processes that are occurring within.

The ability to place numerous targeting vectors and an imaging moiety on a monodisperse polymer in a site specific and selective manner makes dendrimers appealing for the development of targeted molecular imaging agents. Indeed, this strategy

continues to be utilized for imaging enzymes/receptors that are known to be overexpressed in different types of cancer.

Targeting angiogenesis, which is the growth of new blood vessels, is useful due to its association with tumour tissue.[63] This is because as the tumour grows, new vasculature is necessary to supply oxygen and nutrients for the increased metabolism required by the cancer cells. The integrin $\alpha_v\beta_{III}$ belongs to a class of receptors that are closely linked to angiogenesis and are known to be overexpressed in cancerous tissue, particularly those that are invasive in nature.[64] Targeting this integrin using the tripeptide arginine-glycine-aspartic acid (RGD) or the cyclic analogue (cRGD) is a well known strategy that has been previously employed to decorate the periphery of dendrimers.[65–68] Multimerization of RGD is an attractive strategy owing to the increased affinity that is almost universally observed. For example, synthesis of a dendrimer with sixteen RGD units at the periphery results in 125 fold increase in affinity compared to the monomeric unit.[69]

Another targeting vector that has been used in combination with dendrimers is folic acid.[70,71] The importance of the linker was demonstrated by attaching folic acid via a PEG spacer, which was found to increase tumour accumulation *in vivo*.[70] By using PAMAM dendrimers as the scaffold, the resulting folic acid targeted probes were found to be stable *in vitro* and *in vivo*.

The bis-MPA scaffold has been extensively explored for *in vivo* applications ranging from drug delivery to imaging. Previous work has shown that high generation hydrophilic bis-MPA dendrimers clear rapidly via the kidneys, presumably due to their small size, well below the renal filtration cut-off.[72] The same dendrimer backbone has

been used to target the integrin $\alpha_v\beta_{III}$, as stated above. Therefore, the biocompatible bis-MPA scaffold seems ideal to use as a backbone for the development of multivalent, targeted molecular imaging agents, which will be the focus of this thesis.

1.6.3. Competing Technologies

While the use of dendritic scaffolds is the primary focus of this thesis, it is important to briefly highlight competing technologies that exist, in order to properly assess the current work in the broader context of molecular imaging, particularly those based on multivalent scaffolds.[73–75] For example, inorganic nanoparticles have been extensively investigated as a multivalent scaffold, owing to their facile synthesis, tunable and narrow size distributions (typically sub 20 nm) and inherent optical properties which lend itself towards imaging applications via fluorescence.[76,77] Unlike many dendrimers, inorganic nanoparticles are not biodegradable and, depending on their composition, can be toxic. However, this limitation can be overcome through surface coating with a benign substance to form core/shell structures.[78]

Nanoparticles based on organic polymers have also demonstrated promising results.[79,80] Typically comprised of block copolymers, these nanoparticles are prepared via self-assembly, resulting is sizes often ranging from 40-200 nm. While primarily used as a scaffold for drug delivery,[81–83] these nanoparticles have shown to be effective for targeted molecular imaging.[84]

Lastly, liposomes have received significant attention owing to their ease of formulation and favorable pharmacokinetic properties.[85] Several liposomal formulations

have been actively investigated in the clinic, further underscoring the importance of this class of scaffolds for both drug delivery and imaging.[86] Studies have also been conducted that compare and contrast the aforementioned scaffolds, with each technology showing benefits and limitations.[87] Therefore, it is prudent to investigate all technologies in order to develop an array of effective diagnostic tools that clinicians can utilize.

1.7. Goals of the Thesis

The goal for this thesis was to implement a bis-MPA dendritic scaffold into a nuclear molecular imaging platform. It was envisioned that the dendritic imaging platform would contain an imaging moiety at the site isolated core and targeting ligands at the periphery. The attachment of multiple targeting vectors at the periphery of the dendrimer would impart multi-valency to the imaging agent, with the hope that the multi-valency would lead to enhanced binding to the target and result in a higher target:non-target ratio. The design, synthesis and radiolabeling of the dendritic imaging platform is outlined in Chapter 2. This includes the preparation of alkyne-decorated dendrimers that can be readily functionalized with targeting vectors bearing azide moieties using the CuAAC reaction. A DPA ligand was attached to the core of the dendrimer for radiolabelling with ^{99m}Tc. The metal chelate was also coordinated to Re, resulting in a precursor that could be used as a non-radioactive "cold" standard for HPLC analysis and *in vitro* assays. Chapter 2 also addresses the feasibility of transmetalation of the CuDPA ligand with ^{99m}Tc, thus overcoming a major obstacle in using the CuAAC reaction for coupling targeting vectors to the DPA ligand for subsequent imaging with ^{99m}Tc.

Chapters 3, 4 and 5 apply the dendritic scaffold towards targeting enzymes that are overexpressed in different types of cancer. In chapter 3, the synthesis, characterization, and *in vitro* evaluation of acyloxymethyl ketone (AOMK) functionalized dendrimers is reported. These AOMK functionalized dendrimers were evaluated for their affinity toward cathepsin B, an enzyme that is overexpressed in breast cancer. Subsequently, chapters 4 and 5 focus on targeting the prostate specific membrane antigen (PSMA), that is commonly overexpressed in prostate cancer. Chapter 4 describes the synthesis and *in vitro* evaluation of glu-urea-lys dipeptide functionalized dendrimers that target PSMA. The use of different linkers was shown to have an effect on binding affinity towards PSMA, particularly at the first generation. Chapter 5 describes the synthesis, radiolabeling and *in vivo* bio-distribution of a G2 PSMA targeted dendrimer having four glu-urea-lys targeting vectors at the periphery. Lastly, chapter 6 describes the synthesis, radiolabeling and plasma stability of two PSMA targeted G2 dendrimers with a more robust linkages in lieu of non-neopentyl esters. The objective of this effort is to overcome the hydrolysis of the non-neopentyl esters that was observed.

Overall, this thesis reports the synthetic protocols required for using bis-MPA dendrimers in targeted molecular imaging applications. The dendritic imaging platform is applied to two targets: cathepsin B and PSMA, with the latter demonstrating improved affinity attributed to multivalency. Lastly, an improvement in *in vitro* stability was demonstrated by replacing the peripheral non-neopentyl esters with ether linkages, paving the ground work for future efforts in utilizing the bis-MPA scaffold for *in vivo* applications.

1.8. References

(1) Andrady, A. L.; Neal, M. A. *Philos. Trans. R. Soc. Lond. B. Biol. Sci.* **2009**, *364* (1526), 1977–1984.

(2) Plunkett, R. J. Tetrafluoroethylene Polymers. US Patent 2,230,654, 1941.

(3) Kwoleck, S. L. Wholly Aromatic Carbocyclic Polycarbonamide Fiber Having Orientation Angle of Less Than About 45 degrees. US Patent 3,819,587, 1974.

(4) Acharya, G.; Park, K. *Adv. Drug Deliv. Rev.* **2006**, *58* (3), 387–401.

(5) Langer, R. *Nature* **1998**, *392*, 5–10.

(6) Kataoka, K.; Harada, a; Nagasaki, Y. *Adv. Drug Deliv. Rev.* **2001**, *47* (1), 113–131.

(7) Gillies, E. R.; Fréchet, J. M. J. *Drug Discov. Today* **2005**, *10* (1), 35–43.

(8) Langer, R.; Vacanti, J. P. *Science.* **1993**, *260* (5110), 920–926.

(9) Lee, Y. L.; Mooney, D. J. *Chem. Rev.* **2001**, *101* (7), 1869–1879.

(10) Lutolf, M. P.; Hubbell, J. A. *Nat. Biotechnol.* **2005**, *23* (1), 47–55.

(11) Hawker, C. J.; Malmstrom, E. E.; Frank, C. W.; Kampf, J. P. *J. Am. Chem. Soc.* **1997**, *119* (41), 9903–9904.

(12) Walter, M. V; Malkoch, M. *Chem. Soc. Rev.* **2012**, *41* (13), 4593–4609.

(13) Jansen, J. F.; de Brabander-van den Berg, E. M.; Meijer, E. W. *Science* **1994**, *266* (5188), 1226–1229.

(14) Jansen, J.F.G.A., Meijer, E.W., De Brabander-van Den Berg, E. M. M. *J. Am. Chem. Soc.* **1995**, *117*, 4417–4418.

(15) Flory, P. J. *J. Am. Chem. Soc.* **1952**, *74* (1932), 2718–2723.

(16) Buhleier, E.; Wehner, W.; Vogtle, F. *Synthesis (Stuttg).* **1978**, *2*, 155–158.

(17) Berg, E. M. M. D. B. Den; Meijer, E. W. *Angew. Chemie Int. Ed.* **1993**, *32* (9), 1308–1311.

(18) Wörner, C.; Mülhaupt, R. *Angew. Chemie Int. Ed.* **1993**, *32* (9), 1306–1308.

(19) Tomalia, D. A.; Baker, H.; Dewald, J.; Hall, M.; Kallos, G.; Roeck, M. J.; Ryder, J.; Smith, P. *Polym. Chem.* **1985**, *17* (1), 117–132.

(20) Hawker, C. J.; Frechet, J. M. J. *J. Am. Chem. Soc.* **1990**, *112* (21), 7638–7647.

(21) Newkome, G. R.; Yao, Z.; Baker, G. R.; Gupta, V. K. *J. Org. Chem.* **1985**, No. 50, 2004–2006.

(22) Hawker, C. J.; Frechet, J. M. J. *Macromolecules* **1990**, *23* (21), 4726–4729.

(23) Wooley, K. L.; Hawker, C. J.; Frechet, J. M. J. *Angew. Chem. Int. Ed.* **1994**, *33* (1), 82–85.

(24) Gilat, S. L.; Adronov, A.; Fréchet, J. M. J. *Angew. Chem. Int. Ed.* **1999**, *38* (10), 1422–1427.

(25) Wooley, K. L.; Hawker, C. J.; Frechet, J. M. J. *J. Am. Chem. Soc.* **1991**, *113* (11), 4252–4261.

(26) Spindler, R.; Fréchet, J. M. J. *J. Chem. Soc. Perkin Trans.* **1993**, No. 8, 913.

(27) Zeng, F.; Zimmerman, S. C. *J. Am. Chem. Soc.* **1996**, *118*, 5326–5327.

(28) Grayson, S. M.; Fréchet, J. M. J. *Chem. Rev.* **2001**, *101* (12), 3819–3867.

(29) Walter, M. V; Malkoch, M. *Chem. Soc. Rev.* **2012**, *41* (13).

(30) Freeman, A. W.; Fréchet, J. M. J. *Org. Lett.* **1999**, *1* (4), 685–688.

(31) Maraval, V.; Laurent, R.; Marchand, P.; Caminade, A. M.; Majoral, J. P. *J.*

Organomet. Chem. **2005**, *690* (10), 2458–2471.

(32) Kolb, H. C.; Finn, M. G.; Sharpless, K. B. *Angew. Chemie Int. Ed.* **2001**, *40*, 2004–2021.

(33) Antoni, P.; Nyström, D.; Hawker, C. J.; Hult, A.; Malkoch, M. *Chem. Commun.* **2007**, No. 22, 2249–2251.

(34) Antoni, P.; Robb, M. J.; Campos, L.; Montanez, M.; Hult, A.; Malmström, E.; Malkoch, M.; Hawker, C. J. *Macromolecules* **2010**, *43* (16), 6625–6631.

(35) Reek, J. N. H.; Arévalo, S.; van Heerbeek, R.; Kamer, P. C. J.; van Leeuwen, P. W. N. M. *Adv. Catal.* **2006**, *49*, 71–151.

(36) Adronov, A.; Fréchet, J. M. J. *Chem. Commun.* **2000**, No. 18, 1701–1710.

(37) Cooper, A. I.; Londono, J. D.; Wignall, G.; McClain, J. B.; Samulski, E. T.; Lin, J. S.; Dobrynin, A.; Rubinstein, M.; Burke, A. L. C.; Frechet, J. M. J.; DeSimone, J. M. *Nature* **1997**, *389* (6649), 368–371.

(38) Balzani, V.; Ceroni, P.; Gestermann, S.; Kauffmann, C.; Gorka, M.; Vögtle, F. *Chem. Commun.* **2000**, No. 10, 853–854.

(39) Leung, K. C.-F.; Lau, K.-N. *Polym. Chem.* **2010**, *1* (7), 988.

(40) Yang, J. P.; Chen, Z. K.; Yang, G.; Fu, S. Y.; Ye, L. *Polymer.* **2008**, *49* (13-14), 3168–3175.

(41) Asif, A.; Shi, W.; Shen, X.; Nie, K. *Polymer.* **2005**, *46* (24), 11066–11078.

(42) Zhang, Z. Y.; Smith, B. D. *Bioconjug. Chem.* **2000**, *11* (6), 805–814.

(43) Malik, N.; Wiwattanapatapee, R.; Klopsch, R.; Lorenz, K.; Frey, H.; Weener, J. W.; Meijer, E. W.; Paulus, W.; Duncan, R. *J. Control. Release* **2000**, *65* (1-2),

133–148.

(44) Jevprasesphant, R.; Penny, J.; Jalal, R.; Attwood, D.; McKeown, N. B.; D'Emanuele, A. *Int. J. Pharm.* **2003**, *252* (1-2), 263–266.

(45) Lee, C. C.; MacKay, J. a; Fréchet, J. M. J.; Szoka, F. C. *Nat. Biotechnol.* **2005**, *23* (12), 1517–1526.

(46) Gillies, E. R.; Dy, E.; Fréchet, J. M. J.; Szoka, F. C. *Mol. Pharm.* **2005**, *2* (2), 129–138.

(47) Matsumura, Y.; Maeda, H. *Cancer Res.* **1986**, *46*, 6387–6392.

(48) Dy, E. E.; Lee, C. C.; Gillies, E. R.; Fox, M. E.; Guillaudeu, S. J.; Fréchet, J. M. J.; Szoka, F. C. **2006**, *103* (45).

(49) McCarthy, T. D.; Karellas, P.; Henderson, S. A; Giannis, M.; O'Keefe, D. F.; Heery, G.; Paull, J. R. A; Matthews, B. R.; Holan, G. *Mol. Pharm.* **2005**, *2* (4), 312–318.

(50) Uy, H. S.; Kenyon, K. R. *J. Cataract Refract. Surg.* **2013**, *39* (11), 1668–1674.

(51) Parrott, M. C.; Marchington, E. B.; Valliant, J. F.; Adronov, A. *J. Am. Chem. Soc.* **2005**, *127* (34), 12081–12089.

(52) Tang, J.; Sheng, Y.; Hu, H.; Shen, Y. *Prog. Polym. Sci.* **2013**, *38* (3-4), 462–502.

(53) Wiener, E.; Brechbiel, M. W.; Brothers, H.; Magin, R. L.; Gansow, O. A.; Tomalia, D. A.; Lauterbur, P. C. *Magn. Reson. Med.* **1994**, *31* (1), 1–8.

(54) Kobayashi, H.; Saga, T.; Kawamoto, S.; Sato, N.; Hiraga, a.; Ishimori, T.; Konishi, J.; Togashi, K.; Brechbiel, M. W. *Cancer Res.* **2001**, *61* (13), 4966–4970.

(55) Eckelman, W. C. *JACC Cardiovasc. Imaging* **2009**, *2* (3), 364–368.

(56) Einstein, A. J. *JACC Cardiovasc. Imaging* **2009**, *2* (3), 369–371.

(57) Boyd, R. E. *Radiochim. Acta* **1987**, *41* (2-3), 59–63.

(58) Guerin, B.; Tremblay, S.; Rodrigue, S.; Rousseau, J. A.; Dumulon-Perreault, V.; Lecomte, R.; van Lier, J. E.; Zyuzin, A.; van Lier, E. J. *J. Nucl. Med.* **2010**, *51* (4), 13–17.

(59) Bénard, F.; Buckley, K. R.; Ruth, T. J.; Zeisler, S. K.; Klug, J.; Hanemaayer, V.; Vuckovic, M.; Hou, X.; Celler, A.; Appiah, J.-P.; Valliant, J.; Kovacs, M. S.; Schaffer, P. *J. Nucl. Med.* **2014**, *55* (6), 1017–1022.

(60) Beaver, J. E.; Hupf, H. B. *J. Nucl. Med.* **1971**, *12* (11), 739–741.

(61) Wackers, F. J.; Berman, D. S.; Maddahi, J.; Watson, D. D.; Beller, G. A.; Strauss, H. W.; Boucher, C. A.; Picard, M.; Holman, B. L.; Fridrich, R. *J. Nucl. Med.* **1989**, *30* (3), 301–311.

(62) Coover, L. R.; Caravaglia, G.; Kuhn, P. **2004**, 553–558.

(63) Carmeliet, P.; Jain, R. K. *Nature* **2000**, *407*, 249–257.

(64) Liapis, H.; Flath, A.; Kitazawa, S. *Diagnostic Molecular Pathology*, 1996, *5*, 127–135.

(65) Thumshirn, G.; Hersel, U.; Goodman, S. L.; Kessler, H. *Chem. - A Eur. J.* **2003**, *9* (12), 2717–2725.

(66) Wu, Y.; Zhang, X.; Xiong, Z.; Cheng, Z.; Fisher, D. R.; Liu, S.; Gambhir, S. S.; Chen, X. *J. Nucl. Med.* **2005**, *46* (10), 1707–1718.

(67) Li, Z.-B.; Cai, W.; Cao, Q.; Chen, K.; Wu, Z.; He, L.; Chen, X. *J. Nucl. Med.* **2007**, *48* (7), 1162–1171.

(68) Almutairi, A.; Rossin, R.; Shokeen, M.; Hagooly, A.; Ananth, A.; Capoccia, B.; Guillaudeu, S.; Abendschein, D.; Anderson, C. J.; Welch, M. J.; Fréchet, J. M. J. *Proc. Natl. Acad. Sci. U. S. A.* **2009**, *106* (3), 685–690.

(69) Wängler, C.; Maschauer, S.; Prante, O.; Schäfer, M.; Schirrmacher, R.; Bartenstein, P.; Eisenhut, M.; Wängler, B. *ChemBioChem* **2010**, *11* (15), 2168–2181.

(70) Zhang, Y.; Sun, Y.; Xu, X.; Zhang, X.; Zhu, H.; Huang, L.; Qi, Y.; Shen, Y. M. *J. Med. Chem.* **2010**, *53* (8), 3262–3272.

(71) Zhang, Y.; Sun, Y.; Xu, X.; Zhu, H.; Huang, L.; Zhang, X.; Qi, Y.; Shen, Y. M. *Bioorganic Med. Chem. Lett.* **2010**, *20* (3), 927–931.

(72) Parrott, M. C.; Benhabbour, S. R.; Saab, C.; Lemon, J. A.; Parker, S.; Valliant, J. F.; Adronov, A. *J. Am. Chem. Soc.* **2009**, *131* (21), 2906–2916.

(73) Boase, N. R. B.; Blakey, I.; Thurecht, K. J. *Polym. Chem.* **2012**, *3* (6), 1384.

(74) Xie, J.; Lee, S.; Chen, X. *Adv. Drug Deliv. Rev.* **2010**, *62* (11), 1064–1079.

(75) Lim, E.; Kim, T.; Paik, S.; Haam, S.; Huh, Y.; Lee, K. **2012**.

(76) Swierczewska, M.; Lee, S.; Chen, X. *Mol. Imaging* **2011**, *10* (1), 3–16.

(77) Weissleder, R.; Kelly, K.; Sun, E. Y.; Shtatland, T.; Josephson, L. *Nat. Biotechnol.* **2005**, *23* (11), 1418–1423.

(78) Kirchner, C.; Liedl, T.; Kudera, S.; Pellegrino, T.; Gaub, H. E.; Sto, S.; Fertig, N.; Parak, W. J. *Nano* **2005**, *5*, 331–338.

(79) Movassaghian, S.; Merkel, O. M.; Torchilin, V. P. *Wiley Interdiscip. Rev. Nanomedicine Nanobiotechnology* **2015**, *7* (5), 691–707.

(80) Oerlemans, C.; Bult, W.; Bos, M.; Storm, G.; Nijsen, J. F. W.; Hennink, W. E. *Pharm. Res.* **2010**, *27* (12), 2569–2589.

(81) Byrne, J. D.; Betancourt, T.; Brannon-Peppas, L. *Adv. Drug Deliv. Rev.* **2008**, *60* (15), 1615–1626.

(82) McNeil, S. E. *Wiley Interdiscip. Rev. Nanomed. Nanobiotechnol.* **2009**, *1* (3), 264–271.

(83) Tyler, B.; Gullotti, D.; Mangraviti, A.; Utsuki, T.; Brem, H. *Adv. Drug Deliv. Rev.* **2016**.

(84) Shokeen, M.; Pressly, E. D.; Hagooly, A.; Zheleznyak, A.; Ramos, N.; Fiamengo, A. L.; Welch, M. J.; Hawker, C. J.; Anderson, C. J. *ACS Nano* **2011**, *5* (2), 738–747.

(85) Boerman, O. C.; Laverman, P.; Oyen, W. J. G.; Corstens, F. H. M.; Storm, G. *Prog. Lipid Res.* **2000**, *39* (5), 461–475.

(86) Petersen, A. L.; Hansen, A. E.; Gabizon, A.; Andresen, T. L. *Adv. Drug Deliv. Rev.* **2012**, *64* (13), 1417–1435.

(87) Saad, M.; Garbuzenko, O. B.; Ber, E.; Chandna, P.; Khandare, J. J.; Pozharov, V. P.; Minko, T. *J. Control. Release* **2008**, *130* (2), 107–114.

Chapter 2 – Synthesis, Peripheral Functionalization and Radiolabelling of Alkyne Dendrimers Based on the Bis-MPA Dendrimer Scaffold.

**The contents of this chapter is part of the following manuscript:*

Sadowski, L. P., Edem, P. E., Valliant, J. F. and Adronov, A. (2016), Synthesis of Polyester Dendritic Scaffolds for Biomedical Applications. Macromol. Biosci.. doi: 10.1002/mabi.201600154.

All work presented in this chapter was carried out by Lukas Sadowski.

Abstract

To enable facile and mild functionalization of the periphery of G1-G3 bis-MPA dendrimers, the peripheral alcohols were functionalized with the anhydride of 4-pentynoic acid. The subsequent alkyne dendrimers were decorated with triethylene glycol monomethyl ether (TEG) as a model compound using Cu(I) catalyzed alkyne-azide cycloaddition (CuAAC). Removal of Cu(II) from the DPA ligand was successfully accomplished on G1 and G2 functionalized dendrimers. A transmetalation procedure was developed to enable radiolabeling of the G3 dendrimer. The methodology developed herein paves the way for utilizing bis-MPA dendrimers as targeted molecular imaging agents and as a theranostic scaffold.

2.1. Introduction

In order to develop high affinity MI agents, we were interested in taking advantage of multi-valent binding. Dendrimers present themselves as ideal scaffolds for the precise attachment of multiple targeting ligands to an imaging moiety, owing to their precise synthetic control and well-defined structure.[1–3] Although dendrimers have been exploited for numerous biomedical applications,[3,4] dendrimers remain predominantly utilized as a delivery vehicle for drugs[5] and gene transfection.[6] With regards to molecular imaging, the attachment of Gd-DOTA to the periphery of dendrimers has been successfully shown to increase relaxation time and enhance contrast in MRI.[7] With respect to targeted molecular imaging, the attachment of multiple targeting ligands to an imaging moiety confers several potential advantages over their monomeric counterparts, which may include increased affinity towards the target and improved circulation times. In particular, commercially available bis-MPA dendrimers are ideally suited for biomedical applications due to their intrinsic properties that include biocompatibility, hydrophilicity, quick clearance *in vivo* and no undesirable non-specific binding.[8–10] In fact, bis-MPA dendrimers have already been employed for a number of biomedical applications. A bis-MPA dendritic scaffold has been shown *in vivo* to serve as an efficient drug delivery vehicle for doxorubicin.[11] Not only did the dendritic scaffold prove to be an effective means of delivering a chemotherapeutic to the site of disease, a reduced toxicity was observed owing to the covalent attachment of the drug to the scaffold and slow release at the target site. The same dendritic backbone has also been used in the preparation of a nuclear molecular imaging probe used to visualize angiogenesis. This

was performed via the attachment of multiple RGD units to the dendrimer periphery via a PEG spacer.[12] The resulting probe exhibited a 50 fold improvement in affinity to the $\alpha_v\beta_3$ receptors compared to a single RGD unit, displayed increased clearance from non-target tissue, while radiolabeling with ^{76}Br at the core afforded a reduced rate of dehalogenation.

To date, there exist limited examples of well-defined multi-valent radioimaging platforms.[13] Herein, we present a dendritic platform for applications in targeted molecular imaging and therapy.

2.2. Results and Discussion

2.2.1. Functionalization of the Dendrimer Periphery and Activation of the Core

PMPA dendrimers bearing a metal chelate at the core and alkyne moieties at the periphery were employed as a multivalent platform for the attachment of targeting ligands using the CuAAC reaction. The alkyne dendrimers were prepared starting from a para-toluenesulfonylethanol (pTSe) core via divergent synthesis to obtain hydroxyl terminated dendrimers of generation 1 – 3 (**1**, **4** and **7**, Scheme 2.1).[10] The pTSe core serves as a convenient protecting group that is stable to standard dendrimer growth conditions yet is readily removed under moderately basic conditions. The alcohol periphery was functionalized with the anhydride of 4-pentynoic acid to yield the alkyne-decorated dendrons (**2**, **5**, and **8**) in excellent yields under standard dendrimer growth conditions (Scheme 2.1).[14,15] The resulting alkyne-decorated dendrons were subsequently deprotected at the core using DBU, a non-nucleophilic base, liberating a carboxylic acid

functional group (Figure 2.1). The core carboxylic acid of G1, G2, and G3 dendrimers (**3**, **6** and **9**, respectively) can be readily functionalized with an imaging moiety, while the alkyne periphery serves as a site for the attachment of targeting ligands.

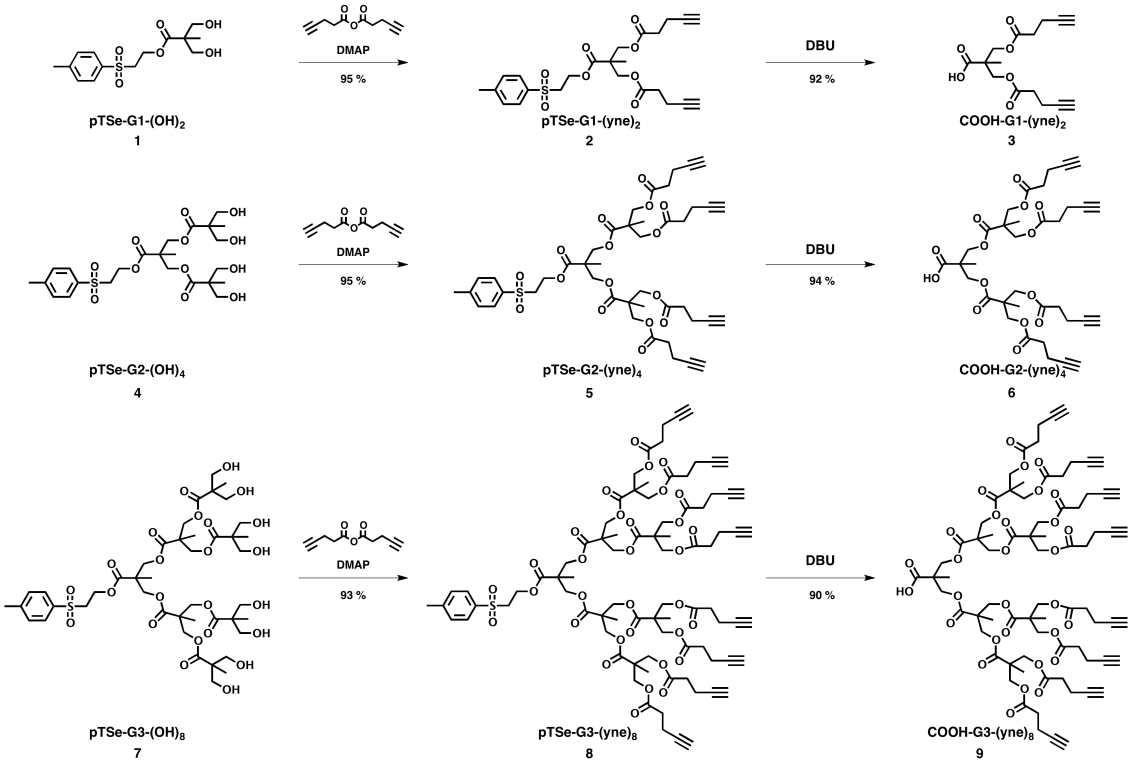

Scheme 2.1. Synthesis of alkyne-decorated dendrons G1-G3.

2.2.2. Functionalization of the Dendrimer Core with a Dipicolylamine (DPA) Metal Chelate

Radiolabeling of the dendritic structures requires the attachment of a dipicolylamine (DPA) metal chelate to the core of the dendrimer, which allows for chelation of ^{99m}Tc. Conversely, the ligand can be metalated with Re, a non-radioactive analogue of ^{99m}Tc, to prepare "cold" standards. Starting with mono-Boc protected 1,4-diaminobutane (**10**),[16] reductive amination with 2-pyridinecarbaldehyde produced the DPA metal chelate **11** (Scheme 2.2). Subsequent removal of the tert-butoxycarbonyl (^{t}Boc) group produced the free amine **12**, which was reacted with the anhydride of pentynoic acid to form the model compound bearing a single alkyne moiety **13**. This model compound was rheniated to produce **14** in near quantitative yield via reaction with $[Re(CO)_3(H_2O)_3]Br$. Introduction of **12** at the core of the G1, G2, and G3 dendrons was accomplished by first forming the succinimidyl esters (**15**, **18**, and **21**), followed by amidation with **12** to yield the ligand-functionalized dendrons **16**, **19**, and **22** (Scheme 2.2). Metalation of the DPA ligand with Re was again accomplished by refluxing with $[Re(CO)_3(H_2O)_3]Br$ in a mixture of acetonitrile/water.[17] This step was monitored by ^{1}H NMR spectroscopy, which showed a distinct signal for the aromatic protons, as well as the disappearance of the methylene (CH_2) singlet adjacent to the aromatic ring at 3.80 (4H) ppm (Figure 2.1). The two doublets at 4.62 (2H) and 5.91 (2H) ppm arise from the methylene bridge protons, which are distinct because of the locked conformation that forms upon chelation to rhenium. Owing to the challenges of preparing and working with

radioactive compounds, the non-radioactive Re analogues were utilized for *in vitro* assays and as HPLC reference standards.

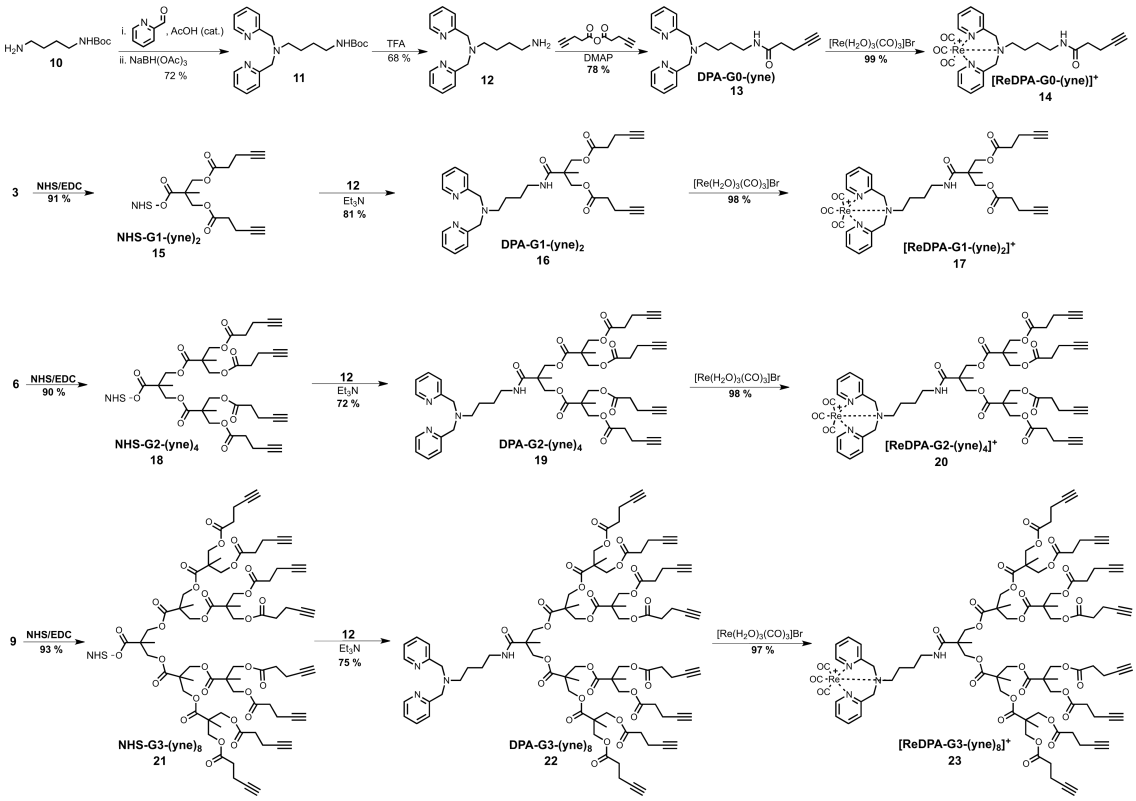

Scheme 2.2. Synthesis of rheniated, alkyne terminated G1-G3 dendrimers and the G0 model compound.

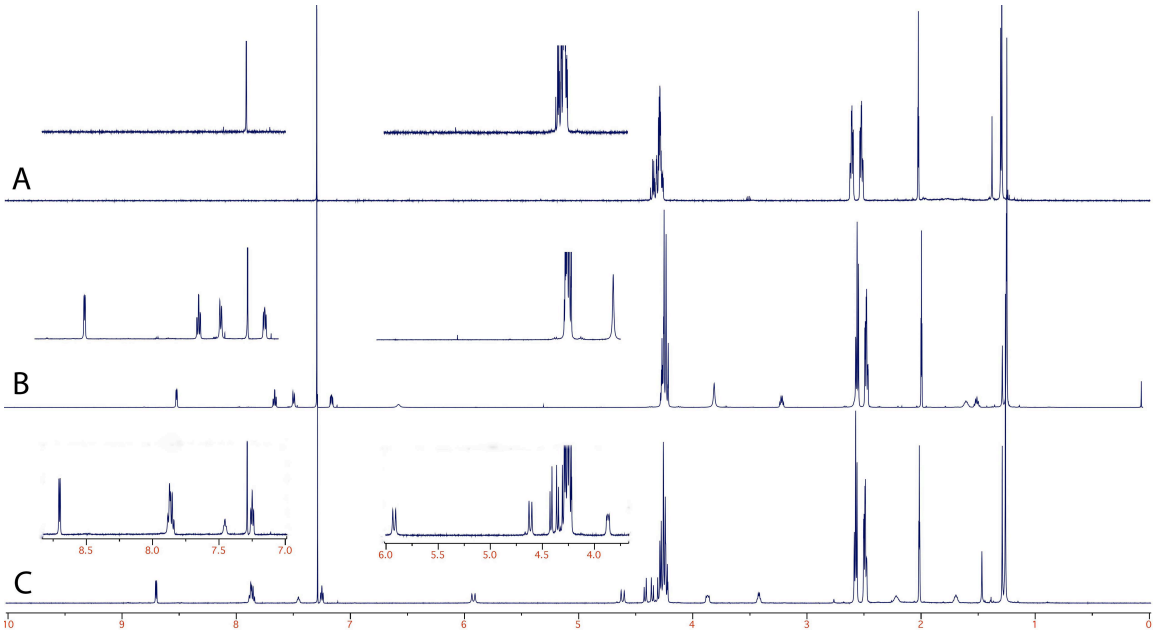

Figure 2.1. ^{1}H-NMR spectra of COOH-G3-(yne)$_8$ (A), DPA-G3-(yne)$_8$ (B), ReDPA-G3-(yne)$_8$ (C) in $CDCl_3$.

The alkyne decorated dendrons bearing the DPA ligand at the core represent a modular multivalent platform that enables efficient attachment of targeting ligands for the preparation of SPECT molecular imaging agents using CuAAC chemistry. The mild CuAAC reaction conditions are particularly amenable to the attachment of targeting ligands that are acid/base sensitive or prone to epimerization. Compounds **14**, **17**, **20**, and **23** serve as monomeric, dimeric, tetrameric, and octameric scaffolds, respectively, for the preparation of non-radioactive analogues of technetium based molecular imaging agents. Upon attachment of targeting ligands to the periphery, the rhenium analogues enable *in vitro* investigation of the effect of multi-valency on the affinity for a specific target.

2.2.3. Conjugation of Model Compound and Subsequent Removal of Cu from the DPA Ligand

To assess the feasibility of coupling multiple ligands to the dendrimer periphery, we chose to use the azide functionalized triethylene glycol monomethyl ether (TEG-N_3) as a model compound, which was readily prepared according to a modified literature procedure.[18] The CuAAC reaction was carried out between our alkyne-terminated structures and the TEG-N_3. Unfortunately, catalytic amounts of copper in the "click" reaction yielded only partially functionalized dendrimers. We hypothesized that the poor results with CuAAC may have been due to copper chelation by the DPA ligand, causing inactivation of the catalyst.[19] When copper was added in excess of stoichiometric amounts (relative to the dendrimer), complete TEGylation of the dendrimer periphery was possible, albeit in lower than expected yields (Scheme 2.3).[20] Analysis of the click coupling reaction mixture by LC-MS confirmed that Cu was quantitatively chelated to the DPA ligand. Removal of the bound copper was possible in a buffered solution of sodium sulfide (Scheme 2.3), as has previously been demonstrated in the case of Cu chelation by DOTA.[20,21] Addition of Na_2S resulted in immediate precipitation of CuS, affording the free base DPA ligand. However, this Cu removal method was noticeably less efficient with each increase in generation, likely because this process leads to the production of base (SH^-), which causes degradation of the polyester dendrimer backbone. For G2, the isolated yield of the free-base dendrimer was ~40%, and at the third generation the free base product could not be isolated. Other reagents commonly used for copper chelation, including cuprisorb, chelex, and ethylenediaminetetraacetic acid (EDTA), were found to

be ineffective in removing copper from the DPA ligand even with the first-generation structure.

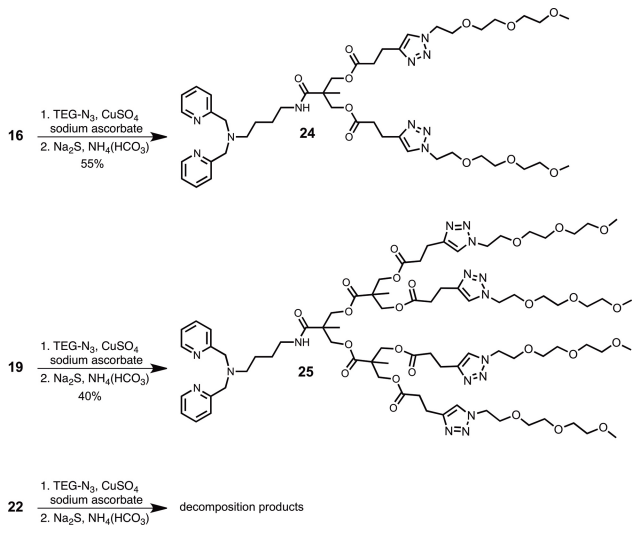

Scheme 2.3. Peripheral TEGylation by CuAAC of structures bearing a free base DPA ligand at the core.

In accord with these results, the CuAAC chemistry proceeded efficiently with the series of corresponding rheniated dendrimers (**17**, **20**, and **23**), even when using catalytic quantities of copper (supporting information, Scheme S2.1). TEGylation of all three rheniated dendrimer generations was accomplished in reasonable yield (64-71%) after preparative HPLC. Characterization of the crude reaction mixtures indicated that complete functionalization of the peripheral alkynes was achieved in each case.

2.2.4. Radiolabeling of Dendrimers with ^{99m}Tc

After obtaining the DPA-G1-(TEG)$_2$ (**24**) and DPA-G2-(TEG)$_4$ (**25**) dendrimers, we proceeded to investigate the radiolabeling of these compounds. Using [^{99m}Tc(CO)$_3$(OH$_2$)$_3$]$^+$,[22] we observed quantitative complexation to ^{99m}Tc by the dendrimer after 5 min of microwave irradiation at 80 °C in a saline solution at pH 4-5 (Scheme 2.4). A 2,2'-bipyridine challenge to determine if any ^{99m}Tc was loosely bound to the dendrimer structures resulted in no radiolabeled 2,2'-bipyridine, indicating quantitative uptake by the DPA ligand to form the stable technetium tricarbonyl complex. Thus, the presence of multiple triazole moieties in the dendritic scaffold does not affect the radiolabeling efficiency of the DPA ligand at the core. Furthermore, the HPLC retention time of [TcDPA-G1-(TEG)$_2$]$^+$ and [TcDPA-G2-(TEG)$_4$]$^+$, monitored using a gamma detector, was in agreement with the retention time of the rhenium analogues, monitored with a UV-Vis detector (Figure 2.2).

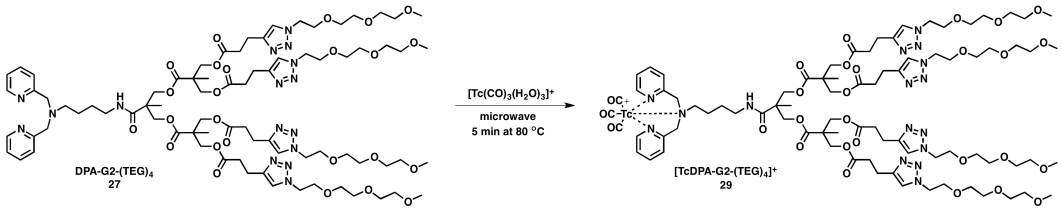

Scheme 2.4. Radiolabeling of DPA-G2-(TEG)$_4$ with ^{99m}Tc.

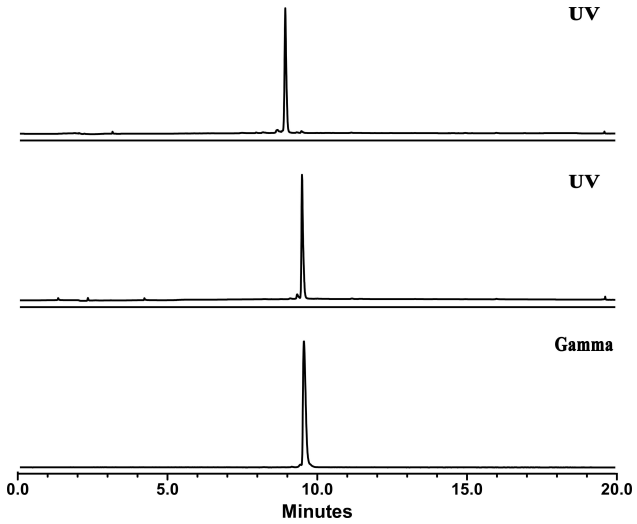

Figure 2.2. HPLC trace of DPA-G2-$(TEG)_4$ (top), $[ReDPA\text{-}G2\text{-}(TEG)_4]^+$ (middle) and $[TcDPA\text{-}G2\text{-}(TEG)_4]^+$ (bottom).

2.2.5. Transmetallation of the CuDPA complex with ^{99m}Tc

In order to produce the radiolabeled third-generation dendrimer, an alternative strategy involving transmetalation was investigated to determine if technetium can displace the chelated copper within the DPA metal chelate of **Cu-27** (Scheme 2.5). The transmetallation reaction has previously been reported with a similar DPA ligand in a "click then chelate" approach, with Tc displacing all traces of Cu in the ligand.[20] To assess the feasibility of this method, a model compound, $[CuDPA\text{-}TEG]^{2+}$ (**Cu-26**), was prepared via CuAAC of **13** with TEG-N_3 (Scheme 2.5). The transmetallation procedure was found to proceed efficiently at a pH of 7 after 5 minutes of microwave heating at 90 °C. Higher temperatures and longer reaction times resulted in product degradation, while shorter reaction times led to incomplete conversion (supporting information, Figures

S2.2-S2.4). Upon translation of this procedure to the third-generation dendrimer, the optimized conditions did not liberate the radiolabeled product in reasonable yield, likely due to steric hindrance reducing access to the DPA ligand. Adjusting the temperature to 100 °C, the pH to 5.5, and the reaction time to 10 minutes allowed isolation of the desired [^{99m}TcDPA-G3-(TEG)$_8$]$^+$, albeit in a modest 36 ± 4 % radiochemical yield (Scheme 2.5 and Figure 2.3).

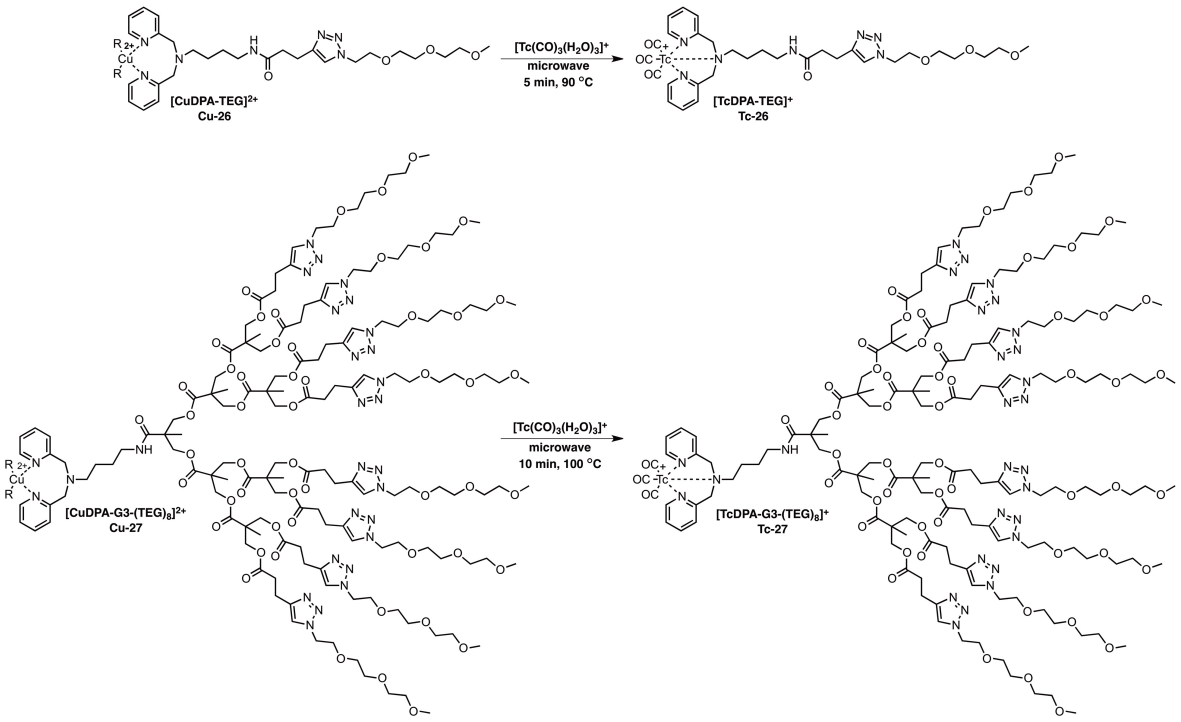

Scheme 2.5. Radiolabeling via transmetalation of model compound **Cu-26** and the third-generation dendrimer **Cu-27**.

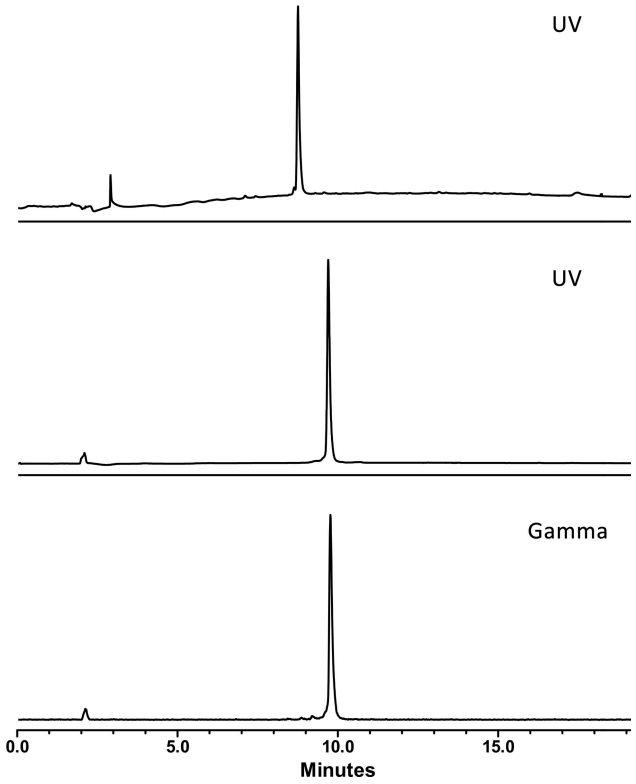

Figure 2.3: HPLC data for the product of the transmetalation reaction, $[^{99m}$TcDPA-G3-$(TEG)_8]^+$, carried out at 100 °C for 10 min at pH 5.5 on $[$CuDPA-G3-$(TEG)_8]^{2+}$ with ^{99m}Tc. Chromatograms correspond to $[$CuDPA-G3-$(TEG)_8]^{2+}$ (top), [ReDPA-G3-$(TEG)_8]^+$ (middle) and $[^{99m}$TcDPA-G3-$(TEG)_8]^+$ (bottom).

2.3. Conclusion

The work described herein provides a solution to many obstacles of using bis-MPA dendrimers for targeted molecular imaging applications. Functionalization of the periphery hydroxyl groups with the anhydride of 4-pentynoic acid resulted in terminal alkynes, which could be subsequently employed for "Click" coupling to a targeting moiety under mild conditions. A model compound, TEG, was attached to the periphery of

the dendrimers in quantitative conversions under mild reaction conditions. Removal of Cu(II) from the DPA ligand proved to be challenging, particularly at higher generation dendrimers. Nevertheless, a transmetalation reaction was developed to displace the Cu(II) with ^{99m}Tc, yielding radiolabeled dendrimers up to G3 with eight peripheral functional groups.

2.4. Experimental

2.4.1. Materials and Characterization

Pentynoic acid was purchased from GFS Chemicals and all other chemicals were purchased from Sigma Aldrich. Dry dichloromethane was dispensed from solvent system equipped with an activated alumina column and pyridine was stored over KOH pellets. NMR spectra were collected on a Bruker Avance 600 MHz or 700 MHz NMR spectrometer and calibrated to the solvent peak. A Micromass QTOF Global Ultima was used to obtain exact masses and HPLC was conducted on an Agilent HPLC equipped with PDA detector and a Phenomenex Luna C18(2) 4.6x150 mm column. HPLC analysis of radiolabeled compounds was performed on a Waters 1525 HPLC equipped with a Waters 2998 PDA detector for UV and Bio-Rad gamma detector.

2.4.2. General Procedures

General procedure 1: Synthesis of pTSe-Gx-(yne)$_y$. To a flame dried round bottom flask was added 1 eq. of pTSe-Gx-(OH)$_y$, 2 eq/OH of alkyne anhydride and 0.2 eq/OH of DMAP. The reaction mixture was dissolved in 2:1 mixture of CH_2Cl_2/pyridine and stirred for 12 hours. The anhydride was quenched by addition of 2 mL distilled water and further stirring at room temperature for 16 hours. The reaction mixture was diluted with 100 mL CH_2Cl_2 and washed with $NaHSO_4$ (3 x 100 mL), Na_2CO_3 (2 x 100 mL) and brine (100 mL). After rotary evaporation, the resulting alkyne dendrimers were purified by silica gel column chromatography (Hex/EtOAc) to give clear thick oils in excess of 90% yields.

General procedure 2: Synthesis of COOH-Gx-(yne)$_y$. To a flame dried round bottom flask was added 1 eq of pTSe-Gx-(yne)$_y$ and 6 eq of DBU in CH_2Cl_2. The reaction mixture was monitored by TLC for disappearance of starting material (approx. 1 hr). The reaction mixture was diluted with CH_2Cl_2 (100 mL) and washed with $NaHSO_4$ (3 x 100 mL) and brine (100 mL). After rotary evaporation, the crude product was purified via column chromatography (CH_2Cl_2/MeOH) to give clear viscous oil in excess of 90% yield.

General procedure 3: Synthesis of NHS-Gx-(yne)$_y$. To a flame dried round bottom flask was added 2 eq N-hydroxysuccinimide, 1 eq COOH-Gx-(yne)$_y$, and 2 eq EDC-HCl in CH_2Cl_2. The reaction mixture was stirred at room temperature overnight. The crude reaction mixture was diluted with CH_2Cl_2 and washed with brine. After rotary evaporation, the product was rapidly purified via silica gel column chromatography (CH_2Cl_2/MeOH) to yield product in excess of 90% yield as a clear viscous oil.

General procedure 4: Synthesis of DPA-Gx-(yne)$_y$. To a flame dried round bottom flask was added 2 eq DPA-NH_2 (**12**), 1 eq NHS-Gx-(yne)$_y$ and 2 eq Et_3N in CH_2Cl_2. The reaction mixture was stirred at room temperature and monitored by TLC for disappearance of dendrimer starting material (approx. 1 - 5 hrs). The crude reaction mixture was diluted with CH_2Cl_2 and washed with Na_2CO_3 and brine. After rotary evaporation, the product was purified via silica gel column chromatography (CH_2Cl_2/MeOH) to yield product in excess of 70% yield as a viscous oil.

General procedure 5: Synthesis of ReDPA-Gx-(yne)$_y$. 1 eq of DPA-Gx-(yne)$_y$ and 1.1 eq of $[Re(CO)_3(H_2O)_3]Br$ were dissolved in a 2:1 mixture of ACN/H_2O in a 5 mL round bottom flask and heated to reflux. After complete conversion (monitored by ^{1}H-NMR, disappearance of peak at approximately 8.50 ppm and appearance of a new peak at around 8.65 ppm), typically after 1 - 2 hrs, the solvent was evaporated and the crude reaction mixture was re-dissolved in $CHCl_3$, dried with Na_2SO_4, filtered and concentrated *in vacuo* to yield the product as a dark orange solid in quantitative yield.

General procedure 6: CuAAC reaction conditions. 1 eq of DPA-Gx-(yne)$_y$ or ReDPA-Gx-(yne)$_y$, 1.2 eq of azide/alkyne and 0.8 eq/alkyne of sodium ascorbate were dissolved in DMF. The flask was evacuated under vacuum and backfilled with nitrogen three times. 0.2 eq/alkyne of $CuSO_4$ in H_2O was added to the reaction vessel and stirred at room temperature overnight. The crude reaction mixture was concentrated by rotary evaporation and purified by semi-prep HPLC to afford the product. A method comprised of water and acetonitrile as eluents, each containining 0.1% formic acid, was utilized. For TEG functionalized dendrimers, the HPLC method was as follows: 95% water for 3 minutes, followed by a gradient ramp to 100% acetonitrile over 15 minutes. 100% acetonitrile was maintained for 3 minutes, followed by a sharp gradient to 95% water over 0.5 minutes and re-equilibration at 95% water for 2.5 minutes. Note: One extra equivalent of $CuSO_4$ and 4 equivalents of sodium ascorbate were utilized for reactions

involving DPA-G_x-$(yne)_y$ dendrimers, due to the chelation of copper by the DPA metal chelate.

2.4.3. Radiochemistry

General Procedure 7: Radiolabeling conditions. $[^{99m}TcO_4]^-$ was eluted from a ^{99m}Tc/Mo generator into an evacuated vial using 10 mL of saline. Preparation of $[^{99m}Tc(CO)_3(OH_2)_3]^+$ involved addition of potassium sodium tartrate (22 mg, 78 μmol), borax (20 mg, 52 μmol), sodium carbonate (15 mg, 142 μmol) and boranocarbonate (10 mg, 74 μmol) to a 5 mL microwave vial. The vial was sealed and purged with argon for 10 min. 4 mL of $[^{99m}TcO_4]^-$ in saline was added to the vial and the reaction mixture was heated in a microwave reactor for 3.5 min at 110 °C resulting in the formation of $[^{99m}Tc(CO)_3(OH_2)_3]^+$. The pH of the solution was adjusted to pH 4.5-6.5 with 1 M HCl. 1 mL of the reaction mixture was added to approx. 250 nmol of dendrimer in 0.1 mL of MeOH in a 2 mL microwave vial, and the reaction mixture was heated in a microwave reactor for 5 min at 80 °C (or higher for the transmetalation reaction). The compound were analyzed by HPLC on a Phenomenex Luna C18(2) column using a water/acetonitrile gradient (containing 0.1% formic acid) using the following method: 0-2 min at 95% water followed by a gradient to 100% acetonitrile between 2 min and 15 min. 100% acetonitrile was maintained until 17 min, followed by a rapid gradient to 95% water between 17-18 minutes. 95% water was maintained until 20 min.

2.4.4. Synthesis

pTSe-G1-(yne)$_2$ (2): Using general procedure 1, pTSe-G1-(OH)$_2$ (1.0 g, 3.16 mmol), pentynoic anhydride (2.25 g, 12.64 mmol, 4 eq.) and DMAP (154 mg, 1.26 mmol, 0.4 eq.) were dissolved in 20 mL dry CH_2Cl_2 and 10 mL pyridine. Yield: 1.43 g (95%). ^{1}H-NMR (600 MHz; $CDCl_3$): δ = 7.84-7.82 (m, 2H), 7.42 (dd, *J* = 8.5, 0.6 Hz, 2H), 4.48 (dd, *J* = 7.4, 4.8 Hz, 2H), 4.21 (s, 2H), 4.19 (d, *J* = 11.0 Hz, 4H), 3.47-3.44 (m, 2H), 2.58-2.56 (m, 4H), 2.51-2.49 (m, 7H), 2.00 (d, *J* = 5.2 Hz, 2H), 1.16 (s, 3H). ^{13}C-NMR (150 MHz, $CDCl_3$): δ = 172.2, 171.2, 145.4, 136.3, 130.3, 128.3, 82.4, 69.4, 65.4, 58.4, 55.1, 46.4, 33.3, 21.8, 17.7, 14.5. HR-MS calc. for $C_{24}H_{28}O_8S$ $[M+NH_4]^+$ m/z = 494.1849. Found: 494.1881.

pTSe-G2-(yne)$_4$ (5): Using general procedure 1, pTSe-G2-(OH)$_4$ (1.0 g, 1.82 mmol), pentynoic anhydride (2.60 g, 14.58 mmol, 8 eq.) and DMAP (180 mg, 1.46 mmol, 0.8 eq.) were dissolved in 20 mL dry CH_2Cl_2 and 10 mL pyridine. Yield: 1.50 g (95%). ^{1}H-NMR (600 MHz; $CDCl_3$): δ = 7.85-7.84 (d, *J* = 7.9 Hz, 2H), 7.42 (d, *J* = 7.9 Hz, 2H), 4.50 (t, *J* = 6.0 Hz, 2H), 4.29-4.22 (m, 12H), 3.48 (t, *J* = 6.0 Hz, 2H), 2.60-2.57 (t, *J* = 7.2 Hz, 8H), 2.52-2.49 (m, 11H), 2.01 (t, *J* = 2.6 Hz, 4H), 1.27 (s, 6H), 1.22 (s, 3H). ^{13}C-NMR (150 MHz, $CDCl_3$): δ = 172.0, 171.3, 145.3, 136.4, 130.3, 128.3, 58.5, 54.9, 33.3, 18.0, 17.5, 14.5. HR-MS calc. for $C_{44}H_{52}O_{16}S$ $[M+H]^+$ m/z = 869.3054. Found 869.3064.

pTSe-G3-(yne)$_8$ (8): Using general procedure 1, pTSe-G3-(OH)$_8$ (1.0 g, 0.99 mmol), pentynoic anhydride (2.81 g, 15.79 mmol, 16 eq.) and DMAP (194 mg, 1.58 mmol, 1.6

eq.) were dissolved in 20 mL dry CH_2Cl_2 and 10 mL pyridine. Yield: 1.52 g (93%). ^{1}H-NMR (600 MHz; $CDCl_3$): δ = 7.76-7.74 (d, *J* = 8.0 Hz, 2H), 7.34 (d, *J* = 8.0 Hz, 2H), 4.43 (t, *J* = 5.9 Hz, 2H), 4.21-4.13 (m, 28H), 3.40 (t, *J* = 5.9 Hz, 2H), 2.50-2.48 (m, 16H), 2.43-2.40 (m, 19H), 1.92 (t, *J* = 2.6 Hz, 8H), 1.19-1.16 (m, 21H). ^{13}C-NMR (150 MHz, $CDCl_3$): δ = 172.1, 171.8, 171.6, 171.3, 144.7, 136.1, 130.3, 128.2, 82.3, 69.5, 65.5, 65.4, 62.2, 58.5, 54.9, 46.5, 33.3, 21.5, 18.0, 17.7, 17.4, 14.4. HR-MS calc. for $C_{84}H_{100}O_{32}S$ $[M+NH_4]^+$ m/z = 1670.6262. Found 1670.6188.

COOH-G1-(yne)$_2$ (3): Using general procedure 2, pTSe-G1-(yne)$_2$ (1.0 g, 2.1 mmol) was dissolved in 50 ml of toluene and DBU (1.88 mL, 12.6 mmol) was added to the reaction mixture. Yield: 569 mg (92%). ^{1}H-NMR (600 MHz; $CDCl_3$): δ = 4.30 (q, *J* = 10.2 Hz, 4H), 2.59-2.56 (m, 4H), 2.51-2.48 (m, 4H), 1.98 (t, *J* = 2.6 Hz, 2H), 1.31 (s, 3H). ^{13}C-NMR (150 MHz, $CDCl_3$): δ = 177.7, 170.6, 81.8, 69.2, 65.3, 45.8, 33.2, 17.8, 14.2. HR-MS calc. for $C_{15}H_{18}O_6$ $[M+Na]^+$ m/z = 317.1001. Found 317.0997.

COOH-G2-(yne)$_4$ (6): Using general procedure 2, pTSe-G2-(yne)$_4$ (1.0 g, 1.2 mmol) was dissolved in 25 ml of toluene and DBU (1.03 mL, 6.9 mmol) was added to the reaction mixture. Yield: 773 mg (94%). ^{1}H-NMR (600 MHz; $CDCl_3$): δ = 4.30-4.23 (m, 12H), 2.58-2.55 (m, 8H), 2.50-2.47 (m, 8H), 1.99 (t, *J* = 2.6 Hz, 4H), 1.31 (s, 3H), 1.27 (s, 6H). ^{13}C-NMR (150 MHz, $CDCl_3$): δ = 174.5, 171.9, 171.3, 81.2, 69.3, 65.8, 65.5, 46.4, 46.3, 33.2, 17.8, 17.6, 14.3. HR-MS calc. for $C_{35}H_{42}O_{14}$ $[M+NH_4]^+$ m/z = 704.2918. Found 704.2898.

COOH-G3-(yne)$_8$ (9): Using general procedure 2, pTSe-G3-(yne)$_8$ (1.0 g, 0.6 mmol) was dissolved in 20 ml of toluene and DBU (0.54 mL, 3.6 mmol) was added to the reaction mixture. Yield: 792 mg (90%). ^{1}H-NMR (600 MHz; $CDCl_3$): δ= 4.36-4.25 (m, 28H), 2.61-2.59 (m, 16H), 2.53-2.50 (m, 16H), 2.02 (td, *J* = 2.6, 0.8 Hz, 8H), 1.37 (s, 3H), 1.29 (s, 18H). ^{13}C-NMR (150 MHz, $CDCl_3$): δ = 172.9, 171.9, 171.5, 82.3, 69.4, 66.7, 65.6, 65.5, 65.4, 46.8, 46.4, 33.2, 17.9, 17.6, 17.4, 14.3. HR-MS calc. for $C_{75}H_{90}O_{30}$ $[M+NH_4]^+$ m/z = 1488.5861. Found 1488.5872.

NHS-G1-(yne)$_2$ (15): Using general procedure 3, COOH-G1-(yne)$_2$ (0.5 g, 1.7 mmol), N-hydroxysuccinimide (391 mg, 3.4 mmol) and EDC-HCl (652 mg, 3.4 mmol) were dissolved in 20 mL CH_2Cl_2. Yield: 607 mg (91%). ^{1}H-NMR (600 MHz; $CDCl_3$): δ = 4.38 (s, 4H), 2.83 (s, 4H), 2.64-2.62 (m, 4H), 2.53-2.50 (m, 4H), 1.98 (t, *J* = 2.6 Hz, 2H), 1.47 (s, 3H). ^{13}C-NMR (150 MHz, $CDCl_3$): δ = 171.1, 168.4, 82.2, 69.2, 65.0, 46.4, 33.2, 25.6, 17.8, 14.2. HR-MS calc. for $C_{19}H_{21}NO_8$ $[M+Na]^+$ m/z = 414.1165. Found 414.1160.

NHS-G2-(yne)$_4$ (18): Using general procedure 3, COOH-G2-(yne)$_4$ (0.5 g, 0.7 mmol), N-hydroxysuccinimide (168 mg, 1.5 mmol) and EDC-HCl (285 mg, 1.5 mmol) were dissolved in 15 mL CH_2Cl_2. Yield: 516 mg (90%). ^{1}H-NMR (600 MHz; $CDCl_3$): δ = 4.42-4.26 (m, 12H), 2.85 (s, 4H), 2.57-2.47 (m, 16H), 1.98 (t, *J* = 2.6 Hz, 4H), 1.47 (s, 3H), 1.29 (s, 6H). ^{13}C-NMR (150 MHz, $CDCl_3$): δ = 172.1, 171.3, 168.6, 168.1, 82.5, 69.4, 65.5, 65.4, 46.8, 46.7, 33.3, 25.7, 17.8, 17.7, 14.4. HR-MS calc. for $C_{39}H_{45}NO_{16}$ $[M+NH_4]^+$ m/z = 801.3082. Found 801.3091.

NHS-G3-(yne)$_8$ (21): Using general procedure 3, COOH-G3-(yne)$_8$ (0.5 g, 0.34 mmol), N-hydroxysuccinimide (0.78 g, 0.68 mmol) and EDC-HCl (0.13 g, 0.68 mmol) were dissolved in CH_2Cl_2. Yield: 504 mg (94 %). ^{1}H-NMR (600 MHz; $CDCl_3$): δ = 4.44-4.24 (m, 28H), 2.88-2.87 (m, 4H), 2.60-2.58 (m, 16H), 2.52-2.49 (m, 16H), 2.01 (t, *J* = 2.6 Hz, 8H), 1.53 (s, 3H), 1.32 (s, 6H), 1.26 (s, 12H). ^{13}C-NMR (150 MHz, $CDCl_3$): δ = 172.1, 171.6, 171.3, 168.8, 82.2, 69.4, 66.3, 65.6, 65.5, 46.7, 46.5, 46.5, 33.3, 25.8, 17.9, 17.7, 17.5, 14.4. HR-MS calc. for $C_{79}H_{93}NO_{32}$ $[M+NH_4]^+$ m/z = 1585.5786. Found 1585.5846.

DPA-C$_4$-NHBoc (11): Mono ^{t}Boc protected 1,4-diaminobutane[2] (0.5 g, 2.7mmol) and pyridine-2-carbaldehyde (758 μL, 8.0 mmol, 3 eq.) were added to 15 mL CH_2Cl_2, followed by AcOH (31 μL, 0.5 mmol, 0.2 eq) and was allowed to stir for 45 min at room temperature. The reaction mixture was then cooled to 0 °C followed by addition of $NaHB(OAc)_3$ (636 mg, 8 mmol, 3 eq.). The reaction mixture was allowed to warm to room temperature, and stirred overnight. The reaction mixture was diluted with 75 mL of CH_2Cl_2 and washed with 1M NaOH (3 x 50 ml) and the organic fractions were combined and washed with brine. The crude reaction mixture was concentrated by rotary evaporation and purified by silica gel column chromatography (CH_2Cl_2/MeOH) to yield 724 mg (72%) of product as a pale yellow oil. ^{1}H NMR (600 MHz; $CDCl_3$): δ = 8.52 (dd, *J* = 4.8, 0.8 Hz, 2H), 7.63 (td, *J* = 7.7, 1.8 Hz, 2H), 7.49 (d, *J* = 7.8 Hz, 2H), 7.13 (ddd, *J* = 7.4, 4.9, 1.0 Hz, 2H), 3.79 (s, 4H), 3.07-3.04 (m, 2H), 2.54 (t, *J* = 7.2 Hz, 2H), 1.56 (m, 2H), 1.45 (m, 2H), 1.42 (s, 9H). ^{13}C-NMR (150 MHz, $CDCl_3$): δ = 159.8, 156.0, 149.0,

136.4, 123.0, 121.9, 78.8, 60.4, 53.9, 40.3, 28.5, 27.8, 24.3. HR-MS calc. for $C_{21}H_{30}N_4O_2$ $[M+H]^+$ m/z = 371.2447. Found 371.2441.

DPA-C_4-NH_2 (12): To a stirring solution of DPA-C_4-NHBoc (0.5 g, 1.3 mmol) in 15 mL of CH_2Cl_2 at room temperature was added 5 mL of TFA dropwise, resulting in a red solution. After stirring at room temperature for 1.5 hours, the reaction mixture was diluted with CH_2Cl_2 and brought to pH 13-14 using 1M NaOH. The aqueous layer was extracted with CH_2Cl_2 (5 x 30 ml) and the organic fractions combined and washed with brine. The product was concentrated by rotary evaporation to yield 248 mg (68%) of product as a yellow oil. ^{1}H NMR (600 MHz; $CDCl_3$): δ 8.51 (d, *J* = 4.2 Hz, 2H), 7.64 (t, *J* = 7.8 Hz, 2H), 7.50 (d, *J* = 7.8 Hz, 2H), 7.14 (t, *J* = 6.1 Hz, 2H), 3.79 (s, 4H), 2.66 (t, *J* = 6.9 Hz, 2H), 2.55-2.50 (t, *J* = 7.2 Hz, 2H), 1.60-1.53 (m, 2H), 1.45 (m, 2H). ^{13}C-NMR (150 MHz, $CDCl_3$): δ = 159.8, 149.1, 136.6, 123.1, 122.1, 60.5, 54.2, 41.7, 30.8, 24.5. HR-MS calc. for $C_{16}H_{22}N_4$ $[M+Na]^+$ m/z = 293.1742. Found 293.1734.

DPA-Pentynoic alkyne (13): DPA-NH_2 (0.2 g, 740 μmol) and pentynoic anhydride (198 mg, 1.1 mmol, 1.5 eq) were stirred in 15 mL CH_2Cl_2 at room temperature overnight. The solution was diluted with 50 mL of CH_2Cl_2 and washed with Na_2CO_3 (2 x 75 mL) and brine. The crude reaction mixture was concentrated by rotary evaporation and purified by silica gel column chromatography (CH_2Cl_2/MeOH) to yield: 201 mg (78%) of a pale yellow oil. ^{1}H-NMR (600 MHz; $CDCl_3$): δ = 8.52-8.51 (m, 2H), 7.63 (td, *J* = 7.7, 1.7 Hz, 2H), 7.43 (d, *J* = 7.8 Hz, 2H), 7.14 (dd, *J* = 7.0, 5.3 Hz, 2H), 6.55 (s, 1H), 3.77 (s, 4H),

3.21 (q, *J* = 6.3 Hz, 2H), 2.55-2.49 (m, 4H), 2.38 (t, *J* = 7.3 Hz, 2H), 1.97 (t, *J* = 2.6 Hz, 1H), 1.59 (quintet, *J* = 7.1 Hz, 2H), 1.49 (quintet, *J* = 7.1 Hz, 2H). ^{13}C-NMR (150 MHz, $CDCl_3$): δ = 171.1, 159.6, 149.1, 136.5, 123.4, 122.1, 83.4, 69.3, 60.4, 53.8, 39.1, 35.4, 27.2, 23.8, 15.1. HR-MS calc. for $C_{21}H_{26}N_4O$ $[M]^+$ m/z = 351.2185. Found 351.2173.

DPA-G1-(yne)$_2$ (16): Using general procedure 4, NHS-G1-(yne)$_2$ (200 mg, 511 μmol) and DPA-NH_2 (276 mg, 1.0 mmol) were dissolved in 10 mL of CH_2Cl_2, followed by addition of Et_3N (143 μL, 1.0 mmol). Yield: 225 mg (81%). ^{1}H NMR (600 MHz; $CDCl_3$): δ 8.52 (ddd, *J* = 4.9, 1.7, 0.9 Hz, 2H), 7.66 (td, *J* = 7.7, 1.8 Hz, 2H), 7.48 (d, *J* = 7.8 Hz, 2H), 7.16 (ddd, *J* = 7.4, 4.9, 1.1 Hz, 2H), 6.37-6.36 (m, 1H), 4.29-4.24 (m, 4H), 3.81 (s, 4H), 3.21 (q, *J* = 6.4 Hz, 2H), 2.58-2.54 (m, 6H), 2.49-2.46 (m, 4H), 1.98 (t, *J* = 2.6 Hz, 2H), 1.58 (quintet, *J* = 7.2 Hz, 2H), 1.50 (quintet, *J* = 7.2 Hz, 2H), 1.24 (s, 3H). ^{13}C-NMR (150 MHz, $CDCl_3$): δ = 172.1, 171.3, 149.1, 136.6, 123.3, 122.2, 82.2, 69.5, 66.7, 60.3, 53.5, 46.2, 39.3, 33.4, 27.1, 23.7, 18.1, 14.5. HR-MS calc. for $C_{31}H_{38}N_4O_5$ $[M+H]^+$ m/z = 547.2920. Found 547.2910.

DPA-G2-(yne)$_4$ (19): Using general procedure 4, NHS-G2-(yne)$_4$ (200 mg, 255 μmol) and DPA-NH_2 (138 mg, 510 μmol) were dissolved in 5 mL of CH_2Cl_2, followed by addition of Et_3N (71 μL, 510 μmol). Yield: 173 mg (72%). ^{1}H NMR (600 MHz; $CDCl_3$): δ = 8.56-8.55 (bs, 2H), 7.70-7.68 (m, 2H), 7.54-7.50 (bs, 2H), 7.21-7.18 (bs, 2H), 6.45 (bs, 1H), 4.31-4.23 (m, 12H), 3.87-3.80 (bs, 4H), 3.26-3.23 (m, 2H), 2.61-2.56 (m, 10H), 2.51-2.48 (m, 8H), 2.00 (t, *J* = 2.8 Hz, 4H), 1.63 (bs, 2H), 1.56-1.51 (quintet, 2H), 1.27 (s,

9H). ^{13}C-NMR (150 MHz, $CDCl_3$): δ = 172.0, 171.5, 171.2, 149.0, 136.5, 123.1, 122.0, 82.3, 69.3, 66.9, 65.4, 60.2, 53.4, 46.5, 46.4, 39.4, 33.2, 27.1, 23.6, 17.9, 17.8, 14.3. $C_{51}H_{62}N_4O_{13}$ $[M+H]^+$ m/z = 939.4392. Found 939.4376.

DPA-G3-(yne)$_8$ (22): Using general procedure 4, NHS-G3-(yne)$_8$ (200 mg, 128 μmol) and DPA-NH_2 (7 mg, 256 μmol) were dissolved in 3 mL of CH_2Cl_2, followed by addition of Et_3N (143 μL, 256 μmol). Yield: 167 mg (75%). ^{1}H NMR (600 MHz; $CDCl_3$): δ = 8.55-8.55 (m, 2H), 7.69-7.67 (m, 2H), 7.56-7.53 (m, 2H), 7.20-7.18 (m, 2H), 4.30-4.23 (m, 28H), 3.84-3.82 (s, 4H), 3.24 (d, *J* = 6.1, 2H), 2.60-2.56 (m, 16H), 2.51-2.48 (m, 16H), 2.01 (d, *J* = 5.2, 8H), 1.53 (dt, *J* = 7.9, 3.5, 2H), 1.28 (s, 21H). NMR (150 MHz, $CDCl_3$): δ = 172.0, 171.6, 171.3, 171.2, 149.1, 136.5, 123.2, 122.1, 82.4, 69.4, 67.2, 65.5, 65.3, 60.2, 53.6, 46.8, 46.4, 39.5, 33.2, 27.2, 17.9, 17.6, 14.4. $C_{91}H_{110}N_4O_{29}$ $[M+H]^+$ m/z = 1723.7334. Found 1723.7281.

[ReDPA-Pentynoic alkyne]$^+$ (14): DPA-Pentynoic alkyne (50 mg, 143 μmol) and $[Re(CO)_3(H_2O)_3]Br$ (63 mg, 157 μmol, 1.1 eq.) were stirred in 2 mL of a 2:1 mixture of ACN/H_2O for 1.5 hrs at reflux. The product was concentrated by rotary evaporation and re-dissolved in $CHCl_3$, filtered, dried with Na_2SO_4 and concentrated to give product as an orange semi-solid in quantitative yield. ^{1}H-NMR (600 MHz; $CDCl_3$): δ = 8.66 (d, *J* = 5.6 Hz, 2H), 7.91 (d, *J* = 7.8 Hz, 2H), 7.83 (t, *J* = 7.7 Hz, 2H), 7.22 (t, *J* = 6.5 Hz, 2H), 7.10 (t, *J* = 6.3 Hz, 1H), 5.89 (d, *J* = 16.5 Hz, 2H), 4.53 (d, *J* = 16.5 Hz, 2H), 3.86-3.83 (m, 2H), 3.44-3.41 (m, 2H), 2.58-2.52 (m, 4H), 2.23-2.21 (m, 2H), 2.17 (s, 1H), 1.71 (m, 4H).

^{13}C-NMR (150 MHz, $CDCl_3$): δ = 195.9, 172.1, 161.3, 150.8, 140.4, 125.4, 125.1, 83.7, 71.0, 69.6, 67.4, 38.4, 35.4, 27.0, 23.0, 15.1. HR-MS calc. for $C_{24}H_{26}N_4O_4Re$ $[M]^+$ m/z = 621.1512. Found 621.1523.

[ReDPA-G1-(yne)$_2$]$^+$ (17): Using general procedure 5, DPA-G1-(yne)$_2$ (50 mg, 91 μmol) and $[Re(CO)_3(H_2O)_3]Br$ (40 mg, 100 μmol) were dissolved in 1 mL of a 2:1 mixture of ACN/H_2O. ^{1}H NMR (600 MHz; $CDCl_3$): δ = 8.62 (d, *J* = 5.0 Hz, 2H), 7.77 (td, *J* = 7.8, 1.5 Hz, 2H), 7.55 (d, *J* = 7.9 Hz, 2H), 7.19 (t, *J* = 6 Hz, 2H), 6.47 (dd, *J* = 7.7, 4.4 Hz, 1H), 4.96 (d, *J* = 16.7 Hz, 2H), 4.52 (d, *J* = 16.6 Hz, 2H), 4.32 (d, *J* = 11.2 Hz, 2H), 4.17 (d, *J* = 11.2 Hz, 2H), 3.76-3.73 (m, 2H), 3.31 (dt, *J* = 9.5, 4.6 Hz, 2H), 2.52-2.48 (m, 4H), 2.43-2.40 (m, 4H), 1.98-1.93 (m, 2H), 1.88 (t, *J* = 2.6 Hz, 2H), 1.57-1.52 (m, 2H), 1.25 (s, 3H). ^{13}C-NMR (150 MHz, $CDCl_3$): δ = 172.7, 171.4, 161.2, 150.9, 140.5, 125.5, 125.1, 82.4, 71.1, 69.4, 67.5, 66.7, 39.0, 33.5, 26.7, 23.4, 18.1, 14.5. HR-MS calc. for $C_{34}H_{38}N_4O_8Re$ $[M]^+$ m/z = 817.2247. Found 817.2259.

[ReDPA-G2-(yne)$_4$]$^+$ (20): Using general procedure 5, DPA-G2-(yne)$_4$ (50 mg, 53 μmol) and $[Re(CO)_3(H_2O)_3]Br$ (23 mg, 58 μmol) were dissolved in 1 mL of a 2:1 mixture of ACN/H_2O. ^{1}H NMR (600 MHz; $CDCl_3$): δ 8.62 (d, *J* = 5.5, 2H), 8.62 (d, *J* = 5.5, 2H), 7.86 (s, 1H), 7.78-7.72 (m, 4H), 7.18-7.15 (m, 2H), 5.62 (d, *J* = 16.7, 2H), 4.58 (d, *J* = 16.6, 2H), 4.35 (dd, *J* = 90.2, 11.1, 4H), 4.22-4.14 (m, 8H), 3.77 (t, *J* = 8.1, 2H), 3.34 (d, *J* = 5.7, 2H), 2.50-2.47 (m, 8H), 2.41-2.38 (m, 8H), 2.11 (s, 2H), 1.93 (t, *J* = 2.6, 4H), 1.58-1.57 (m, 2H), 1.33 (s, 3H), 1.19 (s, 6H). ^{13}C-NMR (150 MHz, $CDCl_3$): δ = 195.7,

172.5, 172.1, 171.3, 161.5, 150.8, 140.2, 125.3, 124.6, 82.3, 71.0, 69.3, 67.5, 66.8, 65.4, 65.4, 46.6, 46.4, 38.9, 33.2, 29.7, 26.5, 23.3, 17.9, 17.8, 14.3, 14.3. HR-MS calc. for $C_{54}H_{62}N_4O_{16}Re$ $[M]^+$ m/z = 1209.3804. Found 1209.3805.

$[ReDPA\text{-}G3\text{-}(yne)_8]^+$ (23): Using general procedure 5, DPA-G3-$(yne)_8$ (50 mg, 29 μmol) and $[Re(CO)_3(H_2O)_3]Br$ (13 mg, 32 μmol) were dissolved in 0.5 mL of a 2:1 mixture of ACN/H_2O. ^{1}H NMR (600 MHz; CDCl3): δ 8.70 (d, *J* = 5.4, 2H), 7.89-7.84 (m, 4H), 7.46-7.44 (m, 1H), 7.25 (t, *J* = 6.4, 2H), 5.92 (d, *J* = 16.7, 2H), 4.61 (d, *J* = 16.4, 2H), 4.39 (dd, *J* = 37.7, 11.1, 4H), 4.31-4.22 (m, 25H), 3.88-3.86 (m, 2H), 3.44-3.41 (m, 2H), 2.58 (s, 16H), 2.50-2.48 (m, 16H), 2.24-2.19 (m, 2H), 2.02 (d, *J* = 5.1, 8H), 1.72-1.68 (m, 2H), 1.46 (s, 3H), 1.29 (s, 6H), 1.26 (s, 12H). ^{13}C-NMR (150 MHz, $CDCl_3$): δ = 195.8, 172.0, 172.0, 171.7, 171.2, 161.3, 150.8, 140.2, 125.3, 124.8, 82.4, 71.0, 69.4, 67.3, 67.2, 65.4, 65.3, 46.4, 39.1, 33.2, 26.6, 23.5, 18.0, 17.9, 17.7, 14.3. HR-MS calc. for $C_{94}H_{110}N_4O_{32}Re$ $[M]^+$ m/z = 1993.6661. Found 1993.6709.

TEG-OTs: Following previous literature precedence,[3] to a cooled solution of triethylene glycol monomethyl ether (1 g, 6.1 mmol) in 3 mL of THF and NaOH (0.44 g, 11 mmol) in 3 mL of dH_2O was added pTsCl (1.16 g, 6.1 mmol) in 4 mL THF dropwise. The reaction mixture was slowly warmed to R.T. and allowed to stir for 12 hours. The crude reaction mixture was diluted with dH_2O (10 mL) and extracted with ether (3 × 10 mL). The combined organic layers were dried using Na_2SO_4, filtered and concentrated *in vacuo* to yield 1.7 g (88 %). ^{1}H NMR (600 MHz; $CDCl_3$): δ 7.79-7.78 (m, 2H), 7.34-7.33 (m,

2H), 4.16-4.14 (m, 2H), 3.74-3.72 (m, 1H), 3.68-3.67 (m, 2H), 3.61-3.57 (m, 6H), 3.53-3.51 (m, 2H), 3.36 (s, 3H), 2.44 (s, 3H). ^{13}C-NMR (150 MHz, $CDCl_3$): δ = 144.82, 132.99, 129.85, 127.93, 71.88, 70.69, 70.51, 69.30, 68.63, 67.93, 58.98, 21.6. HR-MS calc. for $C_{14}H_{22}O_6S$ $[M+NH_4]^+$ m/z = 336.1475. Found 336.1475.

TEG-N_3: TEG-OTs (1 g, 3.1 mmol) was dissolved in 25 mL of DMSO and NaN_3 (820 mg, 12.6 mmol) was added and the reaction was heated to 50 C for 5 hours. The crude reaction mixture was diluted with dH_2O (50 mL) and extracted with Et_2O (3 × 20 mL). The combined organic layers were washed with water (15 mL) and dried with Na_2SO_4 to yield 450 mg (77 %). ^{1}H NMR (700 MHz; $CDCl_3$): δ 3.64-3.61 (m, 8H), 3.52-3.51 (m, 2H), 3.36-3.34 (m, 5H). ^{13}C NMR (150 MHz, $CDCl_3$): δ = 71.95, 70.72, 70.67, 70.62, 70.05, 59.03, 50.70. HR-MS calc. for $C_7H_{15}N_3O_3$ $[M+NH_4]^+$ m/z = 207.1452. Found 207.1454.

DPA-G1-$(TEG)_2$ (25): Using general procedure 6, DPA-G1-$(yne)_2$ (10 mg, 18.3 μmol) and TEG-N_3 (8 mg, 43.9 μmol) was dissolved in 0.5 mL of DMF, followed by addition of sodium ascorbate (5.8 mg, 29.3 μmol). After evacuation and backfilling with argon, $CuSO_4$ (1.8 mg, 7.3 μmol) was added in 0.1 mL H_2O. Upon complete functionalization of the dendrimer, DMF was removed by rotary evaporation and the reaction mixture was dissolved in 5 mL of dH_2O. Addition of a buffered solution of NaS resulted in precipitation of CuS, which was filtered off. The reaction mixture was purified by semi-prep HPLC to yield 9.3 mg (55%). ^{1}H NMR (600 MHz; DMSO): δ 8.46 (d, J = 4.8, 2H),

7.81 (s, 2H), 7.74 (td, *J* = 7.6, 1.8, 2H), 7.70 (t, *J* = 3.0, 1H), 7.50 (d, *J* = 7.8, 2H), 7.23 (dd, *J* = 7.4, 4.9, 2H), 4.45 (t, *J* = 5.3, 4H), 4.11 (q, *J* = 14.9, 4H), 3.79-3.77 (t, *J* = 5.4, 4H), 3.70 (s, 4H), 3.52-3.50 (m, 4H), 3.48-3.46 (m, 8H), 3.40 (dd, *J* = 5.7, 3.7, 4H), 3.23-3.22 (s, 6H), 3.00 (q, *J* = 6.0, 2H), 2.85 (t, *J* = 7.8, 4H), 2.65-2.62 (t, *J* = 7.8 4H), 2.44-2.42 (t, *J* = 6.6, 3H), 1.46-1.44 (quintet, *J* = 7.2, 2H), 1.38-1.36 (quintet, *J* = 7.2, 2H), 1.07 (s, 3H). HR-MS calc. for $C_{45}H_{68}N_{10}O_{11}$ $[M+H]^+$ m/z = 925.5147. Found 925.5128.

DPA-G2-(TEG)$_4$ (26): Using general procedure 6, DPA-G2-(yne)$_4$ (10 mg, 10.6 μmol) and TEG-N_3 (10 mg, 51.1 μmol) were dissolved in 0.4 mL of DMF, followed by addition of sodium ascorbate (6.7 mg, 33.9 μmol). After evacuation and backfilling with argon, $CuSO_4$ (2.1 mg, 8.5 μmol) was added in 0.1 mL H_2O. Upon complete functionalization of the dendrimer, DMF was removed by rotary evaporation and the reaction mixture was dissolved in 5 mL of dH_2O. Addition of a buffered solution of NaS resulted in precipitation of CuS, which was filtered off. The reaction mixture was purified by semi-prep HPLC to yield 7.1 mg (40 %). ^{1}H NMR (600 MHz; DMSO): δ 8.45 (dd, *J* = 4.8, 0.8, 2H), 8.22 (bs, 1H), 7.81 (s, 4H), 7.76-7.72 (m, 3H), 7.50 (d, *J* = 7.9, 2H), 7.23-7.20 (dd, *J* = 7.2, 4.8, 2H), 4.44 (t, *J* = 5.3, 8H), 4.15 (q, *J* = 11.9, 4H), 4.10 (s, 8H), 3.77 (t, *J* = 5.3, 8H), 3.70 (s, 4H), 3.51-3.49 (m, 8H), 3.46 (dt, *J* = 6.0, 2.9, 16H), 3.40 (dd, *J* = 5.7, 3.7, 8H), 3.21 (s, 12H), 2.97 (q, *J* = 6.4, 2H), 2.84 (t, *J* = 7.5, 8H), 2.64 (t, *J* = 7.6, 8H), 2.42 (t, *J* = 7.0, 2H), 1.45 (quintet, *J* = 7.8, 2H), 1.36 (quintet, *J* = 7.8, 2H), 1.10 (s, 3H), 1.08 (s, 6H). HR-MS calc. for $C_{79}H_{122}N_{16}O_{25}$ $[M+H]^+$ m/z = 1695.8845. Found 1695.8813.

[ReDPA-TEG]$^+$ (Re-24): Using general procedure 6, [ReDPA-yne]$^+$ (10 mg, 16.1 μmol) and TEG-N_3 (4.6 mg, 25.2 μmol) were dissolved in 0.4 mL DMF, followed by addition of sodium ascorbate (1.6 mg, 8.1 μmol). After evacuation and backfilling with argon, $CuSO_4$ (0.5 mg, 2.0 μmol) was added in 0.1 mL H_2O. Upon completion, the reaction mixture was purified by semi-prep HPLC to yield 8.3 mg (62 %). ^{1}H NMR (700 MHz; DMSO): δ 8.81 (d, *J* = 5.5, 2H), 8.00 (t, *J* = 7.8, 2H), 7.96 (t, *J* = 5.6, 1H), 7.80 (s, 1H), 7.56 (d, *J* = 7.9, 2H), 7.40 (t, *J* = 6.6, 2H), 4.90 (d, *J* = 16.7, 2H), 4.84 (d, *J* = 16.7, 2H), 4.46 (t, *J* = 5.2, 2H), 3.77 (m, 6H), 3.51 (m, 3H), 3.48 (m, 4H), 3.41 (t, *J* = 4.7, 3H), 3.23 (s, 3H), 3.15 (q, *J* = 6.4, 2H), 2.86 (t, *J* = 7.7, 2H), 2.45 (t, *J* = 7.7, 2H), 1.81 (m, 2H), 1.49 (m, 2H). HR-MS calc. for $C_{31}H_{40}N_7O_7Re$ $[M]^+$ m/z = 808.2592. Found 808.2590.

[ReDPA-G1-(TEG)$_2$]$^+$ (Re-25): Using general procedure 6, [ReDPA-G1-(yne)$_2$]$^+$ (10 mg, 12.2 μmol) and TEG-N_3 (6 mg, 29.3 μmol) were dissolved in 0.4 mL of DMF, followed by addition of sodium ascorbate (3.9 mg, 19.5 μmol). After evacuation and backfilling with argon, $CuSO_4$ (1.2 mg, 4.9 μmol) was added in 0.1 mL H_2O. Upon completion, the reaction mixture was purified by semi-prep HPLC to yield 10.4 mg (71 %). ^{1}H NMR (600 MHz; DMSO): δ= 8.82-8.81 (m, 2H), 8.00 (td, *J* = 7.8, 1.4, 2H), 7.90-7.88 (t, 1H), 7.84 (s, 2H), 7.54 (d, *J* = 7.9, 2H), 7.42-7.40 (t, *J* = 6.0 Hz, 2H), 4.94-4.84 (dd, *J* = 41.4, 16.8, 4H), 4.45 (t, *J* = 5.3, 4H), 4.16 (dd, *J* = 30.3, 11.0, 4H), 3.81-3.77 (m, 6H), 3.52 – 3.51 (m, 4H), 3.49 – 3.47 (m, 8H), 3.42 – 3.40 (m, 5H), 3.23 (s, 6H), 3.19 – 3.16 (q, *J* = 6.6, 2H), 2.88 (dd, *J* = 9.5, 5.5, 4H), 2.69 (dd, *J* = 9.9, 5.2, 4H), 1.83-1.80 (m, 2H), 1.53-1.51

(m, 2H), 1.13 (s, 3H). HR-MS calc. for $C_{48}H_{68}N_{10}O_{14}Re$ $[M]^+$ m/z = 1195.4478. Found 1195.4678.

$[ReDPA\text{-}G2\text{-}(TEG)_4]^+$ (Re-26): Using general procedure 6, $[ReDPA\text{-}G2\text{-}(yne)_4]^+$ (10 mg, 8.3 μmol) and TEG-N_3 (8 mg, 39.7 μmol) were dissolved in 0.4 mL of DMF, followed by addition of sodium ascorbate (5.3 mg, 26.6 μmol). After evacuation and backfilling with argon, $CuSO_4$ (1.2 mg, 4.9 μmol) was added in 0.1 mL H_2O. Upon completion, the reaction mixture was purified by semi-prep HPLC to yield 10.9 mg (67 %). ^{1}H NMR (700 MHz; DMSO): δ 8.81 (d, *J* = 5.5, 2H), 7.98 (td, *J* = 7.8, 1.2, 2H), 7.95 (t, *J* = 5.5, 1H), 7.81 (s, 4H), 7.54 (d, *J* = 7.9, 2H), 7.40 (t, *J* = 6.7, 2H), 4.89 (q, *J* = 21.7, 4H), 4.44 (t, *J* = 5.3, 8H), 4.18 (dd, *J* = 30.9, 10.9, 4H), 4.12 (s, 8H), 3.76 (t, *J* = 5.3, 8H), 3.50 (m, 8H), 3.47-3.46 (m, 14H), 3.40 (m, 8H), 3.21 (s, 12H), 3.15-3.11 (m, 2H), 2.85 (t, *J* = 7.5, 8H), 2.66 (t, *J* = 7.6, 8H), 1.82 (m, 2H), 1.51 (dt, *J* = 14.5, 7.4, 2H), 1.16 (s, 3H), 1.11 (s, 6H) HR-MS calc. for $C_{82}H_{122}N_{16}O_{25}$ $[M]^+$ m/z = 1965.8172. Found 1965.8102.

$[ReDPA\text{-}G3\text{-}(TEG)_8]^+$ (Re-27): Using general procedure 6, $[ReDPA\text{-}G3\text{-}(yne)_8]^+$ (10 mg, 5.0 μmol) and TEG-N_3 (11.4 mg, 60.2 μmol) were dissolved in 0.4 mL of DMF, followed by addition of sodium ascorbate (4.0 mg, 20.1 μmol). After evacuation and backfilling with argon, $CuSO_4$ (1.0 mg, 4.0 μmol) was added in 0.1 mL H_2O. Upon completion, the reaction mixture was purified by semi-prep HPLC to yield 11.1 mg (64 %). ^{1}H NMR (600 MHz; DMSO): δ= 8.81 (d, *J* = 5.6, 2H), 8.51 (s, 2H), 7.98 (q, *J* = 8.1, 3H), 7.81 (s, 8H), 7.54 (d, *J* = 7.8, 2H), 7.40 (t, *J* = 6.8, 2H), 6.84 (bs, 3H), 4.90 (q, *J* =

15.5, 4H), 4.44 (t, *J* = 5.3, 16H), 4.21-4.16 (m, 12H), 4.11 (s, 16H), 3.77 (t, *J* = 5.3, 16H), 3.48 (m, 44H), 3.40 (m, 16H), 3.22 (s, 24H), 3.16 (s, 2H), 2.85 (t, *J* = 7.5, 16H), 2.66 (t, *J* = 7.5, 16H), 1.84 (bs, 2H), 1.52 (bs, 2H), 1.21 (s, 3H), 1.17 (s, 6H), 1.11 (s, 12H). HR-MS calc. for $C_{150}H_{230}N_{28}O_{56}Re$ $[M+2H]^{3+}$ m/z = 1169.8583. Found 1169.8525.

$[CuDPA\text{-}TEG]^{2+}$ (Cu-24): Using general procedure 6, DPA-yne (10 mg, 28.5 μmol) and TEG-N_3 (8.1 mg, 42.8 μmol) were dissolved in 0.4 mL of DMF, followed by addition of sodium ascorbate (2.3 mg, 11.6 μmol). After evacuation and backfilling with argon, $CuSO_4$ (0.7 mg, 2.9 μmol) was added in 0.1 mL H_2O. Upon completion, the reaction mixture was purified by semi-prep HPLC to yield 6.4 mg (37 %). HR-MS calc. for $C_{28}H_{40}N_7O_4Cu$ $[M]^+$ m/z = 601.244. Found 601.244.

$[CuDPA\text{-}G3\text{-}(TEG)_8]^{2+}$ (Cu-27): Using general procedure 6, DPA-G3-$(yne)_8$ (10 mg, 5.8 μmol) and TEG-N_3 (13.3 mg, 70 μmol) were dissolved in 0.4 mL of DMF, followed by addition of sodium ascorbate (3.7 mg, 18.6 μmol). After evacuation and backfilling with argon, $CuSO_4$ (1.2 mg, 4.6 μmol) was added in 0.1 mL H_2O. Upon completion, the reaction mixture was purified by semi-prep HPLC to yield 8.6 mg (45 %). HR-MS calc. for $C_{147}H_{230}N_{28}O_{53}Cu$ $[M+H]^{3+}$ m/z = 1100.5133. Found 1100.5188 (Figure S1).

2.4.5. Radiolabeling

[TcDPA-TEG]$^+$ (Tc-24): Using general procedure 7, CuDPA-TEG (1 mg, 1.66 μmol) in 0.1 mL MeOH and 1 mL of [^{99m}Tc(CO)$_3$(OH$_2$)$_3$]$^+$ (adjusted to the appropriate pH) in saline were heated under microwave irradiation for the specified amount of time (Figure S2.2-S2.4). RT: 8.90 min.

[TcDPA-G1-(TEG)$_2$]$^+$ (Tc-25): Using general procedure 7, DPA-G1-(TEG)$_2$ (0.23 mg, 250 nmol) in 0.1 mL MeOH and 1 mL of [^{99m}Tc(CO)$_3$(OH$_2$)$_3$]$^+$ in saline were heated under microwave irradiation for 5 min at 80 °C. HPLC: RT = 9.15 min. Isolated RCY: 86 ± 4 % (Figure S2.5).

[TcDPA-G2-(TEG)$_4$]$^+$ (Tc-26): Using general procedure 7, DPA-G2-(TEG)$_4$ (0.42 mg, 250 nmol) in 0.1 mL MeOH and 1 mL of [^{99m}Tc(CO)$_3$(OH$_2$)$_3$]$^+$ in saline were heated under microwave irradiation for 5 min at 80 °C. HPLC: RT = 9.09 min. Isolated RCY: 80 ± 6 %.

[TcDPA-G3-(TEG)$_8$]$^+$ (Tc-27). Using general procedure 7, [CuDPA-G3-(TEG)$_8$]$^{2+}$ (2.0 mg, 610 nmol) in 0.1 mL MeOH and 1 mL of [^{99m}Tc(CO)$_3$(OH$_2$)$_3$]$^+$ in saline adjusted to pH 5.5 were heated under microwave irradiation for 10 min at 100 °C. HPLC: RT = 9.88 min. Isolated RCY: 36 ± 4.

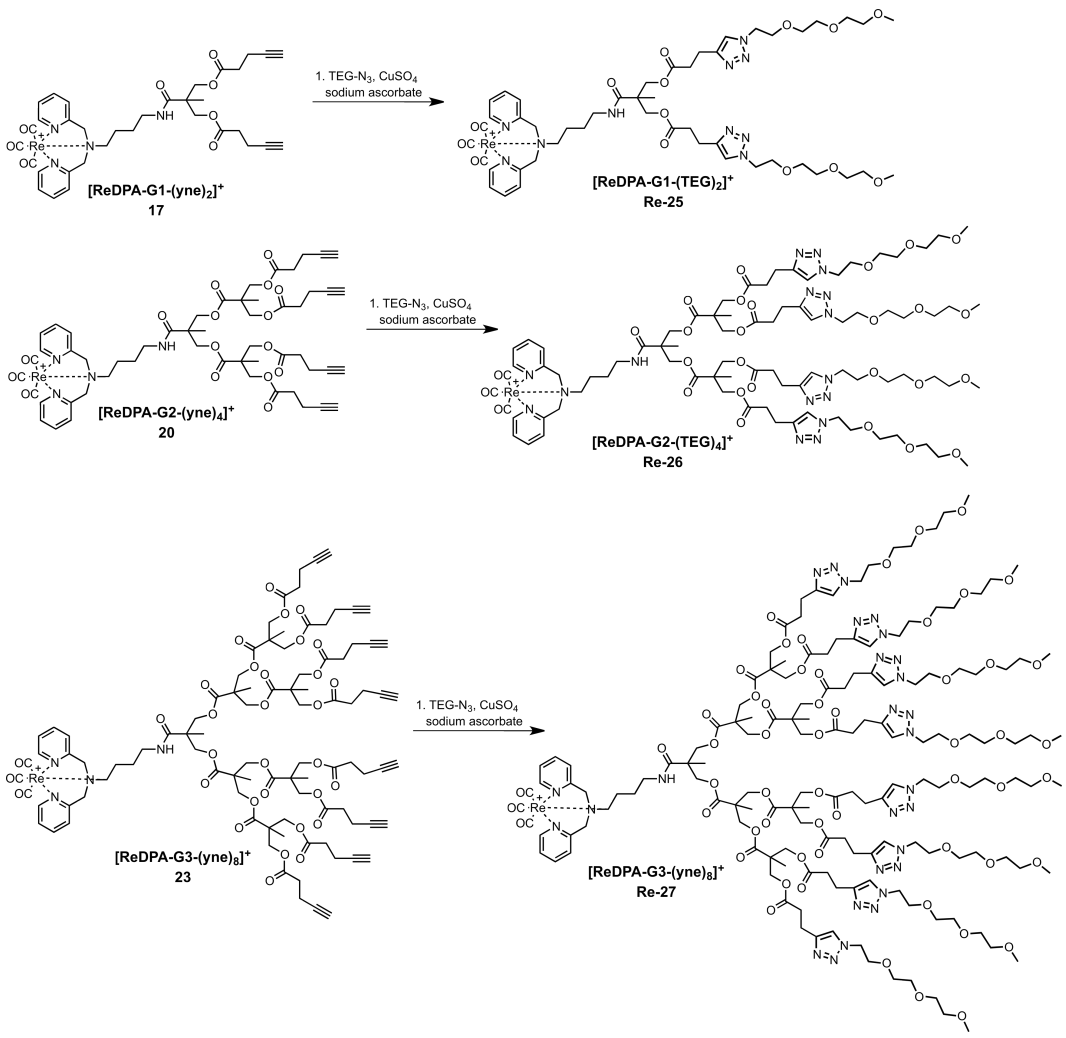

Scheme S2.1. Synthesis of TEGylated dendrimers from the rheniated alkyne-terminated precursors.

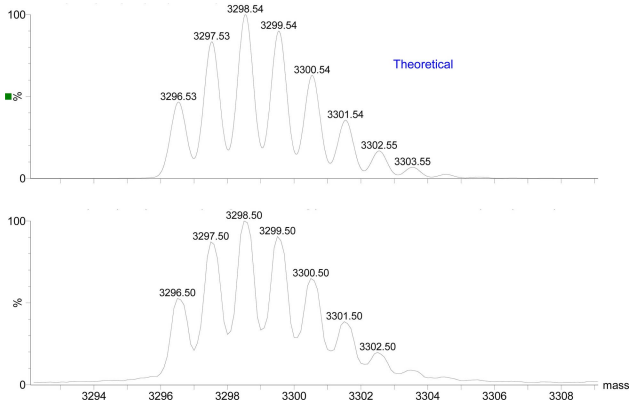

Figure S2.1. Theoretical mass spectra of $[CuDPA\text{-}G3\text{-}(TEG)_8]^{2+}$ (top) and experimental data (bottom).

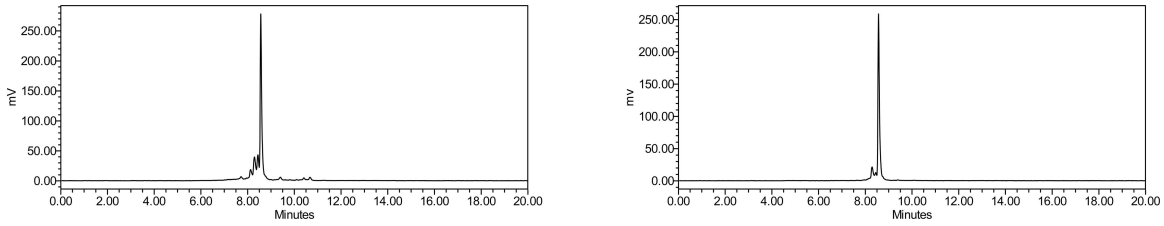

Figure S2.2. Gamma HPLC traces from the radiolabeling of $[CuDPA\text{-}TEG]^{2+}$ with $[^{99m}Tc(CO)_3(H_2O)_3]^+$ at pH 7 for 3 min at 90 °C (left) and 110 °C (right).

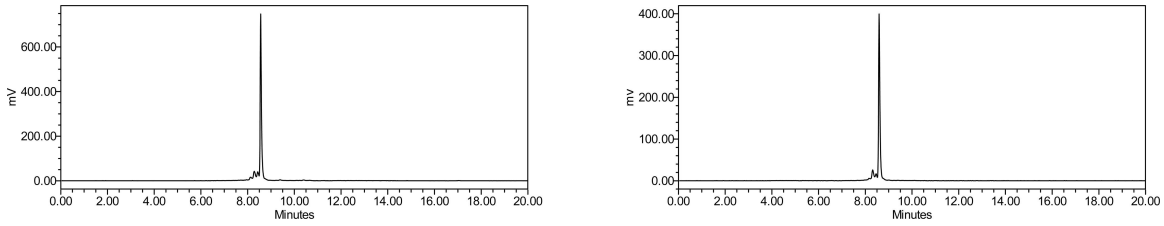

Figure S2.3. Gamma HPLC traces from the radiolabeling of $[CuDPA\text{-}TEG]^{2+}$ with $[^{99m}Tc(CO)_3(H_2O)_3]^+$ at pH 7 for 5 min at 90 °C (left) and 110 °C (right).

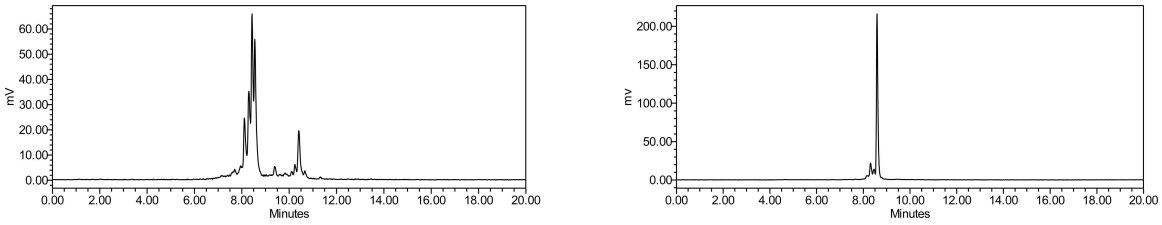

Figure S2.4. Gamma HPLC traces from the radiolabeling of $[CuDPA\text{-}TEG]^{2+}$ with $[^{99m}Tc(CO)_3(H_2O)_3]^+$ at pH 7 for 10 min at 90 °C (left) and 110 °C (right).

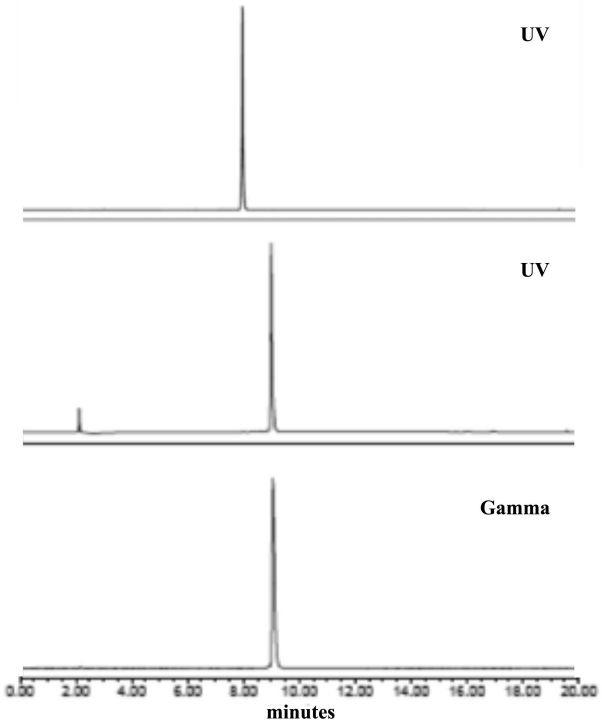

Figure S2.5. HPLC chromatograms of DPA-G1-$(TEG)_2$ (top), $[ReDPA\text{-}G1\text{-}(TEG)_2]^+$ (middle), and $[TcDPA\text{-}G1\text{-}(TEG)_2]^+$ (bottom).

2.5. References

(1) Hawker, C. J.; Fréchet, J. M. J. *Macromolecules* **1990**, *23* (21), 4726–4729.

(2) Wooley, K. L.; Hawker, C. J.; Fréchet, J. M. J. J. *Chem. Soc., Perkin Trans. 1.* **1991**, 1059-1076.

(3) Mintzer, M. A.; Grinstaff, M. W. *Chem. Soc. Rev.* **2011**, 173–190.

(4) Cheng, Y.; Zhao, L.; Xu, T. *Chem. Soc. Rev.* **2011**, *40*, 2673–2703.

(5) Svenson, S. *Eur. J. Pharm. Biopharm.* **2009**, *71* (3), 445–462.

(6) Liu, X.; Rocchi, P.; Peng, L. *New J. Chem.* **2012**, *36*, 256–263.

(7) Tang, J.; Sheng, Y.; Hu, H.; Shen, Y. *Prog. Polym. Sci.* **2013**, *38* (3-4), 462–502.

(8) Ihre, H.; Hult, A.; Soderlind, E. *J. Am. Chem. Soc.* **1996**, *118* (27), 6388–6395.

(9) Ihre, H.; Padilla De Jesús, O. L.; Fréchet, J. M. *J. Am. Chem. Soc.* **2001**, *123* (25), 5908–5917.

(10) Parrott, M. C.; Benhabbour, S. R.; Saab, C.; Lemon, J. A.; Parker, S.; Valliant, J. F.; Adronov, A. *J. Am. Chem. Soc.* **2009**, *131* (21), 2906–2916.

(11) Lee, C. C.; Gillies, E. R.; Fox, M. E.; Guillaudeu, S. J.; Fréchet, J. M. J.; Dy, E. E.; Szoka, F. C. *Proc. Natl. Acad. Sci. U. S. A.* **2006**, *103* (45), 16649–16654.

(12) Almutairi, A.; Rossin, R.; Shokeen, M.; Hagooly, A.; Ananth, A.; Capoccia, B.; Guillaudeu, S.; Abendschein, D.; Anderson, C. J.; Welch, M. J.; Fréchet, J. M. J. *Proc. Natl. Acad. Sci. U. S. A.* **2009**, *106* (3), 685–690.

(13) Ghobril, C.; Lamanna, G.; Kueny-Stotz, M.; Garofalo, A.; Billotey, C.; Felder-Flesch, D. *New J. Chem.* **2012**, *36* (2), 310–323.

(14) Malkoch, M.; Schleicher, K.; Drockenmuller, E.; Hawker, C. J.; Russell, T. P.;

Wu, P.; Fokin, V. V. *Macromolecules* **2005**, *38* (9), 3663–3678.

(15) Wu, P.; Malkoch, M.; Hunt, J. N.; Vestberg, R.; Kaltgrad, E.; Finn, M. G.; Fokin, V. V; Sharpless, K. B.; Hawker, C. J. *Chem. Comm.* **2005**, 5775–5777.

(16) Pittelkow, M.; Lewinsky, R.; Christensen, J. B. *Synthesis (Stuttg).* **2002**, *2* (15), 2195–2202.

(17) Lazarova, N.; James, S.; Babich, J.; Zubieta, J. *Inorg. Chem. Commun.* **2004**, *7* (9), 1023–1026.

(18) Ouchi, M.; Inoue, Y.; Liu, Y.; Nagamune, S.; Nakamura, S.; Wada, K.; Hakushi, T. *Bull. Chem. Soc. Jpn.* **1990**, *63* (4), 1260–1262.

(19) Benoist, E.; Coulais, Y.; Almant, M.; Kovensky, J.; Moreau, V.; Lesur, D.; Artigau, M.; Picard, C.; Galaup, C.; Gouin, S. G. *Carbohydr. Res.* **2011**, *346* (1), 26–34.

(20) Kasten, B. B.; Ma, X.; Liu, H.; Hayes, T. R.; Barnes, C. L.; Qi, S.; Cheng, K.; Bottorff, S. C.; Slocumb, W. S.; Wang, J.; Cheng, Z.; Benny, P. D. *Bioconjug. Chem.* **2014**.

(21) Knör, S.; Modlinger, A.; Poethko, T.; Schottelius, M.; Wester, H. J.; Kessler, H. *Chem. A Eur. J.* **2007**, *13* (21), 6082–6089.

(22) Alberto, R.; Ortner, K.; Wheatley, N.; Schibli, R.; Schubiger, A. P. *J. Am. Chem. Soc.* **2001**, *123* (13), 3135–3136.

(23) Snow, A. W.; Foos, E. E. *Synthesis (Stuttg).* **2003**, *2003* (04), 0509–0512.

Chapter 3 – Functionalization and Evaluation of Bis-MPA Dendrimers with Peripheral Acyloxymethyl Ketone (AOMK) Derivatives for Targeting Cathepsin B for Molecular Imaging Applications

**The contents of this chapter is part of the following manuscript:*

Sadowski, L. P., Edem, P. E., Valliant, J. F. and Adronov, A. (2016), Synthesis of Polyester Dendritic Scaffolds for Biomedical Applications. Macromol. Biosci.. doi: 10.1002/mabi.201600154.

The synthesis of azide functionalized AOMK derivatives and in vitro assays was carried out by Patricia Edem. Synthesis of AOMK functionalized dendrimers was carried out by Lukas Sadowski.

Abstract

Imaging of cathepsin B, a lysosomal cysteine protease that is overexpressed in numerous cancer types, can lead to better diagnostic tools. Herein, we examined the effect of attaching multiple cathepsin B inhibitors to the periphery of a bis-MPA dendrimer, with the aim of preparing high affinity molecular imaging agents for the visualization of cathepsin B *in vivo*. An Acyloxymethyl ketone (AOMK) derivative, which serves as a irreversible cathepsin B inhibitor was chosen as the targeting vector. Attachment of the targeting vector via different linkers was evaluated to determine the effect on the length and type of linker used. Although mono-valent AOMK derivatives demonstrated good affinity towards cathepsin B (K_i = 350-440 nM), multivalent AOMK inhibitors demonstrated poor affinity towards the enzyme.

3.1. Introduction

The discreet, stepwise synthesis of dendrimers allows the production of well-defined, monodisperse structures that can be precisely modified at their core, interior, and periphery.[1–4] This enables the preparation of modular, multi-functional macromolecules that are useful in a range of biomedical applications,[5–9] including as drug delivery and gene transfection agents,[10–16] tissue repair scaffolds,[17,18] and vehicles for magnetic resonance imaging (MRI) contrast agents.[19–22] In particular, poly(2,2-bis(hydroxymethyl)propanoic acid) (PMPA) dendrimers are ideally suited for biological applications due to their intrinsic biocompatibility, hydrophilicity, rapid clearance *in vivo* and the lack of undesirable non-specific binding.[23–25] The PMPA dendrimer structure has been demonstrated as an efficient drug delivery vehicle for doxorubicin, allowing complete regression of colon carcinoma cells in mice after a single treatment.[26] In addition, the multi-valent periphery of dendrimers allows them to display multiple copies of targeting or therapeutic moieties on their surface. Multi-valent interactions between the plurality of peripheral ligands and multiple copies of a receptor on a cell surface or in extracellular spaces can lead to enhanced efficiency of binding between a macromolecule and its biological target.[27–35] This has been demonstrated using the PMPA dendrimer backbone for the preparation of a nuclear molecular imaging probe used to visualize angiogenesis. Attachment of multiple RGD units to the dendrimer periphery via a poly(ethylene glycol) (PEG) spacer[36] led to a 50-fold improvement in affinity to the $\alpha_v\beta_3$ receptors, relative to the mono-valent model compound, while exhibiting improved clearance from non-target tissue. Thus, radiolabeled dendritic structures are ideal for

applications in diagnostic radioimaging, including positron emission tomography (PET) and single photon emission computed tomography (SPECT).[25,37] However, broad applicability of dendrimers in diagnostic imaging requires efficient decoration of the dendrimer periphery with appropriate targeting vectors that promote binding to sites of disease.

Cathepsin B (CB) is a cysteine protease capable of degrading laminin, fibronectin, and type IV collagen within the extracellular matrix.[38] This enzyme is known to be overexpressed at the invasive edge of aggressively growing metastatic tumors, and has attracted significant interest as a target for diagnostic imaging agents, as it has the potential to enable early-stage detection of tumors and improve the outcome for cancer patients.[39–43] Peptidyl acyloxymethyl ketones (AOMKs) are a class of compounds known to selectively and irreversibly inhibit cysteine proteases, such as cathepsins B, L, S, and X, by alkylating a cysteine residue in the active site, forming a thioether.[44–46] AOMKs can therefore serve as effective targeting vectors for sites of CB overexpression, and have been coupled to optical imaging and near infrared fluorescent (NIRF) agents to investigate protease activity in living organisms.[41,42,47] More recently, activity-based probes (ABPs) for CB, modeled after the AOMK structure, that can be used for PET imaging have been developed by coupling an AOMK derivative to 1,4,7,10-tetraazacyclododecane-1,4,7,10-tetraacetic acid (DOTA) and subsequently radiolabeling with ^{64}Cu.[43] The resulting imaging agent was found to exhibit low tumor uptake, but nevertheless allowed for visualization of tumor tissue with reasonable signal to noise levels.[43] Iodinated AOMKs were also developed where different linkers containing aryl

iodides were tested for their affinity for cathepsin B. Lead compounds were then radiolabeled and tested in murine tumor models. Although these compounds were able to detect cathepsin B activity *in vitro*, they underwent deiodination *in vivo*, thus exhibiting low tumor uptake.[48] Encouraged by this work, we set out to derivatize the periphery of a PMPA dendrimer with multiple AOMK ligands using different length linkers, with the aim of investigating the effect of linker chemistry and multivalent interactions on affinity to cathepsin B. More broadly, we present a dendritic platform for applications in targeted molecular imaging. The PMPA dendron structure consists of a core carboxylic acid that enables precise attachment of a single radiolabel,[25] while the periphery is functionalized with terminal alkyne groups, which allow facile attachment of targeting ligands under mild conditions using the Cu catalyzed azide alkyne cycloaddition (CuAAC) reaction. In our studies, we show that an azide derivative of the AOMK inhibitor for CB can be coupled to the dendron periphery using CuAAC. The attachment of a bis(picolyl) amine ligand to the core of the dendrimer allows for coordination to ^{99m}Tc for SPECT imaging. Overall, the modular dendrimer platform we describe can be applied to a number of different imaging modalities and a variety of disease targets by changing the functionality at the core and the periphery, respectively.

3.2. Results and Discussion

3.2.1. Synthesis of AOMK Derivatives with Different Spacers

Having developed the platform for functionalizing the dendrimer periphery under mild conditions, and radiolabeling the core with ^{99m}Tc, we investigated the ability to introduce multiple AOMK targeting agents for cathepsin B at the dendrimer periphery. This was accomplished by converting the free amine of the lysine residue on AOMK, prepared according to literature procedures,[48] to an azide functionality via amidation with either an aliphatic azide-terminated acid of various length, or a commercially available triethylene glycol unit bearing an azide on one end and an acid group on the other (Scheme 3.1). In order to determine the effect of spacer length, the aliphatic chains used for amidation included a C_2, C_4, or C_6 chain length. The triethylene glycol linker was employed to determine the effect of introducing greater hydrophilicity to the dendrimer periphery. Coupling of the azide linkers to the AOMK derivative was accomplished at room temperature using isobutyl chloroformate (IBCF) or benzotriazol-1-yl-oxytripyrrolidinophosphonium hexafluorophosphate (PyBOP) to form the amide bond between the inhibitor and azide functionalized linker (Scheme 3.1).[49] This mild coupling strategy was required as the AOMK derivative tends to epimerize upon treatment with strong acids, bases, or heat, which results in a loss of affinity toward cathepsin B.

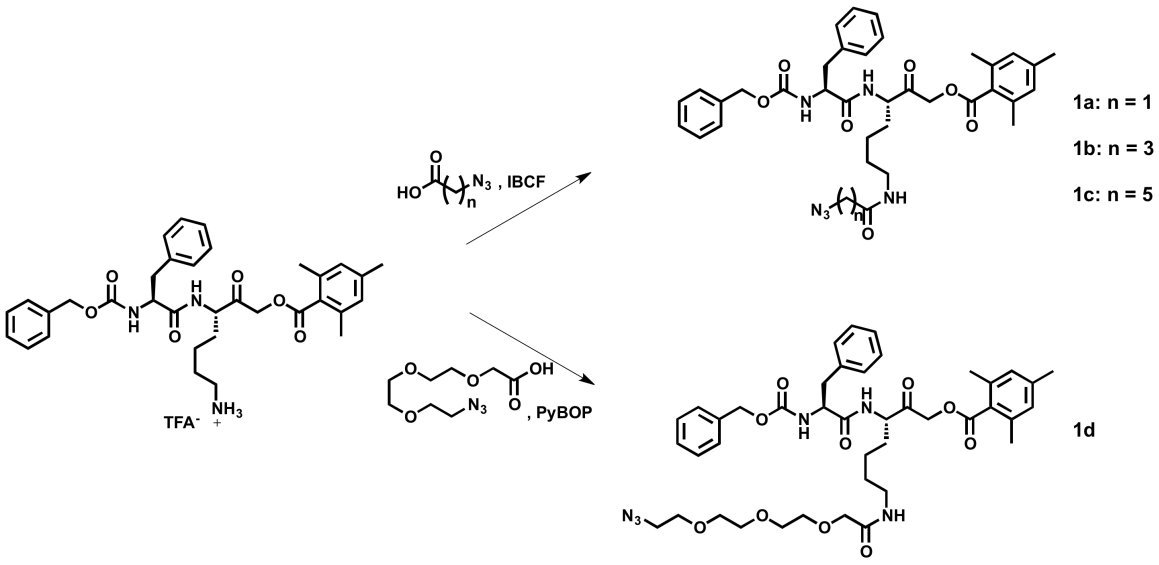

Scheme 3.1. Preparation of AOMK targeting ligands attached to an azide group via different linkers.

3.2.2. Conjugation of Targeting Ligands and *in vitro* Evaluation

The AOMK analogues bearing C_2, C_4, and C_6 spacers (**1a-c**) were first coupled to $[ReDPA\text{-}G1\text{-}(yne)_2]^+$ to produce first-generation dendrimers **3-5** (Figure 3.1), allowing determination of the effect of spacer length. A colorimetric kinetic assay previously employed to evaluate iodinated AOMK derivatives[48] was used to determine the binding affinities of the non-radioactive imaging agent analogues (for details, see experimental section). Briefly cathepsin B, isolated from human liver, was added to solutions of the colorimetric cathepsin B substrate (Z-RR-pNA) and the AOMK derivatives. Enzyme activity was monitored over time by measuring the release of para-nitroanilide by measuring absorption at 405 nm. From this data, the inhibition and second-order rate constants (K_i and k_i/K_i, respectively) were determined.

In vitro evaluation of compounds **3**-**5** revealed that attachment of the AOMK to the dendrimer via the C_4 spacer (compound **4**) displayed the best affinity toward cathepsin B among the G1 derivatives (Figure 3.2A). Thus, the C_4 derivative of AOMK (**1b**) was coupled to $[ReDPA\text{-}G2\text{-}(yne)_4]^+$ and its monovalent analogue $[ReDPA\text{-}yne]^+$, to produce compounds **8** and **2**, respectively (Figure 3.1). Furthermore, the analogous dendron series bearing the more hydrophilic TEG spacer was prepared via the attachment of **1d** to the G0, G1, and G2 dendrons, producing compounds **2**, **7**, and **9** (Figure 3.1). Attachment of the AOMK targeting ligands to the dendron periphery was carried out using $CuSO_4$/Na ascorbate in DMF under Ar. The reaction was followed by LC-MS, which indicated rapid disappearance of the dendron starting material and no detectable partially functionalized dendrimer present after 8 h. Removal of any residual copper was accomplished by semi-preparative HPLC.

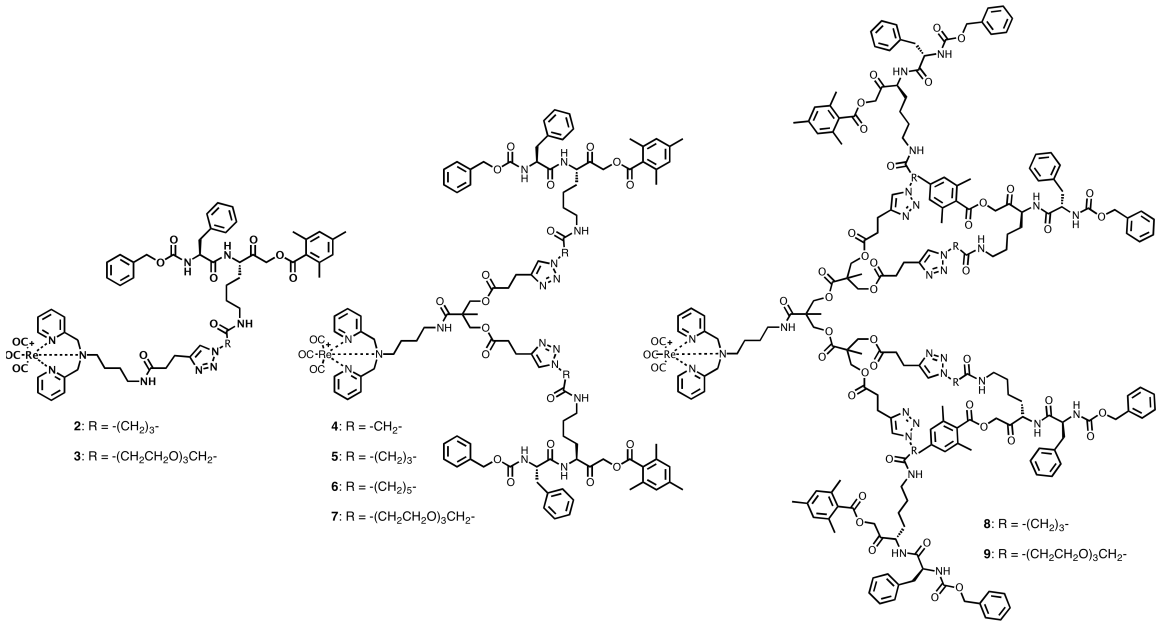

Figure 3.1. Structures of the investigated AOMK-dendrimer conjugates.

The resulting affinity of the AOMK-dendrimer conjugates proved to not only be sensitive to the spacer length, but also its hydrophobicity, as summarized in Figure 3.2. The monovalent G0 analogues **2** and **3** had the highest affinity toward cathepsin B, with second-order rate constants (k_i/K_i) of 13,400 ± 700 and 11,300 ± 400 $s^{-1}M^{-1}$ (Figure 3.2B) and K_i values of 350 ± 40 nM and 440 ± 20 nM respectively (data not shown). Unfortunately, the attachment of multiple copies of AOMK resulted in a decrease in affinity, likely due to steric effects and possibly also to the hydrophobicity of the molecules (Figure 3.2B). A similar trend was observed by Liskamp and co-workers in their preparation and evaluation of [Try^3]octeotride multivalent radioimaging probes targeting somatostatin receptors.[50,51] In that study, the authors attributed the decreased affinity to increasing lipophilicity of the multivalent targeted derivatives. For this reason, the TEG spacer was utilized in an attempt to increase the hydrophilicity of the targeting vectors. Surprisingly, the dendrimer-TEG-AOMK derivatives exhibited even lower affinity toward cathepsin B. This result may be attributed to aggregation of the hydrophobic AOMK ligands to form multi-dendrimer assemblies that internalize the ligands, making them inaccessible to the enzyme. Alternatively, it is possible that the AOMK structures undergo backfolding in aqueous solution, exposing the triethylene glycol chains to the dendrimer periphery, which sterically block their access to the active site of cathepsin B.

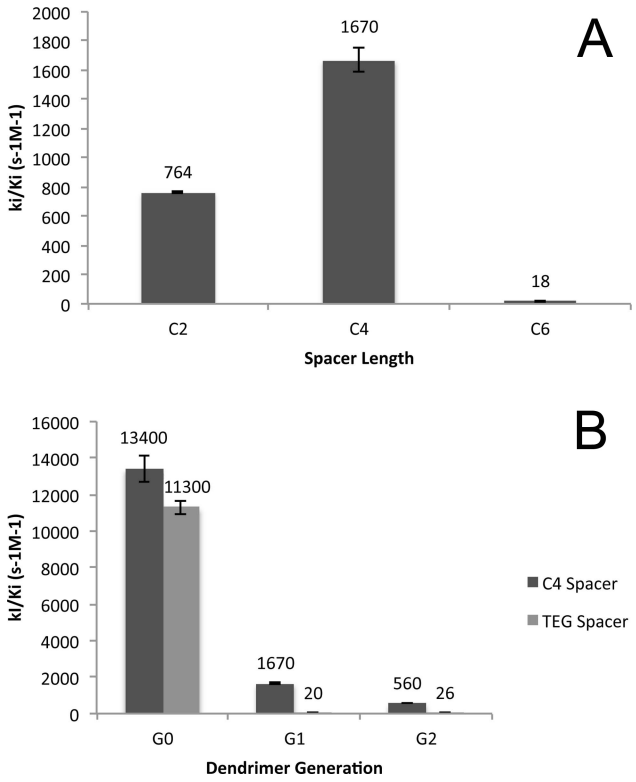

Figure 3.2. Comparison of second-order rate constants for G1 dendrimer with different length alkyl linkers (A) and comparison of second-order rate constant between the C4 and TEG spacers on different generation dendrimers (B).

3.3. Conclusions

A series of derivatives bearing different spacers between the AOMK derivative and the dendrimer reveal the importance of the spacer. Although affinity of the AOMK-dendrimer conjugates increases with increasing spacer length, a decrease in affinity is observed with increasing generation. Imparting hydrophilicity while extending the spacer length with a short TEG spacer did not resolve the problem. We hypothesize that hydrophobicity coupled with steric congestion around the periphery of the dendrimer

results in the ligand being unable to access the active site of the enzyme. Thus, efficient coupling of complex macromolecules to the periphery of dendrimers has been demonstrated, however, AOMK derivatives are not suitable for taking advantage of the multivalent platform offered herein. Future work will explore this dendrimer scaffold with other targeting ligands that can take advantage of multivalent binding.

3.4. Experimental

3.4.1. General

All chemicals, unless otherwise stated, were purchased from Sigma−Aldrich, TCI, GFS, Novabiochem, or Bachem and used without further purification. For screening studies, human liver cathepsin B and Cbz-Arg-Arg- pNA were purchased from Calbiochem and Enzo Life Sciences, respectively. (S)-5-((S)-2-(((Benzyloxy)carbonyl)amino)-3-phenylpropan-amido)-6-oxo-7-((2,4,6-trimethylbenzoyl)oxy)heptan-1-ammonium trifluoroacetate was synthesized as previously described.[48] NMR spectra were collected on a Bruker Avance 600 MHz NMR spectrometer and calibrated to the solvent peak. A Micromass QTOF Global Ultima was used to obtain exact masses and HPLC was conducted on an Agilent HPLC equipped with PDA detector and a Phenomenex Luna C18 column. Reagents used in the assay buffer were from Sigma Aldrich. Inhibitors were dissolved in biological-grade DMSO and diluted in the assay buffer. Black, clear-bottom 96-well plates were obtained from BD Biosciences. L-3-Trans-(propylcarbamyl)oxirane-2- carbonyl-L-isoleucyl-L-proline (CA-074) was obtained from EMD Biosciences, precast gels were from Bio-Rad, and the gel drying kit was from Promega. According to HPLC analysis, supported by ^{1}H and ^{13}C NMR spectroscopy and high-resolution mass spectrometry (HRMS), the chemical purity of all compounds screened for cathepsin B inhibition was >95%.

General procedure for CuAAC. 1 eq of ReDPA-Gx-$(yne)_y$, 1.2 eq of azide/alkyne and 0.8 eq/alkyne of sodium ascorbate were dissolved in DMF. The flask was evacuated

under vacuum and backfilled with nitrogen three times. 0.2 eq/alkyne of $CuSO_4$ in H_2O was added to the reaction vessel and stirred at room temperature overnight. The crude reaction mixture was concentrated by rotary evaporation and purified by semi-prep HPLC to afford the product. A method comprised of water and acetonitrile as eluents, each containining 0.1% formic acid, was utilized. For AOMK functionalized dendrimers, the HPLC method was as follows: A gradient of 97% water to 5% water over 15 minutes, followed by 3 minutes at 5% water. This was followed by a sharp gradient to 97% water over 1 minute and re-equilibration at 97% water over 4 minutes.

3.4.2. Synthesis

(S)-7-(2-azidoacetamido)-3-((S)-2-(((benzyloxy)carbonyl)amino)-3-phenylpropanamido)-2-oxoheptyl 2,4,6-trimethylbenzoate – AOMK-C_2-N_3 (1a). In a flame dried round bottom flask containing a solution of azidoacetic acid[52] (35.4 mg, 350 μmol) in $CHCl_3$ (5 mL) at -20 °C, NMM (38 μL, 350 μmol) and IBCF (45 μL, 350 μmol) were added and left to stir for 1 min. To this, (S)-5-((S)-2-(((Benzyloxy)carbonyl)amino)-3-phenylpropanamido)-6-oxo-7-((2,4,6-trimethylbenzoyl)oxy)heptan-1-ammonium trifluoroacetate[48] (246 mg, 350 μmol) and NMM (38 μL, 350 μmol) were added and the solution was left to stir overnight while warming to room temperature. The solvent was removed under reduced pressure, EtOAc (25 mL) was added, and then extracted with sat. $NaHCO_3$ (3 × 15 mL), water (20 mL), 5% (w/v) citric acid (3 × 15 mL), water (20 mL), brine (20 mL) and dried over Na_2SO_4. The solvent was removed by rotary evaporation and the product was isolated as a white solid following column chromatography using

EtOAc/hexanes (2:1). Yield (35.1 mg, 15%). TLC (2:1 EtOAc/Hex): R_f = 0.28. ^{1}H NMR (500 MHz; DMSO): δ 8.50 (d, *J* = 7.5, 1H), 8.06 (t, *J* = 5.3, 1H), 7.64 (d, *J* = 8.2, 1H), 7.34-7.18 (m, 10H), 6.92 (s, 2H), 4.97 (s, 2H), 4.90 (d, *J* = 17.2, 1H), 4.80 (d, *J* = 17.2, 1H), 4.37-4.31 (m, 2H), 3.79 (s, 2H), 3.10-3.01 (m, 3H), 2.82 (dd, *J* = 13.5, 9.8, 1H), 2.27 (s, 6H), 2.25 (s, 3H), 1.84-1.77 (m, 1H), 1.61-1.53 (m, 1H), 1.46-1.36 (m, 2H), 1.35-1.23 (m, 2H). ^{13}C NMR (126 MHz; DMSO): δ 202.5, 171.8, 168.0, 166.8, 155.7, 138.9, 137.6, 136.8, 134.8, 129.8, 129.1, 128.10, 128.06, 127.92, 127.53, 127.35, 126.2, 66.4, 65.1, 55.9, 55.7, 50.6, 38.2, 37.1, 28.9, 28.3, 22.1, 20.5, 19.2.

(S)-7-(4-azidobutanamido)-3-((S)-2-(((benzyloxy)carbonyl)amino)-3-phenylpropanamido)-2-oxoheptyl 2,4,6-trimethylbenzoate – AOMK-C_4-N_3 (1b). In a flame dried round bottom flask containing a solution of 4-azidobutanoic acid[53] (73.6 mg, 570 μmol) in THF (12 mL) at -30 °C, NMM (63 μL, 570 μmol) and IBCF (75 μL, 570 μmol) were added and left to stir 20 min. under Ar. To this, (S)-5-((S)-2-(((Benzyloxy)carbonyl)amino)-3-phenylpropanamido)-6-oxo-7-((2,4,6-trimethylbenzoyl)oxy)heptan-1-ammonium trifluoroacetate[48] (400 mg, 570 μmol) and NMM (126 μL, 1.14 mmol) were added and the solution was left to stir overnight while warming to room temperature. The solvent was removed under reduced pressure, CH_2Cl_2 (50 mL) was added, and then extracted with sat. $NaHCO_3$ (3 × 20 mL), water (30 mL), 5% (w/v) citric acid (3 × 20 mL), water (30 mL), brine (3 × 20 mL) and the organic layer dried over Na_2SO_4. The solvent was removed by rotary evaporation and the product was isolated as a white solid following flash chromatography using a gradient of 50%-66%

EtOAc/hexanes (2:1). Yield (187 mg, 47%). TLC (5% MeOH/CH_2Cl_2): R_f = 0.46. ^{1}H NMR (600 MHz; DMSO): δ 8.49 (d, *J* = 7.5, 1H), 7.81 (t, *J* = 5.4, 1H), 7.63 (d, *J* = 8.3, 1H), 7.34-7.18 (m, 10H), 6.92 (s, 2H), 4.96 (s, 2H), 4.90 (d, *J* = 17.2, 1H), 4.80 (d, *J* = 17.2, 1H), 4.36-4.31 (m, 2H), 3.29 (t, *J* = 6.8, 2H), 3.04-3.01 (m, 3H), 2.83-2.79 (m, 1H), 2.27 (s, 6H), 2.25 (s, 3H), 2.13 (t, *J* = 7.4, 2H), 1.81-1.77 (m, 1H), 1.76-1.70 (m, 2H), 1.58-1.53 (m, 1H), 1.42-1.23 (m, 4H). ^{13}C NMR (151 MHz; DMSO): δ 202.6, 172.0, 170.9, 168.2, 155.8, 139.1, 137.8, 136.9, 134.9, 129.9, 129.24, 129.20, 128.26, 128.22, 128.08, 127.69, 127.50, 126.3, 66.6, 65.3, 56.04, 55.88, 50.3, 38.2, 37.2, 32.2, 29.1, 28.7, 24.5, 22.4, 20.7, 19.3. HRMS Calcd. for $C_{38}H_{46}N_6O_7Na$ $[M+Na]^+$: 721.3326. Found: 721.3312.

(S)-7-(6-Azidohexanamido)-3-((S)-2-(((benzyloxy)carbonyl)amino)-3-phenylpropanamido)-2-oxoheptyl 2,4,6-trimethylbenzoate – AOMK-C_6-N_3 (1c). In a flame dried round bottom flask containing PyBOP (291 mg, 560 μmol) and 6-azidohexanoic acid[54] (88 mg, 560 μmol) were dissolved in anhydrous DMF (10 mL) under Ar at 0 °C. Et_3N (78 μL, 560 μmol) was added the reaction was left to stir for 5 min. Et_3N (156 μL, 1.12 mmol) and (S)-5-((S)-2-(((Benzyloxy)carbonyl)amino)-3-phenylpropanamido)-6-oxo-7-((2,4,6-trimethylbenzoyl)oxy)heptan-1-ammonium trifluoroacetate[48] (393 mg, 560 μmol) were added and the reaction was stirred at room temperature for 16 h. Water (15 mL) was added and the mixture was extracted with CH_2Cl_2 (3 × 15 mL). The combined organic fractions were extracted with sat. $NaHCO_3$ (3 × 15 mL), brine (3 × 15 mL) and dried over $MgSO_4$. The solvent was removed under

reduced pressure and the product was isolated following flash chromatography using a gradient of 1% - 20% MeOH/CH_2Cl_2 as a white solid. Yield (250 mg, 66%). TLC (5%MeOH/CH_2Cl_2): R_f = 0.49. ^{1}H NMR (600 MHz; DMSO): δ 8.50 (d, *J* = 7.5, 1H), 7.74 (t, *J* = 5.7, 1H), 7.64 (d, *J* = 8.3, 1H), 7.35-7.19 (m, 10H), 6.93 (s, 2H), 4.98 (d, *J* = 6.7, 2H), 4.92 (d, *J* = 17.2, 1H), 4.81 (d, *J* = 17.2, 1H), 4.37-4.33 (m, 2H), 3.30-3.27 (m, 3H), 2.85-2.82 (m, 1H), 2.28 (s, 6H), 2.26 (s, 3H), 2.07-2.04 (m, 2H), 1.84-1.77 (m, 1H), 1.61-1.56 (m, 1H), 1.53-1.49 (m, 5H), 1.41-1.30 (m, 3H), 1.30-1.26 (m, 4H). ^{13}C NMR (151 MHz; DMSO): δ 202.6, 172.0, 171.7, 168.2, 155.9, 139.1, 137.8, 136.9, 134.9, 129.9, 129.2, 128.26, 128.22, 128.08, 127.69, 127.50, 126.3, 66.6, 65.3, 56.05, 55.90, 50.5, 38.1, 37.2, 35.2, 29.1, 28.8, 28.0, 25.8, 24.8, 22.4, 20.7, 19.3. HRMS Calcd. for $C_{40}H_{51}N_6O_7$ $[M+H]^+$: 727.3819. Found: 727.3844.

(S)-1-azido-17-((S)-2-(((benzyloxy)carbonyl)amino)-3-phenylpropanamido)-11,18-dioxo-3,6,9-trioxa-12-azanonadecan-19-yl 2,4,6-trimethylbenzoate – AOMK-TEG-N_3 (1d). In a flame dried round bottom flask containing a solution of 11-azido-3,6,9-trioxoundecanoic acid (70 mg, 300 mmol) in THF (12 mL) at -18 °C, NMM (33 µL, 300 µmol) and IBCF (40 µL, 300 µmol) were added and left to stir 20 min. To this, (S)-5-((S)-2-(((Benzyloxy)carbonyl)amino)-3-phenylpropanamido)-6-oxo-7-((2,4,6-trimethylbenzoyl)oxy)heptan-1-ammonium trifluoroacetate (211 mg, 300 µmol) was added and the solution was left to stir overnight while warming to room temperature. The solvent was removed under reduced pressure, CH_2Cl_2 (25 mL) was added, and the solution was extracted with water (10 mL), sat. $NaHCO_3$ (3 × 10 mL), water (10 mL), 5%

(w/v) citric acid (3 × 10 mL), water (10 mL), brine (3 × 10 mL) and dried over Na_2SO_4. The solvent was removed by rotary evaporation and the product was isolated as a yellow oil following flash chromatography using a gradient of 1% - 10% MeOH/CH_2Cl_2. Yield (154 mg, 64%). TLC (5%MeOH/CH_2Cl_2): R_f = 0.33. ^{1}H NMR (600 MHz; DMSO): δ 8.50 (t, *J* = 6.8, 1H), 7.67-7.64 (m, 1H), 7.64-7.62 (m, 1H), 7.35-7.19 (m, 10H), 6.93 (s, 2H), 4.98 (s, 2H), 4.92 (d, *J* = 17.2, 1H), 4.82 (d, *J* = 17.2, 1H), 4.37-4.32 (m, 2H), 3.87 (s, 2H), 3.61-3.55 (m, 10H), 3.39 (t, *J* = 4.9, 2H), 3.12-3.08 (m, 2H), 3.05-3.02 (m, 1H), 2.84-2.80 (m, 1H), 2.28 (s, 6H), 2.26 (s, 3H), 1.84-1.78 (m, 1H), 1.62-1.55 (m, 1H), 1.47-1.37 (m, 2H), 1.38-1.24 (m, 2H). 13-C NMR (151 MHz; DMSO): δ 202.6, 172.0, 169.0, 168.2, 164.2, 139.1, 137.8, 134.9, 133.1, 129.9, 129.2, 128.26, 128.22, 128.08, 127.69, 127.51, 126.3, 70.2, 70.0, 69.76, 69.65, 69.55, 69.2, 66.6, 65.3, 50.0, 37.8, 37.3, 29.1, 28.8, 22.3, 20.7, 19.3. HRMS Calcd. for $C_{42}H_{55}N_6O_{10}$ $[M+H]^+$: 803.3980. Found: 803.3964.

[ReDPA-(C_4-AOMK)]$^+$ (2): Using the general procedure, [ReDPA-(Pentynoic alkyne)]$^+$ (10 mg, 16.1 μmol) and AOMK-C_4-N_3 (14 mg, 20 μmol) were dissolved in 0.4 mL of DMF, followed by addition of sodium ascorbate (2.6 mg, 12.9 μmol). After evacuation and backfilling with argon, $CuSO_4$ (0.8 mg, 3.2 μmol) was added in 0.1 mL H_2O. Upon completion, the reaction mixture was purified by semi-prep HPLC to yield 13.6 mg of product as a white solid (64 %). ^{1}H NMR (600 MHz; DMSO): δ 8.81 (d, *J* = 5.4, 2H), 8.52-8.51 (d, *J* = 7.2, 1H), 8.01-7.96 (m, 3H), 7.83-7.81 (m, 2H), 7.65-7.64 (d, *J* = 8.4, 1H), 7.56 (d, *J* = 7.9, 2H), 7.40 (t, *J* = 6.6, 2H), 7.34-7.26 (m, 9H), 7.22-7.19 (m, 1H),

6.92 (s, 2H), 4.97-4.79 (m, 8H), 4.36-4.32 (m, 2H), 4.30-4.26 (t, *J* – 6.6, 2H), 3.80-3.75 (m, 4H), 3.63-3.59 (t, *J* = 6.0, 1H), 3.16-3.13 (q, *J* = 6.0, 2H), 3.05-2.99 (m, 3H), 2.90-2.74 (m, 4H), 2.47-2.44 (t, *J* = 7.2, 2H), 2.26-2.24 (m, 9H), 2.08-2.04 (m, 3H), 2.01-1.97 (quintet, *J* = 6.6, 2H), 1.84-1.76 (m, 4H), 1.58-1.46 (m, 3H), 1.40-1.22 (m, 6H). HR-MS calc. for $C_{62}H_{75}N_{10}O_{11}Re$ $[M]^{2+}$ m/z = 660.2506. Found 660.2530.

[ReDPA-(TEG-AOMK)]$^+$ (3): Using the general procedure, [ReDPA-(Pentynoic alkyne)]$^+$ (10 mg, 16.1 μmol) and AOMK-TEG-N_3 (16 mg, 19.3 μmol) were dissolved in 0.4 mL of DMF, followed by addition of sodium ascorbate (2.6 mg, 12.9 μmol). After evacuation and backfilling with argon, $CuSO_4$ (0.8 mg, 3.2 μmol) was added in 0.1 mL H_2O. Upon completion, the reaction mixture was purified by semi-prep HPLC to yield 15.8 mg of product as a white solid (69 %). ^{1}H NMR (600 MHz; DMSO): δ 8.74 (d, *J* = 5.1, 2H), 8.44 (d, *J* = 7.5, 1H), 7.93-7.89 (m, 3H), 7.73 (s, 1H), 7.61 (t, *J* = 5.9, 1H), 7.56 (d, *J* = 8.3, 1H), 7.49 (d, *J* = 7.9, 2H), 7.33 (t, *J* = 6.6, 2H), 7.30-7.16 (m, 9H), 7.17-7.11 (m, 1H), 6.85 (s, 2H), 4.90-4.73 (m, 8H), 4.38 (t, *J* = 5.3, 2H), 4.29-4.23 (m, 2H), 3.79 (s, 2H), 3.74-3.65 (m, 4H), 3.45-3.42 (m, 37H), 3.08 (q, *J* = 6.4, 2H), 3.01 (q, *J* = 6.6, 2H), 2.96 (dd, *J* = 13.5, 5.2, 1H), 2.79 (t, *J* = 7.7, 2H), 2.75 (dd, *J* = 13.7, 9.9, 1H), 2.38 (t, *J* = 7.7, 2H), 2.19 (d, *J* = 11.8, 9H), 1.75-1.73 (m, 3H), 1.52-1.49 (m, 1H), 1.42 (quintet, *J* = 7.1, 2H), 1.37-1.32 (m, 2H), 1.29-1.13 (m, 3H). HR-MS calc. for $C_{66}H_{80}N_{10}O_{14}Re$ $[M+H]^{2+}$ m/z = 712.2743. Found 712.2736.

[ReDPA-G1-(C_2-AOMK)$_2$]$^+$ (4): Using the general procedure, [ReDPA-G1-(yne)$_2$]$^+$ (1.4 mg, 1.7 μmol) and AOMK-C_2-N_3 (2.6 mg, 3.6 μmol) were dissolved in 0.4 mL of DMF, followed by addition of sodium ascorbate (0.5 mg, 2.7 μmol). After evacuation and backfilling with argon, $CuSO_4$ (0.2 mg, 0.7 μmol) was added in 0.1 mL H_2O. Upon completion, the reaction mixture was purified by semi-prep HPLC to yield 2.3 mg of a white solid (63 %). HR-MS calc. for $C_{106}H_{121}N_{16}O_{22}Re$ $[M+H]^{2+}$ m/z = 1079.4277. Found 1079.4310.

[ReDPA-G1-(C_4-AOMK)$_2$]$^+$ (5): Using the general procedure, [ReDPA-G1-(yne)$_2$]$^+$ (10 mg, 12.2 μmol) and AOMK-C_4-N_3 (21 mg, 30.1 μmol) were dissolved in 0.4 mL of DMF, followed by addition of sodium ascorbate (3.9 mg, 19.5 μmol). After evacuation and backfilling with argon, $CuSO_4$ (1.2 mg, 4.9 μmol) was added in 0.1 mL H_2O. Upon completion, the reaction mixture was purified by semi-prep HPLC to yield 13.0 mg of product as a white solid (48 %). ^{1}H NMR (600 MHz; DMSO): δ 8.73 (d, *J* = 5.4, 2H), 8.47 (m, 4H), 7.90 (t, *J* = 7.8, 2H), 7.80 (t, *J* = 5.6, 1H), 7.75 (s, 4H), 7.60-7.58 (m, 2H), 7.46 (t, *J* = 7.0, 2H), 7.34-7.31 (t, *J* = 5.4, 2H), 7.26-7.18 (m, 18H), 7.12 (m, 2H), 6.84, (s, 4H), 4.89-4.71 (m, 12H), 4.29-4.24 (m, 4H), 4.18 (t, *J* = 7.0, 4H), 4.07 (q, *J* = 13.8, 4H), 3.73-3.69 (m, 2H), 3.08 (dt, *J* = 10.3, 5.0, 2H), 2.96-2.93 (m, 6H), 2.79 (t, *J* = 7.4, 4H), 2.60 (t, *J* = 7.5, 4H), 2.19 (m, 18H), 1.97-1.96 (m, 4H), 1.90 (quintet, *J* = 6.6, 4H),1.75-1.69 (m, 4H), 1.52-1.41 (m, 4H), 1.35-1.16 (m, 8H), 1.07-1.03 (s, 3H). HR-MS calc. for $C_{110}H_{129}N_{16}O_{22}Re$ $[M+H]^{2+}$ m/z = 1107.4591. Found 1107.5606.

[ReDPA-G1-(C_6-AOMK)$_2$]$^+$ (6): Using the general procedure, [ReDPA-G1-(yne)$_2$]$^+$ (10 mg, 12.2 μmol) and AOMK-C_6-N_3 (22 mg, 30.3 μmol) were dissolved in 0.4 mL of DMF, followed by addition of sodium ascorbate (3.9 mg, 19.5 μmol). After evacuation and backfilling with argon, $CuSO_4$ (1.2 mg, 4.9 μmol) was added in 0.1 mL H_2O. Upon completion, the reaction mixture was purified by semi-prep HPLC to yield 16.1 mg of product as a white solid (58 %). ^{1}H NMR (600 MHz; DMSO): δ 8.80 (d, *J* = 5.7, 2H), 8.50 (d, *J* = 7.4, 2H), 8.12 (s, 1H), 8.03-7.94 (m, 3H), 7.86 (t, *J* = 5.8, 1H), 7.81 (s, 2H), 7.72 (t, *J* = 6.2, 2H), 7.64 (d, *J* = 8.1, 1H), 7.52 (d, *J* = 7.7, 2H), 7.39 (t, *J* = 7.1, 2H), 7.34-7.24 (m, 12H), 7.20 (q, *J* = 6.4, 2H), 6.92 (s, 4H), 4.96-4.79 (m, 12H), 4.64 (d, *J* = 6.9, 2H), 4.34 (dt, *J* = 15.6, 6.9, 4H), 4.22 (t, *J* = 7.1, 4H), 4.18-4.11 (m, 4H), 3.78 (t, *J* = 8.0, 2H), 3.16 (q, *J* = 6.7, 2H), 3.05-2.94 (m, 6H), 2.90-2.80 (m, 6H), 2.75-2.69 (m, 4H), 2.67 (t, *J* = 7.5, 4H), 2.28-2.24 (m, 12H), 2.02 (t, *J* = 7.6, 4H), 1.83-1.76 (m, 4H), 1.73 (dt, *J* = 13.6, 6.4, 4H), 1.56-1.46 (m, 8H), 1.40-1.22 (m, 10H), 1.17 (dt, *J* = 15.3, 7.8, 4H), 1.12 (s, 3H).. HR-MS calc. for $C_{114}H_{137}N_{16}O_{22}Re$ $[M+H]^{2+}$ m/z = 1135.4905. Found 1135.4908.

[ReDPA-G1-(TEG-AOMK)$_2$]$^+$ (7): Using the general procedure, [ReDPA-G1-(yne)$_2$]$^+$ (10 mg, 12.2 μmol) and AOMK-TEG-N_3 (24 mg, 29.9 μmol) were dissolved in 0.4 mL of DMF, followed by addition of sodium ascorbate (3.9 mg, 19.5 μmol). After evacuation and backfilling with argon, $CuSO_4$ (1.2 mg, 4.9 μmol) was added in 0.1 mL H_2O. Upon completion, the reaction mixture was purified by semi-prep HPLC to yield 16.1 mg of product as a white solid (55 %). 1-H NMR (600 MHz; DMSO): δ 8.73 (d, *J* = 5.6, 2H),

8.43 (d, *J* = 7.4, 2H), 7.94-7.88 (m, 3H), 7.78 (t, *J* = 5.5, 1H), 7.74 (s, 2H), 7.61-7.54 (m, 4H), 7.45 (d, *J* = 8.0, 2H), 7.32 (t, *J* = 6.5, 2H), 7.29-7.15 (m, 17H), 7.13-7.11 (m, 2H), 6.84 (s, 4H), 4.89 (s, 4H), 4.87-4.70 (m, 8H), 4.57 (d, *J* = 6.9, 1H), 4.36 (t, *J* = 5.3, 4H), 4.30-4.22 (m, 4H), 4.07 (dd, *J* = 28.0, 11.0, 4H), 3.79-3.75 (m, 4H), 3.74-3.67 (m, 6H), 3.49-3.38 (m, 16H), 3.12-3.06 (q, *J* = 6.0, 2H), 3.04-2.92 (m, 6H), 2.83-2.82 (m, 3H), 2.82-2.77 (m, 5H), 2.69-2.65 (m, 4H), 2.21-2.16 (m, 16H), 1.76-1.68 (m, 4H), 1.60-1.25 (m, 16H) 1.07 (s, 3H). HR-MS calc. for $C_{116}H_{146}N_{16}O_{28}Re$ $[M+Na]^{2+}$ m/z = 1211.5052. Found 1211.5021.

$[ReDPA\text{-}G_2\text{-}(C_4\text{-}AOMK)_4]^+$ (8): Using the general procedure, $[ReDPA\text{-}G2\text{-}(yne)_4]^+$ (10 mg, 8.3 μmol) and AOMK-C_4-N_3 (28 mg, 40.1 μmol) were dissolved in 0.4 mL of DMF, followed by addition of sodium ascorbate (5.2 mg, 26.5 μmol). After evacuation and backfilling with argon, $CuSO_4$ (1.6 mg, 6.6 μmol) was added in 0.1 mL H_2O. Upon completion, the reaction mixture was purified by semi-prep HPLC to yield 16.6 mg of a white solid (50 %). ^{1}H NMR (600 MHz; CDCl3): δ 8.82-8.77 (m, 2H), 8.53 (dd, *J* = 17.1, 8.1, 4H), 7.99-7.91 (m, 3H), 7.80 (d, *J* = 21.0, 4H), 7.64 (d, *J* = 8.1, 2H), 7.53 (q, *J* = 7.4, 2H), 7.37 (dd, *J* = 11.6, 5.1, 2H), 7.35-7.22 (m, 18H), 7.19 (q, *J* = 8.6, 4H), 6.92 (s, 4H), 4.95-4.73 (m, 13H), 4.38-4.29 (m, 6H), 4.25 (t, *J* = 7.0, 4H), 4.22-4.07 (m, 10H), 3.81-3.74 (m, 3H), 3.06-2.94 (m, 8H), 2.87-2.81 (m, 6H), 2.65 (t, *J* = 7.6, 4H), 2.25 (d, *J* = 30.9, 16H), 2.05 (t, *J* = 7.2, 4H), 1.96 (dd, *J* = 14.0, 7.2, 4H), 1.79 (ddd, *J* = 23.0, 14.5, 5.5, 4H), 1.60-1.45 (m, 6H), 1.42-1.25 (m, 10H), 1.19-1.14 (s, 3H), 1.16-1.04 (s, 6H). HR-MS calc. for $C_{206}H_{245}N_{28}O_{44}Re$ $[M+2H]^{3+}$ m/z = 1334.2538. Found 1335.2255.

[ReDPA-G2-(TEG-AOMK)$_4$]$^+$ (9): Using the general procedure, [ReDPA-G2-(yne)$_4$]$^+$ (10 mg, 8.3 μmol) and AOMK-TEG-N_3 (32 mg, 39.9 μmol) were dissolved in 0.4 mL of DMF, followed by addition of sodium ascorbate (5.2 mg, 26.5 μmol). After evacuation and backfilling with argon, $CuSO_4$ (1.6 mg, 6.6 μmol) was added in 0.1 mL H_2O. Upon completion, the reaction mixture was purified by semi-prep HPLC to yield 22.4 mg of a white solid (61 %). 1-H NMR (600 MHz; DMSO): δ 8.80 (d, *J* = 5.3, 2H), 8.51 (d, *J* = 7.4, 4H), 7.99-7.95 (t, *J* = 4.2, 2H), 7.96-7.92 (t, *J* = 5.4, 1H), 7.80 (s, 4H), 7.70-7.60 (m, 7H), 7.54 (d, *J* = 7.9, 2H), 7.42-7.36 (m, 2H), 7.39 (t, *J* = 6.6, 2H), 7.33-7.25 (m, 32H), 7.21-7.18 (m, 4H), 7.03-6.80 (s, 8H), 4.99 (s, 8H), 4.97-4.79 (m, 16H), 4.43 (t, *J* = 5.3, 7H), 4.37-4.29 (m, 8H), 4.21-4.14 (m, 4H), 4.15-4.05 (s, 8H), 3.87-3.82 (m, 8H), 3.76 (t, *J* = 5.3, 8H), 3.54-3.45 (m, 32H), 3.17-3.12 (m, 2H), 3.13-2.98 (m, 12H), 2.87-2.80 (m, 10H), 2.67-2.62 (m, 8H), 2.31-2.21 (m, 32H), 1.82-1.76 (m, 4H), 1.61-1.50 (m, 6H), 1.47-1.21 (m, 22H), 1.19-1.16 (m, 3H), 1.14-1.09 (m, 6H). HR-MS calc. for $C_{222}H_{276}N_{28}O_{56}Re$ $[M+3H]^{4+}$ m/z = 1105.7383. Found 1105.7264.

3.4.3. Determination of Inhibition Constants

Cathepsin B (200 nM) was preincubated for 30 min at 37 °C in a solution of 5 mM DTT and 0.01% (v/v) Tween-20. The substrate, Cbz-Arg-Arg-pNA (25 μL), and the AOMKs (50 μL) were added the wells of a 96-well microplate containing the assay buffer. The reaction was initiated by the addition of cathepsin B, resulting in a substrate concentration of 500 μM, inhibitor concentrations from 25 nM to 1 μM, and an enzyme concentration of 5 nM. Formation of the p-NA product was monitored for 60 min at 405

nm at 37 °C using a Bio-Rad EL 808 plate reader. Measurements were obtained in triplicate. Absorbance vs. time measurements were analyzed using non-linear regression to determine the pseudo first-order rate constant (k_{obs}) in accordance to: Absorbance = $Ae^{-kobs(t)} + B$. The second-order rate constant, (k_i/K_i), the apparent inactivation rate (k_i), and the inhibition constant (K_i) (where possible) were determined in accordance to: $k_{obs} = \frac{\boldsymbol{ki}[\boldsymbol{I}]}{\boldsymbol{Ki}+[\boldsymbol{I}]}$ for hyperbolic relationships or $k_{obs} = \frac{\boldsymbol{ki}}{\boldsymbol{Ki}}[\boldsymbol{I}]$ for linear relationships. Equations were solved using GraphPad Prism software.

3.5. References

(1) Fréchet, J. M. J. *Science* **1994**, *263* (5154), 1710–1715.

(2) Bosman, A. W.; Janssen, H. M.; Meijer, E. W. *Chem. Rev.* **1999**, *99* (7), 1665–1688.

(3) Carlmark, A.; Hawker, C.; Hult, A.; Malkoch, M. *Chem. Soc. Rev.* **2009**, *38* (2), 352–362.

(4) Grayson, S. M.; Fréchet, J. M. J. *Chem. Rev.* **2001**, *101* (12), 3819–3867.

(5) Svenson, S.; Tomalia, D. A. *Adv. Drug Deliv. Rev.* **2005**, *57*, 2106–2129.

(6) Lee, C. C.; MacKay, J. A; Fréchet, J. M. J.; Szoka, F. C. *Nat. Biotechnol.* **2005**, *23* (12), 1517–1526.

(7) Boas, U.; Heegaard, P. M. H. *Chem. Soc. Rev.* **2004**, *33* (1), 43–63.

(8) Calderón, M.; Quadir, M. A.; Sharma, S. K.; Haag, R. *Adv. Mater.* **2010**, *22*, 190–218.

(9) Guillaudeu, S. J.; Fox, M. E.; Haidar, Y. M.; Dy, E. E.; Szoka, F. C.; Fréchet, J. M. J. *Bioconjug. Chem.* **2008**, *19*, 461–469.

(10) Svenson, S. *Eur. J. Pharm. Biopharm.* **2009**, *71* (3), 445–462.

(11) Cheng, Y.; Xu, Z.; Ma, M.; Xu, T. *J. Pharm. Sci.*, **2008,** *97*, 123–143.

(12) Darbre, T.; Reymond, J. L. *Acc. Chem. Res.* **2006**, *39*, 925–934.

(13) Nanjwade, B. K.; Bechra, H. M.; Derkar, G. K.; Manvi, F. V.; Nanjwade, V. K. *Eur. J. Pharm. Sci.* **2009**, *38* (3), 185–196.

(14) Gillies, E. R.; Fréchet, J. M. J. *Drug Discov. Today* **2005**, *10* (1), 35–43.

(15) Padilla De Jesús, O. L.; Ihre, H. R.; Gagne, L.; Fréchet, J. M. J.; Szoka, F. C.

Bioconjug. Chem. **2002**, *13* (3), 453–461.

(16) Kukowska-Latallo, J. F.; Bielinska, A. U.; Johnson, J.; Spindler, R.; Tomalia, D. A.; Baker, J. R. *Proc. Natl. Acad. Sci. U. S. A.* **1996**, *93*, 4897–4902.

(17) Grinstaff, M. W. *Chemistry* **2002**, *8* (13), 2839–2846.

(18) Mintzer, M. A.; Grinstaff, M. W. *Chem. Soc. Rev.* **2011**, *40* (1), 173–190.

(19) Langereis, S.; de Lussanet, Q. G.; van Genderen, M. H. P.; Backes, W. H.; Meijer, E. W. *Macromolecules* **2004**, *37*, 3084–3091.

(20) Koyama, Y.; Talanov, V. S.; Bernardo, M.; Hama, Y.; Regino, C. A. S.; Brechbiel, M. W.; Choyke, P. L.; Kobayashi, H. *J. Magn. Reson. Imaging* **2007**, *25*, 866–871.

(21) Kobayashi, H.; Kawamoto, S.; Jo, S. K.; Bryant, H. L.; Brechbiel, M. W.; Star, R. A. *Bioconjug. Chem.* **2003**, *14*, 388–394.

(22) Majoros, I. J.; Williams, C. R.; Baker, J. R. *Curr. Top. Med. Chem.* **2008**, *8* (14), 1165–1179.

(23) Ihre, H.; Hult, A.; Soderlind, E. *J. Am. Chem. Soc.* **1996**, *118* (27), 6388–6395.

(24) Ihre, H.; Padilla De Jesús, O. L.; Fréchet, J. M. *J. Am. Chem. Soc.* **2001**, *123* (25), 5908–5917.

(25) Parrott, M. C.; Benhabbour, S. R.; Saab, C.; Lemon, J. A.; Parker, S.; Valliant, J. F.; Adronov, A. *J. Am. Chem. Soc.* **2009**, *131* (21), 2906–2916.

(26) Lee, C. C.; Gillies, E. R.; Fox, M. E.; Guillaudeu, S. J.; Fréchet, J. M. J.; Dy, E. E.; Szoka, F. C. *Proc. Natl. Acad. Sci. U. S. A.* **2006**, *103* (45), 16649–16654.

(27) Mammen, M.; Choi, S.-K.; Whitesides, G. M. *Angew. Chemie Int. Ed.* **1998**, *37*, 2754–2794.

(28) Cairo, C. W.; Gestwicki, J. E.; Kanai, M.; Kiessling, L. L. *J. Am. Chem. Soc.* **2002**, *124* (8), 1615–1619.

(29) Gray, B. P.; Li, S.; Brown, K. C. *Bioconjug. Chem.* **2013**, *24*, 85–96.

(30) Röglin, L.; Lempens, E. H. M.; Meijer, E. W. *Angew. Chem. Int. Ed. Engl.* **2011**, *50* (1), 102–112.

(31) Banerjee, S. R.; Pullambhatla, M.; Shallal, H.; Lisok, A.; Mease, R. C.; Pomper, M. G. *Oncotarget* **2011**, *2* (12), 1244–1253.

(32) Wu, P.; Malkoch, M.; Hunt, J. N.; Vestberg, R.; Kaltgrad, E.; Finn, M. G.; Fokin, V. V; Sharpless, K. B.; Hawker, C. J. *Chem. Commun.* **2005**, 5775–5777.

(33) Shokeen, M.; Pressly, E. D.; Hagooly, A.; Zheleznyak, A.; Ramos, N.; Fiamengo, A. L.; Welch, M. J.; Hawker, C. J.; Anderson, C. J. *ACS Nano* **2011**, *5*, 738–747.

(34) Buffet, K.; Gillon, E.; Holler, M.; Nierengarten, J. F.; Imberty, A.; Vincent, S. P. *Org. Biomol. Chem.* **2015**, *13* (23), 6482–6492.

(35) Nierengarten, I.; Nierengarten, J. F. *Chem. An Asian J.* **2014**, *9* (6), 1436–1444.

(36) Almutairi, A.; Rossin, R.; Shokeen, M.; Hagooly, A.; Ananth, A.; Capoccia, B.; Guillaudeu, S.; Abendschein, D.; Anderson, C. J.; Welch, M. J.; Fréchet, J. M. J. *Proc. Natl. Acad. Sci. U. S. A.* **2009**, *106* (3), 685–690.

(37) Seo, J. W.; Baek, H.; Mahakian, L. M.; Kusunose, J.; Hamzah, J.; Ruoslahti, E.; Ferrara, K. W. *Bioconjug. Chem.* **2014**, *25* (2), 231–239.

(38) Yoshii, A.; Kageshita, T.; Tsushima, H.; Ono, T. *Arch. Dermatol. Res.* **1995**, *287* (2), 209–213.

(39) Kato, D.; Boatright, K. M.; Berger, A. B.; Nazif, T.; Blum, G.; Ryan, C.; Chehade,

K. A. H.; Salvesen, G. S.; Bogyo, M. *Nat. Chem. Biol.* **2005**, *1* (1), 33–38.

(40) Mohamed, M. M.; Sloane, B. F. *Nat. Rev. Cancer* **2006**, *6*, 764–775.

(41) Blum, G.; von Degenfeld, G.; Merchant, M. J.; Blau, H. M.; Bogyo, M. *Nat. Chem. Biol.* **2007**, *3* (10), 668–677.

(42) Edgington, L. E.; Berger, A. B.; Blum, G.; Albrow, V. E.; Paulick, M. G.; Lineberry, N.; Bogyo, M. *Nat. Med.* **2009**, *15* (8), 967–973.

(43) Ren, G.; Blum, G.; Verdoes, M.; Liu, H.; Syed, S.; Edgington, L. E.; Gheysens, O.; Miao, Z.; Jiang, H.; Gambhir, S. S.; Bogyo, M.; Cheng, Z. *PLoS One* **2011**, *6* (11), 1–9.

(44) Smith, R. A.; Copp, L. J.; Coles, P. J.; Pauls, H. W.; Robinson, V. J.; Spencer, R. W.; Heard, S. B.; Krantz, A. *J. Am. Chem. Soc.* **1988**, *110* (13), 4429–4431.

(45) Krantz, a; Copp, L. J.; Coles, P. J.; Smith, R. A; Heard, S. B. *Biochemistry* **1991**, *30* (19), 4678–4687.

(46) Powers, J. C.; Asgian, J. L.; Ekici, Ö. D.; James, K. E. *Chem. Rev.* **2002**, *102* (12), 4639–4750.

(47) Blum, G.; Mullins, S. R.; Keren, K.; Fonovic, M.; Jedeszko, C.; Rice, M. J.; Sloane, B. F.; Bogyo, M. *Nat. Chem. Biol.* **2005**, *1* (4), 203–209.

(48) Edem, P. E.; Czorny, S.; Valliant, J. F. *J. Med. Chem.* **2014**, *57* (22), 9564–9577.

(49) Chen, Q.; Deady, L. W.; Baguley, B. C.; Denny, W. A. *J. Med. Chem.* **1994**, *37* (5), 593–597.

(50) Yim, C.-B.; Dijkgraaf, I.; Merkx, R.; Versluis, C.; Eek, A.; Mulder, G. E.; Rijkers, D. T. S.; Boerman, O. C.; Liskamp, R. M. J. *J. Med. Chem.* **2010**, *53* (10), 3944–

3953.

(51) Yim, C.; Boerman, O. C.; Visser, M. De; Jong, M. De; Dechesne, A. C.; Rijkers, D. T. S.; Liskamp, R. M. J. *Bioconjug. Chem.* **2009**, *20* (7), 1323–1331.

(52) Dyke, J. M.; Groves, A. P.; Morris, A.; Ogden, J. S.; Dias, A. A.; Oliveira, A. M. S.; Costa, M. L.; Barros, M. T.; Cabral, M. H.; Moutinho, A. M. C. *J. Am. Chem. Soc.* **1997**, *119* (29), 6883–6887.

(53) Khoukhi, N.; Vauitier, M.; Carrié, R. *Tetrahedron* **1987**, *43* (8), 1811–1822.

(54) Liu, S. Q.; Rachel E, P. L.; Ke, C. Y.; Hedrick, J. L.; Yang, Y. Y. *Biomaterials* **2009**, *30* (8), 1453–1461.

Chapter 4. Synthesis and *In Vitro* Affinity of PSMA Targeted Dendrimers for Molecular Imaging Applications.

**All synthesis work presented in this chapter was carried out by Lukas Sadowski. Synthesis of compound 9 was first performed by Stuart McNelles. In vitro assays were carried out by Nancy Janzen.*

Abstract

Multimerization of lys-urea-glu dipeptide for targeting of PSMA was accomplished via attachment to a G1 and G2 bis-MPA dendrimer. Attachment of the targeting vector to the dendrimer was achieved via either a hydrophobic or hydrophilic linker of similar length. *In vitro* affinity of the resulting compounds indicated an increase in affinity of G2 targeted dendrimers compared to the G1 analogues. Furthermore, the dendrimers utilizing the hydrophobic linker resulted in derivatives with the highest affinity towards PSMA. From these results, a lead compound was chosen for further evaluation *in vivo*.

4.1. Introduction

Prostate cancer (PCa) is one of the most widely diagnosed cancers in developed countries.[1] Therefore, the need for early diagnosis and treatment is of utmost importance for survival. Imaging prostate cancer is not only important for detection and initial staging, but also for therapeutic monitoring.[2] Imaging of PCa with ^{18}F-FDG is of limited utility in early detection, despite showing uptake in advanced PCa.[3] Although certain imaging agents have been shown to exhibit uptake in PCa, including ^{11}C-choline, ^{18}F-fluorocholine and ^{11}C-acetate, unfortunately, these compounds also display uptake in benign inflammatory processes.[4,5] Yet another strategy that has been employed for the early detection of PCa involves the overexpression of the Prostate Specific Membrane Antigen (PSMA). PSMA has become a well-established biomarker of PCa, and small molecule inhibitors have been developed to target this enzyme.[6] Of particular interest is the urea-based inhibitor of glutamic acid and lysine (or cysteine), first developed by Pomper and co-workers.[7,8] The high affinity and excellent specificity of these urea inhibitors stems from their resemblance to N-acetylaspartylglutamate (NAAG), the natural substrate for PSMA. The primary amine of the lysine residue serves as a convenient handle for further conjugation to imaging moieties, enabling visualization of PSMA *in vivo*. To date, a number of radionuclides have been conjugated to urea based PSMA inhibitors, including ^{18}F, ^{111}In, ^{123}I and ^{131}I, ^{68}Ga and ^{99m}Tc as well as fluorophores.[2,9-11] Trofex™ (MIP-1072 and MIP 1095), the first of this class of compounds that is being actively investigated in a clinical setting, illustrates the potential of urea based PSMA inhibitors.

It is important to note that the radionuclide or it's corresponding chelate can have a significant impact on the resulting pharmacokinetics (PK) of the imaging agent.[12] Presumably, the further the imaging moiety is from the targeting vector, the smaller an effect it will have on the resulting PK. Dendrimers represent an ideal scaffold for this purpose due to their site isolated core which can be functionalized to accommodate imaging moieties.[13] Furthermore, the attachment of multiple PSMA inhibitors to the periphery of a dendrimer can impart higher affinity toward the target. In fact, it has been shown that a dimeric analogue of a urea PSMA inhibitor not only possessed greater affinity towards PSMA, but also exhibited longer tumor retention versus the monomeric analogue.[9] Dendrimers based on 2-bis(methylol)propionic acid (bis-MPA) are an attractive scaffold for this purpose owing to their hydrophilicy, biocompatibility and ease of functionalization at the periphery and core. Furthermore, the polyester backbone, albeit degradable, has been shown to be resilient towards hydrolysis for days,[14] particularly at lower pH, such as those found in the vicinity of tumors. Given that patients are typically imaged within hours of being administered a molecular imaging agent, the stability of bis-MPA dendrimers seems to be sufficient to warrant their use for *in vivo* biomedical applications.

4.2. Results and Discussion

4.2.1. Synthesis

It has been shown that a minimum linker length is required to attach larger imaging moieties to the urea inhibitor, due to the location of the active site on PSMA. To investigate the importance of the nature of the linker, we decided to functionalize the lysine residue with a hydrophobic and a hydrophilic spacer of similar length. Suberic acid has previously been employed to prepare PSMA targeted imaging agents with high affinity, and thus, served as a convenient hydrophobic spacer for the purpose of our study.[15] In order to attach the PSMA inhibitor to the periphery of the dendritic scaffold bearing alkynes at the periphery, we needed to attach an azide functionality to one end of suberic acid. To accomplish this, suberic acid di-NHS ester (**1**) was mono-substituted with 6-amino-1-propanol to give an alcohol moiety on one side and an activated NHS ester on the other side (**2**). Upon purification, the compound was immediately reacted with the lysine residue of the PSMA inhibitor to yield compound **3**. This was done to ensure that polymerization or cyclization of the alcohol functionality with the NHS activated ester was avoided. Subsequent mesylation of the alcohol, followed by nucleophilic substitution yielded the azide functionalized PSMA inhibitor (**5**).

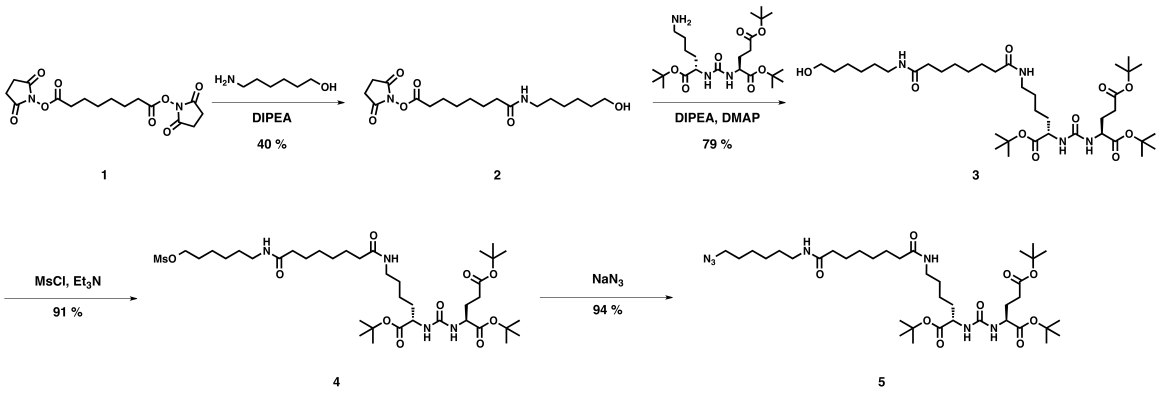

Scheme 4.1. PSMAi-SA-N_3 synthesis.

Tetraethylene glycol was chosen as the second spacer owing to its similar length to suberic acid while possessing a more hydrophilic nature. Mono functionalization of tetraethylene glycol with para-nitrophenyl chloroformate, followed by reaction with the amino group of the lysine residue on the PSMA inhibitor yielded a carbamate linked compound **7**. Subsequent mesylation of the alcohol and substitution with sodium azide yielded the target azide functionalized PSMA inhibitor with a tetraethylene glycol spacer (**9**).

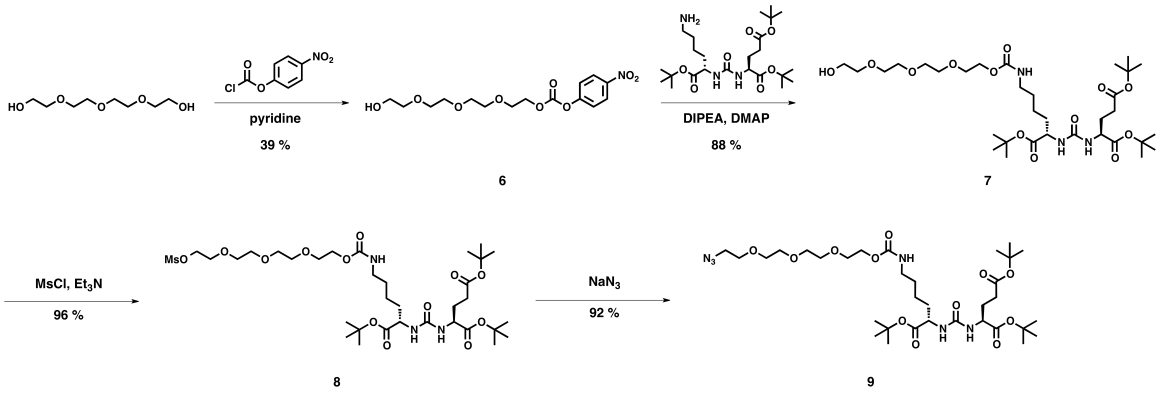

Scheme 4.2. PSMAi-PEG-N_3 synthesis.

"Click" chemistry was utilized to attach the PSMA inhibitors to the alkyne periphery of G1 and G2 Bis-MPA dendrimers bearing an ReDPA ligand at the core. The rhenium core serves as a convenient non-radioactive analogue to ^{99m}Tc, the most widely used radionuclide in diagnostic imaging. The click coupling proceeded smoothly at ambient temperatures using the commonly used $CuSO_4$/sodium ascorbate combination. After semi-preparative HPLC purification of the products, the resulting dendrimers were treated with TFA to remove the tert-butyl groups, liberating the carboxylic acid moieties on the PSMA targeting vector. Despite the polyester backbone, negligible hydrolysis was observed during the course of the reaction. The final compounds were purified again using semi-preparative HPLC to ensure purity of the products for *in vitro* evaluation.

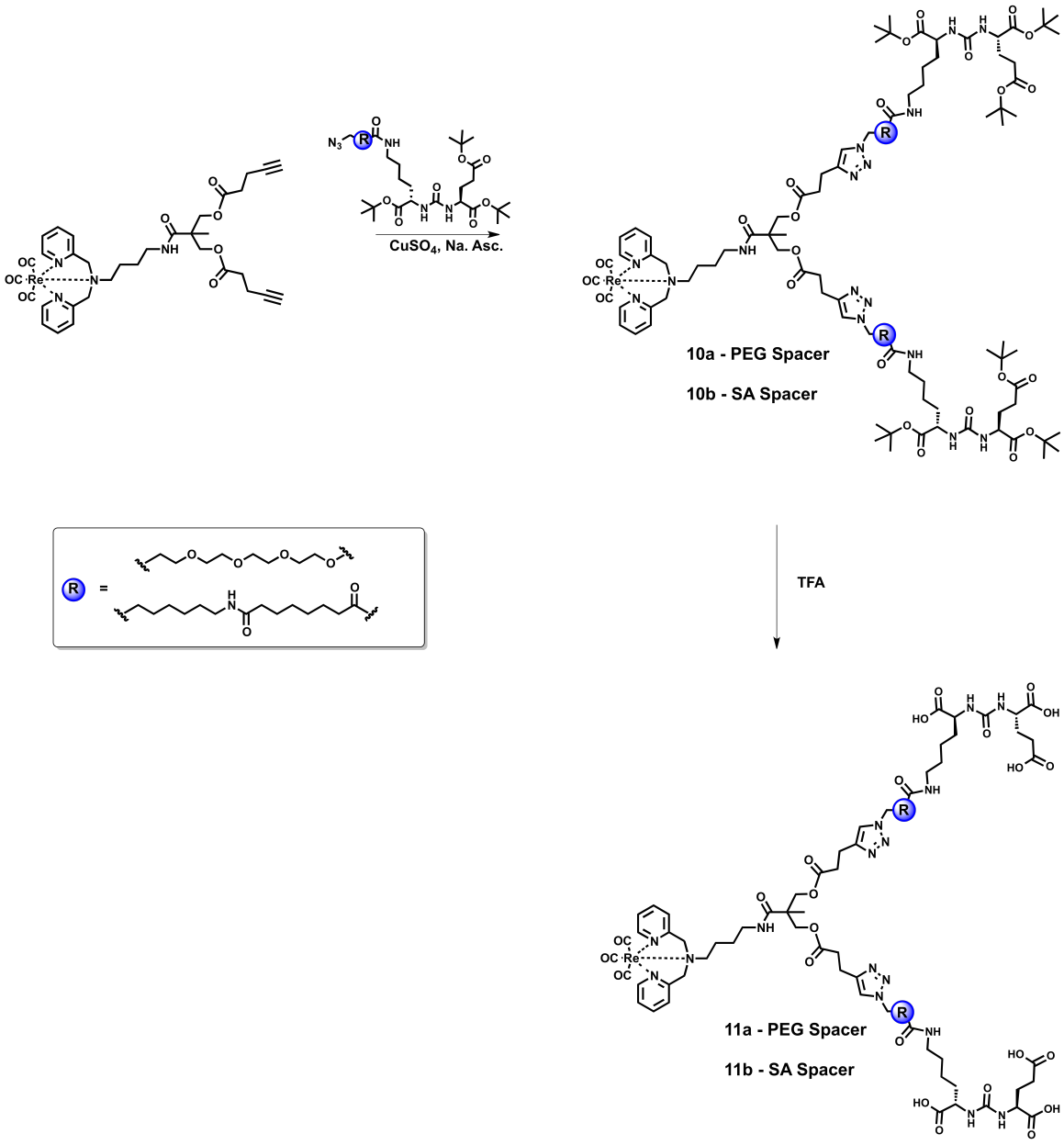

Scheme 4.3. $[ReDPA\text{-}G1\text{-}(PSMAi)_2]^+$ synthesis with hydrophilic and hydrophobic linker.

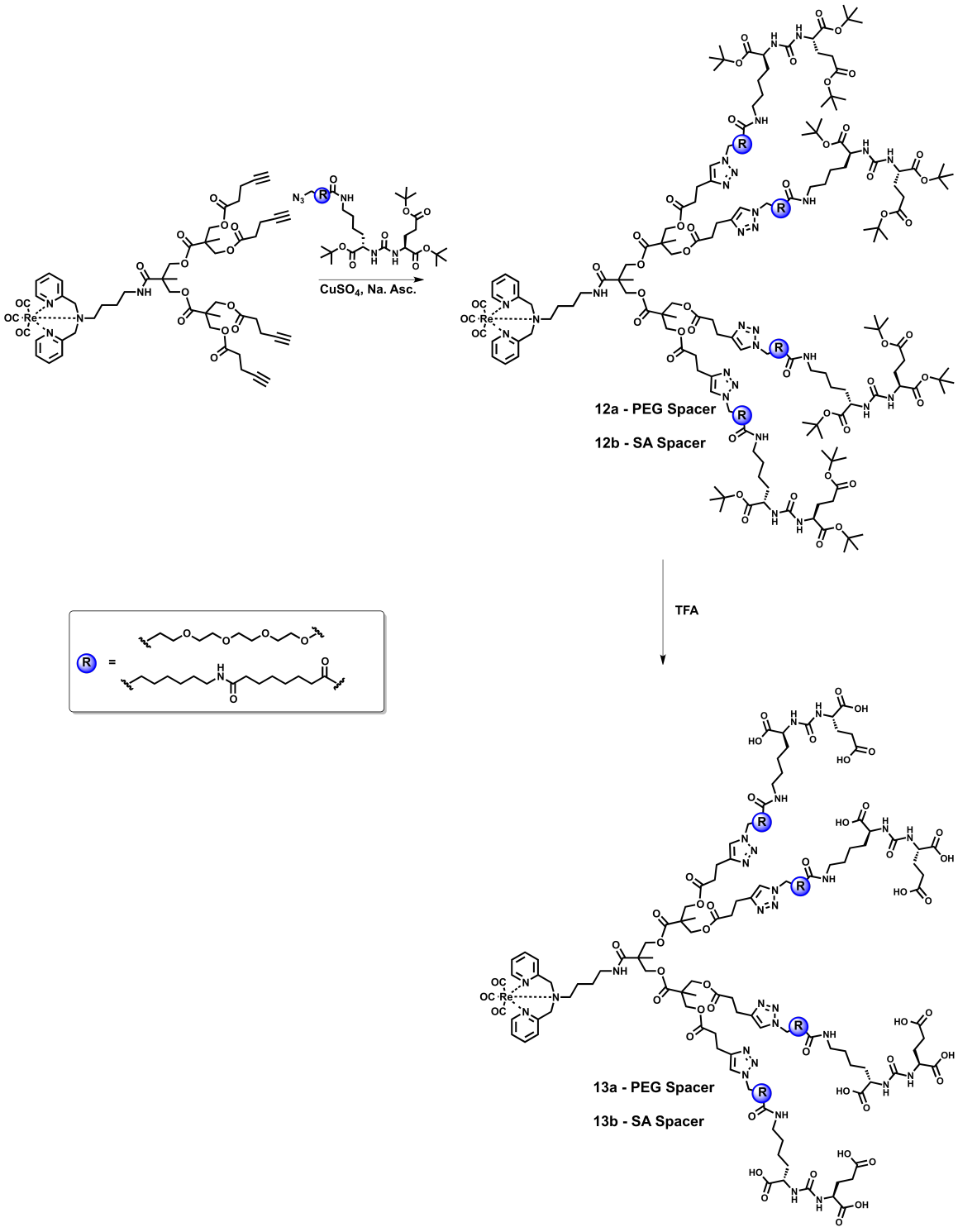

Scheme 4.4. $[ReDPA\text{-}G2\text{-}(PSMAi)_4]^+$ synthesis with hydrophilic and hydrophobic linker.

4.2.2. *In Vitro* Affinity of PSMA Targeted Dendrimers

The affinity of the multivalent molecular imaging agents was evaluated using a competitive inhibition assay. Upon evaluation of the IC50 of lys-urea-glu attached to the dendrimer via a PEG spacer, the G2 dendrimer exhibited an order of magnitude increase in affinity toward PSMA compared to G1 (IC50 of 383.0 ± 233.7 vs 26.6 ± 4.9 nM), demonstrating a pronounced effect with increasing multi-valency. The suberic acid based hydrophobic spacer exhibited the highest affinity toward PSMA. Increasing multivalency further resulted in a decrease in IC50 from 16.4 ± 3.0 nM for the G1 derivative to 8.2 ± 0.4 nM for the G2 derivative. Interestingly, the affinity towards PSMA doubles when twice the amount of targeting vectors are present, implying a linear correlation in this set of derivatives.

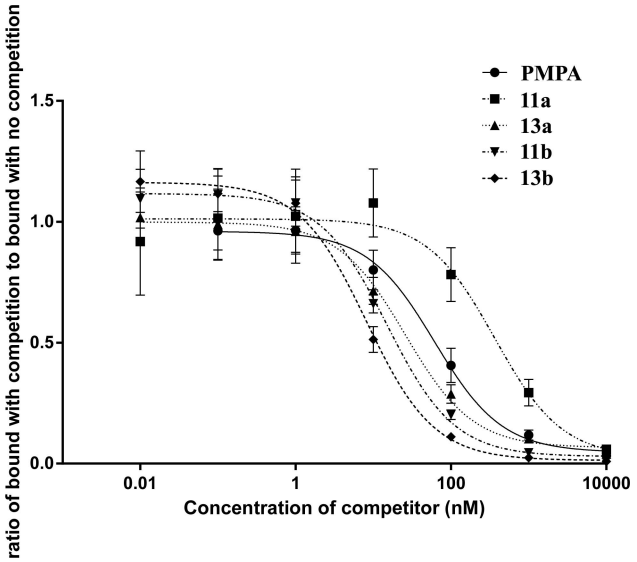

Figure 4.1. IC_{50} curves for PSMA targeted compounds and control (PMPA).

Table 4.1. Summary of compound IC_{50} and 95% Confidence Interval.

Compound	IC_{50} (nM)	95% Confidence Interval
PMPA	61.5	52.3 - 72.4
11a	366.1	206.1 - 650.3
13a	25.9	19.1 - 34.9
11b	15.1	12.1 - 18.7
13b	8.2	6.7 - 9.9

4.3. Conclusions

Multimerization of lys-urea-glu is a strategy that has been shown effective in improving affinity towards PSMA. In addition, the nature of the spacer has been demonstrated to have a considerable impact on the affinity of the targeting moiety. Interestingly, the hydrophobic spacer attaching the PSMA inhibitor to the dendrimer resulted in the highest affinity towards PSMA. From these results, a lead compound has been developed that merits further investigation *in vivo*.

4.4. Experimental

4.4.1. Materials and Characterization

Suberic acid and N-hydroxysuccinimide were purchased from Chem-Impex and all other chemicals were purchased from Sigma Aldrich. Dry dichloromethane was dispensed from a solvent system equipped with an activated alumina column. NMR spectra were collected on a Bruker Avance 600 MHz or 700 MHz NMR spectrometer and calibrated to the solvent peak. A Micromass QTOF Global Ultima was used to obtain exact masses and HPLC was conducted on Waters 2695 HPLC equipped with Waters 2996 PDA detector and a Phenomenex Luna 5u C18(2) 150 x 10.0 mm column. The desired products were eluted using a water/acetonitrile gradient containing 0.1% formic acid for dendrimers containing tBu groups at the periphery and 0.1% trifluoroacetic acid for dendrimers with –COOH groups at the periphery. Additionally, water contained 5% acetonitrile. The method used for purification was 0-2 min for 100% water, followed by a gradient to 100% acetonitrile over 15 min. Tert-Butyl protected analogues would typically elute around 90% ACN, while final compounds bearing carboxylic acids at the periphery would elute around 45% ACN.

4.4.2. Synthesis

4.4.2.1. N_3-SA-PSMAi Synthesis

HO-SA-NHS (2): To a 500 mL round bottom flask, equipped with a magnetic stir bar, was added the di-NHS ester of suberic acid (2.20 g, 5.97 mmol) in CH_2Cl_2 (150 mL), aminohexanol (0.18 g, 1.49 mmol), and DIPEA (0.26 mL, 1.49 mmol). The reaction was allowed to stir at R.T. for 1 hour. The reaction mixture was diluted with CH_2Cl_2 (150 mL) and washed with $NaHSO_4$ (2 x 100 mL) and brine. The reaction mixture was dried with Na_2SO_4 and concentrated in vacuo. The product was rapidly purified via silica gel column chromatography (5-10% CH_3OH in CH_2Cl_2) to yield 220 mg of the product as a clear viscous oil (40 % based on aminohexanol). ^{1}H NMR (700 MHz; DMSO): δ 7.70 (t, *J* = 5.5, 1H), 4.31 (t, *J* = 5.2, 1H), 3.36 (q, *J* = 5.9, 2H), 3.00 (q, *J* = 6.4, 2H), 2.80 (s, 4H), 2.64 (t, *J* = 7.3, 2H), 2.03 (t, *J* = 7.5, 2H), 1.60 (quintet, *J* = 7.5, 2H), 1.47 (dt, *J* = 15.0, 7.5, 2H), 1.38-1.35 (m, 6H), 1.26-1.22 (m, 6H). ^{13}C NMR (175 MHz, DMSO): δ = 171.76, 170.23, 168.93, 60.65, 38.34, 35.33, 32.49, 30.15, 29.22, 28.14, 27.74, 26.32, 25.43, 25.23, 25.09, 24.16. HR-MS calc. for $C_{18}H_{30}N_2O_6$ $[M+H]^+$= 371.2182. Found: 371.2191.

HO-SA-PSMAi (3): To a 100 mL round bottom flask, equipped with a magnetic stir bar, was added HO-SA-NHS (0.20 g, 0.54 mmol) in CH_2Cl_2 (20 mL), PSMAi-NH_2 (0.29 g, 0.59 mmol), and DIPEA (0.10 mL, 0.59 mmol). The reaction was allowed to stir at R.T. for 2 hour. The reaction mixture was diluted with CH_2Cl_2 (50 mL) and washed with $NaHSO_4$ (2 x 50 mL) and brine. The reaction mixture was dried with Na_2SO_4 and

concentrated in vacuo to yield 317 mg of the product as a white solid (79 %). ^{1}H NMR (700 MHz; DMSO): δ 7.70 (m, 2H), 6.27 (dd, *J* = 26.0, 8.3, 2H), 4.32 (t, *J* = 5.1, 1H), 4.03 (ddd, *J* = 11.2, 7.1, 4.0, 1H), 3.97-3.94 (m, 1H), 3.37 (q, *J* = 5.9, 2H), 3.01-2.98 (m, 4H), 2.23-2.20 (m, 2H), 2.01 (t, *J* = 6.6, 4H), 1.87-1.84 (m, 1H), 1.69-1.65 (m, 1H), 1.60-1.58 (m, 1H), 1.49-1.46 (m, 6H), 1.43-1.37 (m, 32H), 1.25-1.22 (m, 10H). ^{13}C NMR (175 MHz, DMSO): δ = 172.20, 171.85, 171.81, 171.39, 157.08, 80.56, 80.27, 79.72, 60.65, 53.02, 52.15, 38.24, 38.16, 35.41, 32.48, 31.76, 30.87, 29.22, 28.83, 28.49, 28.46, 27.72, 27.63, 26.32, 25.23, 22.48. HR-MS calc. for $C_{38}H_{70}N_4O_{10}$ $[M+H]^+$: 743.5170. Found: 743.5134.

MsO-SA-PSMAi (4): To a 100 mL round bottom flask, equipped with a magnetic stir bar, was added HO-SA-PSMAi (300 mg, 404 μmol) and Et_3N (62 μL, 444 μmol, 1.1 eq) in 20 mL of dry CH_2Cl_2, and cooled in an ice bath. MsCl (35 μL, 444 μmol, 1.1 eq) in 1 mL of dry CH_2Cl_2 was added dropwise over 5 min. The reaction was stirred at 0 °C for 1.5 hours. The reaction mixture was diluted with 50 mL of CH_2Cl_2 and washed with cold water (20 mL), $NaHSO_4$ (2 x 25 mL) and brine. The organic layer was dried with Na_2SO_4 and concentrated by rotary evaporation to yield 301 mg of a white solid (91 %). ^{1}H NMR (700 MHz; DMSO): δ 7.70 (t, *J* = 5.4, 2H), 6.27 (dd, *J* = 26.1, 8.4, 2H), 4.17 (t, *J* = 6.5, 2H), 4.03 (td, *J* = 8.5, 5.3, 1H), 3.95 (q, *J* = 6.9, 1H), 3.19-3.12 (s, 3H), 3.00 (dq, *J* = 11.8, 6.0, 4H), 2.27-2.17 (m, 2H), 2.03-2.00 (m, 4H), 1.86-1.84 (m, 1H), 1.67-1.64 (m, 3H), 1.60-1.57 (m, 1H), 1.51-1.45 (m, 5H), 1.40-1.35 (m, 27H), 1.32 (dd, *J* = 15.0, 7.6, 2H), 1.27 (dt, *J* = 15.9, 8.0, 4H), 1.21 (bs, 4H). ^{13}C NMR (175 MHz; DMSO): δ 172.34,

171.97, 171.52, 157.20, 80.69, 80.39, 79.85, 70.48, 53.13, 52.26, 38.33, 38.27, 36.64, 35.52, 31.87, 30.98, 29.10, 28.94, 28.58, 27.74, 25.96, 25.35, 24.73, 22.60. HR-MS calc. for $C_{39}H_{72}N_4O_{12}S$ $[M+H]^+$: 821.4946. Found: 821.4909.

N_3-SA-PSMAi (5): To a 25 mL round bottom flask, equipped with a magnetic stir bar, was added MsO-SA-PSMAi (200 mg, 244 μmol) in DMSO (5 mL), and NaN_3 (63 mg, 974 μmol, 4 eq). The reaction mixture was allowed to stir overnight at 50 °C. The reaction mixture was diluted with water (40 mL) and extracted with Et_2O (4 x 25 mL). The combined organic layers were washed with brine and dried with Na_2SO_4. The product was concentrated by rotary evaporation to yield 178 mg of a white solid (94 %). ^{1}H NMR (700 MHz; DMSO): δ 7.71 (m, 2H), 6.28 (dd, *J* = 25.9, 8.3, 2H), 4.04 (td, *J* = 8.5, 5.2, 1H), 3.96 (td, *J* = 8.0, 5.6, 1H), 3.31 (t, *J* = 6.9, 2H), 3.02-2.99 (m, 4H), 2.23-2.21 (m, 2H) 2.04-2.01 (m, 4H), 1.88-1.86 (m, 1H), 1.68-1.65 (m, 1H), 1.60-1.57 (m, 1H), 1.51-1.48 (m, 7H), 1.42-1.38 (m, 27H), 1.29-1.26 (m, 6H), 1.21 (bs, 4H). ^{13}C NMR (175 MHz; DMSO): δ 172.30, 171.93, 171.48, 157.17, 80.66, 80.35, 79.81, 53.10, 52.24, 50.65, 38.32, 38.26, 35.50, 31.85, 30.96, 29.10, 28.91, 28.58, 28.55, 28.27, 27.80, 27.71, 26.00, 25.93, 25.33, 22.57. HR-MS calc. for $C_{38}H_{69}N_7O_9$ $[M+Na]^+$: 790.5054. Found: 790.5029.

4.4.2.2. N_3-PEG-PSMAi Synthesis

HO-PEG-NP (6): To a 250 mL round bottom flask, equipped with a magnetic stir bar, was added tetraethylene glycol (4.0 g, 20.6 mmol) in 100 mL of dry CH_2Cl_2, p-

nitrophenyl chloroformate (4.2 g (20.6 mmol), and Et_3N (4.3 mL, 30.9 mmol). After stirring overnight, the reaction mixture was diluted with 100 mL of CH_2Cl_2 and washed with $NaHSO_4$ (2 x 150 mL) and brine. The combined organic layers were dried with Na_2SO_4 and concentrated by rotary evaporation. The product was purified by column chromatography, using 3:1 EtOAc/Hex to remove the nitrophenol, followed by 5% MeOH in CH_2Cl_2 to yield 1.93 g of the product as a pale yellow viscous oil (39%). ^{1}H-NMR (600 MHz; DMSO): δ 8.34-8.31 (dt, *J* = 9.2, 2.2, 2H), 7.59-7.56 (dt, *J* = 9.2, 2.3, 2H), 4.58 (bs, 1H), 4.38 (dt, J = 4.1, 2.3, 2H), 3.73-3.72 (m, 2H), 3.60-3.58 (m, 2H), 3.57-3.52 (m, 6H), 3.50-3.48 (m, *J* = 4.8, 2H), 3.43 (t, *J* = 5.2, 2H). ^{13}C NMR (175 MHz; DMSO): δ 155.29, 152.08, 145.15, 125.39, 122.57, 72.36, 69.85, 69.79, 68.30, 67.92, 60.22. HR-MS calc. for $C_{15}H_{21}NO_9$ $[M+H]^+$: 360.1295. Found: 360.1306.

HO-PEG-PSMAi (7): To a 100 mL round bottom flask, equipped with a magnetic stir bar, was added HO-PEG-NP (200 mg, 557 μmol) in 25 mL of CH_2Cl_2, PSMAi-NH_2 (326 mg, 668 μmol, 1.2 eq), DIPEA (115 μL, 668 μmol, 1.2 eq), and DMAP (41 mg, 334 μmol, 0.6 eq). The reaction mixture was stirred at room temperature overnight. The reaction was diluted with 25 mL of CH_2Cl_2 and washed with $NaHSO_4$ (3 x 50 mL) and brine. The organic layer was concentrated by rotary evaporation and purified on silica gel column chromatography eluting with 3:1 EtOAc/Hex to remove the nitrophenol and subsequently 5% MeOH in CH_2Cl_2 to yield 346 mg of the product as a clear viscous oil (88 %). ^{1}H NMR (700 MHz; DMSO): δ 7.18 (t, *J* = 5.6, 1H), 6.27 (dd, *J* = 28.3, 8.3, 2H), 4.56 (t, *J* = 5.5, 1H), 4.03 (s, 3H), 3.95 (q, *J* = 7.2, 1H), 3.55 (t, *J* = 4.7, 2H), 3.52-3.50

(m, 6H), 3.49 (q, *J* = 5.4, 2H), 3.41 (t, *J* = 5.2, 2H), 2.95 (q, *J* = 6.4, 2H), 2.24-2.21 (m, *J* = 14.5, 2H), 1.89-1.86 (m, 1H), 1.68-1.65 (m, 1H), 1.61-1.59 (m, 1H), 1.52-1.50 (m, 1H), 1.41-1.29 (m, 9H), 1.27-1.25 (m, 2H). ^{13}C NMR (175 MHz, $CDCl_3$): δ = 172.31, 171.96, 171.50, 160.93, 157.18, 156.21, 80.68, 80.38, 79.84, 72.44, 69.93, 69.86, 69.82, 68.99, 63.09, 60.31, 59.84, 55.01, 53.14, 52.25, 31.83, 31.79, 30.97, 29.16, 28.76, 22.54, 22.43, 20.87, 14.20. HR-MS calc. for $C_{33}H_{61}N_3O_{13}$ $[M+H]^+$: 708.4277. Found: 708.4277.

MsO-PEG-PSMAi (8): To a 25 mL round bottom flask, equipped with a magnetic stir bar, was added HO-PEG-PSMAi (300 mg, 424 μmol) and Et_3N (65 μL, 466 μmol, 1.1 eq) in dry CH_2Cl_2 (10 mL), and cooled in an ice bath. MsCl (36 μL, 466 μmol, 1.1 eq) in 1 mL of CH_2Cl_2 was added dropwise over 5 min. The reaction mixture was stirred at 0 °C for 1.5 hours. The reaction mixture was diluted with CH_2Cl_2 and washed with cold water, $NaHSO_4$ and brine. The organic layer was dried with Na_2SO_4 and concentrated by rotary evaporation to yield the product as a white solid (96 %). ^{1}H NMR (700 MHz; DMSO): δ 7.17 (s, 1H), 6.28 (d, *J* = 25.4, 2H), 4.30 (t, *J* = 4.4, 2H), 4.02 (t, *J* = 4.7, 3H), 3.94 (t, *J* = 6.0, 1H), 3.67-3.66 (m, 2H), 3.55-3.53 (m, 10H), 2.94 (q, *J* = 6.1, 2H), 2.38 (s, 2H), 2.27-2.16 (m, 2H), 1.87-1.85 (m, 1H), 1.68-1.63 (m, 1H), 1.59-1.58 (m, 1H), 1.50-1.49 (m, 1H), 1.39-1.38 (m, 29H), 1.27-1.25 (m, 2H). ^{13}C NMR (175 MHz, $CDCl_3$): δ = 172.34, 171.99, 171.52, 157.20, 156.22, 80.68, 80.38, 79.85, 69.85, 69.81, 69.77, 69.00, 68.39, 63.09, 55.03, 53.15, 52.27, 36.92, 31.83, 30.99, 29.18, 27.84, 27.75, 27.71, 22.45. HR-MS calc. for $C_{34}H_{63}N_3O_{15}S$ $[M+H]^+$: 786.4053. Found: 786.4054.

N_3-PEG-PSMAi (9): To a 10 mL round bottom flask, equipped with a magnetic stir bar, was added MsO-PEG-PSMAi (200 mg, 254 μmol) in DMSO (5 mL), and NaN_3 (0.07 g, 1.02 mmol, 4 eq). The reaction mixture was allowed to stir overnight at 50 °C. The reaction mixture was diluted with water (40 mL) and extracted with Et_2O (4 x 25 mL). The combined organic layers were washed with brine and dried with Na_2SO_4. The product was concentrated by rotary evaporation to yield 173 mg of the product as a white solid (92 %). ^{1}H NMR (600 MHz; DMSO): δ 7.18 (t, *J* = 5.6, 1H), 6.28 (dd, *J* = 24.2, 8.3, 2H), 4.06-4.03 (m, 3H), 3.98-3.94 (m, 1H), 3.61 (t, *J* = 5.0, 2H), 3.58-3.54 (m, 10H), 3.40 (t, *J* = 4.9, 2H), 2.95 (q, *J* = 6.4, 2H), 2.28-2.17 (m, 2H), 1.89-1.86 (m, 1H), 1.70-1.65 (m, 1H), 1.59 (dt, *J* = 14.1, 6.7, 1H), 1.53-1.49 (m, 1H), 1.43-1.37 (m, 30H), 1.28 (dt, *J* = 15.1, 7.4, 3H). ^{13}C NMR (150 MHz, DMSO): δ = 172.20, 171.85, 171.38, 157.05, 156.09, 80.55, 80.25, 79.70, 69.79, 69.69, 69.23, 68.88, 62.97, 53.02, 52.13, 49.98, 31.72, 30.85, 29.05, 27.71, 27.61, 22.31. HR-MS calc. for $C_{33}H_{60}N_6O_{12}$ $[M+H]^+$: 733.4342. Found: 733.4344.

4.4.2.3. PSMAi Functionalized Dendrimers

$[ReDPA\text{-}G1\text{-}(PEG\text{-}PSMAi)_2]^+$ (10a): To a 5 mL round bottom flask, equipped with a magnetic stir bar, was added $[ReDPA\text{-}G1\text{-}(yne)_2]^+$ (10 mg, 12 μmol), PSMAi-PEG-N_3 (22 mg, 31 μmol, 2.5 eq) and sodium ascorbate (2.4 mg, 12.0 μmol, 1 eq) in 0.5 mL of DMF. The reaction flask was evacuated and back filled with N_2 three times. $CuSO_4$ (0.6 mg, 2.4 μmol, 0.2 eq) in 0.1 mL of dH_2O was added to the reaction vessel and the reaction mixture was allowed to stir at room temperature overnight. The product was

purified via semi-prep HPLC to yield 16.8 mg of the title compound as a white solid after lyophilization (60 %). ^{1}H NMR (700 MHz; DMSO): δ 8.81 (d, *J* = 5.4, 2H), 8.49 (s, 2H), 7.99 (td, *J* = 7.8, 1.4, 2H), 7.93 (t, *J* = 5.6, 1H), 7.83 (s, 2H), 7.54 (d, *J* = 7.9, 2H), 7.40 (t, *J* = 6.6, 2H), 7.20 (t, *J* = 5.6, 2H), 6.40 (dd, *J* = 30.9, 8.3, 4H), 4.89 (q, *J* = 21.5, 4H), 4.44 (t, *J* = 5.3, 4H), 4.15 (dd, *J* = 34.4, 11.0, 4H), 4.03 (td, *J* = 8.6, 5.2, 6H), 3.94 (td, *J* = 7.8, 5.7, 2H), 3.80-3.76 (m, 6H), 3.54 (t, *J* = 4.8, 4H), 3.51-3.47 (m, 14H), 3.17 (q, *J* = 6.5, 2H), 2.94 (q, *J* = 6.5, 4H), 2.88 (t, *J* = 7.5, 4H), 2.68 (t, *J* = 7.5, 4H), 2.27-2.17 (m, 4H), 1.88-1.85 (m, 2H), 1.83-1.79 (m, 2H), 1.67 (dtd, *J* = 14.0, 8.6, 5.7, 2H), 1.59-1.56 (m, 2H), 1.50 (td, *J* = 13.9, 6.2, 4H), 1.39 (d, *J* = 5.5, 47H), 1.26 (dt, *J* = 15.3, 7.7, 4H), 1.13 (s, 3H). HR-MS calc. for $C_{100}H_{156}N_{16}O_{32}Re$ $[M+2H]^{3+}$: 760.3607. Found: 760.3625.

$[ReDPA\text{-}G1\text{-}(PEG\text{-}PSMAi\text{-}COOH)_2]^+$ (11a): To a 5 mL round bottom flask, equipped with a magnetic stir bar, was added $[ReDPA\text{-}G1\text{-}(PEG\text{-}PSMAi)_2]^+$ (15.0 mg, 6.6 μmol) in 1 mL of CH_2Cl_2, followed by addition of 1 mL of TFA dropwise. The reaction mixture was allowed to stir at room temperature for 4 hours. The volatiles were removed by blowing N_2 over the reaction mixture and the product was purified via semi-prep HPLC and lyophilized to yield 4.8 mg of a white solid (37 %). ^{1}H NMR (700 MHz; MeOD): δ 8.88 (d, *J* = 5.4, 2H), 7.95 (t, *J* = 8.5, 2H), 7.84 (s, 2H), 7.55 (d, *J* = 7.7, 2H), 7.38 (t, *J* = 6.3, 2H), 4.53 (t, *J* = 5.1, 4H), 4.32 (dd, *J* = 8.6, 5.1, 2H), 4.26 (dd, *J* = 8.2, 4.7, 2H), 4.23 (q, *J* = 11.0, 4H), 4.15 (t, *J* = 4.7, 3H), 3.90 (d, *J* = 6.8, 2H), 3.87 (t, *J* = 5.1, 4H), 3.66 (t, *J* = 4.7, 4H), 3.63-3.60 (m, 12H), 3.09 (t, *J* = 6.9, 3H), 3.02 (t, *J* = 7.3, 4H), 2.78 (t, *J* = 7.4, 4H), 2.44-2.42 (m, 4H), 2.16-2.14 (m, 2H), 1.96-1.94 (m, 2H), 1.91-1.90 (m, 2H),

1.84-1.82 (m, 2H), 1.66-1.63 (m, 5H), 1.52-1.50 (m, 4H), 1.43-1.41 (m, 4H), 1.31-1.29 (m, 4H), 1.23 (s, 3H), 1.14 (d, J = 6.4, 2H). HR-MS calc. for $C_{76}H_{109}N_{16}O_{32}Re$ $[M+H]^{2+}$: 973.3552. Found: 973.3468.

$[ReDPA\text{-}G2\text{-}(PEG\text{-}PSMAi)_4]^+$ (12a): A 5 mL round bottom flask, equipped with a magnetic stir bar, was added $[ReDPA\text{-}G2\text{-}(yne)_4]^+$ (10.0 mg, 8.3 μmol), PSMAi-PEG-N_3 (30 mg, 41 μmol, 5 eq) and sodium ascorbate (3.3 mg, 17.0 μmol, 2 eq) in 0.5 mL of DMF. The reaction flask was evacuated and back filled with N_2 three times. $CuSO_4$ (0.8 mg, 3.3 μmol, 0.4 eq) in 0.1 mL of dH_2O was added to the reaction vessel and the reaction mixture was allowed to stir at room temperature overnight. The product was purified via semi-prep HPLC to yield 23 mg of the title compound as a white solid after lyophilization (65 %). ^{1}H NMR (700 MHz; DMSO): δ 8.80 (d, J = 5.4, 2H), 7.98 (t, J = 8.5, 2H), 7.81 (s, 4H), 7.54 (d, J = 7.9, 2H), 7.39 (t, J = 6.9, 2H), 7.18 (t, J = 5.7, 4H), 6.36-6.34 (m, 8H), 4.92 (d, J = 16.7, 2H), 4.87 (d, J = 16.8, 2H), 4.44 (t, J = 5.3, 8H), 4.18 (dd, J = 30.7, 10.9, 4H), 4.12 (s, 6H), 4.04-3.99 (m, 12H), 3.95-3.93 (m, 4H), 3.77 (t, J = 5.3, 8H), 3.60 (dd, J = 5.5, 4.5, 2H), 3.50-3.47 (m, 36H), 3.39 (t, J = 4.9, 4H), 3.13-3.12 (m, 2H), 2.94-2.93 (m, 7H), 2.85 (t, J = 7.5, 8H), 2.66 (t, J = 7.5, 8H), 2.23-2.21 (m, 8H), 1.86-1.84 (m, 6H), 1.68-1.65 (m, 4H), 1.58-1.57 (m, 4H), 1.52-1.49 (m, 8H), 1.43-1.37 (m, 89H), 1.26-1.23 (m, 8H), 1.16 (s, 3H), 1.11 (s, 6H). HR-MS calc. for $C_{186}H_{301}N_{28}O_{64}Re$ $[M+3H]^{4+}$: 1035.0245. Found: 1035.0221.

[ReDPA-G2-(PEG-PSMAi-COOH)$_4$]$^+$ (13a): To a 5 mL round bottom flask, equipped with a magnetic stir bar, was added [ReDPA-G2-(PEG-PSMAi)$_4$]$^+$ (15.0 mg, 3.6 μmol) in 1 mL of CH_2Cl_2, followed by addition of 1 mL of TFA dropwise. The reaction mixture was allowed to stir at room temperature for 4 hours. The volatiles were removed by blowing N_2 over the reaction mixture and the product was purified via semi-prep HPLC and lyophilized to yield 6.3 mg of a white solid (50 %). ^{1}H NMR (700 MHz; MeOD): δ 8.87 (d, *J* = 5.7, 2H), 7.95 (t, *J* = 7.8, 3H), 7.83 (s, 4H), 7.57 (d, *J* = 7.8, 2H), 7.38 (t, *J* = 6.6, 2H), 4.54 (t, *J* = 5.1, 8H), 4.33 (dd, *J* = 8.5, 5.1, 4H), 4.26 (t, *J* = 6.4, 8H), 4.20 (q, *J* = 9.9, 8H), 4.15 (t, *J* = 4.7, 8H), 3.92-3.90 (m, 2H), 3.88 (t, *J* = 5.1, 8H), 3.66 (t, *J* = 4.6, 8H), 3.62-3.58 (m, 28H), 3.09 (t, *J* = 6.9, 8H), 2.99 (q, *J* = 7.1, 8H), 2.75 (t, *J* = 7.0, 8H), 2.44-2.35 (m, 10H), 2.17-2.12 (m, 4H), 1.99-1.95 (m, 2H), 1.90 (dtd, *J* = 14.2, 8.6, 5.7, 4H), 1.86-1.81 (m, 4H), 1.68-1.65 (m, *J* = 7.4, 8H), 1.51 (qd, *J* = 14.7, 7.4, 8H), 1.42 (quintet, *J* = 7.7, 8H), 1.33-1.30 (m, 12H), 1.21 (s, 6H). HR-MS calc. for $C_{138}H_{205}N_{28}O_{64}Re$ $[M+2H]^{3+}$: 1156.4487. Found: 1156.4368.

[ReDPA-G1-(SA-PSMAi)$_2$]$^+$ (10b): A 5 mL round bottom flask, equipped with a magnetic stir bar, was added [ReDPA-G1-(yne)$_2$]$^+$ (10 mg, 12 μmol), PSMAi-SA-N_3 (24 mg, 31 μmol, 2.5 eq) and sodium ascorbate (2.4 mg, 12.0 μmol, 1 eq) in 0.5 mL of DMF. The reaction flask was evacuated and back filled with N_2 three times. $CuSO_4$ (0.6 mg, 2.4 μmol, 0.2 eq) in 0.1 mL of dH_2O was added to the reaction vessel and the reaction mixture was allowed to stir at room temperature overnight. The product was purified via semi-prep HPLC to yield 17.9 mg of the title compound as a white solid after

lyophilization (64 %). ^{1}H NMR (700 MHz; DMSO): δ 8.80 (d, *J* = 5.4, 2H), 8.53 (s, 2H), 7.98 (t, *J* = 7.8, 2H), 7.95 (m, 2H), 7.84 (s, 2H), 7.78 (t, *J* = 5.6, 2H), 7.73 (t, *J* = 5.6, 2H), 7.53 (d, *J* = 7.9, 2H), 7.40 (t, *J* = 6.6, 3H), 6.43 (dd, *J* = 33.4, 8.2, 4H), 4.89 (q, *J* = 22.0, 4H), 4.25 (t, *J* = 7.1, 4H), 4.14 (dd, *J* = 34.9, 11.0, 4H), 4.02 (td, *J* = 8.5, 5.2, 2H), 3.94 (td, *J* = 7.9, 5.5, 2H), 3.78 (m, 2H), 3.16 (q, *J* = 6.5, 2H), 2.99 (dq, *J* = 12.5, 6.3, 8H), 2.86 (t, *J* = 7.4, 4H), 2.68 (t, *J* = 7.5, 4H), 2.27-2.17 (m, 4H), 2.01 (t, *J* = 7.5, 8H), 1.87-1.84 (m, 2H), 1.82-1.80 (m, 2H), 1.74 (quintet, *J* = 7.3, 4H), 1.67-1.65 (m, 2H), 1.60-1.57 (m, 2H), 1.53-1.51 (m, 4H), 1.44 (t, *J* = 6.9, 8H), 1.39-1.33 (m, 51H), 1.26-1.24 (m, 8H), 1.20-1.19 (m, 10H), 1.11 (s, 3H). HR-MS calc. for $C_{110}H_{175}N_{18}O_{26}Re$ $[M+H]^{2+}$: 1177.1332. Found: 1177.1261.

$[ReDPA-G1-(SA-PSMAi-COOH)_2]^+$ (11b): To a 5 mL round bottom flask, equipped with a magnetic stir bar, was added $[ReDPA-G1-(SA-PSMAi)_2]^+$ (15.0 mg, 6.4 μmol) in 1 mL of CH_2Cl_2, followed by addition of 1 mL of TFA dropwise. The reaction mixture was allowed to stir at room temperature for 4 hours. The volatiles were removed by blowing N_2 over the reaction mixture and the product was purified via semi-prep HPLC and lyophilized to yield 7.2 mg of a white solid (56 %). ^{1}H NMR (700 MHz; MeOD): δ 8.87 (d, *J* = 5.5, 2H), 7.95 (td, *J* = 7.8, 1.4, 2H), 7.77 (s, 2H), 7.55 (d, *J* = 7.8, 2H), 7.38 (t, *J* = 6.6, 2H), 4.34 (t, *J* = 6.7, 4H), 4.29-4.28 (m, 2H), 4.22 (m, 5H), 3.90-3.89 (m, 2H), 3.16 (dt, *J* = 14.9, 7.3, 8H), 3.01 (t, *J* = 7.3, 4H), 2.77 (t, *J* = 7.3, 4H), 2.42-2.40 (m, 4H), 2.17 (t, *J* = 7.5, 6H), 2.15-2.13 (m, 3H), 1.96-1.83 (m, 11H), 1.67-1.61 (m, 12H), 1.49-1.44

(m, 13H), 1.36-1.30 (m, 19H), 1.22 (s, 3H). HR-MS calc. for $C_{86}H_{127}N_{18}O_{26}Re$ $[M+H]^{2+}$: 1008.4440. Found: 1008.4409.

$[ReDPA-G2-(SA-PSMAi)_4]^+$ (12b): To a 5 mL round bottom flask, equipped with a magnetic stir bar, was added $[ReDPA-G2-(yne)_4]^+$ (10.0 mg, 8.3 μmol), PSMAi-SA-N_3 (32 mg, 41 μmol, 5 eq) and sodium ascorbate (3.3 mg, 16.5 μmol, 2 eq) in 0.5 mL of DMF. The reaction flask was evacuated and back filled with N_2 three times. $CuSO_4$ (0.8 mg, 3.3 μmol, 0.4 eq) in 0.1 mL of dH_2O was added to the reaction vessel and the reaction was allowed to stir at room temperature overnight. The product was purified via semi-prep HPLC to yield 21 mg of the title compound as a white solid after lyophilization (60 %). ^{1}H NMR (700 MHz; DMSO): δ 8.80 (d, *J* = 5.5, 2H), 8.44-8.44 (m, 2H), 8.00-7.97 (m, 4H), 7.82 (s, 2H), 7.72-7.68 (m, 10H), 7.54 (d, *J* = 7.9, 1H), 7.48 (d, *J* = 7.8, 2H), 7.40 (t, *J* = 6.7, 1H), 7.20 (dd, *J* = 7.0, 5.2, 2H), 6.30 (dt, *J* = 26.5, 7.6, 8H), 4.90 (dd, *J* = 44.5, 16.7, 4H), 4.45-4.41 (m, 6H), 4.29 (t, *J* = 7.1, 6H), 4.28-4.23 (m, 4H), 4.23-4.14 (m, 4H), 4.11-4.09 (m, 4H), 4.04 (ddd, *J* = 12.9, 8.7, 4.4, 6H), 3.95 (q, *J* = 6.8, 4H), 3.69 (s, 3H), 3.46-3.43 (m, 8H), 3.14-3.13 (m, 2H), 2.99 (tquintet, *J* = 12.6, 6.3, 16H), 2.84 (t, *J* = 7.5, 4H), 2.65 (t, *J* = 7.5, 4H), 2.43-2.40 (m, 2H), 2.27-2.16 (m, 8H), 2.00 (t, *J* = 7.5, 16H), 1.89-1.84 (m, 4H), 1.75 (tt, *J* = 15.7, 7.8, 8H), 1.66 (dtd, *J* = 14.0, 8.6, 5.7, 6H), 1.59 (dd, *J* = 14.1, 6.3, 4H), 1.52-1.43 (m, 24H), 1.36-1.31 (m, 99H), 1.30-1.16 (m, 34H), 1.00 (s, 3H). HR-MS calc. for $C_{206}H_{338}N_{32}O_{52}Re$ $[M+3Na]^{4+}$: 1087.6022. Found: 1087.6003.

[ReDPA-G2-(SA-PSMAi-COOH)$_4$]$^+$ (13b): To a 5 mL round bottom flask, equipped with a magnetic stir bar, was added [ReDPA-G2-(SA-PSMAi)$_4$]$^+$ (10.0 mg, 2.3 μmol) in 1 mL of CH_2Cl_2, followed by addition of 1 mL of TFA dropwise. The reaction was allowed to stir at room temperature for 4 hours. The volatiles were removed by blowing N_2 over the reaction mixture and the product was purified via semi-prep HPLC and lyophilized to yield 5.3 mg of a white solid (67 %). ^{1}H NMR (700 MHz; MeOD): δ 8.78-8.74 (m, 2H), 7.84 (dd, *J* = 14.5, 6.8, 2H), 7.70-7.61 (s, 4H), 7.45 (t, *J* = 9.9, 2H), 7.28-7.24 (m, 2H), 4.27-4.18 (m, 6H), 4.18-4.15 (m, 4H), 4.12-4.00 (m, 8H), 3.84-3.77 (m, 4H), 3.08-2.98 (m, 7H), 2.90-2.83 (m, 4H), 2.66-2.60 (m, 4H), 2.38-2.25 (m, 6H), 2.11-2.03 (m, 8H), 1.93-1.83 (m, 4H), 1.84-1.67 (m, 9H), 1.60-1.53 (m, 4H), 1.53-1.44 (m, 8H), 1.49-1.36 (m, 12H), 1.32 (td, J = 14.6, 7.2, 4H), 1.29-1.17 (m, 16H), 1.11-1.09 (m, 3H), 1.09-1.00 (m, 4H). HR-MS calc. for $C_{158}H_{241}N_{32}O_{52}Re$ $[M+3H]^{4+}$: 902.6741. Found: 902.6771.

4.4.3. *In vitro* Competitive Inhibition Assay

LNCaP cells were plated in 24 well plates for confluency at time of use. Growth media was removed and 300 μL of binding buffer, [RPMI 1640 with 2mM glutamine + 0.5% BSA containing a fixed amount of 125I-TAAG-PSMA (0.45 nM), a previously published PSMA inhibitor, and increasing concentrations of competitor (0 nM - 10 000 nM)].[9] After 1h at RT, binding buffer and cells were transferred to microcentrifuge tubes (1.5 mL), binding buffer was removed and cells were washed 3 times with wash buffer (RPMI 1640 with 2mM glutamine + 0.5% BSA) using centrifugation for 30 s at max speed. After washing, cells were lysed in 500 μL RIPA buffer (100 mM Tris pH 8, 50

mM NaCl, 1% NP40, 0.5% Na deoxycholate, 0.1% SDS) and incubated at 37˚C for 30 min. A 400 µL aliquot of lysate was transferred to gamma counting tubes and counted for 10 min. in a Perkin Elmer Wizard 1470 Automatic Gamma Counter. The resulting CPM values were used to calculate the relative binding with respect to the control (no competitor present). The assay was repeated three times for all compounds with each experiment done in triplicate. For each repeat the positive control, PMPA was also measured in triplicate. GraphPad Prism 5 software was used to determine the IC50 values.

[ReDPA-G1-(PEG-PSMAi-COOH)$_2$]$^+$:

Table S4.1. IC_{50} data for [ReDPA-G1-(PEG-PSMAi-COOH)$_2$]$^+$ over 3 trials.

	Trial 1	**Trial 2**	**Trial 3**
IC_{50} (nM)	652.1	266.0	230.8
95% CI	223.4 – 1904	178.0 – 397.4	128.1 – 415.8
Std Error of curve fit	1.67	1.21	1.32
R^2	0.8454	0.9777	0.9525

Table S4.2. Combined analysis of IC_{50} data for [ReDPA-G1-(PEG-PSMAi-COOH)$_2$]$^+$.

	Combined Aggregate Data (GraphPad)	**Combined Experimental Averaged data (Excel)**
IC_{50} (nM)	366.1	383.0
95% CI	206.1 – 650.3	176.5 – 905.7
Std Error	1.33	233.7 (std dev between experiments)
R^2	0.8578	

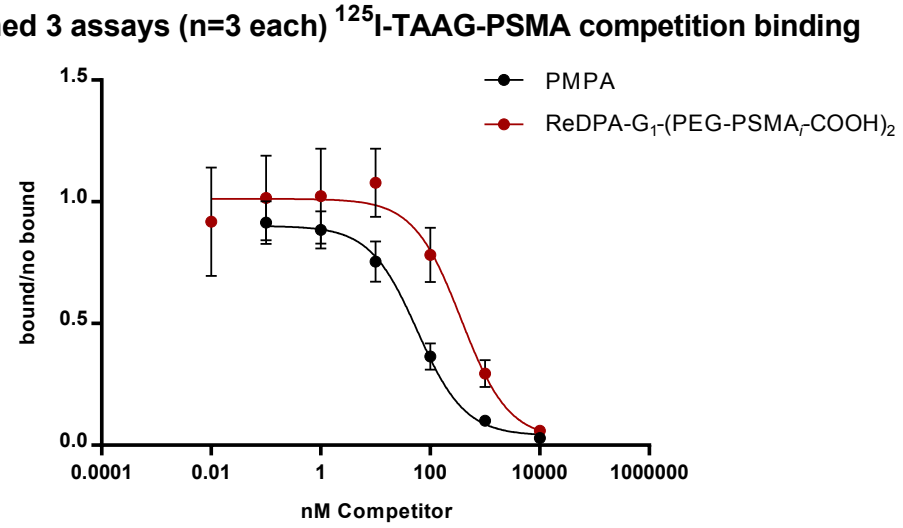

Figure S4.1. Competition binding assay curve for [ReDPA-G1-(PEG-PSMAi-COOH)$_2$]$^+$.

$[ReDPA\text{-}G2\text{-}(PEG\text{-}PSMAi\text{-}COOH)_4]^+$:

Table S4.3. IC_{50} data for $[ReDPA\text{-}G2\text{-}(PEG\text{-}PSMAi\text{-}COOH)_4]^+$ over 3 trials.

	Trial 1	Trial 2	Trial 3
IC50 (nM)	28.89	29.79	20.97
95% CI	20.03 – 41.65	17.64 – 50.33	13.79 – 31.89
Std Error of curve fit	1.19	1.28	1.21
R^2	0.9828	0.9653	0.9850

Table S4.4. Combined analysis of IC_{50} data for $[ReDPA\text{-}G2\text{-}(PEG\text{-}PSMAi\text{-}COOH)_4]^+$.

	Combined Aggregate Data (GraphPad)	Combined Experimental Averaged data (Excel)
IC50 (nM)	25.86	26.55
95% CI	19.14 – 34.94	17.15 – 41.29
Std Error	1.16	4.85 (std dev between experiments)
R^2	0.9621	

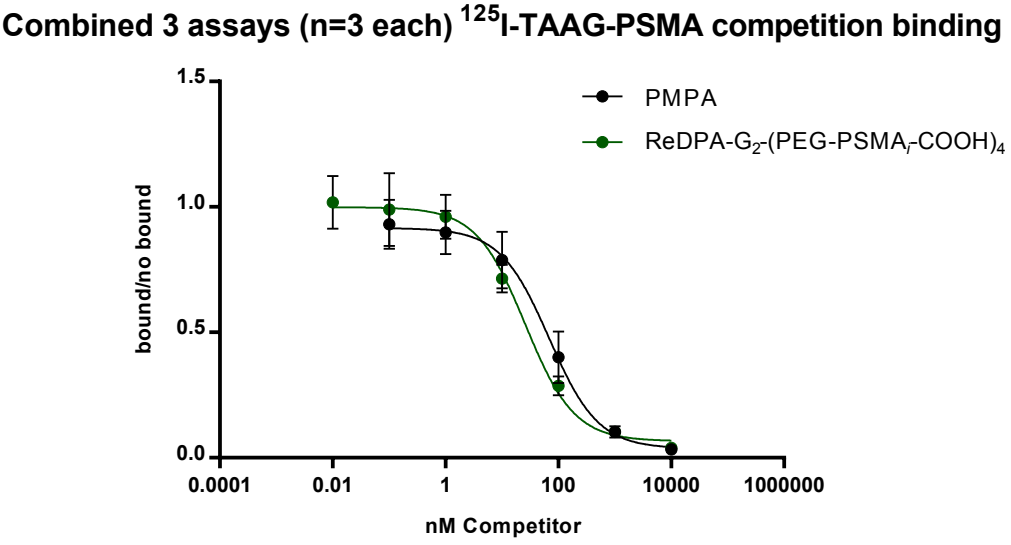

Figure S4.2. Competition binding assay curve for $[ReDPA\text{-}G2\text{-}(PEG\text{-}PSMAi\text{-}COOH)_4]^+$.

[ReDPA-G1-(SA-PSMAi-COOH)$_2$]$^+$:

Table S4.5. IC_{50} data for [ReDPA-G1-(SA-PSMAi-COOH)$_2$]$^+$ over 3 trials.

	Trial 1	Trial 2	Trial 3
IC50 (nM)	12.84	14.72	18.73
95% CI	9.27 – 17.79	11.74 – 18.46	15.41 – 22.75
Std Error of curve fit	1.17	1.11	1.1
R^2	0.9843	0.9925	0.9947

Table S4.6. Combined analysis of IC_{50} data for [ReDPA-G1-(SA-PSMAi-COOH)$_2$]$^+$.

	Combined Aggregate Data (GraphPad)	Combined Experimental Averaged data (Excel)
IC50 (nM)	15.05	15.43
95% CI	12.13 – 18.66	12.14 – 19.67
Std Error	1.11	3.01 (std dev between experiments)
R^2	0.9757	

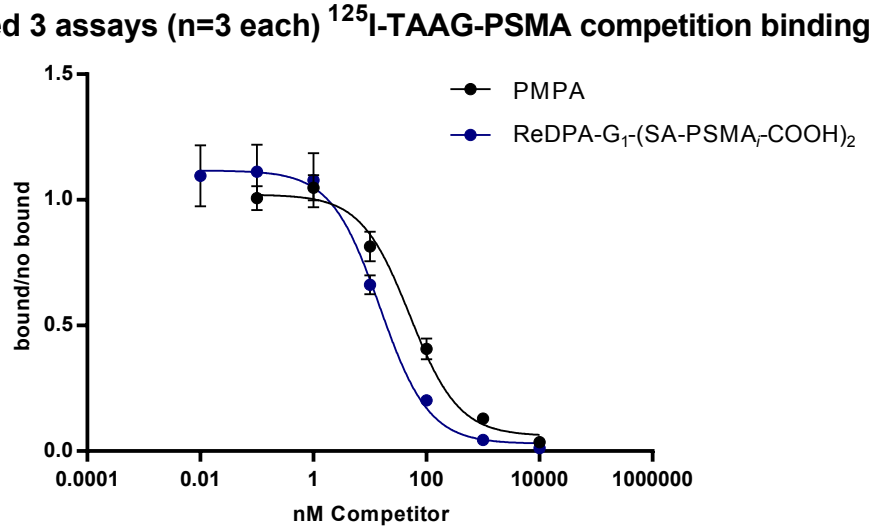

Figure S4.3. Competition binding assay curve for [ReDPA-G1-(SA-PSMAi-COOH)$_2$]$^+$.

[ReDPA-G2-(SA-PSMAi-COOH)$_4$]$^+$:

Table S4.7. IC_{50} data for [ReDPA-G2-(SA-PSMAi-COOH)$_4$]$^+$ over 3 trials.

	Trial 1	Trial 2	Trial 3
IC50 (nM)	7.835	8.009	8.611
95% CI	6.431 – 9.546	6.468 – 9.918	6.257 – 11.85
Std Error of curve fit	1.1	1.11	1.16
R^2	0.9942	0.9932	0.9848

Table S4.8. Combined analysis of IC_{50} data for [ReDPA-G2-(PEG-PSMAi-COOH)$_4$]$^+$.

	Combined Aggregate Data (GraphPad)	Combined Experimental Averaged data (Excel)
IC50 (nM)	8.155	8.152
95% CI	6.698 – 9.93	6.385 – 10.44
Std Error	1.1	0.407 (std dev between experiments)
R^2	0.979	

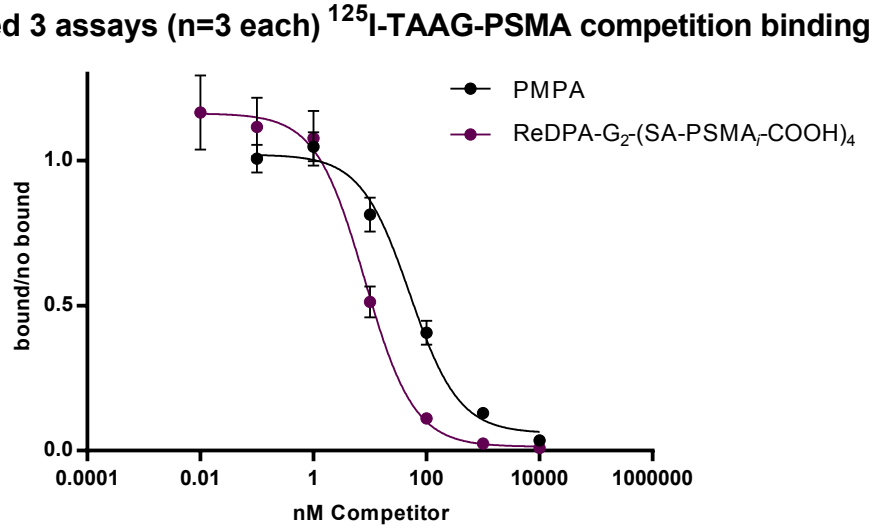

Figure S4.4. Competition binding assay curve for [ReDPA-G2-(SA-PSMAi-COOH)$_4$]$^+$.

4.5. References

(1) Statistics, C. C. *Canadian Cancer Statistics*; 2013; pp. 1–114.

(2) Chen, Y.; Pullambhatla, M.; Foss, C. A.; Byun, Y.; Nimmagadda, S.; Senthamizhchelvan, S.; Sgouros, G.; Mease, R. C.; Pomper, M. G. *Clin. Cancer Res.* **2011**, *17*, 7645–7653.

(3) Morris, M. J.; Akhurst, T.; Larson, S. M.; Ditullio, M.; Chu, E.; Siedlecki, K.; Verbel, D.; Heller, G.; Kelly, W. K.; Slovin, S.; Schwartz, L.; Scher, H. I. *Clin. Cancer Res.* **2005**, *11*, 3210–3216.

(4) Souvatzoglou, M.; Weirich, G.; Schwarzenboeck, S.; Maurer, T.; Schuster, T.; Bundschuh, R. A.; Eiber, M.; Herrmann, K.; Kuebler, H.; Wester, H. J.; Hoefler, H.; Gschwend, J.; Schwaiger, M.; Treiber, U.; Krause, B. J. *Clinical Cancer Research* **2011**, *17*, 3751–3759.

(5) Bauman, G.; Belhocine, T.; Kovacs, M.; Ward, A.; Beheshti, M.; Rachinsky, I. **2011**, *15*, 45–55.

(6) Bařinka, C.; Rovenská, M.; Mlčochová, P.; Hlouchová, K.; Plechanovová, A.; Majer, P.; Tsukamoto, T.; Slusher, B. S.; Konvalinka, J.; Lubkowski, J. *J. Med. Chem.* **2007**, *50*, 3267–3273.

(7) Foss, C. A.; Mease, R. C.; Fan, H.; Wang, Y.; Ravert, H. T.; Dannals, R. F.; Olszewski, R. T.; Heston, W. D.; Kozikowski, A. P.; Pomper, M. G. *Clin. Cancer Res.* **2005**, *11*, 4022–4028.

(8) Chen, Y.; Foss, C. A.; Byun, Y.; Nimmagadda, S.; Pullambhatla, M.; Fox, J. J.; Castanares, M.; Lupold, S. E.; Babich, J. W.; Mease, R. C.; Pomper, M. G. *J.*

Med. Chem. **2008**, *51*, 7933–7943.

(9) Banerjee, S. R.; Pullambhatla, M.; Shallal, H.; Lisok, A.; Mease, R. C.; Pomper, M. G. *Oncotarget* **2011**, *2*, 1244.

(10) Maresca, K. P.; Hillier, S. M.; Femia, F. J.; Keith, D.; Barone, C.; Joyal, J. L.; Zimmerman, C. N.; Kozikowski, A. P.; Barrett, J. A.; Eckelman, W. C.; Babich, J. W. *J. Med. Chem.* **2009**, *52*, 347–357.

(11) Joyal, J. L.; Barrett, J. A.; Marquis, J. C.; Chen, J.; Hillier, S. M.; Maresca, K. P.; Boyd, M.; Gage, K.; Nimmagadda, S.; Kronauge, J. F.; Friebe, M.; Dinkelborg, L.; Stubbs, J. B.; Stabin, M. G.; Mairs, R.; Pomper, M. G.; Babich, J. W. *Cancer Res.* **2010**, *70*, 4045–4053.

(12) Ray Banerjee, S.; Pullambhatla, M.; Foss, C. A.; Falk, A.; Byun, Y.; Nimmagadda, S.; Mease, R. C.; Pomper, M. G. *J. Med. Chem.* **2013**, *56*, 6108–6121.

(13) Parrott, M. C.; Benhabbour, S. R.; Saab, C.; Lemon, J. A.; Parker, S.; Valliant, J. F.; Adronov, A. *J. Am. Chem. Soc.* **2009**, *131*, 2906–2916.

(14) Feliu, N.; Walter, M. V.; Montañez, M. I.; Kunzmann, A.; Hult, A.; Nyström, A.; Malkoch, M.; Fadeel, B. *Biomaterials* **2012**, *33*, 1970–1981.

(15) Chandran, S. S.; Banerjee, S. R.; Mease, R. C.; Pomper, M. G.; Denmeade, S. R. *Cancer Biol. Ther.* **2008**, *7*, 974–982.

Chapter 5. Synthesis, Radiolabeling and Biodistribution of PSMA Targeted Dendrimers

**All synthesis and radiolabeling work presented in this chapter was carried out by Lukas Sadowski. Plasma stability and biodistribution studies were performed by Nancy Janzen.*

Abstract:

Early detection and imaging of prostate cancer is critical in a disease that affects one in eight men. Lys-urea-glu, a dipeptide with a high affinity toward PSMA has been exploited to target the over-expression of PSMA *in vivo*. Using bis-MPA as a dendritic imaging scaffold, a high affinity PSMA targeted tracer was radiolabeled with ^{99m}Tc and the resulting probe was investigated *in vitro* and *in vivo*. Radiolabeling of the compound proceeded in near quantitative yields, however, the compound was found to have limited stability in mouse plasma. Bio-distribution data resulted in high uptake in the gall bladder and only modest uptake of the radiotracer within the tumor. Plasma stability and bio-distribution data suggest facile hydrolysis of the ester linkages within the dendrimer backbone.

5.1. Introduction

The use of bis-MPA dendrimers for biomedical applications has received considerable attention owing to the favorable properties exhibited by the structural scaffold. These properties include excellent biocompatibility, moderately good stability[1] and ease of functionalization at the periphery and core.[2] Furthermore, circulation times of bis-MPA dendrimers *in vivo* can be tuned via PEGylation of the periphery.[3] As a result, this class of dendrimers has successfully been employed as a scaffold for therapeutic[4–7] and imaging applications.[2,8] With regard to the latter application, dendrimers have been used in multiple imaging modalities, often exploiting the multivalent periphery to improve image quality or disease targeting.[9,10]

A targeting moiety that has shown promising results upon attachment to a divalent scaffold is lys-urea-glu, a dipeptide targeting the prostate specific membrane antigen (PSMA).[11] Imaging the overexpression of PSMA is a useful and attractive method for the early detection of prostate cancer.[12] The lys-urea-glu PSMA inhibitor has been extensively investigated for the early detection of prostate cancer.[13,14] The excellent specificity and high target:non target ratio has warranted nuclear molecular imaging probes based on the aforementioned urea inhibitor to be investigated in a clinical setting. Despite the success of the targeting vector, very little effort has gone into investigating the effects of multivalency on affinity and pharmacokinetics.

Although dendrimers have previously been investigated as theranostic scaffolds for treatment of PSMA, their applications in nuclear imaging has been limited.[15] Herein, we investigate not only the effect of multivalency on the biodistribution of the PSMA

targeted dendrimers, but also the effect of ester linkages on the stability of these compounds *in vitro* and *in vivo*. By using an imaging scaffold with both neopentyl and non-neopentyl esters, we aim to evaluate the robustness of the system as well as determine its limitations.

5.2. Results and Discussion

5.2.1. Synthesis

Based on the affinity of PSMA targeted dendrimers discussed in chapter 4 of this thesis, we opted to investigate the highest affinity dendrimer for radiolabeling and a biodistribution study. Given the difficulty in removing copper from the DPA ligand and the challenges associated with transmetalation of Cu with ^{99m}Tc (as discussed in chapter 2), the lys-urea-glu PSMA inhibitor was attached to the second generation alkyne decorated dendrimer having the pTSe protecting group at the core using the CuAAC (Scheme 5.1). Using the PSMA inhibitor with the alkyl suberic acid linker, the coupling proceeded smoothly to give the desired product (**1**), with no partially functionalized dendrimer visible by HPLC analysis of the crude reaction mixture. Subsequent removal of the pTSe core protecting group was accomplished using DBU to yield the free carboxylic acid (**2**). Activation of the carboxylic acid via N-hydroxy succinimide enabled the DPA ligand to be coupled to the core of the dendrimer in a mild and highly efficient manner.

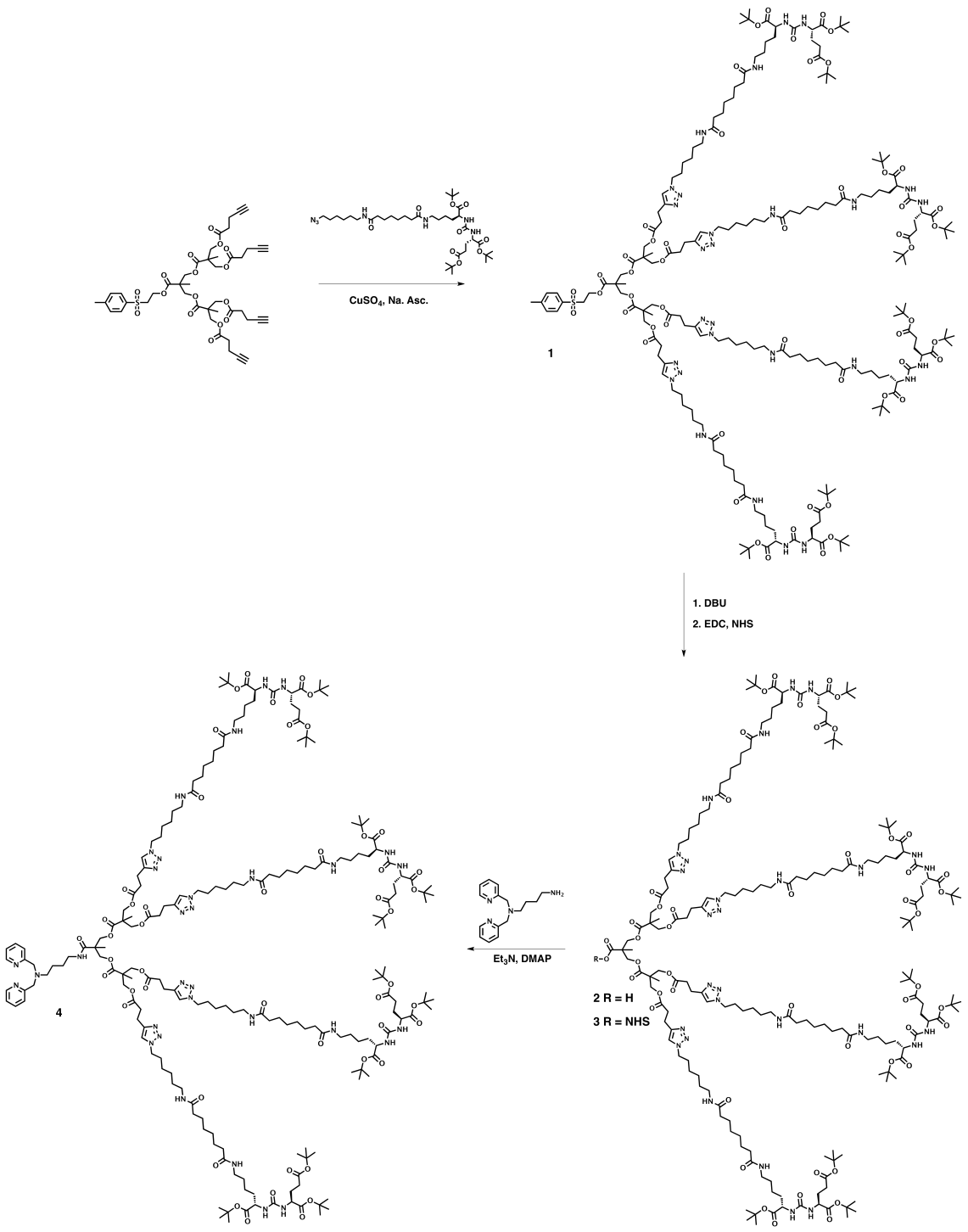

Scheme 5.1. Synthesis of DPA-G2-(SA-PSMAi)$_4$ from pTSe-G2-(yne)$_4$.

The DPA-G2-(SA-PSMAi)$_4$ (**4**) dendrimer was treated with TFA to remove the tert-butyl protecting groups from the carboxylic acids located on the lys-urea-glu PSMA inhibitors at the periphery of the dendrimer (Scheme 5.2). Prior to removal of the tert-butyl groups, the dendrimer could also be treated with the [Re(CO)$_3$(H$_2$O)$_3$]Br salt to co-ordinate Re to the DPA ligand. The acidic nature of the Re salt necessitates the reaction mixture to be buffered (ie. using PBS) in order to prevent premature removal of the tert-butyl protecting groups. This synthetic method provides an alternate route for the synthesis of $^{+}$[ReDPA-G2-(SA-PSMAi-COOH)$_4$] **(6)**, which was first reported in Chapter 4 of this thesis.

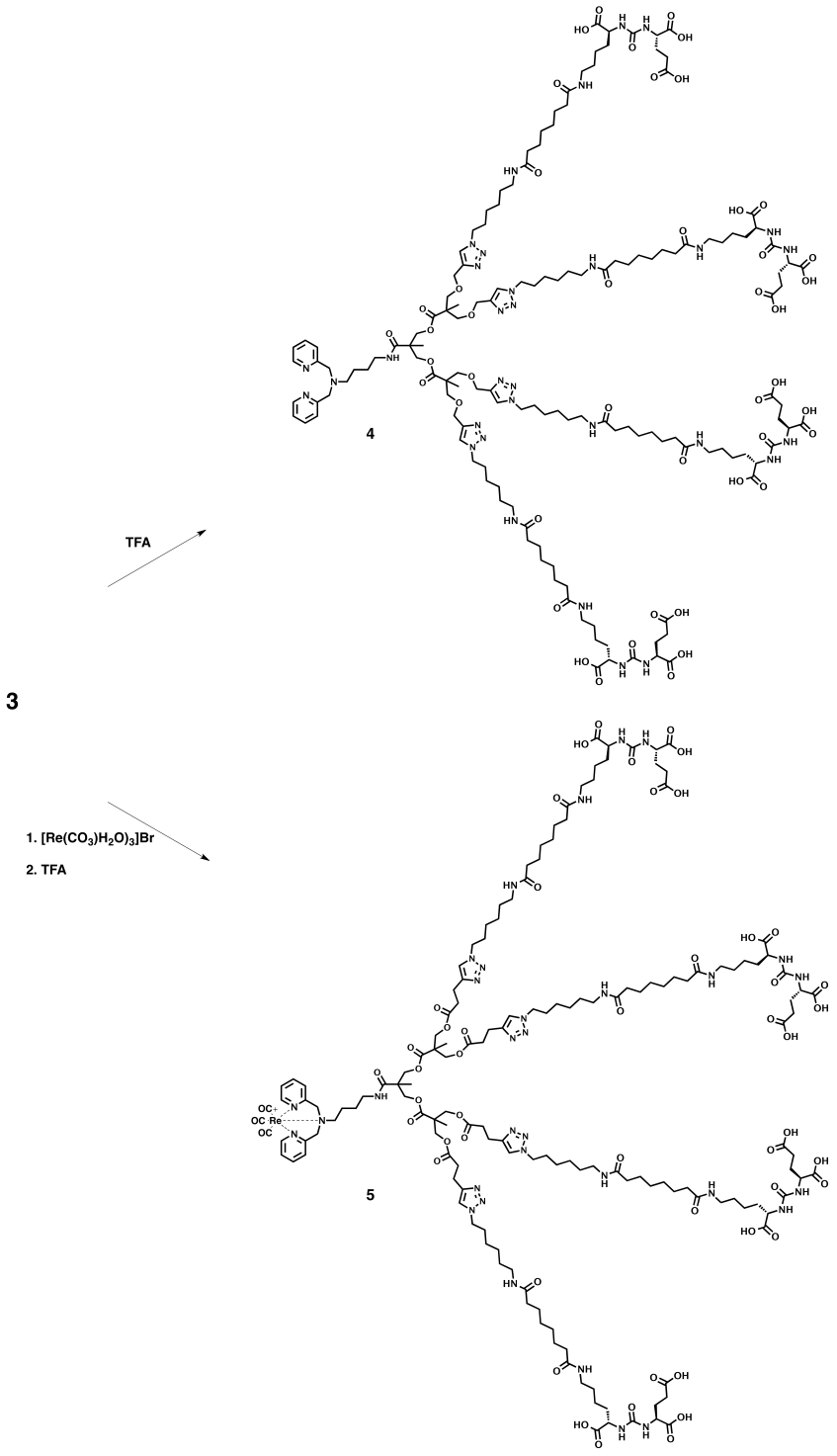

Scheme 5.2. Synthesis of DPA-G2-(SA-PSMAi-COOH)$_4$ and [ReDPA-G2-(SA-PSMAi-COOH)$_4$]$^+$.

5.2.2. Radiolabeling and Plasma Stability

Radiolabeling of the PSMA targeted dendrimer was accomplished using $[Tc(CO)_3(H_2O)_3]^+$, which was prepared by the reduction of TcO_4^- using borano carbonate.[16] Efficient radiolabeling of the dendrimer was accomplished after 5 minutes at 80 °C, while negligible degradation of the dendrimer backbone was visible (Scheme 5.3 and Figure 5.1). Furthermore, a histidine and bipyridine challenge to remove loosely bound Tc resulted in no loss of radioactivity from dendrimer, as determined by HPLC analysis. The radiolabeled $[^{99m}$TcDPA-G2-(SA-PSMAi-COOH)$_4]^+$ dendrimer had a retention time that corresponded to the non-radioactive rhenium analogue (Figure 5.1). The simple and efficient radiolabeling and facile purification of the product enabled preparation of the target compound in high purity, as required for *in vivo* analysis.

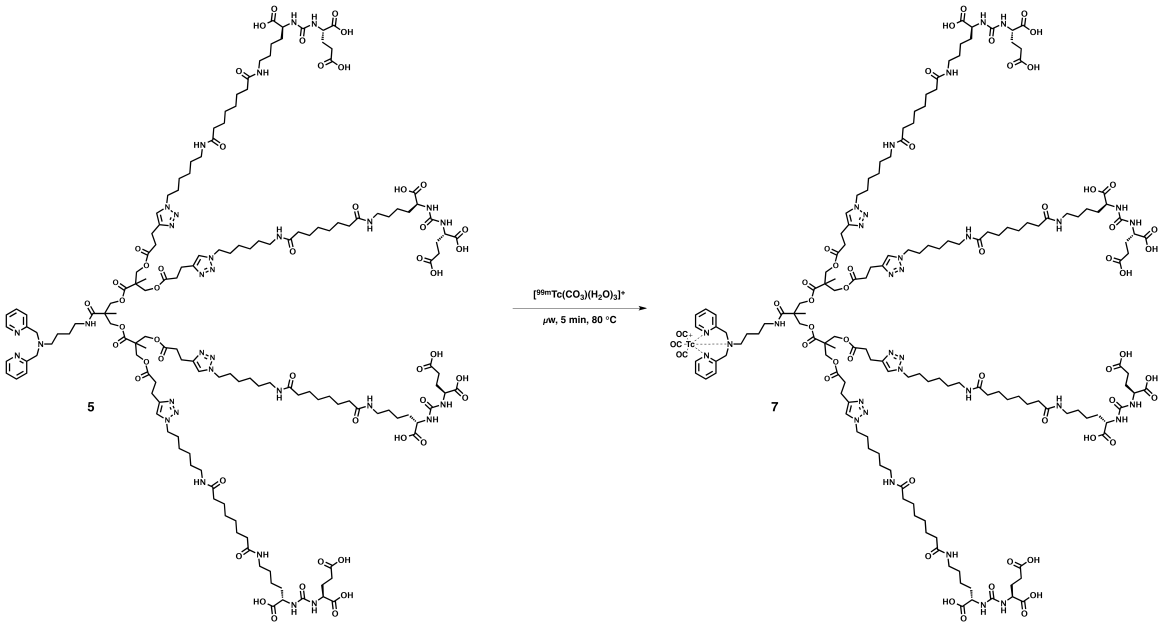

Scheme 5.3: Radiolabeling of DPA-G2-(SA-PSMAi-COOH)$_4$ (**5**) with ^{99m}Tc to prepare $[^{99m}$TcDPA-G2-(SA-PSMAi-COOH)$_4]^+$ (**7**).

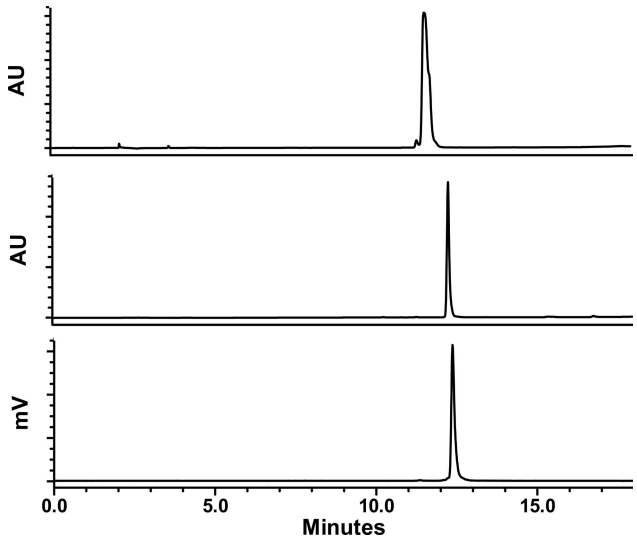

Figure 5.1: UV trace of DPA-G2-(SA-PSMAi-COOH)$_4$ (**5**) (top), [ReDPA-G2-(SA-PSMAi-COOH)$_4$]$^+$ (**6**) (middle) and gamma trace of [^{99m}Tc DPA-G2-(SA-PSMAi-COOH)$_4$]$^+$ (**7**) (bottom).

Log P of the radiolabeled dendrimer (**7**) was calculated to be -3.47, which is consistent with having 12 carboxylic acid moieties on a single molecule. To evaluate the plasma stability of the resulting imaging agent *in vitro*, we incubated the radiolabeled compound in mouse plasma and performed HPLC analysis at various time points up to 4 hours. Each plasma sample was diluted with acetonitrile to precipitate out the proteins followed by centrifugation. No radioactivity was observed in the pellet, indicating no protein binding of the targeting vector (see supplementary info). HPLC analysis of the supernatant revealed extensive degradation of the imaging agent within 15 minutes (Figure 5.2). Complete degradation was observed by the 30 minute time point.

Interestingly, a secondary degradation product was evident at the two hour time point which became more prevalent after four hours. Given the stability of esters *in vivo* and the lack of other readily hydrolysable linkages within the structure, a likely route of degradation would first involve hydrolysis of the non-neopentyl esters, followed by the sterically more hindered neopentyl esters.

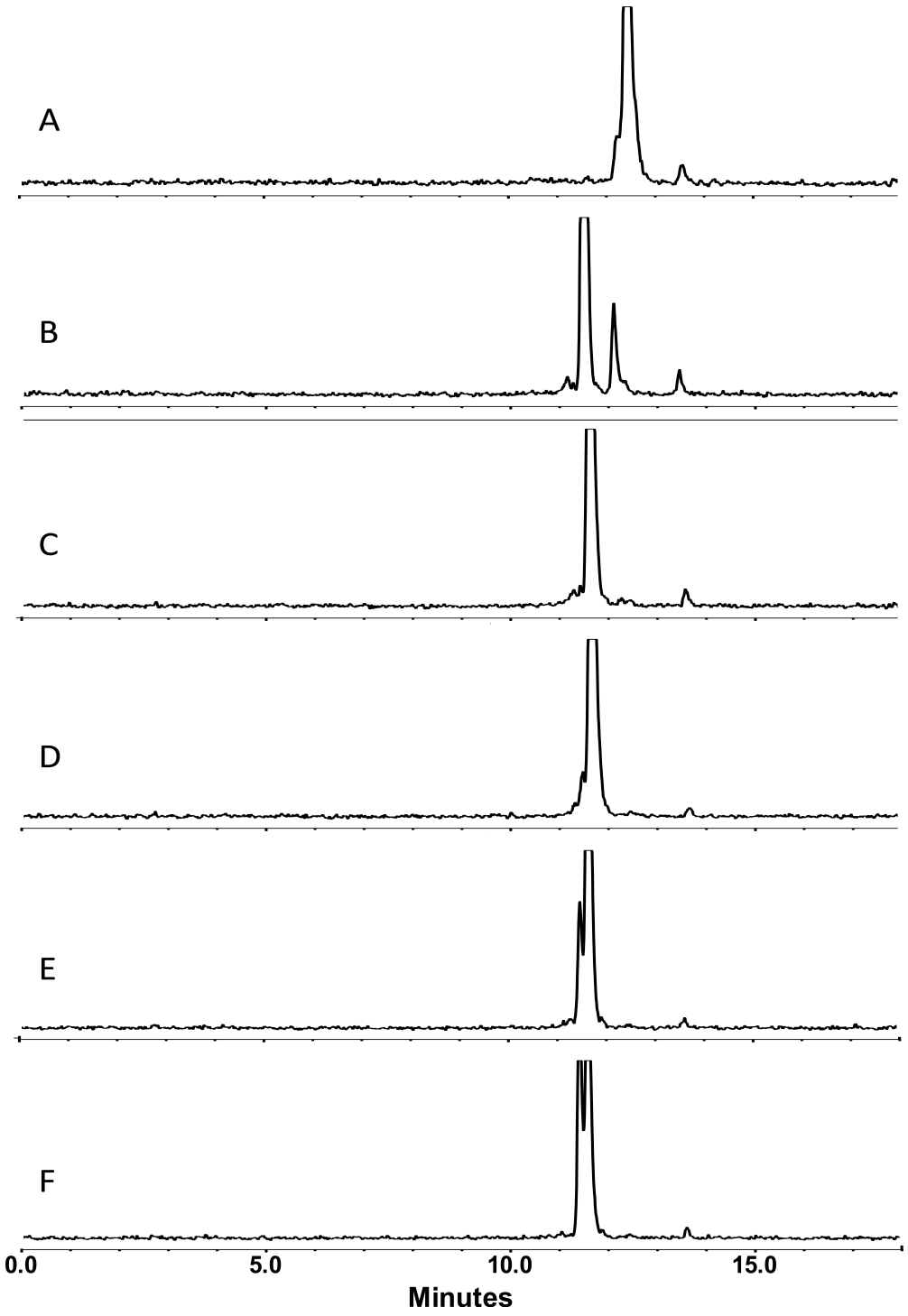

Figure 5.2. Plasma stability of $[TcDPA\text{-}G2\text{-}(SA\text{-}PSMAi\text{-}COOH)_4]^+$ at A) 0 min B) 15 min C) 30 min D) 1 hour E) 2 hours and F) 4 hours.

5.2.4. Bio-Distribution of a PSMA Targeted Dendrimer

A biodistribution of the radiolabeled dendrimer was investigated *in vivo* using nude LNCap tumor bearing mice, a tumor model known to overexpress PSMA. Upon radiolabeling and purification, the dendrimer was evaporated to dryness and formulated in 10 % EtOH/PBS. Three time points were chosen to evaluate the *in vivo* biodistribution of the targeted dendrimer: 1, 6 and 24 hours. After 1 hour, only 0.87 ± 0.19 % ID/g was observed in the tumour (Figure 5.3, Table 5.1, 5.2). A major proportion of the radioactivity was observed in the clearance organs such as the kidney, gallbladder and intestines. The 6 and 24 hour time points indicated a significant clearance of the radioactivity via the intestines and kidney with slow washout of radioactivity from the tumour. This is in contrast to what was observed by Pomper and co-workers for multivalent PSMA targeted molecular imaging agents, who saw an increase in affinity towards PSMA *in vivo* and excellent tumour uptake, particularly, when comparing monovalent and divalent urea dipeptide inhibitor analogues.[11]

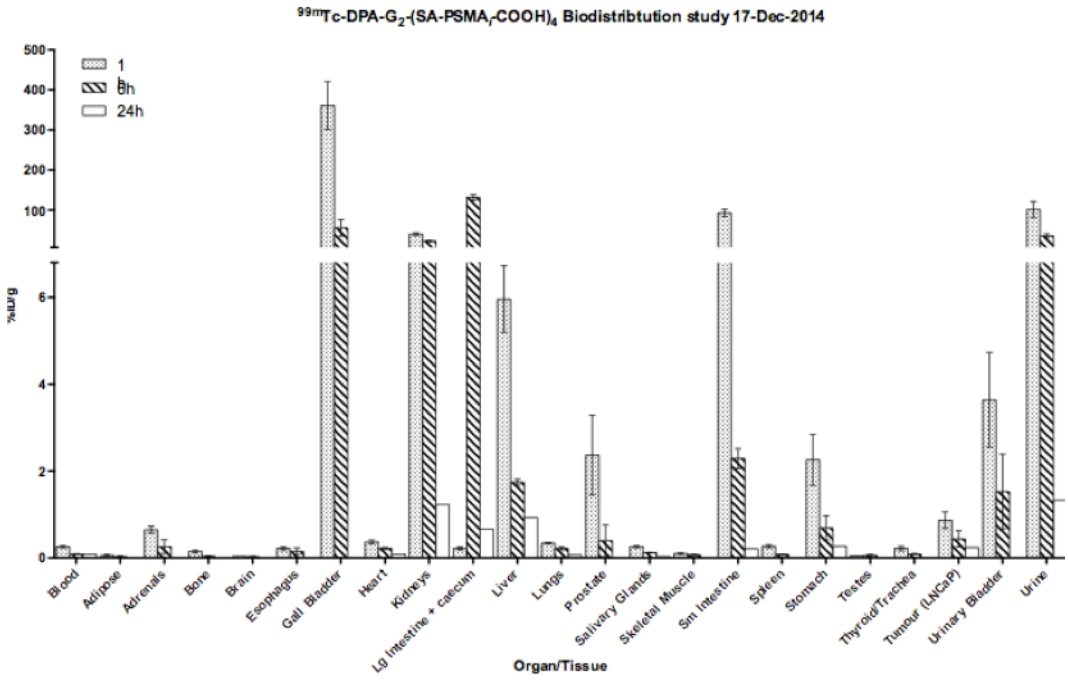

Figure 5.3. *In vivo* biodistribution of $[^{99m}$TcDPA-G2-(SA-PSMAi-COOH)$_4]^+$ in LNCaP xenograft mice. Mice were injected with ~0.3MBq of test article and sacrificed at various timepoints. Data expressed as %ID/g.

Table 5.1: Tissue distribution of $[^{99m}TcDPA\text{-}G2\text{-}(SA\text{-}PSMAi\text{-}COOH)_4]^+$ in NCr nude mice bearing LNCaP xenografts.

	Time (h)		
Organs	**1**	**6**	**24**
Blood	0.26 ± 0.02	0.09 ± 0.00	0.09 ± n/a
Adipose	0.06 ± 0.02	0.03 ± 0.02	0.00 ± n/a
Adrenals	0.65 ± 0.08	0.26 ± 0.16	0.00 ± n/a
Bone	0.15 ± 0.03	0.04 ± 0.01	0.00 ± n/a
Brain	0.04 ± 0.00	0.03 ± 0.00	0.00 ± n/a
Esophagus	0.22 ± 0.04	0.15 ± 0.08	0.00 ± n/a
Gall Bladder	360.96 ± 59.81	55.87 ± 20.94	0.00 ± n/a
Heart	0.37 ± 0.04	0.22 ± 0.02	0.09 ± n/a
Kidneys	40.43 ± 3.24	22.92 ± 2.48	1.23 ± n/a
Lg Intestine + caecum	0.22 ± 0.03	131.49 ± 7.11	0.67 ± n/a
Liver	5.96 ± 0.77	1.74 ± 0.07	0.93 ± n/a
Lungs	0.34 ± 0.01	0.22 ± 0.04	0.07 ± n/a
Prostate	2.37 ± 0.92	0.40 ± 0.36	0.00 ± n/a
Salivary Glands	0.26 ± 0.02	0.12 ± 0.00	0.03 ± n/a
Skeletal Muscle	0.10 ± 0.01	0.07 ± 0.01	0.00 ± n/a
Sm Intestine	93.15 ± 9.08	2.29 ± 0.23	0.21 ± n/a
Spleen	0.27 ± 0.03	0.08 ± 0.01	0.00 ± n/a
Stomach	2.26 ± 0.59	0.69 ± 0.28	0.27 ± n/a
Testes	0.05 ± 0.00	0.06 ± 0.02	0.00 ± n/a
Thyroid/ Trachea	0.22 ± 0.05	0.09 ± 0.01	0.00 ± n/a
Tumour (LNCaP)	0.87 ± 0.19	0.44 ± 0.19	0.24 ± n/a
Urinary Bladder	3.64 ± 1.09	1.53 ± 0.86	0.00 ± n/a
Urine	101.43 ± 19.85	36.09 ± 4.86	1.33 ± n/a

Note: Data are %ID/g, expressed as mean ± SEM.

Table 5.2: Tumour to tissue ratios of $[^{99m}TcDPA\text{-}G2\text{-}(SA\text{-}PSMAi\text{-}COOH)_4]^+$ in NCr nude mice bearing LNCaP xenografts.

	Time (h)			
	1	**6**	**24**	
Tumour/Blood	3.29 ± 0.74	5.07 ± 2.22	2.61	n/a
Tumour/Skeletal Muscle	10.84 ± 3.88	6.92 ± 2.66	n/a	n/a

Note: Data are ratios based on %ID/g, expressed as mean ± SEM.

Similar results were observed by Valliant and co-workers with PSMA targeted carboranes.[17] The results were attributed to the hydrophobic nature of the carborane. A similarly hydrophobic entity would be obtained upon hydrolysis of the esters in the dendrimer backbone, yielding the DPA ligand attached to a partially degraded bis-MPA dendrimer. These findings further corroborate the lack of resilience to hydrolysis within the ester backbone of the dendrimer. Nevertheless, the work herein demonstrates the potential ability for bis-MPA dendrimers to serve as convenient scaffolds for multivalent molecular imaging agents. Further work will focus on replacing non-neopentyl esters with more resilient linkages that are amenable to *in vivo* applications.

5.3. Conclusions

The synthesis of a second generation dendrimer bearing four PSMA targeting peptides at the periphery and a DPA ligand at the core has been realized. Successful radiolabeling of the product was observed in near quantitative yield and formulation of the product was successful in 10% EtOH/PBS. Despite promising *in vitro* data, the resulting compound demonstrated poor *in vitro* stability in mouse plasma. Biodistribution

data indicated poor uptake of the imaging agent within the tumor, indicating potential degradation of the compound. Future work includes replacement of the non-neopentyl esters with linkages that are more resilient to hydrolysis in an effort to increase stability and hence tumor uptake.

5.4. Experimental

5.4.1. General

All chemicals were purchased from Sigma Aldrich. Dry dichloromethane was dispensed from a solvent drying system equipped with an activated alumina column. NMR spectra were collected on a Bruker Avance 600 MHz or 700 MHz NMR spectrometer and calibrated to the solvent peak. A Micromass QTOF Global Ultima was used to obtain exact masses and HPLC was conducted on Waters 2695 HPLC equipped with Waters 2996 PDA detector and a Phenomenex Luna 5u C18(2) 150 x 10.0 mm column. The desired products were eluted using a water/acetonitrile gradient containing 0.1% formic acid for dendrimers containing tBu groups at the periphery and 0.1% trifluoroacetic acid for dendrimers with –COOH groups at the periphery. Additionally, water contained 5% acetonitrile. The method used for purification was 0-2 min for 100% water, followed by a gradient to 100% acetonitrile over 15 min. Tert-Butyl protected analogues would typically elute around 90% ACN, while final compounds bearing carboxylic acids at the periphery would elute around 45% ACN. Radiochemistry was performed with the aid of a Biotage Microwave Reactor and HPLC analysis/purification of the radioactive compounds was performed on a Waters 1525 system equipped with a Waters 2998 PDA detector and a Bio-Rad gamma detector. A Phenomenex Luna C18(2) 4.6 x 150 mm HPLC column was employed, using a mobile phase of water and acetonitrile (each containing 0.1% TFA). The HPLC method consisted of 90 % Water for 2 min, followed by a gradient to 40 % water at 14 minutes, and 0 % water at 16 minutes.

At 16.5 minutes, the water was ramped to 90 % and the column equilibrated until 18 minutes at 90 % water.

5.4.2. Synthesis

pTSe-G2-(SA-PSMAi)$_4$ (1): In a 5 mL round bottom flask, equipped with a magnetic stir bar, was added pTSe-G2-(yne)$_4$ (20 mg, 23 μmol), PSMAi-SA-N_3 (88 mg, 115 μmol, 5 eq) and sodium ascorbate (9 mg, 46 μmol, 2 eq) in 1 mL of DMF. The reaction flask was evacuated and back filled with N_2 three times. $CuSO_4$ (2.3 mg, 9.0 μmol, 0.4 eq) in 0.2 mL of dH_2O was added to the reaction vessel and the reaction was allowed to stir at room temperature overnight. The reaction mixture was concentrated by rotary evaporation and purified via silica gel column chromatography (5-13% CH_3OH in CH_2Cl_2) to yield 68 mg of the product as a white solid (75 %). ^{1}H NMR (700 MHz; DMSO): δ 7.82 (s, 4H), 7.78 (dd, *J* = 8.2, 3.6, 4H), 7.70 (dt, *J* = 15.7, 5.6, 9H), 7.44 (t, *J* = 7.4, 4H), 6.28 (dd, *J* = 25.9, 8.3, 8H), 4.31 (t, *J* = 5.5, 3H), 4.26 (t, *J* = 7.1, 8H), 4.09 (m, 8H), 4.10-4.02 (m, 4H), 4.00 (bs, 4H), 3.95 (dd, *J* = 13.6, 8.0, 4H), 3.69 (t, *J* = 5.4, 3H), 3.65 (dd, *J* = 12.1, 6.4, 2H), 3.40 (t, *J* = 6.5, 2H), 3.17 (d, *J* = 5.2, 3H), 3.02-2.98 (m, 16H), 2.84 (t, *J* = 7.5, 8H), 2.65 (t, *J* = 7.5, 8H), 2.38 (s, 3H), 2.23-2.21 (m, *J* = 6.5, 10H), 2.00 (t, *J* = 6.7, 16H), 1.88-1.84 (m, 7H), 1.76-1.73 (m, 8H), 1.69-1.65 (m, 6H), 1.60-1.58 (m, 7H), 1.51-1.44 (m, 24H), 1.40-1.39 (m, 88H), 1.34 (s, 8H), 1.26-1.20 (m, 36H), 1.08 (s, 6H), 0.99 (s, 3H). HR-MS calc. for $C_{196}H_{328}N_{28}O_{52}S$ $[M+4H]^{4+}$: 985.5974. Found: 985.6019.

COOH-G2-(SA-PSMAi)$_4$ (2): A 5 mL round bottom flask, equipped with a magnetic stir bar, was added pTSe-G2-(SA-PSMAi)$_4$ (60 mg, 15 umol) in 2 mL CH_2Cl_2 and DBU (12 mg, 76 umol, 5 eq). After stirring at room temperature for 1 hour, the reaction mixture was diluted with 15 mL of CH_2Cl_2 and washed with $NaHSO_4$ (2 x 15 mL) and brine. The crude reaction mixture was concentrated by rotary evaporation and purified by silica gel column chromatography (5-20 % CH_3OH in CH_2Cl_2) to yield 57 mg of the product as a white solid (68 %). ^{1}H NMR (700 MHz; DMSO): δ 7.85 (s, 4H), 7.77-7.75 (m, 8H), 7.73-7.70 (m, 8H), 6.42 (dd, *J* = 27.5, 7.0, 8H), 4.26 (t, *J* = 7.0, 8H), 4.15 (dd, *J* = 12.2, 8.1, 8H), 4.07 (dd, *J* = 17.4, 11.4, 8H), 4.03-4.01 (m, 8H), 3.94 (dd, *J* = 13.5, 7.9, 8H), 2.98 (dt, *J* = 12.4, 6.2, 16H), 2.84 (t, *J* = 6.9, 8H), 2.64 (t, *J* = 7.4, 8H), 2.24-2.21 (m, *J* = 9.1, 6.8, 12H), 2.02-2.00 (t, *J* = 7.4, 10H), 1.86 (ddd, *J* = 20.1, 8.2, 5.7, 7H), 1.75 (dt, *J* = 14.5, 7.2, 8H), 1.68-1.64 (m, 8H), 1.60-1.56 (m, 8H), 1.52-1.49 (m, 8H), 1.44 (t, *J* = 6.5, 12H), 1.38-1.35 (m, 56H), 1.28-1.24 (m, 16H), 1.20 (s, 12H), 1.15 (s, 3H), 1.05 (s, 6H), 0.88 (t, *J* = 7.7, 8H). HR-MS calc. for $C_{187}H_{318}N_{28}O_{50}$ $[M+4H]^{4+}$: 940.0873. Found: 940.0878.

DPA-G2-(SA-PSMAi)$_4$ (4): A 5 mL round bottom flask, equipped with a magnetic stir bar, was added COOH-G2-(SA-PSMAi)$_4$ (55 mg, 15 μmol) in 1 mL of CH_2Cl_2, NHS (4 mg, 37 μmol, 2.5 eq) and EDC-HCl (7 mg, 37 μmol, 2.5 eq). The reaction mixture was allowed to stir at room temperature overnight. The reaction mixture was diluted with CH_2Cl_2 and washed with water and $NaHSO_4$ to yield NHS-G2-(carb-SA-PSMAi)$_4$ (**3**). The crude **3** was dissolved in CH_2Cl_2 (2 mL), followed by addition of DPA-NH_2 (8 mg, 29 μmol, 2 eq) and Et_3N (6 μL, 43 μmol, 3 eq). After 6 hours, the reaction mixture was

purified by semi-prep HPLC and lyophilized to afford 27 mg of the title compound as a white solid in 47 % yield. ^{1}H NMR (700 MHz; DMSO): δ 8.44 (d, *J* = 4.8, 2H), 7.81 (s, 4H), 7.72-7.68 (m, 10H), 7.49 (d, *J* = 7.8, 2H), 7.20 (dd, *J* = 7.0, 5.2, 2H), 6.28 (dd, *J* = 25.4, 8.3, 8H), 4.25 (t, *J* = 7.1, 8H), 4.16-4.08 (m, 12H), 4.03 (td, *J* = 8.5, 5.3, 6H), 3.95 (td, *J* = 7.9, 5.6, 6H), 3.69 (s, 4H), 2.99 (td, *J* = 12.6, 6.7, 16H), 2.83 (t, *J* = 7.5, 8H), 2.64 (t, *J* = 7.5, 8H), 2.59 (s, 8H), 2.42-2.40 (m, 4H), 2.26-2.16 (m, 10H), 2.00 (t, *J* = 7.5, 12H), 1.88-1.85 (m, 4H), 1.74 (dt, *J* = 14.5, 7.2, 8H), 1.66 (m, *J* = 5.7, 6H), 1.61-1.56 (m, 6H), 1.52-1.48 (m, 8H), 1.44 (t, *J* = 6.6, 16H), 1.39-1.38 (m, 78H), 1.35-1.31 (m, 10H), 1.26-1.24 (m, 26H), 1.20 (bs, 19H), 1.10 (s, 3H), 1.06 (s, 6H). HR-MS calc. for $C_{203}H_{338}N_{32}O_{49}$ $[M+4H]^{4+}$: 1003.6323. Found: 1003.6313.

DPA-G2-(SA-PSMAi-COOH)$_4$ (5): In a 5 mL round bottom flask, equipped with a magnetic stir bar, was added [DPA-G2-(SA-PSMAi)$_4$] (10.0 mg, 2.5 μmol) in 1 mL of CH_2Cl_2, followed by 1 mL of TFA dropwise. The reaction was allowed to stir at room temperature for 4 hours. The volatiles were removed by blowing N_2 over the reaction mixture and the product was purified via semi-prep HPLC and lyophilized to yield 4.9 mg of a white powder (59 %). ^{1}H NMR (700 MHz; DMSO): δ 8.62 (d, *J* = 4.7, 2H), 7.87 (td, *J* = 7.7, 1.6, 2H), 7.82 (s, 4H), 7.71 (dt, *J* = 11.3, 5.6, 8H), 7.50 (d, *J* = 7.8, 2H), 7.44-7.42 (m, 2H), 6.30 (dd, *J* = 25.1, 8.3, 8H), 4.25 (t, *J* = 7.1, 8H), 4.16-4.09 (m, 12H), 4.04 (td, *J* = 8.0, 5.3, 4H), 3.00-2.97 (m, 16H), 2.83 (t, *J* = 7.4, 8H), 2.65-2.63 (m, 8H), 2.29-2.19 (m, 8H), 2.01 (t, *J* = 7.5, 12H), 1.94-1.89 (m, 4H), 1.75-1.70 (m, 12H), 1.66-1.61 (m, 4H), 1.50 (dd, *J* = 13.8, 7.5, 4H), 1.44 (t, *J* = 6.6, 12H), 1.37-1.33 (m, 14H), 1.27-1.24 (m,

12H), 1.20 (bs, 16H), 1.11 (s, 3H), 1.07 (s, 6H). HR-MS calc. for $C_{155}H_{241}N_{32}O_{49}$ $[M+3H]^{3+}$: 1113.2559. Found: 1113.2554.

5.4.3. Radiolabeling, LogP, Plasma Stability and Biodistribution

$[^{99m}$TcDPA-G2-(SA-PSMAi-COOH)$_4]^+$ (7): To a 2 mL microwave vial containing DPA-G2-(SA-PSMAi-COOH)$_4$ (1 mg, 300 nmol) in 0.1 mL of MeOH was added 1 mL of $[^{99m}Tc(CO)_3(H_2O)_3]^+$ in saline adjusted to pH 4.5-6.5 with 1 M HCl. The reaction vessel was sealed and the reaction mixture was heated under microwave irradiation for 5 min at 80 °C. R.T. = 12.95 min. Isolated RCY: 82 ± 3 %.

Log P of $[^{99m}$TcDPA-G2-(SA-PSMAi-COOH)$_4]^+$: An aqueous solution of $[^{99m}$TcDPA-G2-(SA-PSMAi-COOH)$_4]^+$ was prepared via HPLC purification by collecting the peak between 12 and 13 min. The sample was dried on a V-10 rotary evaporator and reconstituted in distilled water at 500 μCi/mL. 10 μCi (20 μL) of radiolabeled compound was dispensed into 9 vials containing a pre-equilibrated water/octanol solution containing NaH_2PO_4 and Na_2HPO_4. The vials were capped and placed on a shaker for 20 min, followed by centrifugation for 30 min. 10 μL of each layer was taken from every vial and placed in a pre-weighed culture tube. The culture tubes were subsequently re-weighed and the activity in each tube was measured. Log P is calculated by taking the log of the ratio of the mass of solution/counts per minute for the water and octanol. Using this method, the log P was determined to be -3.47.

Plasma Stability of [^{99m}TcDPA-G2-(SA-PSMAi-COOH)$_4$]$^+$: A purified and concentrated sample of [^{99m}TcDPA-G2-(SA-PSMAi-COOH)$_4$]$^+$ was formulated in 10% EtOH/PBS at 100 uL/mCi. 100 µL (12MBq) of the formulated compound was added to 900 µL of pre-warmed (to 37°C) mouse plasma (Innovative Research, IMS-CD1-N), vortexed and incubated at 37°C. At each timpoint (t = 0, 0.25 h, 0.5 h, 1 h, 2 h and 4 h), 100 µL was removed and added to 200 µL ice cold acetonitrile. Samples were vortexed and then centrifuged at maximum speed for 10 min. The amount of activity in the whole sample was measured using a dose calibrator (Capintec Inc, CRC-25R). The supernatant was separated from the pellet and the activity from the supernatant and the pellet was measured using a dose calibrator. HPLC analysis was conducted on the supernatant. The experiment was completed once with the % bound to blood proteins calculated as follows (pellet): [(amount of activity in pellet)/(amount of activity in pellet)+(amount of activity in supernatant)]×100% and the % in the supernatant calculated as follows (supernatant): [(amount of activity in supernatant)/(amount of activity in pellet)+(amount of activity in supernatant)]×100%.

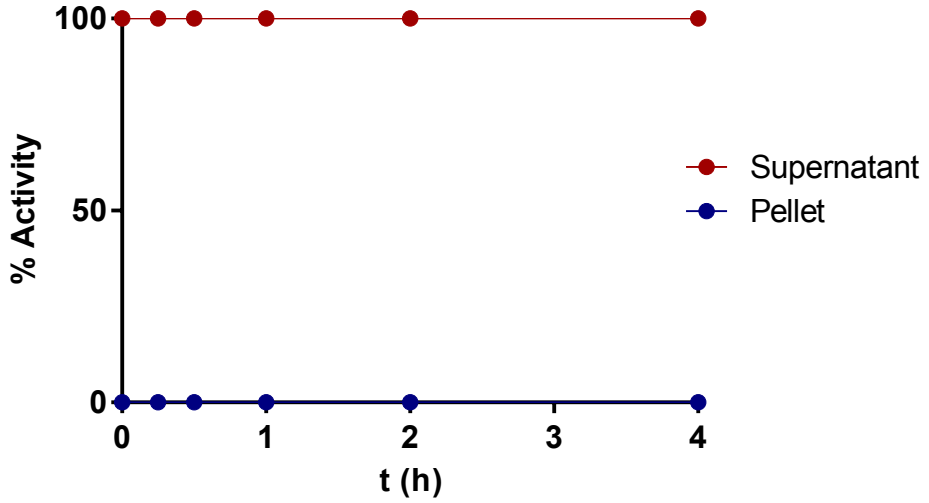

Figure S5.1. Percentage of radioactivity in pellet vs. supernatant at each time point of the plasma stability test.

Bio-Distribution of [^{99m}TcDPA-G2-(SA-PSMAi-COOH)$_4$]$^+$: LNCaP cells derived from lymph node metastases of human prostate carcinoma were purchased from ATCC (CRL-1740). NCr nude homo male mice ordered from Taconic (Germantown, NY, USA) were injected with 2.0×10^6 LNCaP cells in Matrigel:DPBS (1:1) subcutaneously into the right flank. Biodistribution of [^{99m}TcDPA-G2-(SA-PSMAi-COOH)$_4$]$^+$ was performed on mice at 6 weeks post tumour inoculation (n = 5 at t=1 h and 6 h and n = 1 at t=24 h). The animals were injected with approximately 0.3MBq of [^{99m}TcDPA-G2-(SA-PSMAi-COOH)$_4$]$^+$ in PBS via the tail vein. At the specified time points, animals were anesthetized with 3% isoflurane and euthanized by cervical dislocation. Blood, adipose, adrenals, bone, brain, esophagus, gall bladder, heart, kidneys, large intestine and caecum (with contents), liver, lungs, prostate, salivary glands, skeletal muscle, small intestine

(with contents), spleen, stomach (with contents), testes, thyroid/trachea, LNCaP tumour, urinary bladder, urine and tail were collected, weighed and counted in a Perkin Elmer Wizard 1470 Automatic Gamma Counter. Decay correction was used to normalize organ activity measurements to time of dose preparation for data calculations with respect to injected dose (i.e.ID/g).

5.5. References

(1) Feliu, N.; Walter, M. V; Montañez, M. I.; Kunzmann, A.; Hult, A.; Nyström, A.; Malkoch, M.; Fadeel, B. *Biomaterials* **2012**, *33* (7), 1970–1981.

(2) Parrott, M. C.; Benhabbour, S. R.; Saab, C.; Lemon, J. A.; Parker, S.; Valliant, J. F.; Adronov, A. *J. Am. Chem. Soc.* **2009**, *131* (21), 2906–2916.

(3) Gillies, E. R.; Dy, E.; Fréchet, J. M. J.; Szoka, F. C. *Mol. Pharm.* **2005**, *2* (2), 129–138.

(4) Parrott, M. C.; Marchington, E. B.; Valliant, J. F.; Adronov, A. *J. Am. Chem. Soc.* **2005**, 127 (6), 12081–12089.

(5) Lee, C. C.; Gillies, E. R.; Fox, M. E.; Guillaudeu, S. J.; Fréchet, J. M. J.; Dy, E. E.; Szoka, F. C. *Proc. Natl. Acad. Sci. U. S. A.* **2006**, *103* (45), 16649–16654.

(6) Ihre, H. R.; Padilla De Jesús, O. L.; Szoka, F. C.; Fréchet, J. M. J. *Bioconjug. Chem.* **2002**, *13* (3), 443–452.

(7) Padilla De Jesús, O. L.; Ihre, H. R.; Gagne, L.; Fréchet, J. M. J.; Szoka, F. C. *Bioconjug. Chem.* **2002**, 13 (3), 453–461.

(8) Almutairi, A.; Rossin, R.; Shokeen, M.; Hagooly, A.; Ananth, A.; Capoccia, B.; Guillaudeu, S.; Abendschein, D.; Anderson, C. J.; Welch, M. J.; Fréchet, J. M. J. *Proc. Natl. Acad. Sci. U. S. A.* **2009**, *106* (3), 685–690.

(9) Tang, J.; Sheng, Y.; Hu, H.; Shen, Y. *Prog. Polym. Sci.* **2013**, *38* (3-4), 462–502.

(10) Ghobril, C.; Lamanna, G.; Kueny-stotz, M.; Garofalo, A.; Billotey, C.; Felder-flesch, D. *New J. Chem.* **2012**, *36* (2), 310–323.

(11) Banerjee, S. R.; Pullambhatla, M.; Shallal, H.; Lisok, A.; Mease, R. C.; Pomper,

M. G. *Oncotarget* **2011**, *2* (12), 1244–1253.

(12) Foss, C. A.; Mease, R. C.; Fan, H.; Wang, Y.; Ravert, H.; Dannals, R. F.; Olszewski, R. T.; Heston, W. D.; Kozikowski, A. P.; Pomper, M. G. *Clin. Cancer Res.* **2005**, 4022–4028.

(13) Joyal, J. L.; Barrett, J. A.; Marquis, J. C.; Chen, J.; Hillier, S. M. *Cancer Res.* **2010**, 4045–4053.

(14) Hillier, S. M.; Maresca, K. P.; Femia, F. J.; Marquis, J. C.; Foss, C. A; Nguyen, N.; Zimmerman, C. N.; Barrett, J. a; Eckelman, W. C.; Pomper, M. G.; Joyal, J. L.; Babich, J. W. *Cancer Res.* **2009**, *69* (17), 6932–6940.

(15) Lo, S. T.; Kumar, A.; Hsieh, J. T.; Sun, X. *Mol. Pharm.* **2013**, *10* (3), 793–812.

(16) Alberto, R.; Ortner, K.; Wheatley, N.; Schibli, R.; Schubiger, A. P. *J. Am. Chem. Soc.* **2001**, *123* (13), 3135–3136.

(17) El-Zaria, M. E.; Genady, A. R.; Janzen, N.; Petlura, C. I.; Beckford Vera, D. R.; Valliant, J. F. *Dalton Trans.* **2014**, *43* (13), 4950–4961.

Chapter 6. Synthesis, Radiolabeling and Plasma Stability of Targeted Bis-MPA Dendrimers with Ether or Carbamate Linkages at the periphery

**All synthesis and radiolabeling work presented in this chapter was carried out by Lukas Sadowski. Plasma stability studies were performed by Nancy Janzen.*

Abstract

The attachment of alkyne functional groups to the periphery of a G2 bis-MPA dendrimer via linkages that are less prone to hydrolysis than previously investigated esters has been carried out. Attachment of alkynes to the periphery of bis-MPA dendrimers was accomplished separately via carbamate and ether linkages. The two dendrimer derivatives were functionalized with lys-urea-glu dipeptides for targeting of PSMA. Attachment of a dipicolylamine amine ligand to the core of the dendrimer enabled for radiolabeling with ^{99m}Tc. Stability of the radiolabeled compounds was evaluated in mouse plasma and showed improved stability compared to the ester analogue. In particular, replacement of non-neopentyl esters with ethers leads to a remarkable improvement in plasma stability.

6.1. Introduction

The use of bis-MPA dendrimers for biomedical applications has resulted in many promising drug delivery and imaging platforms.[1–4] The ability to tune circulation time of the dendrimers has not only been demonstrated, but has also been exploited for drug delivery via the EPR effect.[1,5] With respect to imaging, bis-MPA dendrimers have been successfully employed as multivalent scaffolds for imaging angiogenesis,[2] while non-functionalized dendrimers have been shown to have rapid clearance via the renal filtration system.[4]

In order to achieve the aforementioned dendrimer properties, efficient functionalization protocols need to exist. A number of synthetic strategies have been demonstrated to be particularly effective in functionalizing the alcohol periphery of bis-MPA dendrimers. Many of these protocols result in formation of another ester moiety, relying on DCC/EDC couplings, anhydride couplings,[6] or the reagent carbonyl diimidazole (CDI).[7] Carbamate formation has been reported by utilizing a carbonate functionalized bis-MPA monomer.[8] The use of para-nitrophenyl chloroformate has also been used for the formation of carbamates at the periphery of bis-MPA dendrimers.[1,9] In addition, the monomeric bis-MPA can be effectively functionalized at the alcohol positions leading to alkenes[10] or alkynes[11] which are attached via an ether linkage.

Despite the success of this dendritic scaffold, there are few studies that look at the stability of bis-MPA dendrimers *in vitro* or *in vivo*.[12,13] Herein, we synthesize and evaluate two linkages for the peripheral functionalization of dendrimers as alternatives to

esters. The need to investigate alternative functionalization strategies in lieu of esters stems from the quick degradation times *in vitro* and *in vivo* that is inherent to many esters.

6.2. Results and Discussion

6.2.1. Synthesis of Alkyne Dendrimers

In an effort to increase the stability of bis-MPA polyester dendrimers *in vivo*, we aimed to replace all non-neopentyl esters with linkages that are more resilient to hydrolysis. The non-neopentyl esters were the result of functionalizing the alcohol periphery of bis-MPA dendrimers with the anhydride of pentynoic acid, in order to decorate the dendrimer periphery with alkynes. Therefore, attachment of alkyne moieties to the periphery of a second generation dendrimer was investigated by alternative methods. Carbamate linkages were envisioned by activating the alcohol periphery with either p-nitrophenyl chloroformate or the reagent carbonyl diimidazole (CDI). CDI has been shown to be an effective reagent for the preparation of carbamates.[14] Therefore, the alcohol periphery of a second generation bis-MPA dendrimer was furnished with carbonyl imidazole and the product (**1**) was purified by collecting the precipitate via filtration (Scheme 6.1). Activation was accomplished with methyl iodide in order to methylate the imidazole ring and render it more susceptible to displacement by a nucleophile. Without methylation, the use of elevated temperatures and a base is required to complete the transformation – conditions that are incompatible with the para-toluenesulfonyl ethanol core-protecting group. Upon methylation, the dendrimer was

reacted with propargyl amine under anhydrous conditions to install alkynes linked via carbamate linkages (**3**).

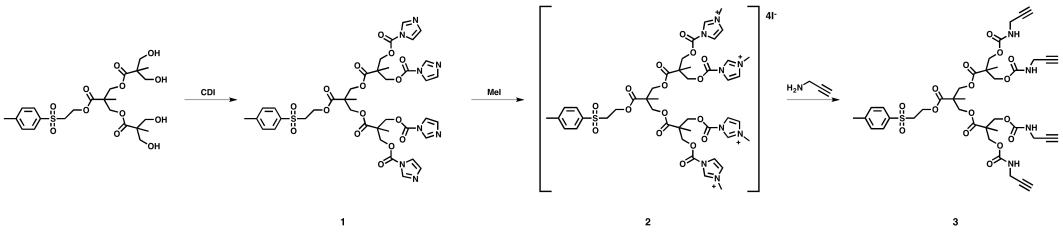

Scheme 6.1. Synthesis of G2 alkyne decorated dendrimer via carbamate linkages.

In addition to carbamates, alkyne functionalization of the dendrimer periphery was accomplished via ethers. Propargyl bromide was used in the first step to functionalize the alcohol groups of the bis-MPA monomer (Scheme 6.2).[11] The resulting alkyne monomer was subsequently coupled to the periphery of a pTSe-G1-$(OH)_2$ dendrimer using EDC/DPTS to form neo-pentyl ester linkages. This synthetic route led to the preparation of a second generation dendrimer with four alkynes at the periphery linked via ether linkages. Chemical shifts of the terminal alkyne protons were observed to be 2.26 ppm for the carbamate derivative and 2.43 ppm for the alkynes linked via the ether functionality (figure 6.1).

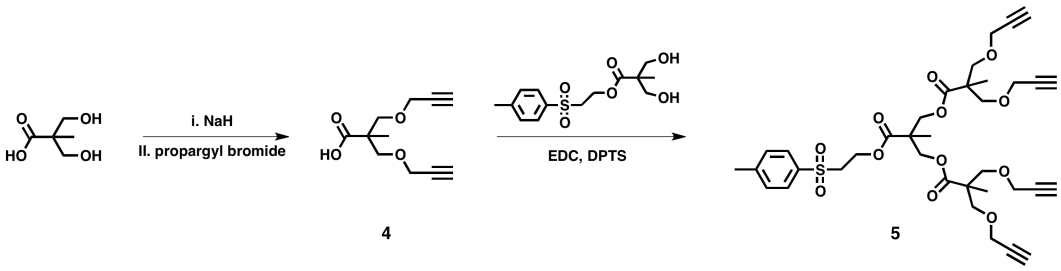

Scheme 6.2. Synthesis of G2 alkyne decorated dendrimer via ether linkages.

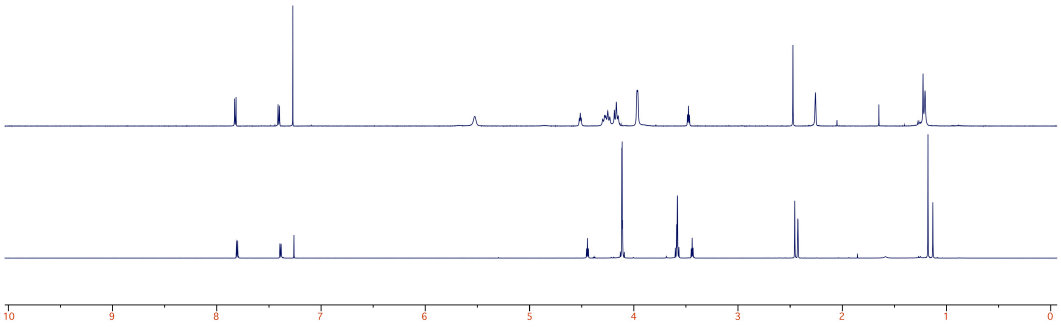

Figure 6.1. ^{1}H-NMR spectrum of pTSe-G2-(carbamate-yne)$_4$ (top) and pTSe-G2-(ether-yne)$_4$ (bottom).

6.3.2. Synthesis of Prostate Specific Membrane Antigen (PSMA) Targeted Dendrimers

The alkyne dendrimer analogues were functionalized with lys-urea-glu,[15] a dipeptide that is known to have affinity towards PSMA.[16–19] Based on our previous results (see chapter 4), we opted to use a hydrophobic suberic acid based spacer to link the targeting vector to the dendrimer. An analogous strategy was used to prepare all dendrimer derivatives for radiolabeling purposes. The copper (I) catalyzed alkyne-azide

cycloaddition (CuAAC) was employed to attach the targeting vector to the alkyne periphery of the dendrimer (Scheme 6.3). Subsequent functionalization of the core required removal of the para-toleuenesulfonyl ethanol group – a carboxylic acid protecting group, which was accomplished using 1,8-diazabicycloundec-7-ene (DBU). The core of the dendrimer was activated using succinimidyl ester chemistry to facilitate the efficient coupling of the dipicolylamine metal chelate (Scheme 6.4). Lastly, removal of the tert-butyl groups on the PSMA targeting vector to unmask the carboxylic acids was accomplished by treating the compounds with trifluoroacetic acid (TFA). The resulting carboxylic acids enable targeting of PSMA via interactions in the active site of the enzyme.[20] A rhenium analogue of each PSMA targeted dendrimer was also prepared to serve as an HPLC standard upon radiolabeling with ^{99m}Tc (Scheme 6.5).

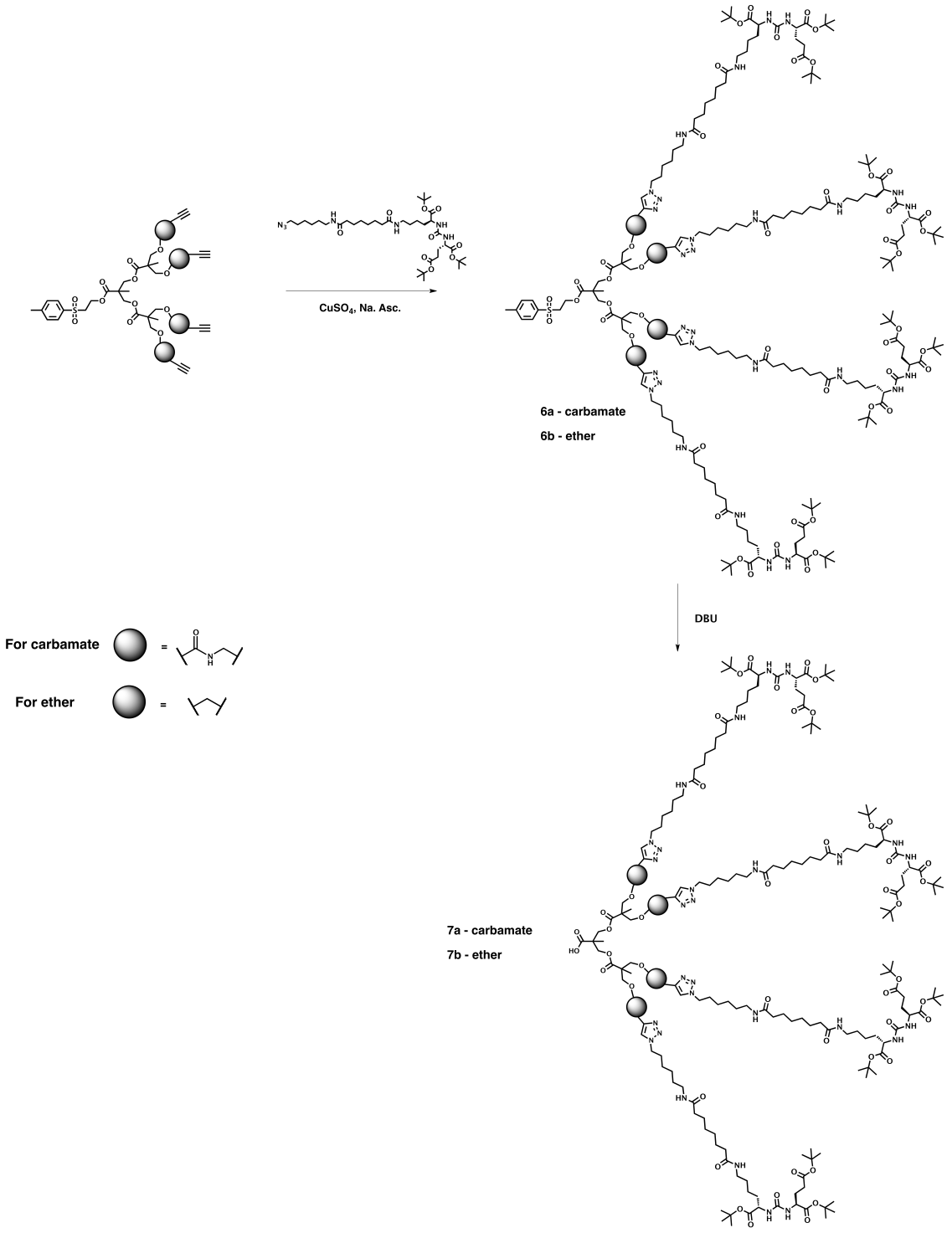

Scheme 6.3. "Click" functionalization of dendrimers with PSMA-SA-N_3 and subsequent removal of core protecting group.

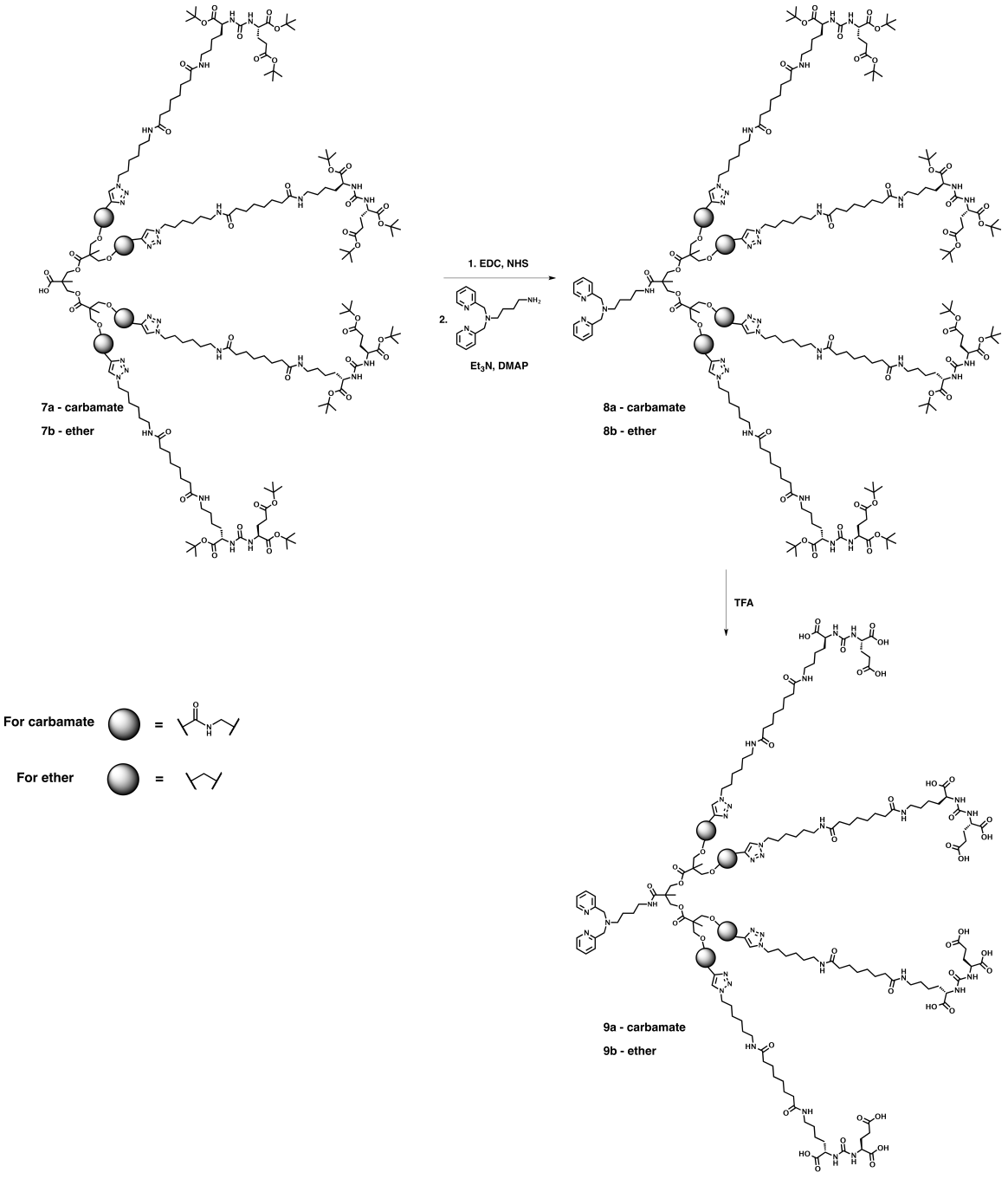

Scheme 6.4. Attachment of DPA ligand to core of dendrimer and subsequent removal of tert-butyl protecting groups.

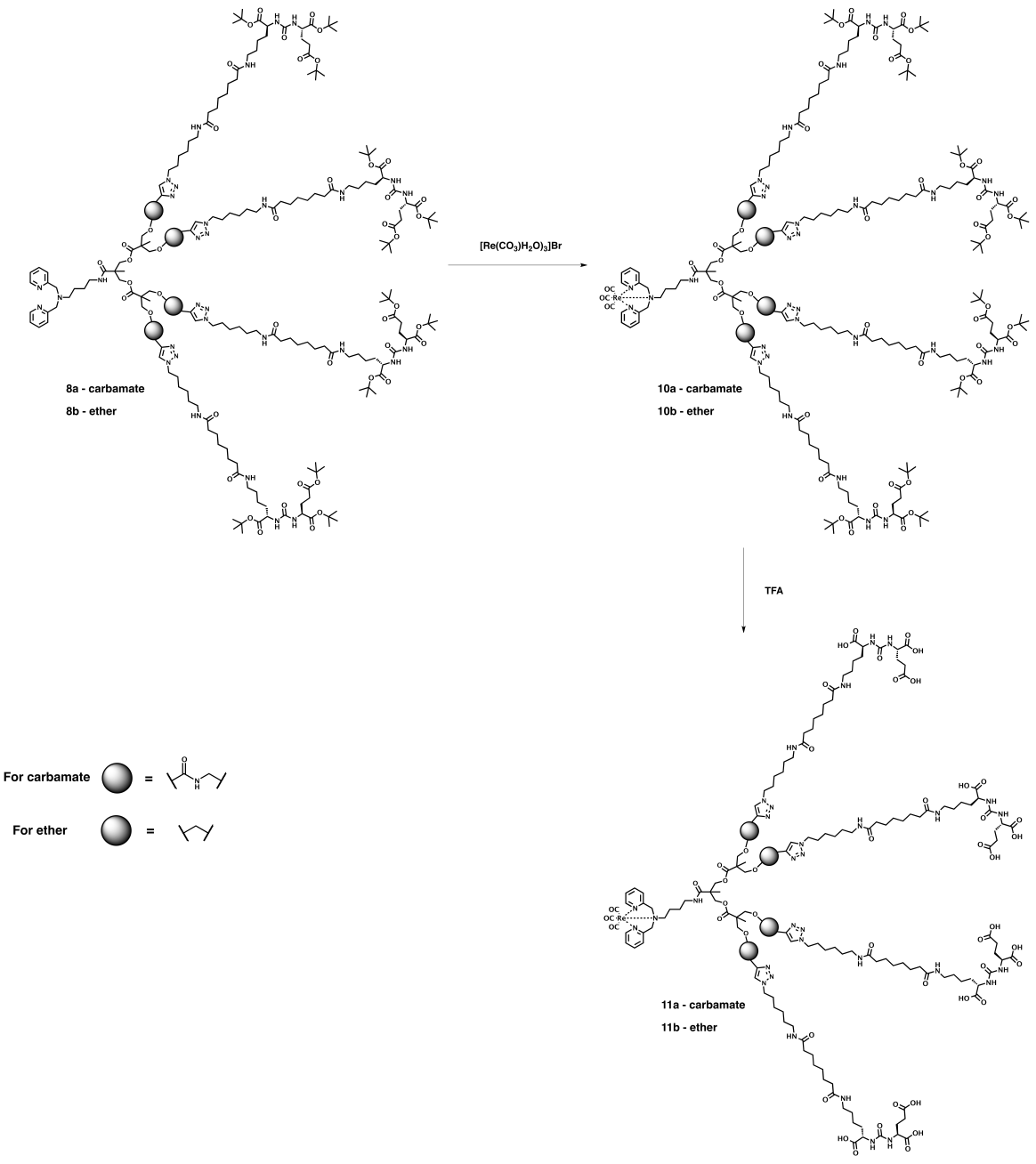

Scheme 6.5. Coordination of rhenium to DPA ligand and subsequent removal of tert-butyl protecting groups.

6.3.3. Radiolabeling and Plasma Stability of PSMA targeted Dendrimers

6.3.3.1. $[TcDPA\text{-}G2\text{-}(carb\text{-}SA\text{-}PSMAi\text{-}COOH)_4]^+$ Synthesis and Plasma Stability

Radiolabeling of the dendrimers with ^{99m}Tc was carried out using the $[^{99m}Tc(CO)_3(H_2O)_3]^+$ salt to prepare stable technetium tricarbonyl derivatives.[21] Using microwave irradiation, the carbamate dendrimer analogue DPA-G2-(carb-SA-PSMAi-$COOH)_4$ was radiolabeled with ^{99m}Tc in an unoptimized 23±3% yield (Scheme 6.6). The radiolabeled $[TcDPA\text{-}G2\text{-}(carb\text{-}SA\text{-}PSMAi\text{-}COOH)_4]^+$ **(12a)** dendrimer had a retention time of 11.55 min, which was in agreement with the expected retention time, based on $[ReDPA\text{-}G2\text{-}(carb\text{-}SA\text{-}PSMAi\text{-}COOH)_4]^+$ **(11a)** (Figure 6.2).

Upon purification and isolation of **12a**, the compound was formulated in phosphate buffered saline (PBS) with 10% EtOH to aid solubility. Compound **12a** was subsequently incubated in mouse plasma at 37°C and aliquots were analyzed at 15, 30 and 45 min, as well as at the 1, 2 and 4 hour time points. Analysis of the mouse plasma up to 4 hours revealed degradation of the dendrimer starting to occur within 30 minutes of incubation (Figure 6.3). Although degradation was clearly visible and continued throughout the course of the experiment, a peak corresponding to the retention time of compound **12a** was still observable after 4 hours. Further analysis of the plasma proteins (via precipitation and centrifugation) revealed nearly 50% protein binding (as determined by the amount of radioactivity measured in the pellet) after 1 hour (Figure 6.4). The results observed herein demonstrate a remarkable improvement in stability compared to PSMA functionalized dendrimers via ester linkages (Chapter 5).

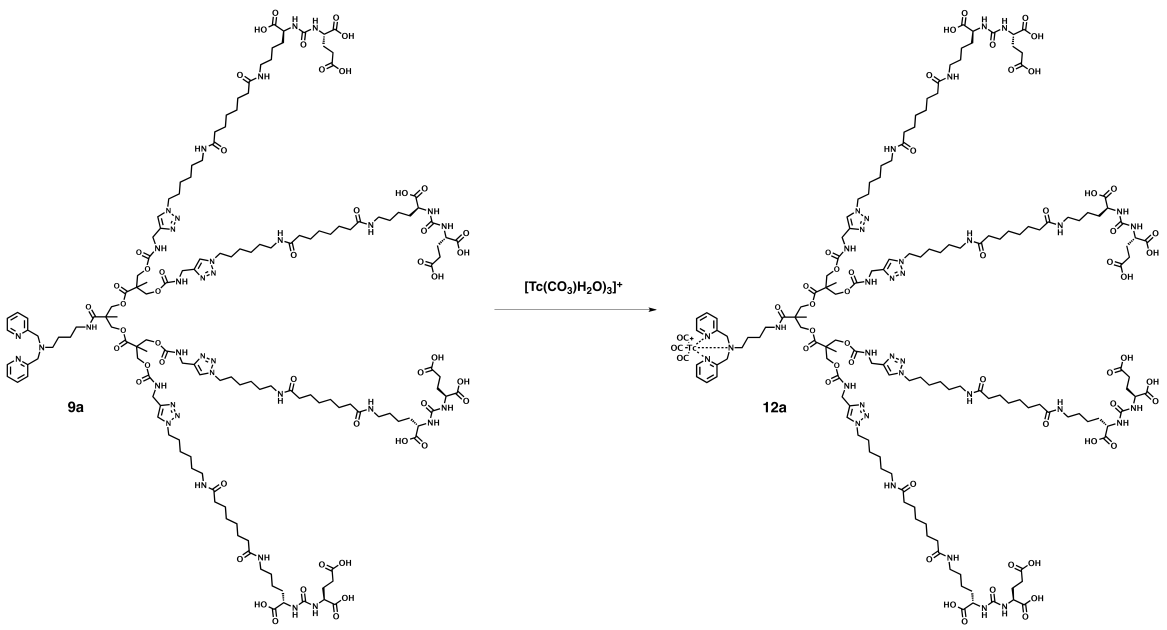

Scheme 6.6. Radiolabeling of DPA-G2-(carb-SA-PSMAi-COOH)$_4$ **(9a)** with ^{99m}Tc.

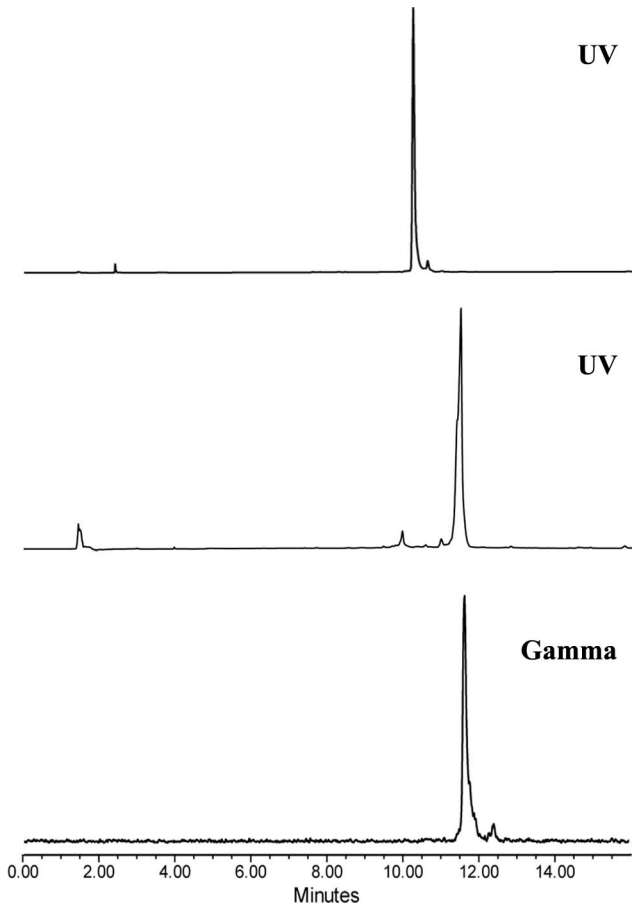

Figure 6.2. UV trace of DPA-G2-(carb-SA-PSMAi-COOH)$_4$ **(9a)** (top), [ReDPA-G2-(carb-SA-PSMAi-COOH)$_4$]$^+$ **(11a)** (middle) and gamma trace of [^{99m}Tc DPA-G2-(carb-SA-PSMAi-COOH)$_4$]$^+$ **(12a)** (bottom).

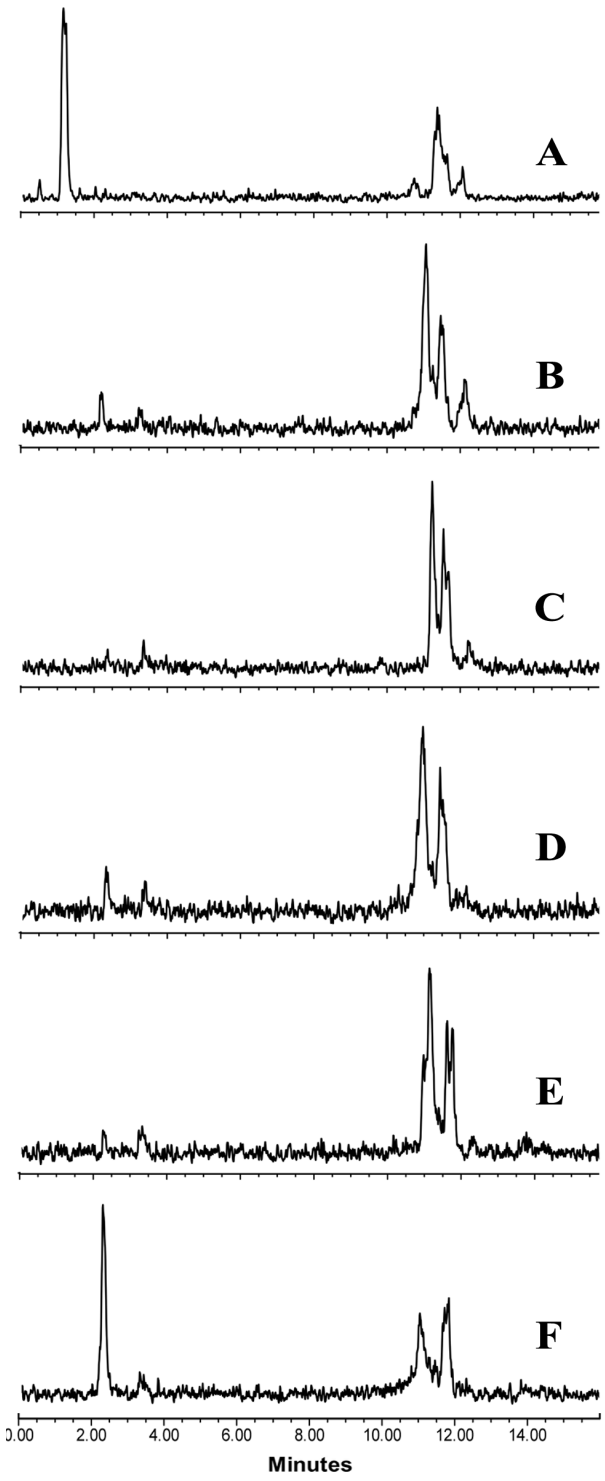

Figure 6.3. Plasma stability of $[TcDPA\text{-}G2\text{-}(carb\text{-}SA\text{-}PSMAi\text{-}COOH)_4]^+$ **(12a)** at A) 0 min B) 15 min C) 30 min D) 1 hour E) 2 hours and F) 4 hours.

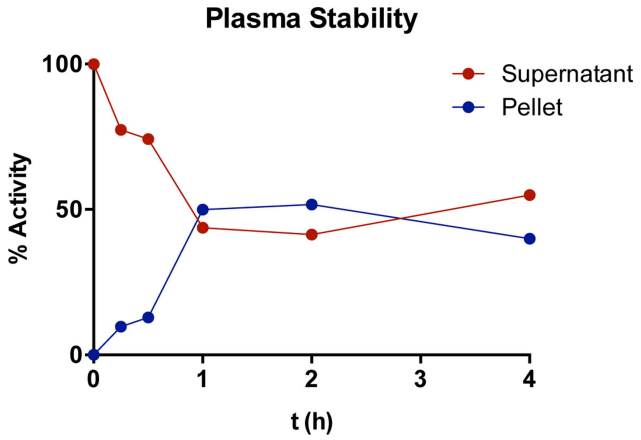

Figure 6.4. Measured radioactivity in supernatant and pellet during plasma stability study of $[TcDPA\text{-}G2\text{-}(carb\text{-}SA\text{-}PSMAi\text{-}COOH)_4]^+$ **(12a).** Radioactivity in the pellet (vs. supernatant) indicates relative protein binding of **12a**.

6.3.3.2. $[TcDPA\text{-}G2\text{-}(pro\text{-}SA\text{-}PSMAi\text{-}COOH)_4]^+$ Synthesis and Plasma Stability

Radiolabeling of $DPA\text{-}G2\text{-}(pro\text{-}SA\text{-}PSMAi\text{-}COOH)_4$ **(9b)** was accomplished using analogous conditions to those used for compound **9a**, as described in section 6.3.3.1. Thus, radiolabeling of dendrimer **9b** with ^{99m}Tc was carried out using the $[^{99m}Tc(CO)_3(H_2O)_3]^+$ salt under microwave irradiation for 5 min at 80°C (Scheme 6.7). Analysis of the reaction mixture indicated quantitative uptake of radioactivity by the dendrimer, yielding compound **12b**, which had a retention time in agreement with the non-radioactive rhenium analogue **11b** (Figure 6.5). A bipyridine challenge to remove loosely bound technetium did not result in any newly formed radiolabeled products, as analyzed by HPLC, further confirming the quantitative co-ordination of the radionuclide by the DPA ligand at the core of the dendrimer.

To assess the plasma stability of compound **12b**, it was formulated in PBS (with 10% EtOH) and incubated in mouse plasma at 37°C. The resulting dendrimer displayed excellent stability over 4 hours with no appreciable decomposition, as monitored by HPLC (Figure 6.6). Analysis of the plasma proteins (via precipitation and centrifugation) revealed a similar protein bound:unbound dendrimer ratio compared to **12a** (Figure 6.7). The observed plasma stability of compound **12b** can thus be attributed to the non-degradable ether linkages utilized in linking the targeting moieties to the bis-MPA scaffold.

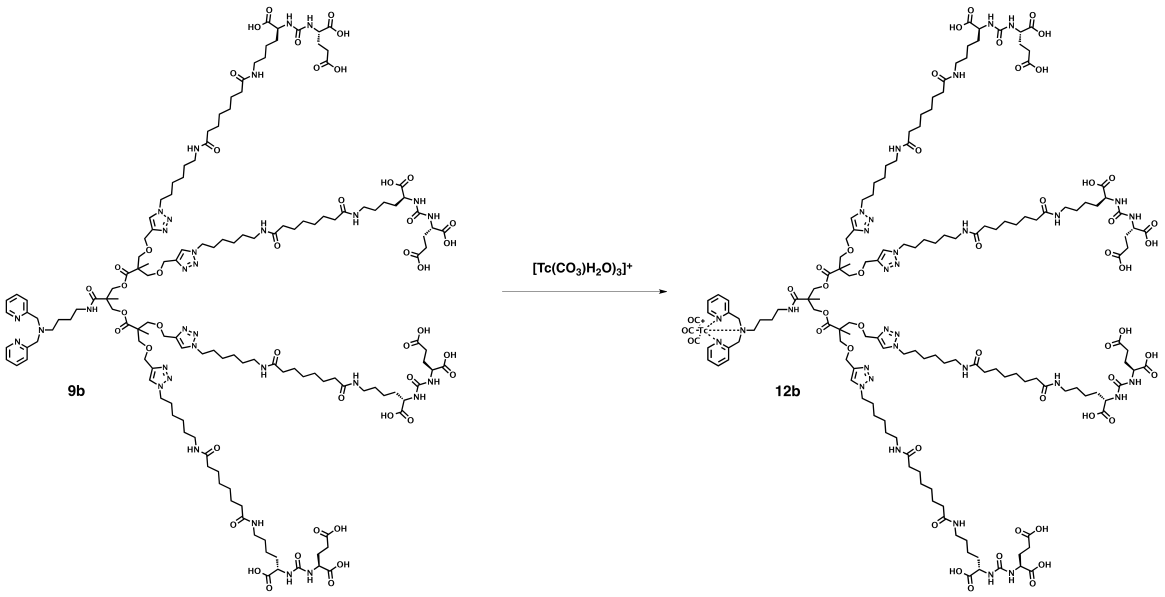

Scheme 6.7. Radiolabeling of DPA-G2-(pro-SA-PSMAi-COOH)$_4$ **(9b)** with ^{99m}Tc.

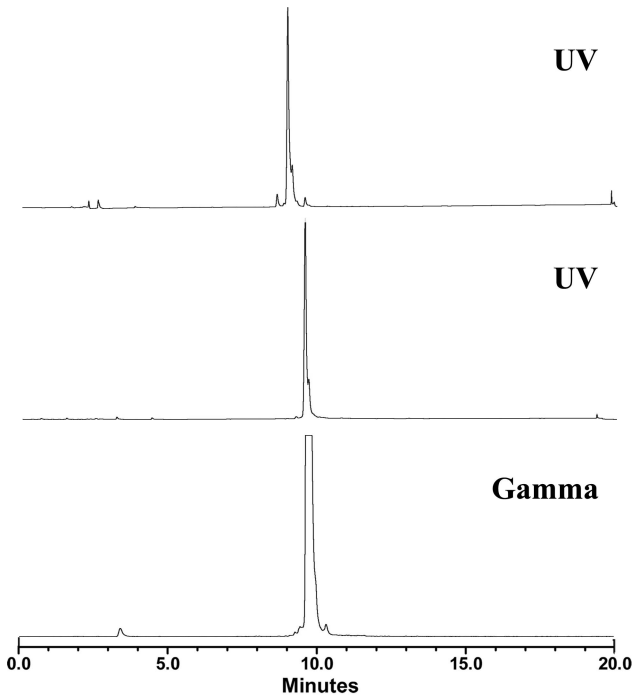

Figure 6.5. UV trace of DPA-G2-(pro-SA-PSMAi-COOH)$_4$ **(9b)** (top), [ReDPA-G2-(pro-SA-PSMAi-COOH)$_4$]$^+$ **(11b)** (middle) and gamma trace of [^{99m}TcDPA-G2-(pro-SA-PSMAi-COOH)$_4$]$^+$ **(12b)** (bottom).

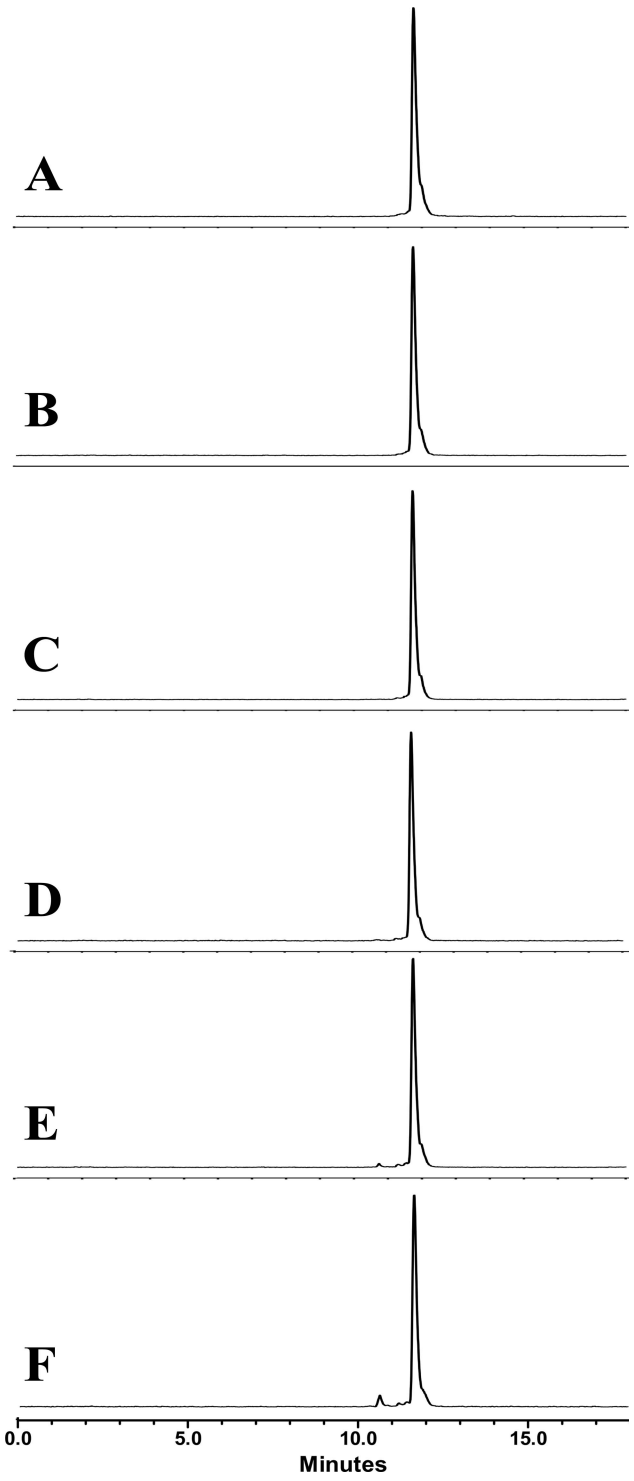

Figure 6.6. Plasma stability of $[TcDPA\text{-}G2\text{-}(pro\text{-}SA\text{-}PSMAi\text{-}COOH)_4]^+$ **(12b)** at A) 0 min B) 15 min C) 30 min D) 1 hour E) 2 hours and F) 4 hours.

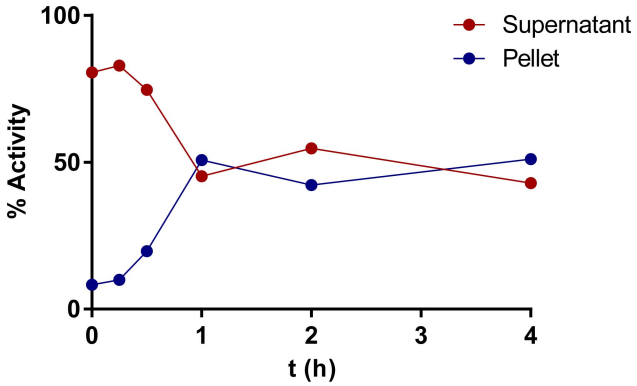

Figure 6.7. Measured radioactivity in supernatant and pellet during plasma stability study of $[TcDPA\text{-}G2\text{-}(pro\text{-}SA\text{-}PSMAi\text{-}COOH)_4]^+$ **(12b)**. Radioactivity in the pellet (vs. supernatant) indicates relative protein binding of **12b**.

6.4. Concluding Remarks

A synthetic protocol has been established to decorate the periphery of bis-MPA dendrimers with alkynes via carbamate or ether linkages. To demonstrate the feasibility of the dendrimer scaffold for biomedical applications, lys-urea-glu peptides were attached at the periphery to enable targeting of PSMA. Radiolabeling and plasma stability of the two dendrimer analogues reveal increased stability (compared to dendrimers bearing non-neopentyl esters). In particular, the remarkable increase in stability of bis-MPA dendrimers having ether linkages (in lieu of non-neopentyl esters or carbamates) makes this scaffold amenable for further *in vivo* investigations.

6.5. Experimental

6.5.1. General

All reagents and solvents, unless otherwise noted were purchased from Sigma-Aldrich, Bachem, Chem-Impex or Carbosynth and used without further purification. Dry dichloromethane and acetonitrile was dispensed from a solvent system equipped with an activated alumina column. NMR spectra were collected on a Bruker Avance 600 MHz or 700 MHz NMR spectrometer and calibrated to the solvent peak. A Micromass QTOF Global Ultima was used to obtain exact masses and semi-preparative HPLC was conducted on a Waters 2695 HPLC equipped with a Waters 2998 PDA detector and a Phenomenex Luna C18(2) 10 x 150 mm HPLC column. Radiochemistry was performed with the aid of a Biotage Microwave Reactor and HPLC analysis/purification of the radioactive compounds was performed on a Waters 1525 system equipped with a Waters 2998 PDA detector and a Bio-Rad gamma detector. A Phenomenex Luna C18(2) 4.6 x 150 mm HPLC column was employed, using a mobile phase of water and acetonitrile (each containing 0.1% FA or TFA). HPLC methods A and C consisted of using a water/acetonitrile gradient (containing 0.1% formic acid for Method A and 0.1% trifluoroacetic acid for Method C) using the following parameters: 0-2 min at 95% water followed by a gradient to 100% acetonitrile between 2 min and 15 min. 100% acetonitrile was maintained until 17 min, followed by a rapid gradient to 95% water between 17-18 minutes. 95% water was maintained until 20 min. HPLC method B consisted of 90 % Water for 2 min, followed by a gradient to 40 % water at 14 minutes, and 0 % water at 16

minutes. At 16.5 minutes, the water was ramped to 90 % and the column equilibrated until 18 minutes at 90 % water.

6.5.2. Synthesis

pTSe-G2-(CI)$_4$ (1): To a 25 mL round bottom flask, equipped with a magnetic stir bar, was added pTSe-G2-(OH)$_4$ (0.20 g, 0.37 mmol) in 8 mL of ACN, and CDI (0.47 g, 2.92 mmol), and the heterogenous reaction mixture was allowed to stir at room temperature overnight. The precipitate was collected and washed with 5 mL of cold ACN to yield 0.16 g of an off white powder (47 %). ^{1}H NMR (600 MHz; DMSO): δ 8.26 (s, 4H), 7.77 (d, *J* = 8.3, 2H), 7.58 (s, 4H), 7.43 (d, *J* = 8.0, 2H), 7.06 (s, 4H), 4.60-4.55 (m, 8H), 4.26 (t, *J* = 5.6, 2H), 4.11-4.06 (m, 4H), 3.67 (t, *J* = 5.6, 2H), 2.38 (s, 3H), 2.08 (s, 4H), 1.33 (s, 6H), 0.98 (s, 3H). ^{13}C NMR (150 MHz; DMSO): 171.32, 171.09, 147.83, 144.65, 137.27, 136.36, 130.27, 129.91, 127.62, 117.48, 67.90, 65.36, 58.35, 53.76, 46.02, 45.81, 20.98, 17.11, 16.33. HR-MS calc. for $C_{40}H_{45}N_8O_{16}S$ $[M+H]^+$: 925.2674. Found: 925.2676.

pTSe-G2-(carbamate-alkyne)$_4$ (3): To a 10 mL flame dried round bottom flask, equipped with a magnetic stir bar, was added pTSe-G2-(CI)$_4$ (0.10 g, 0.11 mmol) in 10 mL of dry ACN, and MeI (0.08 mL, 1.30 mmol, 12 eq), followed by stirring at 50 °C overnight in the sealed vessel. The crude reaction mixture was concentrated by rotary evaporation to remove ACN and the excess MeI, yielding compound **2**, which was subsequently used without further purification. The resulting product (**2**) was redissolved in 5 mL of dry CH_2Cl_2. Freshly distilled propargylamine (0.03 mL, 0.48 mmol, 4.4 eq)

was added and the reaction mixture was allowed to stir at room temperature until complete disappearance of starting material by TLC (ca. 4 hours). The product was purified by silica gel column chromatography using Hex/EtOAc to afford 52 mg of product as a clear viscous oil (73 %). ^{1}H NMR (600 MHz; $CDCl_3$): δ 7.82 (d, *J* = 8.3, 2H), 7.41 (d, *J* = 7.9, 2H), 5.53 (s, 3H), 4.51 (t, *J* = 5.9, 2H), 4.20 (d, *J* = 49.2, 12H), 3.97 (s, 8H), 3.48 (t, *J* = 5.9, 2H), 2.47 (s, 3H), 2.26 (s, 4H), 1.22 (d, *J* = 11.6, 9H). HR-MS calc. for $C_{40}H_{48}N_4O_{16}S$ $[M+H]^+$: 895.2684. Found: 895.2631.

*This compound is not bench stable for prolonged periods (multiple weeks) of time.

pTSe-G2-(propyne)$_4$ (5): To a 50 mL round bottom flask, equipped with a magnetic stir bar, was added pTSe-G1-$(OH)_2$ (0.10 g, 0.32 mmol) in 20 mL of CH_2Cl_2, Bis-MPA-yne (**4**) (0.20 g, 0.95 mmol, 3 eq), DCC (0.20 g, 0.95 mmol, 3 eq) and DPTS (0.03 g, 0.13 mmol, 0.4 eq). The reaction mixture was allowed to stir overnight at room temperature. The urea precipitate was filtered off and the filtrate was concentrated by rotary evaporation and purified via silica gel column chromatography (2:1 to 2:3 Hex/EtOAc) to yield 86 mg of the product as a clear viscous oil (39 %). ^{1}H NMR (700 MHz; CDCl3): δ 7.81 (d, *J* = 8.2, 2H), 7.39 (d, *J* = 7.9, 2H), 4.44 (t, *J* = 6.3, 2H), 4.15-4.03 (m, 12H), 3.68-3.50 (m, 8H), 3.44 (t, *J* = 6.2, 2H), 2.46 (s, 3H), 2.43 (s, 4H), 1.18 (s, 6H), 1.13 (s, 3H). ^{13}C NMR (175 MHz, $CDCl_3$): δ = 173.43, 172.16, 145.38, 136.38, 130.30, 128.26, 79.66, 74.78, 71.85, 65.23, 58.76, 58.33, 55.13, 48.27, 46.70, 21.79, 18.01, 17.50. HR-MS calc. for $C_{36}H_{44}O_{12}S$ $[M+H]^+$: 701.2632. Found: 701.2619.

pTSe-G2-(carb-SA-PSMAi)$_4$ (6a): To a 5 mL round bottom flask, equipped with a magnetic stir bar, was added pTSe-G2-(carbamate-yne)$_4$ (0.22 g, 0.03 mmol), PSMAi-SA-N_3 (0.10 mg, 0.13 mmol, 5 eq) and sodium ascorbate (0.01 g, 0.05 mmol, 2 eq) in 1 mL of DMF. The reaction flask was evacuated and back filled with N_2 three times. $CuSO_4$ (2.00 mg, 7.80 μmol, 0.4 eq) in 0.2 mL of dH_2O was added to the reaction vessel and the reaction was allowed to stir at room temperature overnight. The reaction mixture was concentrated by rotary evaporation and purified via silica gel column chromatography (5-15% CH_3OH in CH_2Cl_2) to yield 82 mg of the product as a white solid (71 %). ^{1}H NMR (700 MHz; DMSO): δ 7.87 (s, 4H), 7.78 (d, *J* = 8.2, 2H), 7.71 (s, 6H), 7.65 (t, *J* = 5.4, 4H), 7.44 (d, *J* = 8.1, 2H), 6.28 (dd, *J* = 25.9, 8.3, 8H), 4.31-4.27 (m, 8H), 4.20 (d, *J* = 5.5, 8H), 4.05 (d, *J* = 8.4, 8H), 3.96 (s, 8H), 3.69 (t, *J* = 5.5, 4H), 3.05-2.92 (m, 12H), 2.31-2.19 (m, 8H), 2.01 (t, *J* = 7.4, 8H), 1.94-1.83 (m, 4H), 1.75 (t, *J* = 7.1, 6H), 1.71-1.62 (m, 4H), 1.61-1.50 (m, 4H), 1.48-1.40 (m, 16H), 1.38–1.25 (m, 55H), 1.24-1.12 (m, 22H), 1.09 (s, 6H), 0.99-0.96 (s, 3H). HR-MS calc. for $C_{192}H_{324}N_{32}O_{52}S$ $[M+4H]^{4+}$: 987.0941. Found: 987.0906.

COOH-G2-(carb-SA-PSMAi)$_4$ (7a): To a 5 mL round bottom flask, equipped with a magnetic stir bar, was added pTSe-G2-(carb-SA-PSMAi)$_4$ (0.80 g, 0.02 mmol) in 2 mL CH_2Cl_2 and DBU (0.02 g, 0.10 mmol, 5 eq). After stirring at room temperature for 1 hour, the reaction mixture was diluted with 15 mL of CH_2Cl_2 and washed with $NaHSO_4$ (2 x 15 mL) and brine. The crude reaction mixture was concentrated by rotary evaporation and purified by silica gel column chromatography (5-20 % CH_3OH in CH_2Cl_2) to yield 57 mg

of the product as a white solid (76 %). ^{1}H NMR (700 MHz; DMSO): δ 7.92 (s, 4H), 7.72 (bs, 8H), 6.30 (dd, *J* = 27.0, 4.9, 8H), 4.26 (t, *J* = 6.9, 8H), 4.19-4.18 (m, 10H), 4.05-4.03 (m, J = 3.3, 12H), 3.96-3.93 (m, 7H), 2.98 (m, 12H), 2.26-2.16 (m, 8H), 2.00 (t, *J* = 6.5, 12H), 1.88-1.83 (m, 4H), 1.74 (t, *J* = 7.1, 8H), 1.67-1.64 (m, 6H), 1.60-1.56 (m, 6H), 1.50-1.47 (m, 7H), 1.44 (t, *J* = 6.8, 12H), 1.39-1.33 (m, 71H), 1.24 (m, 16H), 1.19 (bs, 16H), 1.14 (s, 3H), 1.08 (s, 6H). HR-MS calc. for $C_{183}H_{314}N_{32}O_{50}$ $[M+4H]^{4+}$: 941.5841. Found: 941.5796.

DPA-G2-(carb-SA-PSMAi)$_4$ (8a): To a 5 mL round bottom flask, equipped with a magnetic stir bar, was added COOH-G2-(carb-SA-PSMAi)$_4$ (55 mg, 15 μmol) in 1 mL of CH_2Cl_2, NHS (4.2 mg, 36.5 μmol, 2.5 eq), and EDC-HCl (7.2 mg, 36.5 μmol, 2.5 eq). The reaction mixture was allowed to stir at room temperature overnight. The reaction mixture was diluted with 10 mL CH_2Cl_2 and washed with water (1 x 10 mL) and $NaHSO_4$ (2 x 10 mL). The crude NHS-G2-(carb-SA-PSMAi)$_4$ was concentrated *in vacuo* and re-dissolved in 2 mL of CH_2Cl_2, followed by addition of DPA-NH_2 (8.0 mg, 29.2 μmol, 2 eq) and Et_3N (6.0 μL, 43.8 μmol, 3 eq). The reaction mixture was purified by semi-prep HPLC and lyophilized to afford 33 mg of the title compound as a white solid in 56 % yield. ^{1}H NMR (700 MHz; DMSO): δ 8.53 (s, 4H), 8.44 (d, *J* = 4.8, 2H), 7.86 (s, 4H), 7.72-7.71 (m, 4H), 7.70-7.68 (m, 4H), 7.65-7.63 (m, 4H), 7.49 (d, *J* = 7.9, 2H), 7.20 (dd, *J* = 7.3, 4.9, 2H), 6.86 (bs, 4H), 6.30 (dd, *J* = 27.2, 8.2, 8H), 4.26 (t, *J* = 7.1, 8H), 4.19 (d, *J* = 5.5, 8H), 4.11 (bs, 4H), 4.03 (m, 8H), 3.95 (td, *J* = 8.0, 5.6, 4H), 3.69 (s, 4H), 2.99 (td, *J* = 13.2, 7.2, 12H), 2.27-2.16 (m, 8H), 2.00 (t, *J* = 7.4, 8H), 1.86 (td, *J* = 14.0, 6.6, 4H),

1.74 (m, 4H), 1.69-1.63 (m, 4H), 1.61-1.56 (m, 4H), 1.51-1.48 (m, 4H), 1.45-1.43 (m, 10H), 1.37-1.33 (m, 40H), 1.26-1.24 (m, 9H), 1.20 (t, J = 6.7, 10H), 1.15 (s, 3H), 1.07 (d, J = 0.2, 6H). HR-MS calc. for $C_{199}H_{334}N_{36}O_{49}$ $[M+4H]^{4+}$: 1004.6276. Found: 1004.6293.

DPA-G2-(carb-SA-PSMAi-COOH)$_4$ (9a): To a 5 mL round bottom flask, equipped with a magnetic stir bar, was added DPA-G2-(carb-SA-PSMAi)$_4$ (15.0 mg, 3.7 μmol) in 1 mL of CH_2Cl_2, followed by addition of 1 mL of TFA dropwise. The solution was stirred for 4 hours at room temperature. The reaction mixture was concentrated by rotary evaporation and purified by semi-preparative HPLC (Method B) to give 8.1 mg of a white solid after freeze drying (65% yield). ^{1}H NMR (700 MHz; MeOD): δ 8.65 (d, J = 4.3, 2H), 7.90 (d, J = 9.0, 2H), 7.88 (d, J = 8.4, 4H), 7.51 (d, J = 7.8, 2H), 7.45 (t, J = 6.2, 2H), 4.66 (s, 4H), 4.36-4.32 (m, 18H), 4.28 (dd, J = 8.2, 4.9, 4H), 4.23-4.16 (m, 10H), 3.39 (t, J = 8.0, 2H), 3.21-3.14 (m, 16H), 2.47-2.39 (m, 8H), 2.19-2.14 (m, 18H), 2.05 (s, 2H), 1.94-1.83 (m, 16H), 1.68 (dq, J = 14.2, 7.3, 4H), 1.61-1.58 (m, 16H), 1.58-1.42 (m, 24H), 1.36-1.32 (m, 31H), 1.22-1.19 (m, 8H). HR-MS calc. for $C_{151}H_{238}N_{36}O_{49}$ $[M+3H]^{3+}$: 1114.5702. Found: 1114.5829.

[ReDPA-G2-(carb-SA-PSMAi)$_4$]$^+$ (10a): To a 5 mL round bottom flask, equipped with a magnetic stir bar, was added DPA-G2-(carb-SA-PSMAi)$_4$ (10.0 mg, 2.5 μmol) in 0.5 mL of a 2:1 ACN/PBS solution and $[Re(CO)_3(H_2O)_3]Br$ (1.1 mg, 2.7 μmol, 1.1 eq). The reaction mixture was stirred at 75 °C for 90 min. The product was purified by semi-prep HPLC and lyophilized to afford 3.5 mg as a white powder in 32 % yield. ^{1}H NMR (700

MHz; DMSO): δ 8.81 (d, *J* = 5.5, 2H), 7.98 (t, *J* = 7.8, 2H), 7.88 (s, 4H), 7.72 (dt, *J* = 17.4, 5.5, 8H), 7.66 (t, *J* = 5.1, 3H), 7.54 (d, *J* = 7.8, 2H), 7.40 (t, *J* = 6.5, 2H), 6.32 (dd, *J* = 27.8, 8.4, 8H), 4.90 (dd, *J* = 50.9, 16.7, 4H), 4.28 (t, *J* = 7.0, 8H), 4.20-4.16 (m, 12H), 4.09 (bs, 8H), 4.04 (td, *J* = 8.4, 5.3, 4H), 3.95 (q, *J* = 6.8, 4H), 3.79 (m, 2H), 3.15 (m, 2H), 3.00 (dsextet, *J* = 12.2, 6.2, 18H), 2.28-2.17 (m, 8H), 2.01 (t, *J* = 7.5, 16H), 1.89-1.85 (m, 4H), 1.81 (s, 2H), 1.77-1.73 (m, 8H), 1.67 (m, *J* = 5.7, 4H), 1.62-1.57 (m, 4H), 1.51 (m, 6H), 1.45 (t, *J* = 6.6, 16H), 1.39 (m, 122H), 1.34 (m, 12H), 1.26 (m, 18H), 1.21 (m, 27H), 1.14 (s, 3H), 1.13 (s, 6H). HR-MS calc. for $C_{202}H_{334}N_{36}O_{52}Re$ $[M+3H]^{4+}$: 1071.6097. Found: 1071.6088.

$[ReDPA\text{-}G2\text{-}(carb\text{-}SA\text{-}PSMAi\text{-}COOH)_4]^+$ (11a): To a 5 mL round bottom flask, equipped with a magnetic stir bar, was added $[ReDPA\text{-}G2\text{-}(carb\text{-}SA\text{-}PSMAi)_4]^+$ (2.8 mg, 0.7 μmoles) in 1 mL of CH_2Cl_2, followed by dropwise addition of 1 mL of TFA. The solution was stirred for 4 hours at room temperature. The reaction mixture was concentrated by rotary evaporation to give 2.3 mg of an off-white waxy solid after freeze drying (98% yield). ^{1}H NMR (700 MHz; MeOD): δ 8.88 (d, *J* = 5.4, 2H), 7.95 (t, *J* = 7.3, 2H), 7.89 (s, 4H), 7.58 (d, *J* = 7.6, 2H), 7.39 (t, J = 6.5, 2H), 4.41-4.30 (m, 16H), 4.29-4.18 (m, 12H), 3.92-3.90 (m, 2H), 3.20-3.15 (m, 16H), 2.46-2.40 (m, 8H), 2.19-2.13 (m, 16H), 2.01-1.83 (m, 16H), 1.70-1.65 (m, 4H), 1.65-1.58 (m, 16H), 1.58-1.40 (m, 24H), 1.40-1.28 (m, 32H), 1.28-1.18 (m, 8H). HR-MS calc. for $C_{154}H_{238}N_{36}O_{52}Re$ $[M+H]^{2+}$: 1806.8413. Found: 1806.8466.

pTSe-G2-(pro-SA-PSMAi)$_4$ (6b): A 5 mL round bottom flask, equipped with a magnetic stir bar, was added pTSe-G2-(propyne)$_4$ (20 mg, 29 μmol), PSMAi-SA-N_3 (110 mg, 143 μmol, 5 eq) and sodium ascorbate (11 mg, 57 μmol, 2 eq) in 1 mL of DMF. The reaction flask was evacuated and back filled with N_2 three times. $CuSO_4$ (2.9 mg, 11.4 μmol, 0.4 eq) in 0.2 mL of dH_2O was added to the reaction vessel and the reaction mixture was allowed to stir at room temperature overnight. The reaction mixture was concentrated by rotary evaporation and purified via silica gel column chromatography (5-15% CH_3OH in CH_2Cl_2) to yield 60 mg of the product as a white solid (55 %). ^{1}H NMR (700 MHz; DMSO): δ 8.01 (s, 4H), 7.77 (d, *J* = 8.2, 2H), 7.69 (dt, *J* = 16.4, 5.5, 8H), 7.42 (d, *J* = 8.2, 2H), 6.28 (dd, *J* = 26.1, 8.3, 8H), 4.44 (s, 8H), 4.30 (t, *J* = 7.0, 8H), 4.09 (q, *J* = 5.2, 10H), 4.03 (td, *J* = 8.5, 5.2, 4H), 3.95 (td, *J* = 7.9, 5.6, 4H), 3.91 (s, 4H), 3.66 (t, *J* = 5.5, 4H), 3.47-3.42 (m, 8H), 2.98 (tt, *J* = 11.1, 5.6, 12H), 2.36 (s, 3H), 2.28-2.18 (m, *J* = 6.5, 8H), 2.02-1.99 (t, *J* = 7.2, 10H), 1.88-1.84 (m, 4H), 1.77 (dt, *J* = 14.4, 7.2, 6H), 1.69-1.64 (m, 4H), 1.58 (m, 6H), 1.52-1.49 (m, 4H), 1.44 (t, *J* = 6.5, 10H), 1.37 (m, 57H), 1.36-1.28 (m, 8H), 1.26-1.22 (m, 16H), 1.22-1.19 (m, 15H), 1.01-0.99 (s, 6H), 0.92 (s, 3H), 0.90-0.85 (m, 4H). HR-MS calc. for $C_{188}H_{320}N_{28}O_{48}S$ $[M+4H]^{4+}$: 944.0883. Found: 944.0886.

COOH-G2-(pro-SA-PSMAi)$_4$ (7b): To a 5 mL round bottom flask, equipped with a magnetic stir bar, was added pTSe-G2-(pro-SA-PSMAi)$_4$ (45.0 mg, 11.9 μmol) in 2 mL CH_2Cl_2 and DBU (9.1 mg, 59.6 μmol, 5 eq). After stirring at room temperature for 1 hour, the reaction mixture was diluted with 15 mL CH_2Cl_2 and washed with $NaHSO_4$ (2 x 10 mL) and brine. The crude reaction mixture was concentrated by rotary evaporation and

purified by silica gel column chromatography (5-20 % CH_3OH in CH_2Cl_2) to yield 37 mg of the product as a white solid (87 %). ^{1}H NMR (700 MHz; DMSO): δ 8.03 (bs, 4H), 7.73 (bs, 8H), 4.45 (s, 8H), 4.31 (t, *J* = 6.9, 8H), 4.13-4.07 (m, 3H), 4.03 (td, *J* = 8.5, 5.2, 4H), 3.95 (dd, *J* = 13.5, 8.0, 4H), 3.46 (s, 8H), 2.99 (dq, *J* = 11.6, 5.9, 12H), 2.26-2.22 (m, 8H), 2.01 (t, *J* = 7.5, 10H), 1.90-1.84 (m, 4H), 1.78 (dt, *J* = 14.5, 7.2, 6H), 1.73-1.65 (m, 4H), 1.63-1.54 (m, 4H), 1.50-1.42 (m, 18H), 1.40-1.30 (m, 68H), 1.27-1.20 (m, 24H), 1.02 (s, 3H). HR-MS calc. for $C_{179}H_{310}N_{28}O_{46}$ $[M+4H]^{4+}$: 898.0768. Found: 898.0786.

DPA-G2-(pro-SA-PSMAi)$_4$ (8b): To a 5 mL round bottom flask, equipped with a magnetic stir bar, was added COOH-G2-(pro-SA-PSMAi)$_4$ (35.0 mg, 9.8 μmol) in 1 mL of CH_2Cl_2, NHS (2.2 mg, 19.5 μmol, 2 eq) and EDC-HCl (3.7 mg, 19.5 μmol, 2 eq). The reaction mixture was allowed to stir at room temperature overnight. The reaction mixture was diluted with CH_2Cl_2 and washed with water and $NaHSO_4$. The crude NHS-G2-(pro-SA-PSMAi)$_4$ was dissolved in CH_2Cl_2, followed by addition of DPA-NH_2 (5.3 mg, 19.5 μmol, 2 eq) and Et_3N (4.0 μL, 29.3 μmol, 3 eq). The reaction mixture was purified by semi-prep HPLC and lyophilized to afford 18.2 mg of the title compound as a white solid in 49 % yield. ^{1}H NMR (700 MHz; DMSO): δ 8.44 (d, J = 4.9, 2H), 7.99 (s, 4H), 7.73-7.68 (m, 8H), 7.48 (d, J = 7.9, 2H), 7.20 (dd, J = 6.9, 5.0, 2H), 6.94 (s, 4H), 6.31 (dd, J = 27.7, 8.3, 8H), 4.43 (bs, 8H), 4.29 (t, J = 7.1, 8H), 4.07 (dd, J = 29.9, 7.9, 4H), 4.03 (m, 4H), 3.94 (td, J = 7.9, 5.6, 4H), 3.69 (s, 4H), 3.46-3.43 (m, 8H), 2.98 (m, 12H), 2.41 (s, 2H), 2.22-2.20 (m, 8H), 2.00 (t, J = 7.5, 8H), 1.86 (m, 4H), 1.76 (dt, J = 14.5, 7.2, 8H), 1.69-1.63 (m, 4H), 1.60-1.51 (m, 4H), 1.48-1.41 (m, 16H), 1.40-1.30 (m, 60H), 1.27-1.23

(m, 12H), 1.20-1.17 (m, 12H), 1.02 (s, 3H), 1.00 (s, 6H). HR-MS calc. for $C_{195}H_{330}N_{32}O_{45}$ $[M+3H]^{3+}$: 1281.8265. Found: 1281.8243.

$[ReDPA-G2-(pro-SA-PSMAi)_4]^+$ (10b): To a 5 mL round bottom flask, equipped with a magnetic stir bar, was added DPA-G2-(pro-SA-PSMAi)$_4$ (10 mg, 2.6 μmol) in 0.5 mL of a 2:1 ACN/PBS solution, and $[Re(CO)_3(H_2O)_3]Br$ (1.2 mg, 2.9 μmol , 1.1 eq). The reaction mixture was stirred at 75 °C for 90 min. The product was purified via semi-preparative HPLC (Method A) to give 7.4 mg of a white solid after freeze drying (69% yield). ^{1}H-NMR (700 MHz; DMSO): δ 8.81 (d, *J* = 5.5, 2H), 8.55 (s, 2H), 8.02 (s, 4H), 7.99 (td, *J* = 7.8, 1.3, 2H), 7.89-7.85 (m, 2H), 7.74-7.70 (m, 8H), 7.54 (d, *J* = 8.0, 2H), 7.40 (t, *J* = 6.7, 2H), 6.29 (dd, *J* = 26.8, 8.3, 8H), 4.90 (dd, *J* = 56.8, 16.8, 8H), 4.46 (s, 8H), 4.30 (t, *J* = 7.1, 8H), 4.12 (dd, *J* = 39.3, 10.9, 8H), 4.03 (td, *J* = 8.5, 5.2, 4H), 3.95 (td, *J* = 8.0, 5.6, 4H), 3.83-3.77 (m, 2H), 3.50-3.46 (m, 8H), 3.19-3.14 (m, 2H), 2.99 (td, *J* = 12.0, 6.3, 8H), 2.27-2.17 (m, 8H), 2.01 (t, *J* = 7.5, 8H), 1.88-1.82 (m, 8H), 1.76 (dt, *J* = 14.5, 7.3, 6H), 1.68-1.63 (m, 6H), 1.60-1.58 (m, 4H), 1.52-1.49 (m, 6H), 1.44 (t, *J* = 6.9, 8H), 1.39-1.33 (m, 42H), 1.27-1.24 (m, 8H), 1.20 (s, 12H), 1.15 (s, 2H), 1.08 (s, 3H), 1.03 (s, 6H). HR-MS calc. for $C_{198}H_{330}N_{32}O_{48}Re$ $[M+3H]^{4+}$: 1029.1051. Found: 1029.1005.

DPA-G2-(pro-SA-PSMAi-COOH)$_4$ (9b): To a 5 mL round bottom flask, equipped with a magnetic stir bar, was added DPA-G2-(pro-SA-PSMAi)$_4$ (7.0 mg, 1.8 μmol) in 1 mL of CH_2Cl_2, followed by dropwise addition of 1 mL of TFA. The solution was stirred for 4

hours at room temperature. The reaction mixture was concentrated by rotary evaporation and purified by semi-preparative HPLC (Method B) to give 3.5 mg of a white solid after freeze drying (60% yield). ^{1}H-NMR (700 MHz; MeOD): δ 8.65 (d, *J* = 4.3, 2H), 7.95 (s, 4H), 7.90 (td, *J* = 7.7, 1.6, 2H), 7.51 (d, *J* = 7.8, 2H), 7.45 (dd, *J* = 7.3, 5.1, 2H), 4.66 (s, 4H), 4.55 (s, 8H), 4.40 (t, *J* = 7.1, 8H), 4.33 (dd, *J* = 8.6, 5.0, 4H), 4.28 (dd, *J* = 8.3, 4.9, 4H), 4.18 (dd, *J* = 32.6, 11.0, 4H), 3.60-3.56 (m, 8H), 3.38 (t, *J* = 8.0, 2H), 3.19-3.15 (m, 18H), 2.47-2.39 (m, 8H), 2.19-2.14 (m, 20H), 2.05 (s, 3H), 1.93-1.83 (m, 18H), 1.68 (dq, *J* = 14.3, 7.3, 4H), 1.61 (t, *J* = 6.4, 16H), 1.56-1.42 (m, 28H), 1.39-1.33 (m, 34H), 1.14 (s, 9H). HR-MS calc. for $C_{147}H_{233}N_{32}O_{45}Na$ $[M+3H+Na]^{4+}$: 798.6786. Found: 798.6714.

$[ReDPA-G2-(pro-SA-PSMAi-COOH)_4]^+$ (11b): To a 5 mL round bottom flask, equipped with a magnetic stir bar, was added $[ReDPA-G2-(pro-SA-PSMAi)_4]^+$ (6.0 mg, 1.5 μmol) in 1 mL of CH_2Cl_2, followed by dropwise addition of 1 mL of TFA. The solution was stirred for 4 hours at room temperature. The reaction mixture was concentrated by rotary evaporation to give 5.0 mg of an off-white waxy solid after freeze drying (>99% yield). ^{1}H NMR (700 MHz; MeOD): δ 8.89 (d, *J* = 5.5, 2H), 7.98-7.95 (m, 6H), 7.58 (d, *J* = 7.9, 2H), 7.40 (t, *J* = 6.6, 2H), 4.57 (s, 8H), 4.39 (t, *J* = 7.1, 8H), 4.33 (dd, *J* = 8.6, 5.1, 4H), 4.28 (dd, *J* = 8.3, 4.9, 4H), 4.22 (dd, *J* = 32.3, 11.0, 4H), 3.92-3.90 (m, 2H), 3.61 (q, *J* = 9.9, 8H), 3.19-3.15 (m, 16H), 2.47-2.39 (m, 8H), 2.19-2.13 (m, 20H), 2.05 (s, 2H), 1.98-1.96 (m, 2H), 1.92-1.88 (m, 12H), 1.86-1.84 (m, 4H), 1.69-1.65 (m, 4H), 1.61 (t, *J* = 6.9, 18H), 1.53-1.50 (m, 16H), 1.44 (quintet, *J* = 7.7, 8H), 1.38-1.30

(m, 33H), 1.19 (s, 3H), 1.17 (s, 6H). HR-MS calc. for $C_{150}H_{233}N_{32}O_{48}Re$ $[M+2H]^{3+}$: 1147.2196. Found: 1147.2115.

6.5.3. Radiolabeling and Plasma Stability

$[^{99m}$TcDPA-G2-(carb-PSMAi-COOH)$_4]^+$ (12a): To a 2 mL microwave vial containing DPA-G2-(carb-SA-PSMAi-COOH)$_4$ (1 mg, 300 nmol) in 0.1 mL of MeOH was added 1 mL of $[^{99m}Tc(CO)_3(H_2O)_3]^+$ in saline adjusted to pH 5-6 with 1 M HCl. The reaction vessel was sealed and the reaction mixture was heated under microwave irradiation for 5 min at 80 °C. R.T. = 11.55 min (Method B). Isolated RCY: 23 ± 3 %.

$[^{99m}$TcDPA-G2-(pro-PSMAi-COOH)$_4]^+$ (12b): To a 2 mL microwave vial containing DPA-G2-(pro-SA-PSMAi-COOH)$_4$ (1 mg, 316 nmol) in 0.1 mL of MeOH was added 1 mL of $[^{99m}Tc(CO)_3(H_2O)_3]^+$ in saline adjusted to pH 5-6 with 1 M HCl. The reaction vessel was sealed and the reaction mixture was heated under microwave irradiation for 5 min at 80 °C. R.T. = 9.80 min (Method C). Isolated RCY: 89 ± 5 %.

Plasma binding studies

A purified and concentrated sample of **12a** or **12b** was formulated in 10% EtOH/PBS at 100 µL/mCi. 100 µL (27MBq) of dendrimer was added to 900 µL of pre-warmed (to 37°C) mouse plasma (Innovative Research, IMS-CD1-N), vortexed and incubated at 37°C. At each timpoint (t = 0, 0.25 h, 0.5 h, 1 h, 2 h and 4 h), 100 µL was removed and added to 200 µL ice cold acetonitrile. Samples were vortexed and then centrifuged at

maximum speed for 10 min. The amount of activity in the whole sample was measured using a dose calibrator (Capintec Inc, CRC-25R). The supernatant was separated from the pellet and the activity from the supernatant and the pellet was measured using a dose calibrator. The supernatant was analyzed via HPLC using Method B. For all time points, pellets were washed with 50 μL of ice cold PBS and the amount of activity in the washed pellet was measured. The experiment was completed once, with the % bound to blood proteins calculated as follows (pellet): [(amount of activity in washed pellet)/(amount of activity in pellet)+(amount of activity in supernatant)]×100% and the % in the supernatant calculated as follows (supernatant): [(amount of activity in supernatant)/(amount of activity in pellet)+(amount of activity in supernatant)]×100%.

6.6. References

(1) Lee, C. C.; Gillies, E. R.; Fox, M. E.; Guillaudeu, S. J.; Fréchet, J. M. J.; Dy, E. E.; Szoka, F. C. *Proc. Natl. Acad. Sci. U. S. A.* **2006**, *103* (45), 16649–16654.

(2) Almutairi, A.; Rossin, R.; Shokeen, M.; Hagooly, A.; Ananth, A.; Capoccia, B.; Guillaudeu, S.; Abendschein, D.; Anderson, C. J.; Welch, M. J.; Fréchet, J. M. J. *Proc. Natl. Acad. Sci. U. S. A.* **2009**, *106* (3), 685–690.

(3) Parrott, M. C.; Marchington, E. B.; Valliant, J. F.; Adronov, A. *J. Am. Chem. Soc.* **2005**, *127* (6), 12081–12089.

(4) Parrott, M. C.; Benhabbour, S. R.; Saab, C.; Lemon, J. A.; Parker, S.; Valliant, J. F.; Adronov, A. *J. Am. Chem. Soc.* **2009**, *131* (21), 2906–2916.

(5) Gillies, E. R.; Dy, E.; Fréchet, J. M. J.; Szoka, F. C. *Mol. Pharm.* **2005**, *2* (2), 129–138.

(6) Wu, P.; Malkoch, M.; Hunt, J. N.; Vestberg, R.; Kaltgrad, E.; Finn, M. G.; Fokin, V. V; Barry, K.; Hawker, C. J. *Chem. Comm.* **2005**, 5775–5777.

(7) García-Gallego, S.; Hult, D.; Olsson, J. V.; Malkoch, M. *Angew. Chem. Int. Ed.* **2015**, *54* (8), 2416–2419.

(8) Goodwin, A. P.; Lam, S. S.; Fréchet, J. M. J. *J. Am. Chem. Soc.* **2007**, *129* (22), 6994–6995.

(9) Gillies, E. R.; Fréchet, J. M. J. *J. Am. Chem. Soc.* **2002**, *124* (47), 14137–14146.

(10) Antoni, P.; Robb, M. J.; Campos, L.; Montanez, M.; Hult, A.; Malmström, E.; Malkoch, M.; Hawker, C. J. *Macromolecules* **2010**, *43* (16), 6625–6631.

(11) Wu, W.; Driessen, W.; Jiang, X. *J. Am. Chem. Soc.* **2014**, *136* (8), 3145–3155.

(12) Guillaudeu, S. J.; Fox, M. E.; Haidar, Y. M.; Dy, E. E.; Szoka, F. C.; Fréchet, J. M. J. *Bioconjug. Chem.* **2008**, *19*, 461–469.

(13) Feliu, N.; Walter, M. V; Montañez, M. I.; Kunzmann, A.; Hult, A.; Nyström, A.; Malkoch, M.; Fadeel, B. *Biomaterials* **2012**, *33* (7), 1970–1981.

(14) Vaillard, V. A.; González, M.; Perotti, J. P.; Grau, R. J. a.; Vaillard, S. E. *RSC Adv.* **2014**, *4* (25), 13012.

(15) Maresca, K. P.; Hillier, S. M.; Femia, F. J.; Keith, D.; Barone, C.; Joyal, J. L.; Zimmerman, C. N.; Kozikowski, A P.; Barrett, J. A; Eckelman, W. C.; Babich, J. W. *J. Med. Chem.* **2009**, *52* (2), 347–357.

(16) Banerjee, S. R.; Pullambhatla, M.; Shallal, H.; Lisok, A.; Mease, R. C.; Pomper, M. G. *Oncotarget* **2011**, *2* (12), 1244–1253.

(17) Shallal, H. M.; Minn, I.; Banerjee, S. R.; Lisok, A.; Mease, R. C.; Pomper, M. G. *Bioconj. Chem.* **2014**, *25* (2), 393-405.

(18) Chandran, S. S.; Banerjee, S. R.; Mease, R. C.; Pomper, M. G.; Denmeade, S. R. *Cancer Biol. Ther.* **2008**, *7* (6), 974–982.

(19) Banerjee, S. R.; Foss, C. A.; Castanares, M.; Mease, R. C.; Byun, Y.; Fox, J. J.; Hilton, J.; Lupold, S. E.; Kozikowski, A. P.; Pomper, M. G. *J. Med. Chem.* **2008**, *51*, 4504–4517.

(20) Davis, M. I.; Bennett, M. J.; Thomas, L. M.; Bjorkman, P. J. *Proc. Natl. Acad. Sci. U. S. A.* **2005**, *102* (17), 5981–5986.

(21) Alberto, R.; Ortner, K.; Wheatley, N.; Schibli, R.; Schubiger, A. P. *J. Am. Chem. Soc.* **2001**, *123* (13), 3135–3136.

Chapter 7. Concluding Remarks and Future Directions

7.1. Concluding Remarks

The goal of the thesis from the very beginning was to develop a dendritic molecular imaging platform that could be assembled in a modular manner. In order to accomplish this task, several obstacles needed to be overcome, such as efficient and orthogonal coupling of targeting vectors to the periphery, evaluating and addressing stability of the platform *in vitro* and *in vivo*, and lastly choosing the appropriate targeting vector to show the "proof of concept" of enhanced target affinity via multi-valency.

To enable efficient and orthogonal functionalization of the dendrimer with targeting vectors, the alcohol periphery of the dendrimers were decorated with alkyne moieties to enable "Click" functionalization using the Cu(I) catalyzed alkyne-azide cycloaddition (Chapter 2). Although the "Click" chemistry worked well in attaching model compounds to the periphery of the dendrimer, undesirable chelation of the copper by the DPA ligand was observed. Although removal of copper from the DPA ligand was not trivial (without resulting in significant degradation of the polyester dendritic backbone), a transmetallation reaction with ^{99m}Tc was demonstrated to be a feasible alternative (Chapter 2).

In order to demonstrate the proof of concept, we evaluated two targeting vectors: an acyloxymethyl ketone (AOMK) derivative for targeting cathepsin B (Chapter 3), and a lys-urea-glu dipeptide for targeting the prostate specific membrane antigen (PSMA) (Chapter 4 and 5). Functionalization of dendrimers with AOMK derivatives resulted in

loss of affinity towards cathepsin B, despite the use of both hydrophobic and hydrophilic linkers. This was attributed to the highly hydrophobic nature of the AOMK targeting vector, which resulted in poor aqueous solubility and potential aggregation, rendering the inhibitors inaccessible to the enzyme. Conversely, the lys-urea-glu dipeptide inhibitor for targeting PSMA demonstrated increased affinity with increased multi-valency. The PSMA inhibitor is much more hydrophilic, bearing three carboxylic acid moieties on each targeting vector, and thus resulting in excellent aqueous solubility. A G2 dendrimer functionalized with four PSMA inhibitors linked via an alkyl spacer demonstrated the highest affinity towards PSMA and was further investigated *in vitro* and *in vivo*. Unfortunately, the compound demonstrated poor tumour uptake *in vivo*, which was attributed to the rapid degradation (<15 min) of the dendrimer backbone (hypothesized to occur via hydrolysis) as demonstrated through plasma stability data (Chapter 5).

In order to address the stability of the molecular imaging agent, the non-neopentyl esters were replaced with more resilient linkages. A carbamate and an ether dendrimer analogue were prepared and functionalized with PSMA inhibitors to serve as a direct comparison to the previous data. Both the carbamate and ether dendrimers demonstrated improved plasma stability when functionalized with PSMA inhibitors (Chapter 6). In particular, the ether analogue demonstrated excellent *in vitro* stability (>4 hours) and overcomes the last obstacle that was encountered in developing the dendritic platform.

7.2. Future Directions

Given the progress that has been reported in the design, synthesis and optimization of the aforementioned dendritic scaffold for molecular imaging applications, the immediate future work can focus on validating the *in vitro* stability with *in vivo* results. Upon validating the *in vivo* stability of the dendritic scaffold, future efforts can focus solely on the investigation of targeting vectors. Based on our observations, it would be prudent to choose a targeting vector that is hydrophilic in nature. It is worthy to note that the nature of the linker also warrants careful consideration and design. A hydrophilic PEG spacer, while commonly utilized, is not always the ideal choice for the attachment of a targeting vector to the dendritic scaffold (as shown in Chapter 4). However, with careful consideration, it is possible to prepare high affinity multi-valent molecular imaging agents that warrant further investigation *in vivo*, as demonstrated in this thesis.